UC Irvine
UC Irvine Electronic Theses and Dissertations

Title

Catalysts for C-N Bond Formation, Polymers for the Delivery of mRNA, and Metal-Ligand Mediated Mechanical Gradient Formation

Permalink

https://escholarship.org/uc/item/88h8828k

Author

Oldenhuis, Nathan John

Publication Date

2017

Copyright Information

Peer reviewed|Thesis/dissertation

UNIVERSITY OF CALIFORNIA,
IRVINE

Catalysts for C-N Bond Formation, Polymers for the Delivery of mRNA, and Metal-Ligand
Mediated Mechanical Gradient Formation

DISSERTATION

submitted in partial satisfaction of the requirements
for the degree of

DOCTOR OF PHILOSOPHY

in Chemistry

by

Nathan Oldenhuis

Dissertation Committee:
Professor Zhibin Guan, Co-Chair
Professor Vy Dong, Co-Chair
Professor David Van Vranken
Professor Aaron Esser-Kahn

2017

DEDICATION

To the people who make my life great

TABLE OF CONTENTS

LIST OF FIGURES

Page

LIST OF TABLES

ACKNOWLEDGMENTS

CURRICULUM VITAE

Education

University of Iowa (2008 – 2012)

B.S. in Chemistry with Distinction

University of California Irvine (2012 – 2017)

Ph.D. in Organic Chemistry (Advisor: Zhibin Guan, Vy Dong)

Work Experience

Prof. Zhibin Guan and Prof. Vy Dong – University of California, Irvine (2012 – 2017)

Graduate research member involved in investigating acceptorless dehydrogenation catalysts for amidation, polyamidation, and chiral amine synthesis. Development of siRNA/mRNA delivery reagents.

Prof. Stephen Buchwald – Massachusetts Institute of Technology (Summer 2010, 2011)

Undergraduate research member involved in the synthesis of unsymmetrical N,N diarylureas and of a general system for Negishi Coupling using paladacycle precatalysts.

Prof. Hein Nguyen – University of Iowa (2011 – 2012)

Undergraduate research member involved in development of catalytic system for enantioselective allylic fluorination of allylic trichloroacetimidates.

Touch the Earth – University of Iowa (2009 – 2012)

Advanced climbing instructor responsible for teaching upper-level climbing techniques and skills and leading outdoor adventure trips

Honors and Awards

NIH NRSA F31 Individual Predoctoral Fellowship (GM115077) (2015 – 2017)

Allergan Graduate Fellowship (2015)

Hal Moore Award for Accomplishments in the field of organic chemistry (2016)

NSF GRFP Honorable Mention (2012)

2012 Chemistry Alumni Award Recipient (2012)

Dean's List (all semesters UI 2008 – 2012)

The National Society of Collegiate Scholars

University of Iowa Honors Program

Publications

1. Breitler, S., **Oldenhuis, N.J.,** Fors, B.P. & Buchwald, S.L. Synthesis of Unsymmetrical Diarylureas via Pd-Catalyzed C-N Cross-Coupling Reactions. *Org. Lett.* 13, 3262-3265 (2011).

2. Yang, Y., **Oldenhuis, N.J.** & Buchwald, S.L. Mild and General Conditions for Negishi Cross-Coupling Enabled by the Use of Palladacycle Precatalysts. *Angew. Chem. Int. Ed.* 52, 615-619 (2013).

    a. Highlighted by Synfacts: Yang, Y., Oldenhuis N.J., Buchwald S.L., Negishi Cross-Coupling Using Palladacycle Precatalysts *Synfacts* 9 (04), 0431-0431

3. **Oldenhuis, N.J.,** Dong, V.M. & Guan, Z. Catalytic acceptorless dehydrogenations: Ru-Macho catalyzed construction of amides and imines. *Tetrahedron* 70, 4213-4218 (2014).

4. **Oldenhuis, N.J.,** Dong, V.M. & Guan, Z. From Racemic Alcohols to Enantiopure Amines: Ru-Catalyzed Diastereoselective Amination. *J. Am. Chem. Soc.* 136, 12548-12551 (2014).

    a. Highlighted by Synfacts: **Oldenhuis, N.J.,** Dong, V.M., Guan, Z. Diastereoselective Amination of Alcohols Catalyzed by Ruthenium *Synfacts 10 (11), 1174-1174*

5. Zeng, H., Johnson, M.E., **Oldenhuis, N.J.,** Tiambeng, T.T., Guan, Z. Structure-Based Design of Dendritic Peptide Bolaamphiphiles for siRNA Delivery *ACS Central Science* 1 (6), 303-312

6. **Oldenhuis, N.J.,** Whittaker A.M., Dong. V.M., Green Chemistry in Drug Discovery: From Academia to Industry (Green Methodologies for Amide Synthesis) *Book chapter, accepted: Being published in 2016*.

7. **Oldenhuis, N.J.,** Eldredge, A.C., Burts, A.O., Ryu, K.A., Chung, J., Johnson, M.E., Guan, Z. Biodegradable dendronized polymers for efficient mRNA delivery *ChemistrySelect* 1 (15), 4413-4417 (2016)

8. Elderdge, A.C., Johnson, M.E., **Oldenhuis, N.J.,** Guan Z. A Focused Library Approach to Discover Discrete Dipeptide Bolaamphiphiles for siRNA Delivery *Biomacromolecules* 17 (10), 3138–3144 (2016)

9. Johnson, M.E., Shon, J., Guan, B., Patterson, J., **Oldenhuis, N.J.,** Eldredge A.C., Gianneschi, N., Guan, Z., Fluorocarbon Modified Low-Molecular-Weight Polyethylenimine for siRNA Delivery *Bioconjugate Chemistry* 27 (8), 1784-1788 (2016)

Patents

1. **Oldenhuis, N. J.;** Guan, Z. Biodegradeable dendronized polymers for efficient mRNA delivery App. No. PCT/US17/21978

Presentations and Posters

1. **Oldenhuis, N. J.;** Eldredge, A.C., Burts, A.O., Johnson, M.E., Guan, Z. Biodegradable dendronized polymers for efficient mRNA delivery *Poster, ACS 251st National Meeting San Diego 2016*

    a. Selected for *SciMix*

2. **<u>Oldenhuis, N. J.;</u>** Eldredge, A.C., Burts, A.O., Johnson, M.E., Guan, Z. Biodegradable dendronized polymers for efficient mRNA delivery *Poster, GRS Drug Carriers in Medicine & Biology*

3. **<u>Oldenhuis, N. J.;</u>** Neal, J.A.; Novitsky, A.L.; Samson, E.M.; Guan, Z. Mechanical Gradient Formation via Metal-Ligand Interactions *Presentation, Bristol Meyers Squibb symposium UCI 2017*

ABSTRACT OF THE DISSERTATION

Catalysts for C-N Bond Formation, Polymers for the Delivery of mRNA, and Metal-Ligand

Mediated Mechanical Gradient Formation

By

Nathan John Oldenhuis

Doctor of Philosophy in Organic Chemistry

University of California, Irvine 2017

Professor Zhibin Guan, Co-Chair

Professor Vy Dong, Co-Chair

In this dissertation, I will discuss the primary authored papers I have published over my time at UCI. They cover a broad range of topics, including catalysis, drug delivery, and dynamic materials.

Chapter 1 is a modified version of a yet to be published book chapter I have written. It will discuss green methodology for the construction of amide bonds compared to commonly used methods, which generally produce stoichiometric amounts of waste.

Chapter 2 is reproduced from a published manuscript that describes a catalytic system using a PNP type pincher complex, Ru-Macho, which was discovered to produce amides via dehydrogenative coupling of alcohols and amines. This methodology allows for the creation of secondary and tertiary amides as well as imines, producing only hydrogen and water as the by-products.

Chapter 3 is reproduced from a published manuscript that describes a catalytic system using a PNP type pincher complex, Ru-Macho, which was discovered to produce alpha chiral amines via a hydrogen borrowing methodology from secondary alcohols and Ellman's tert

butanesufinylamide. This methodology allows for the creation of high value added alpha chiral amines, producing only water as the by-product.

Chapter 4 is reproduced from a published manuscript that describes the development of a dendronized polymer system for the delivery of mRNA to immortalized and primary cells *in vitro*. In the past decade mRNA delivery has emerged as a promising way to modulate protein expression without the need for plasmid DNA transfections. In spite of this need, there are very few synthetic vectors currently available for mRNA delivery. We developed a vector, which was able to deliver both eGFP and Luc-2 mRNA to 3T3, DC 2.4, and bone marrow derived dendritic cells.

Chapter 5 is a yet to be published manuscript which, describes the formation of a biomimetic synthetic mechanical gradient material. Large changes in material stiffness at interfaces often causes manifestation of damage at the interface during stressing of the material. In order to solve this problem, we have developed a synthetic mechanical gradient material based of the metal ligand interaction found in the polychaete worm jaw. Using metal imidazole based materials previously studied in the lab, we were able to create a material with a continuous metal gradient of over 2 orders of magnitude in Young's modulus.

Chapter 1 : Introduction to Acceptorless Dehydrogenate Amide Synthesis

(This is a modified version of a yet unpublished book chapter I wrote, which felt appropriate to include as a lengthy but interesting introduction)

1.1 Introduction:

Amide bonds stitch together life's most basic building blocks to create various peptides and proteins. Moreover, amides are common intermediates and targets in the creation of new materials and medicines. Due to the importance of these bonds there now exist many ways to create amide linkages to access endogenous biomolecules, as well as non-endogenous pharmaceuticals, synthetic proteins, and more, by a robust set of reagents and methods [1-3]. Most commonly used are coupling reagents, which operate by activating a carboxylic acid for nucleophilic displacement by an amine nucleophile. (Figure 1.1). These transformations are general and high yielding, but typically require an excess of the coupling reagent, as well as a stoichiometric amount of base to prevent insoluble carboxylate ammonium salt formation. The excess reagent used in these reactions is wasteful and can often be toxic.
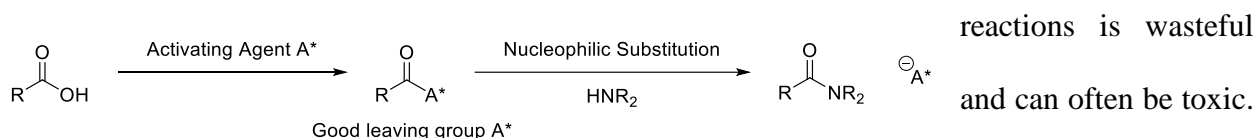
Figure 1.1 Traditional approach to amide bond formation via activated carboxylic group

A recent survey of pharmaceutical manufacturers in 2005 named "amide formation avoiding poor atom economy reagents" the number one challenge to address in the coming years [4]. In response to this challenge, several new amide-forming reactions have emerged to improve atom economy [5-9]. Methods that form amides by catalysis *via* the release or use of small benign molecules, such as H_2O, O_2, N_2, H_2 etc. are targeted to decrease waste. This chapter will survey amide bond formation through the use or loss of H_2. For other promising approaches using catalysis, readers are pointed to recent reviews. [1, 8, 10].

1

1.2 Dehydrogenative Amide Synthesis (DAS) using alcohols and amines:

The first example of amide synthesis from amines and alcohols was explored by Murahashi with the formation of lactams from amino alcohols in the presence of $RuH_2(PPh_3)_4$ [11]. Using aldehydes and secondary amines, both γ and δ lactams were synthesized using this system as well as tertiary amides. In this seminal work, a stoichiometric amount of a hydrogen acceptor (benzylacetone) was required to remove the equivalent of hydrogen from the ruthenium and turn over the catalytic cycle. When the hydrogen acceptor was removed from the reaction, the authors noted that direct amination *via* dehydration occurred instead. Similar catalytic activity for lactam formation was observed using $Ru_3(CO)_{12}$, $RuCl_3•H_2O$, $RuCl_2(PPh_3)_3$, and $RhCl(PPh_3)_3$. Many of these metal complexes make later appearances in this chapter as precursors for more robust catalytic systems.
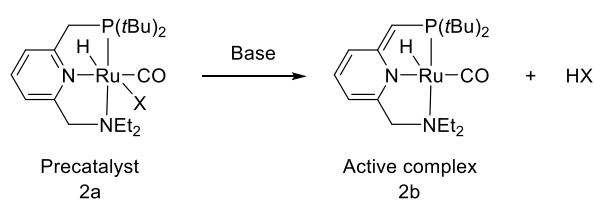
Figure 1.2 Pyridine based PNN pincer complex for amide bond formation

Milstein demonstrated the first dehydrogenative bimolecular amide formation from alcohols and amines using a novel tridentate phosphine-nitrogen-nitrogen (PNN)type ruthenium (II) pincer complex (Figure 1.2) [12]. The pyridine based pincer complex had previously been shown to catalyze ester formation upon activation with base from alcohols *via* the direct elimination of hydrogen gas from the catalyst. The elimination of dihydrogen directly from the catalyst after oxidation was facilitated *via* a Lewis basic site formed through dearomatization of the pyridine on the ligand and the Lewis acidic ruthenium [13-15]. During their optimization studies, the authors found that amide formation was favored over ester formation as well as imine and amine formation. Considering the oxidative route displayed in Figure 1.3, after the alcohol (**3a**) is oxidized to the carbonyl complex (**3b**) both the amine and the alcohol could attack **3b** producing either a
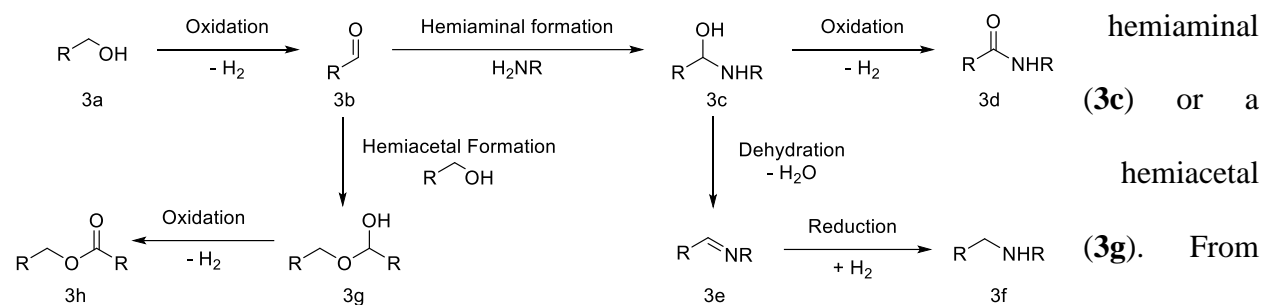
Figure 1.3 Potential amidation side products

hemiaminal (**3c**) or a hemiacetal (**3g**). From there a number of competitive pathways are possible. The hemiacetal can undergo oxidation to generate the ester product (**3h**). The hemiaminal (**3c**), can undergo dehydration to afford the imine (**3e**), which upon reduction by the metal-hydride would yield an amine (**3f**). Finally, the catalyst can oxidize the hemiaminal to yield the amide (**3d**). The robust pincer complex affords a variety of secondary amides, with only 0.1 mol % of the active complex **2b** formed in situ needed for the reaction to go to completion (Figure 1.4). The elimination of stoichiometric reagents, production of hydrogen gas as the only by-product, and eventual commercial availability, demonstrated that not only was green amide bond formation possible, but would become economically viable.

While looking for catalysts for amine alkylation with alcohols, Madsen found that ruthenium (II) N-Heterocyclic carbene (NHC) phosphine complexes formed amides almost exclusively (Figure 1.5) [16]. Considering the reaction pathway outlined in Figure
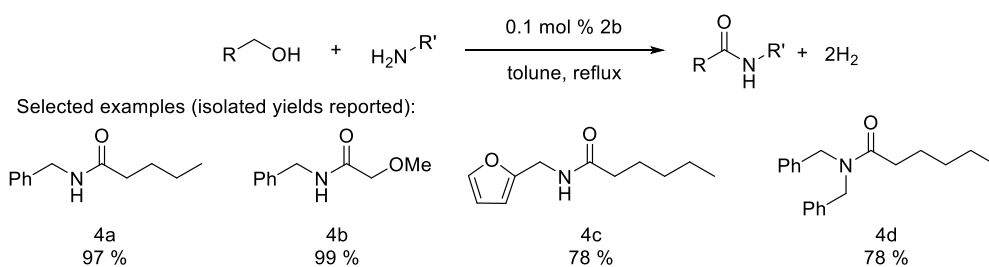
Figure 1.4 Selected examples of DAS using complex 2a.

1.3, it easy to see that dehydrogenative amide synthesis (DAS) could compete with alkylation pathways. The use of Ru(COD)Cl$_2$ with imidazolium salt **5a**, tricyclopentylphosphine, and potassium *tert* butoxide gave the highest yield of amides under reflux in toluene. A variety of

3
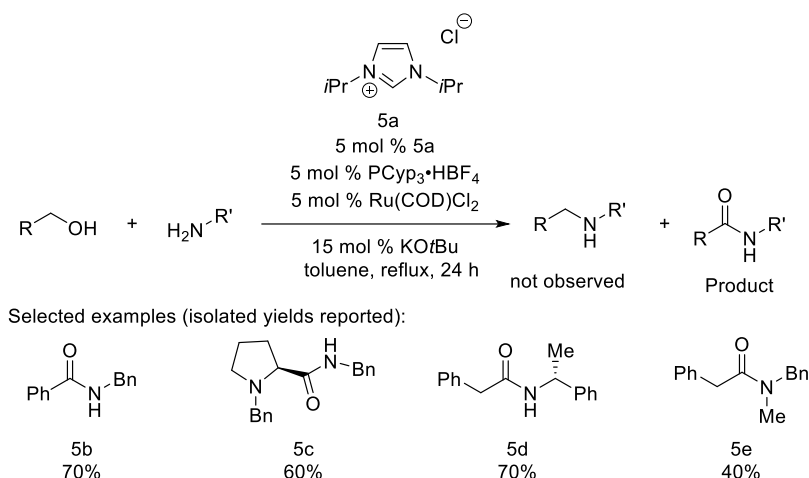
Figure 1.5 Madsen's NHC complex formation for DAS.

primary amines and alcohols yielded secondary amides in excellent yields. Stereocenters on both the alcohol (**5c**) and amine (**5d**) were not racemized during the transformation. One example of a tertiary amide was shown using a secondary amine, but to obtain an appreciable amount (40% isolated yield) of amide, the mixture had to be refluxed in mesitylene (**5e**). This work showed that a ruthenium (II) NHC complex formed *in situ* performed DAS, but required much higher (5 mol % vs 0.1 mol %) catylast loadings and longer reaction times (24 h vs 6-12 h) compared to Milstein's original report.

Milstein's report revived an interest in identifying catalytic methods for DAS. Several studies investigating the mechanism and new catalysts have since appeared. Another ruthenium (II) based system was subsequently discovered by the Williams group [17]. [Ru(*p*-cymene)Cl$_2$]$_2$ was complexed with *bis*(diphenylphosphino)butane
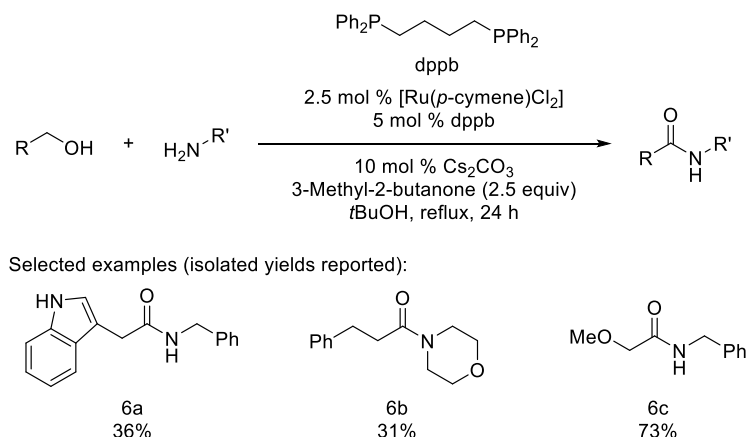
Figure 1.6 DAS using dppb as a ligand and 2-Methyl-3-butanone as a hydrogen acceptor

(dppb) in the presence of cesium carbonate and refluxed in *t*-BuOH to form a variety of amides from alcohols and amines (Figure 1.6). In accordance with the work to date, the methodology was largely limited to less bulky aliphatic amines and alcohols (**6a**, **6c**). Of note, a tertiary amide was

formed using morpholine, but the yield in this case was lower (**6b**). 2.5 equivalents of 3-methyl-2-butanone was used as the hydrogen acceptor, and both this ketone and the corresponding alcohol formed upon reduction can easily be removed after reaction due to their low boiling points (~110 °C). This system was considered advantageous compared to Milstein's PNN complex (**2b**) due to the convenient procedure and use of both a commercially available ligand and ruthenium source at the time. However, lower isolated yields, higher catalyst loadings, and longer reaction times were also observed

The Grützmacher group departed from the use of ruthenium and reported DAS from alcohols and amines using a rhodium (I) complex [18]. This work focused on reducing the high temperatures required for amide formation required by both previously developed methods. While the [Rh(trop$_2$N)(PPh$_3$)] (Figure 1.7, **7b**) looks much different than both the complexes used by Milstein and Madsen, it was designed to contain the same "cooperative ligand" effects as the Milstein catalyst (a Lewis acidic site and a Lewis basic site). According to density
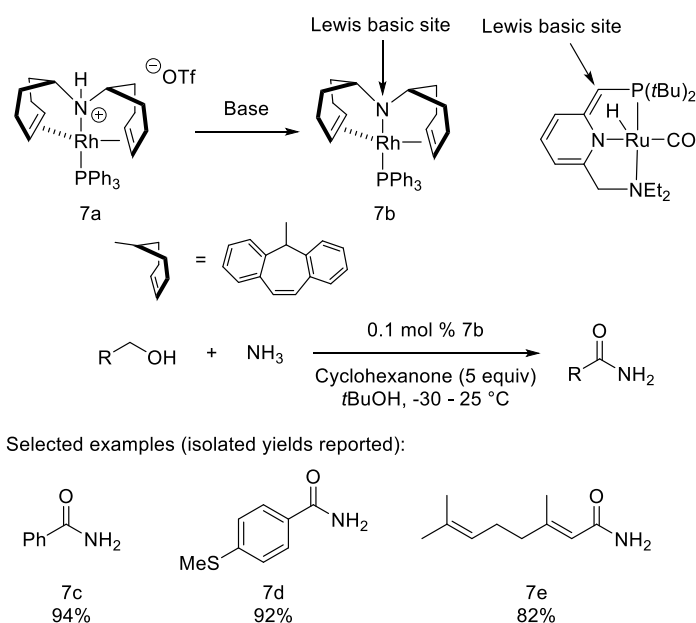
Figure 1.7 Rhodium (I) trop$_2$N complex for DAS

functional theory (DFT) calculations performed by Grützmacher, the Lewis basic nitrogen atom (HOMO) and the Lewis acidic center on the rhodium (LUMO) activate dihydrogen heterolytically. While the protocol formed carboxylic acids, esters, and amides in good yields at ambient temperatures (~25 °C), the procedure required a hydrogen acceptor (5 equiv of cyclohexanone, or
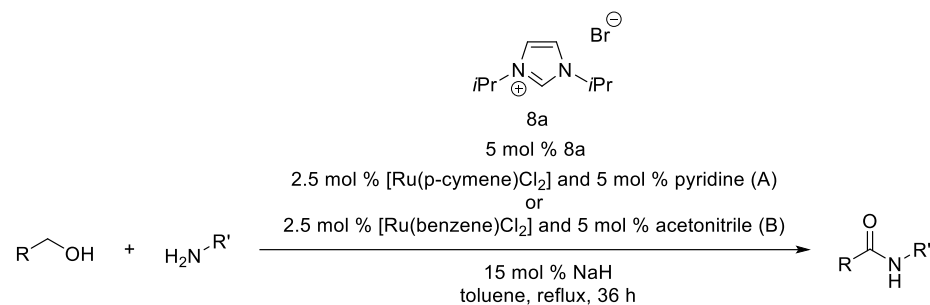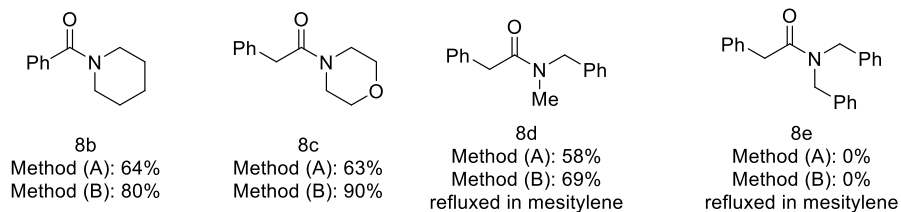
Figure 1.8 Formation of tertiary amides by Ru NHC complexes

methyl methacrylate) to turn over the catalyst. Using the activated complex (**7b**) directly versus the precatalyst (**7a**) and base, one can produce primary amides by DAS from ammonia and primary alcohols (**7c** – **7e**). This result represents the first time ammonia could be activated in a DAS reaction. Benzyl amine was also able to be used to form secondary amides.

Until 2009, all the complexes used for catalytic amide bond formation from amines and alcohols used phosphine ligands to facilitate the reaction. The Hong group sought a phosphine free catalytic system to decrease catalyst deactivation through the decomposition of tertiary phosphines *via* either heat or air [19]. Both [Ru(*p*-cymene)Cl$_2$]$_2$ (method A) and [Ru(benzene)Cl$_2$]$_2$ (method B) in tandem with catalytic amounts of sodium hydride, animidazolium salt (**8a**), and a ligand (pyridine or acetonitrile) produce a variety of amides under reflux conditions in toluene (Figure 1.8). The reaction times were slightly longer (36 h), due to a lower catalyst TON as compared to Milstein's 2007 work. However, compared to the work by Williams ([Ru(*p*-cymene)Cl$_2$]$_2$ and dppb), no hydrogen acceptor was required, thus providing an advantage in terms of atom economy. Both catalyst systems were tolerant of aliphatic alcohols and amines to yield secondary amides, and showed some effectiveness for tertiary amide formation. Piperidine , morpholine , and *N*-methylbenzylamine coupled with various alcohols to give the corresponding

Figure 1.9 Comparison of ruthenium NHC complexes for DAS. Cyp = Cyclopentyl

Ruthenium source	Ligand	Base	Yield of 9b
RuCl$_3$	Pyridine	NaH	80%
RuH$_2$(PPh$_3$)$_4$	Acetonitrile	NaH	96%
RuH$_2$(PMe$_3$)$_4$	Acetonitrile	NaH	21%
RuH$_2$(CO)(PPh$_3$)$_3$	Acetonitrile	NaH	87%
RuH$_2$(CO)(PPh$_3$)$_3$	Pyridine	NaH	74%
RuH$_2$(CO)(PPh$_3$)$_3$	PPh$_3$	NaH	57%
RuHCl(CO)(PPh$_3$)$_3$	Acetonitrile	NaH	49%
Ru(COD)Cl$_2$	PCyp$_3$•HBF$_4$	KOtBu	92%
Ru(cod)(cot)	Acetonitrile	NaH	83%
Ru$_3$(CO)$_{12}$	Acetonitrile	NaH	59%
Ru Black	Acetonitrile	NaH	19%
Ru on Al$_2$O$_3$	Acetonitrile	NaH	15%

tertiary amides **8b**, **8c** and **8d** in good yields. For tertiary amide formation with *N*-methylbenzylamine, reflux in mesitylene was required. Using either method, no reactivity was observed with dibenzylamine, due to the high steric encumbrance.

Several follow up studies were published by Hong [20-22] and Madsen [23] to more thoroughly investigate the formation, mechanism, and substrate scope of the ruthenium NHC based-systems for DAS. The Hong group created amidation catalysis using more economical ruthenium (II) or ruthenium (0) sources (such as RuH$_2$(PPh$_3$)$_4$, RuCl$_3$, Ru(cod)(cot), Ru Black, Ru on Al$_2$O$_3$, and Ru$_3$(CO)$_{12}$), a NHC precursor, base, and a ligand. A comparison of the ligands, bases and ruthenium sources is shown in Figure 1.9. Both Hong and Madsen showed that Grubb's olefin metathesis catalysts are able to mediate the formation of amide bonds from amines and alcohols as well. This work demonstrated that almost any ruthenium-based NHC catalyst showed some degree of activity

Figure 1.10 Triazolylidene ruthenium (II) complex for DAS

for amide bond formation. An additional example was provided by Albrecht using a triazolylidene complex instead of an imidazolium-based one (Figure 1.10) [24].

Tertiary amide formation using primary alcohols and secondary amines has been especially challenging. Both Madsen and Hong tried to enhance the formation of tertiary amides by reducing the steric bulk of the "wingtip" groups

R = Me, *i*Pr, Mes
X = Cl, I
11a

11b
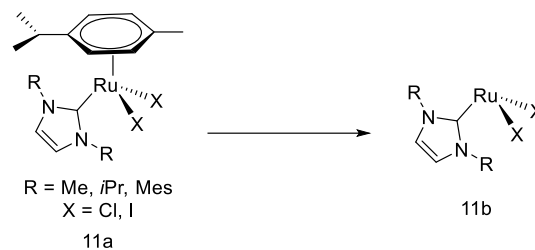
Figure 1.11 In situ generated ruthenium NHC catalyst species

(functional groups on the N position of the imidazolium) on the imidazolium salt. Unfortunately, this change did not enable the formation of tertiary amides, and in all cases to this date, isopropyl substituents remain the best for amide formation. Both Madsen and Hong did not observe primary amides using ammonia (or its surrogates) with the NHC complexes, in contrast to the Rh (I) system reported by Grützmacher. The substrate scope was still largely limited to unhindered aliphatic amines and alcohols, but both Madsen and Hong were able to show lactam formation from α,ω amino alcohols, and tolerance to tertiary amide from minimally hindered secondary amines. Hong further demonstrated that using $RuH_2(PPh_3)_4$ as a precursor rather than $[Ru(p\text{-cymene})Cl_2]_2$ to generate a NHC complex greatly increased the ability of the ruthenium (II) complex to form amides directly from aldehydes and amines as well as from alcohols and amines.

To elucidate the structure of the active catalyst, both Madsen and Hong prepared a variety of ruthenium NHC complexes (**11a**) (Figure 1.11). They postulated that **11b** is the active catalytic species as free *p*-cymene was observed while monitoring the reaction *via* ^{1}H NMR indicating disassociation. Preliminary mechanistic studies showed that the formation of a ruthenium hydride species through the action of a base was likely a key step in forming the active catalytic species. Amide bond formation was not observed when no base was added. An interesting observation by Madsen was that imine formation seemed to hinder amide formation. Amines were combined with mixtures of aldehyde (which condenses with the amine to form the imine immediately) and alcohol

to measure if the amide product was still observed. Formation of the amide product decreased as the amount of aldehyde present in the system increased. This indicated that the aldehyde formed from oxidation of the alcohol must stay partially or fully coordinated to the catalyst during the reaction, and remains on the metal center until a suitable nucleophile approaches.

Hong followed up with a paper addressing the formation of tertiary amides from secondary amines and alcohols using a NHC precatalyst derived from $[Ru(benzene)Cl_2]_2$ (Figure 1.12) [25]. Much like their previous investigations, preparing the ruthenium (II) NHC "precatalyst" beforehand,
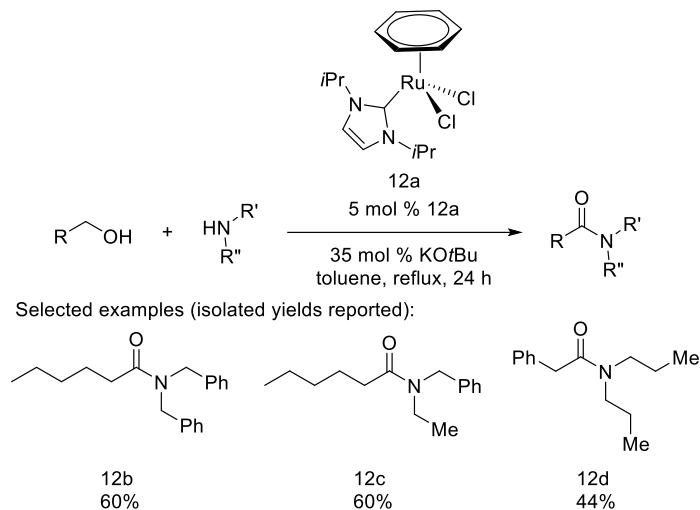
Figure 1.12 Ruthenium NHC complex for tertiary amide formation

rather than *in situ*, led to more efficient tertiary amide bond formation (**12b** – **12d**). They postulated that the dissociation of the arene is necessary to form the active catalytic species. An increased reaction rate was observed using the benzene complex over the cymene complex. This effect was attributed to the less sterically hindered and more electron deficient benzene being able to disassociate faster to form the active complex. However, ester formation was observed using **12a** and not in the case of the *p*-cymene complex. Increasing the amount of base (35 mol %) was necessary to increase tertiary amide formation, with a simultaneous decrease in ester formation. The authors did not rule out the possibility that ester formation might occur followed by trans-amidation with the secondary amine to yield the desired product. In summary, this work was the first to demonstrate tertiary amide synthesis in reasonable yields, as well as the ability to step away from unencumbered secondary amines to use bulkier secondary amines such as dibenzyl amine.

In similar work reported by Milstein in 2013, a new dipyridine PNN (**13a**) type catalyst was shown to have activity towards tertiary amide formation (**13c** - **13d**) but could not react with highly encumbered dibenzylamine (**13b**) (Figure 1.13) [26].

To deduce what components of catalyst design were important for DAS, the Crabtree group studied a variety of diphosphine diamine catalysts (Figure 1.14) based on an amidation catalyst developed by the Williams group (**14a**) in a model lactamization reaction [27]. In the cases where the diphosphine was not present, much lower activity in lactam formation was observed (**14e**). In the diamine, if there were no N-H bonds present, TOFs were reduced (**14b**, **14d**). They reasoned through computational studies that the N-H bond helps stabilize both the aldehyde and hemiaminal intermediates through preventing them from disengaging from the catalyst and forming imines, which can interrupt and

13a

Selected examples (isolated yields reported):

13b	13c	13d
0%	50%	45%

Figure 1.14 Ruthenium NHC complex for tertiary amide formation

	14a	14b	14c	14d
TOF (h-1)	>120	13	>120	23

	14e	14f	14g
TOF (h-1)	40	78	9

Figure 1.13 Diphosphine diamine complexes prepared for study of DAS synthesis

shut down the catalytic cycle (**14a**, **14c**, **14f**). While the structures of these catalysts were similar to previously mentioned systems, Crabtree's study provided insights to influence future catalyst design.

In a follow-up study, Milstein focused on making cyclic dipeptides, as well as pyrazines using their PNN- (**15a**) and PNP-based (**15b**) pincer complexes (Figure 1.15) [28]. β-Amino alcohols in combination with the PNN complex were shown to favor forming the cyclic dipeptide (**15c**, **15d**). When alaninol (R = Me) was used, the polyamide was obtained instead. Pyrazine formation could be promoted with the PNP complex (**15b**) which is known to promote imine formation over amide formation. A cyclic diimine intermediate is obtained that spontaneously oxidizes to the substituted pyrazine (**15e**, **15f**). Accessing symmetrically substituted pyrazines is an important advance because these structures are present in a number of pharmacologically active complexes.

In a related study, the Glorius group used methanol as the alcohol in DAS to form primary formamides. To drive the reaction to completion, a new NHC ruthenium (II) complex was developed derived from [Ru(cod)(2-methylallyl)$_2$] and the imidazolium salt **16a** (Figure 1.16). Previous catalysts were unsuccessful for this transformation because the

Figure 1.15 Synthesis of cyclic dipeptides and pyrazines using amino alcohols and PNN or PNP Ru complexes
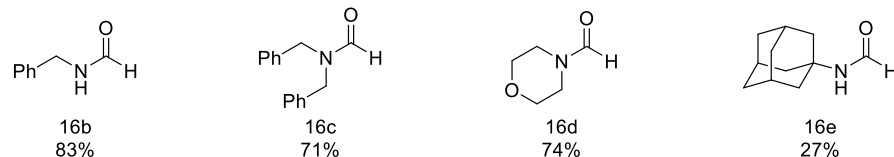
Figure 1.16 Formylation of amines with methanol via DAS

formation of formamides is thermodynamically disfavored. There was a concern that urea derivatives could be formed under the reaction conditions through oxidative amidation of the formamide product. However, formamide formation through DAS proceeded in good yields (**16b** - **16e**). Styrene was required as an additive in the production of the formamides in high yields because the catalyst could not turnover without the assistance of a hydrogen acceptor.

With a focus on the oxygen-source, Milstein developed an amidation methodology using water to oxidize cyclic amines to lactams [29]. With the more active acridine PNP complex **17a**, secondary cyclic amines are activated *via* the removal of hydrogen to form an imine, and then through reversible hydration to form the hemiaminal. Finally, the catalyst oxidizes the hemiaminal to form the lactam in good yields (**17b** – **17e**). They also report the synthesis of
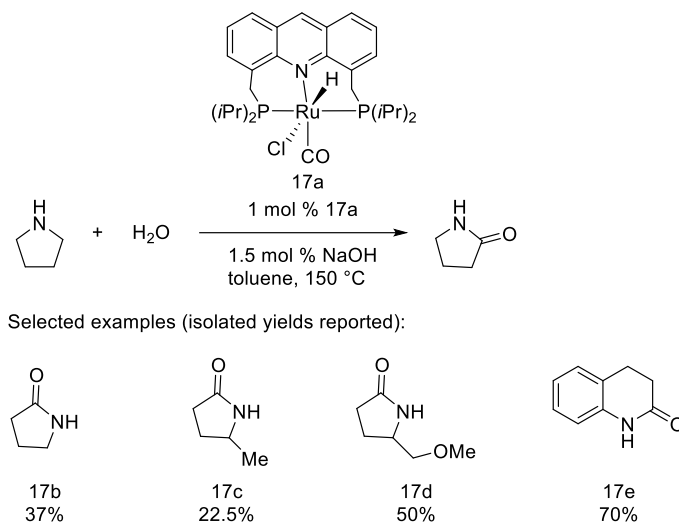
Figure 1.17 DAS of formamides using water as oxidant

lactams from diols and ammonium hydroxide as an ammonia equivalent. The oxidation of amines

12

using water is a major advancement in green oxidation methods for DAS, but at this point requires

rather harsh conditions in the form of high reaction temperatures and only gives modest yields.

1.3 Mechanistic Considerations of Homogeneous DAS:

To date, several mechanistic studies have been published with a focus on DAS

(dehydrogenative amide synthesis). To prevent redundancy, we direct the readers to the studies

themselves for an in depth discussion of the mechanistic

considerations for each of the catalytic systems studied [30-37].

In this brief section, we will provide what we consider the

most important mechanistic facets of DAS from alcohols and

amines across the catalysts previously surveyed. There are

two mechanistic pathways that will be discussed, as well as

the energetics of amide bond formation versus the competing

pathways listed in Figure 1.3.
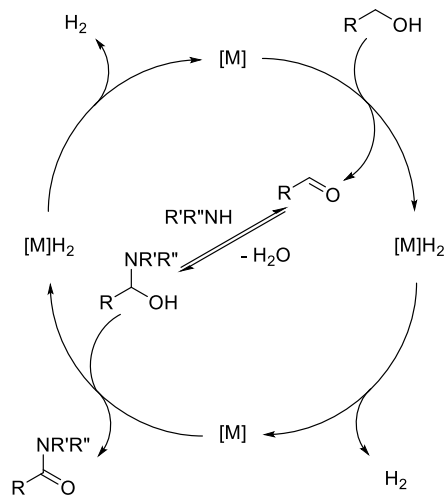
Figure 1.18 Key mechanistic steps of DAS from alcohols and amines

In a simplified view of the reaction, DAS can be summarized in the 4 key steps illustrated

in Figure 1.18. Initially, a metal complex oxidizes an alcohol to an aldehyde *via* removal of

hydrogen. The catalyst then eliminates the equivalent of hydrogen directly or with the help of a
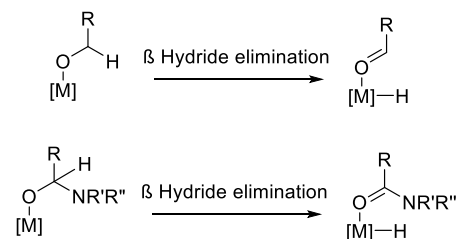
Figure 1.19 Schematic of ß Hydride elimination of alcohols and hemiaminals

hydrogen acceptor while simultaneously the aldehyde

undergoes nucleophilic attack by the amine to form the

hemiaminal intermediate. In the final step, the hemiaminal

is further oxidized by the catalyst to form the amide product

with the catalyst regenerated *via* removal of hydrogen.
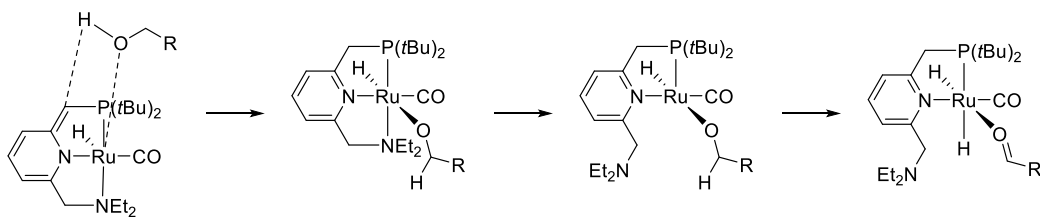
Figure 1.20 Example of hemilable ligand site required for ß-hydride elimination of alcohol using PNN catalyst

Upon the discovery of DAS, the operative mechanism was thought to involve β-hydride eliminations from both the alcohol and hemiaminal as the key steps to form a supposed aldehyde intermediate and product respectively (Figure 1.19). This *β*-hydride elimination could potentially be operative in all the above-mentioned systems, but requires the amine group of the PNN ligand to be hemilabile in order to allow an open coordination site on the ruthenium center. (Figure 1.20). This disassociation is thought to be too high in energy to be feasible. However, pincer ligands presented by Milstein, Grutzmacher, Dong, and Guan could proceed through an additional mechanism involving a bifunctional double hydrogen transfer (BDHT) (Figure 1.21). In the BDHT mechanism, no hemilabile ligand is required, which could explain why the pincer complexes (used by the Grutzmacher group) facilitate DAS despite lacking this feature.

In light of the possible reaction pathways, common observations found during the initial studies help confirm certain mechanistic aspects of DAS from alcohols and amines. For example, the free aldehyde and hemiaminal tend not to be observed during the course of the reaction, despite early theories that the hemiaminal re-binds to the catalyst after being initially formed in solution. This suggests that the aldehydic intermediate must remain bound to the catalyst during the overall oxidation process from alcohol to amide. This proposal is further supported by the observation that the catalysts, which are observed to release the aldehyde after the initial oxidation, favor direct amination and imine formation as opposed to amidation. If hemiaminal formation occurs through a non-catalytic pathway, dehydration to either the imine [34, 38] or amine product out-competes

14
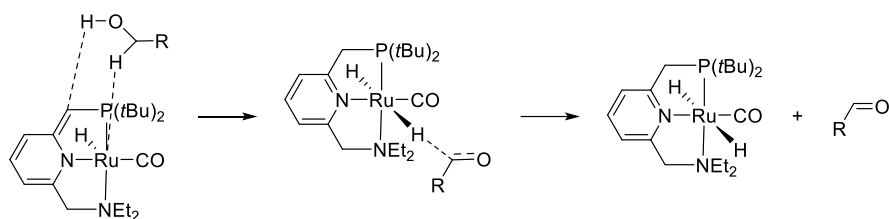
Figure 1.21 BDHT mechanism operating on PNN pincer ligand. No hemilabile site is required

sequential oxidation to form the amide. For a catalyst to be active in DAS, the oxidation of the hemiaminal species by the catalyst must out-compete dehydration to imine intermediates.

These mechanistic studies demonstrate that DAS mainly out-competes dehydrogenative ester synthesis, and computational studies (LANL2DZ) [34] show that hemiaminal formation is favored over hemiacetal formation (the intermediate in dehydrogenative ester synthesis) when using primary amines. Unsurprisingly, when sterically hindered secondary amines are considered, the rate of hemiacetal formation is faster than hemiaminal formation because the lower nucleophilicity of secondary amines makes the hemiaminal formation higher in energy than hemiacetal formation. This trend was observed in several cases, and when highly sterically encumbered amines are used in DAS, ester formation is exclusively observed.

1.4 References:

1.   Valeur, E.; Bradley, M., Amide bond formation: beyond the myth of coupling reagents. *Chem. Soc. Rev.* **2009,** *38* (2), 606-631.

2.   Bode, J. W., Emerging methods in amide- and peptide-bond formation. *Curr. Opin. Drug Discovery Dev.* **2006,** *9* (6), 765-775.

3.   Montalbetti, C. A. G. N.; Falque, V., Amide bond formation and peptide coupling. *Tetrahedron* **2005,** *61* (46), 10827-10852.

4.   Constable, D. J. C.; Dunn, P. J.; Hayler, J. D.; Humphrey, G. R.; Leazer, J. L.; Linderman, R. J.; Lorenz, K.; Manley, J.; Pearlman, B. A.; Wells, A.; Zaks, A.; Zhang, T. Y.,

Key green chemistry research areas - a perspective from pharmaceutical manufacturers. *Green Chem.* **2007,** *9* (5), 411-420.

5.   Allen, C. L.; Williams, J. M. J., Metal-catalyzed approaches to amide bond formation. *Chem. Soc. Rev.* **2011,** *40* (7), 3405-3415.

6.   Gunanathan, C.; Milstein, D., Applications of Acceptorless Dehydrogenation and Related Transformations in Chemical Synthesis. *Science (Washington, DC, U. S.)* **2013,** *341* (6143), 249.

7.   Chen, C.; Hong, S. H., Oxidative amide synthesis directly from alcohols with amines. *Org. Biomol. Chem.* **2011,** *9* (1), 20-26.

8.   Pattabiraman, V. R.; Bode, J. W., Rethinking amide bond synthesis. *Nature (London, U. K.)* **2011,** *480* (7378), 471-479.

9.   Trost, B. M., The Atom Economy - a Search for Synthetic Efficiency. *Science* **1991,** *254* (5037), 1471-1477.

10.   Lundberg, H.; Tinnis, F.; Selander, N.; Adolfsson, H., Catalytic amide formation from non-activated carboxylic acids and amines. *Chem. Soc. Rev.* **2014,** *43* (8), 2714-2742.

11.   Naota, T.; Murahashi, S. I., Ruthenium-Catalyzed Transformations of Amino-Alcohols to Lactams. *Synlett* **1991,** (10), 693-694.

12.   Gunanathan, C.; Ben-David, Y.; Milstein, D., Direct synthesis of amides from alcohols and amines with liberation of H-2. *Science* **2007,** *317* (5839), 790-792.

13.   Zhang, J.; Gandelman, M.; Shimon, L. J. W.; Rozenberg, H.; Milstein, D., Electron-rich, bulky ruthenium PNP-type complexes. Acceptorless catalytic alcohol dehydrogenation. *Organometallics* **2004,** *23* (17), 4026-4033.

14.   Zhang, J.; Leitus, G.; Ben-David, Y.; Milstein, D., Facile conversion of alcohols into esters and dihydrogen catalyzed by new ruthenium complexes. *J. Am. Chem. Soc.* **2005,** *127* (31), 10840-10841.

15.   Zhang, J.; Leitus, G.; Ben-David, Y.; Milstein, D., Efficient homogeneous catalytic hydrogenation of esters to alcohols. *Angew. Chem. Int. Ed.* **2006,** *45* (7), 1113-1115.

16.   Nordstrøm, L. U.; Vogt, H.; Madsen, R., Amide Synthesis from Alcohols and Amines by the Extrusion of Dihydrogen. *J. Am. Chem. Soc.* **2008,** *130* (52), 17672-17673.

17.   Watson, A. J. A.; Maxwell, A. C.; Williams, J. M. J., Ruthenium-Catalyzed Oxidation of Alcohols into Amides. *Org. Lett.* **2009,** *11* (12), 2667-2670.

18.   Zweifel, T.; Naubron, J.-V.; Grützmacher, H., Catalyzed Dehydrogenative Coupling of Primary Alcohols with Water, Methanol, or Amines. *Angewandte Chemie International Edition* **2009,** *48* (3), 559-563.

19.   Ghosh, S. C.; Muthaiah, S.; Zhang, Y.; Xu, X.; Hong, S. H., Direct Amide Synthesis from Alcohols and Amines by Phosphine-Free Ruthenium Catalyst Systems. *Adv. Synth. Catal.* **2009,** *351* (16), 2643-2649.

20.   Zhang, Y.; Chen, C.; Ghosh, S. C.; Li, Y.; Hong, S. H., Well-Defined N-Heterocyclic Carbene Based Ruthenium Catalysts for Direct Amide Synthesis from Alcohols and Amines. *Organometallics* **2010,** *29* (6), 1374-1378.

21.   Ghosh, S. C.; Hong, S. H., Simple RuCl3-Catalyzed Amide Synthesis from Alcohols and Amines. *Eur. J. Org. Chem.* **2010,** (22), 4266-4270, S4266/1-S4266/14.

22.   Muthaiah, S.; Ghosh, S. C.; Jee, J.-E.; Chen, C.; Zhang, J.; Hong, S. H., Direct amide synthesis from either alcohols or aldehydes with amines: activity of Ru(II) hydride and Ru(0) complexes. *J. Org. Chem.* **2010,** *75* (9), 3002-3006.

23.   Dam, J. H.; Osztrovszky, G.; Nordstrom, L. U.; Madsen, R., Amide Synthesis from Alcohols and Amines Catalyzed by Ruthenium N-Heterocyclic Carbene Complexes. *Chem. Eur. J.* **2010,** *16* (23), 6820-6827.

24.   Prades, A.; Peris, E.; Albrecht, M., Oxidations and Oxidative Couplings Catalyzed by Triazolylidene Ruthenium Complexes. *Organometallics* **2011,** *30* (5), 1162-1167.

25.   Chen, C.; Zhang, Y.; Hong, S. H., N-Heterocyclic Carbene Based Ruthenium-Catalyzed Direct Amide Synthesis from Alcohols and Secondary Amines: Involvement of Esters. *J. Org. Chem.* **2011,** *76* (24), 10005-10010.

26.   Srimani, D.; Balaraman, E.; Hu, P.; Ben-David, Y.; Milstein, D., Formation of Tertiary Amides and Dihydrogen by Dehydrogenative Coupling of Primary Alcohols with Secondary Amines Catalyzed by Ruthenium Bipyridine-Based Pincer Complexes. *Adv. Synth. Catal.* **2013,** *355* (13), 2525-2530.

27.   Schley, N. D.; Dobereiner, G. E.; Crabtree, R. H., Oxidative Synthesis of Amides and Pyrroles via Dehydrogenative Alcohol Oxidation by Ruthenium Diphosphine Diamine Complexes. *Organometallics* **2011,** *30* (15), 4174-4179.

28.   Gnanaprakasam, B.; Balaraman, E.; Ben-David, Y.; Milstein, D., Synthesis of Peptides and Pyrazines from ss-Amino Alcohols through Extrusion of H2 Catalyzed by Ruthenium Pincer Complexes: Ligand-Controlled Selectivity. *Angew. Chem. Int. Ed.* **2011,** *50* (51), 12240-12244.

29.   Khusnutdinova, J. R.; Ben-David, Y.; Milstein, D., Oxidant-Free Conversion of Cyclic Amines to Lactams and H2 Using Water As the Oxygen Atom Source. *J. Am. Chem. Soc.* **2014,** *136* (8), 2998-3001.

30.   Gruetzmacher, H., Cooperating ligands in catalysis. *Angew. Chem., Int. Ed.* **2008,** *47* (10), 1814-1818.

31.   Nova, A.; Balcells, D.; Schley, N. D.; Dobereiner, G. E.; Crabtree, R. H.; Eisenstein, O., An experimental-theoretical study of the factors that affect the switch between ruthenium-catalyzed dehydrogenative amide formation versus amine alkylation. *Organometallics* **2010,** *29* (23), 6548-6558.

32.   Gunanathan, C.; Milstein, D., Metal-Ligand Cooperation by Aromatization-Dearomatization: A New Paradigm in Bond Activation and "Green" Catalysis. *Acc. Chem. Res.* **2011,** *44* (8), 588-602.

33.   Li, H.; Wang, X.; Huang, F.; Lu, G.; Jiang, J.; Wang, Z.-X., Computational Study on the Catalytic Role of Pincer Ruthenium(II)-PNN Complex in Directly Synthesizing Amide from Alcohol and Amine: The Origin of Selectivity of Amide over Ester and Imine. *Organometallics* **2011,** *30* (19), 5233-5247.

34.   Zeng, G.; Li, S., Insights into Dehydrogenative Coupling of Alcohols and Amines Catalyzed by a (PNN)-Ru(II) Hydride Complex: Unusual Metal-Ligand Cooperation. *Inorg. Chem.* **2011,** *50* (21), 10572-10580.

35.   Cho, D.; Ko, K. C.; Lee, J. Y., Catalytic Mechanism for the Ruthenium-Complex-Catalyzed Synthesis of Amides from Alcohols and Amines: A DFT Study. *Organometallics* **2013,** *32* (16), 4571-4576.

36.   Mielby, J.; Riisager, A.; Fristrup, P.; Kegnaes, S., Mechanistic investigation of the one-pot formation of amides by oxidative coupling of alcohols with amines in methanol. *Catal. Today* **2013,** *203*, 211-216.

37.   Montag, M.; Zhang, J.; Milstein, D., Aldehyde Binding through Reversible C-C Coupling with the Pincer Ligand upon Alcohol Dehydrogenation by a PNP-Ruthenium Catalyst. *J. Am. Chem. Soc.* **2012,** *134* (25), 10325-10328.

38.   Gunanathan, C.; Gnanaprakasam, B.; Iron, M. A.; Shimon, L. J. W.; Milstein, D., "Long-Range" Metal-Ligand Cooperation in H2 Activation and Ammonia-Promoted Hydride Transfer with a Ruthenium-Acridine Pincer Complex. *J. Am. Chem. Soc.* **2010,** *132* (42), 14763-14765.

Chapter 2 : Catalytic acceptorless dehydrogenations: Ru-Macho catalyzed construction of amides and imines

Abstract:

A commercially available ruthenium (II) PNP type pincer catalyst (Ru-Macho) promotes formation of amides and imines from alcohols and amines via an acceptorless dehydrogenation pathway. The formation of secondary amides, tertiary amides, and secondary ketimines occurs in yields ranging from 35%–95%.

2.1: Introduction

Amide bonds are prevalent in natural products, proteins, and synthetic materials. The formation of amide linkages is one of the most executed transformations in organic chemistry. Traditional methods for amide bond formation often involve harsh conditions and/or generate a stoichiometric amount of waste.[1-3] With growing environmental concerns, there is a need for more efficient, atom economical, and environmentally friendly methods for amide synthesis. As an indication, the formation of amide bonds via green methods was named the number one challenge for organic chemists by the ACS Green Chemistry Institute in 2007.[4] To address this challenge, a variety of new methodologies have emerged.[3] Among them, acceptorless catalytic dehydrogenation has received particular attention for its ability to form amide bonds directly from alcohols and amines[5-10] (Scheme 2.1). Catalytic acceptorless dehydrogenative amide synthesis circumvents the need for a stoichiometric oxidizing agent or sacrificial hydrogen acceptor by evolving hydrogen gas directly from the reaction.[11] A number of laboratories[5-8, 12-17] have demonstrated promising catalysts for amide bond formation via dehydrogenation using Ruthenium catalysis. Our group previously employed the Milstein catalyst (**1**) for the synthesis of polyamides.[18] Others have also applied acceptorless dehydrogenation to the direct synthesis of
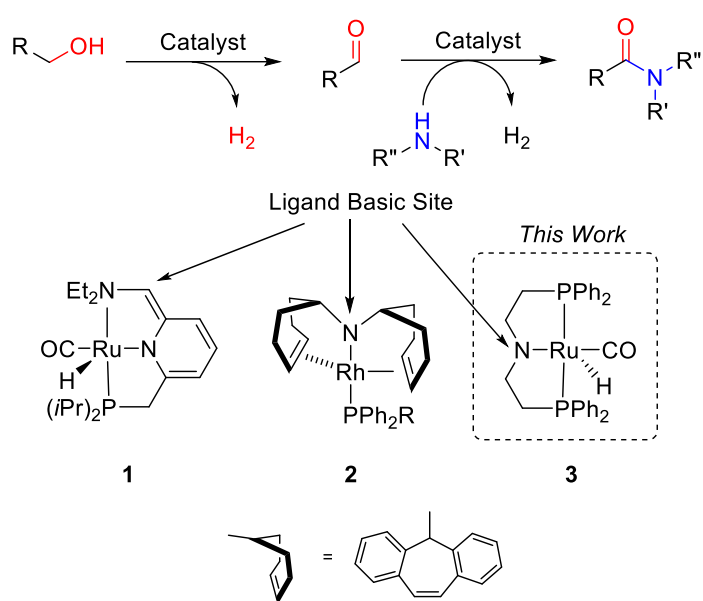
Figure 2.1 Acceptorless dehydrogenation of an amine and alcohol to form an amide. All catalysts shown contain a cooperative basic site on the ligand.

esters,[19-21] lactones,[6, 19] imines, [16, 22-26] and pyrroles[6, 27, 28]. While searching for improved polyamidation catalysts, we discovered in this work that a commercially available, relatively inexpensive catalyst (complex **3**, Scheme 2.1) catalyzed the synthesis of a variety of secondary and tertiary amides, as well as secondary ketimines from alcohols and amines.

Given the potential of acceptorless dehydrogenation for amide bond formation, [29] we sought to identify inexpensive and robust catalysts that could produce amide bonds. Previous studies demonstrated that the catalytic cycle did not rely on redox chemistry at the metal, but rather on metal/ligand cooperation.[14, 30] In both the Milstein catalyst (**1**) and the Grützmacher catalyst (2), the catalytic process was proposed to proceed through cooperative interactions of substrates with the basic site of the ligand and with the electrophilic metal centerutilizing catalysts based off the works of Shvo, Murahashi and others[17, 31-33] (Scheme 2.1). A hydrogen acceptor is not necessary because the ligands play an active role in the hydrogen abstraction and liberation process. The bulky ligands in these catalysts, however, may hinder the ability of the substrate to interact with both sites of the complex, which may explain why tertiary amides are difficult to synthesize via reported acceptorless dehydrogenation systems[5, 6, 8, 9, 15]. Of note, Ru-NHC complexes have also emerged as promising catalysts.[8-10]

The commercially available PNP type ruthenium (II) catalyst, (RuHCl(CO)(HN(CH$_2$CH$_2$PPh$_2$)$_2$)) pioneered by the Saito group (Ru-Macho, Scheme 2.1, complex **3**) has recently been reported to efficiently hydrogenate esters to form the corresponding alcohols.[34, 35] In this context, hydrogenation and dehydrogenation are reversible reactions, we hypothesized that this industrially relevant catalyst could be used for dehydrogenative amide formation. Complex **3** has a number of desirable attributes for our purpose. Firstly, similar to catalysts **1** and **2**, complex **3** contains a basic site on the ligand to provide the desired cooperative interactions between the substrate and the metal/ligand framework (Scheme 2.**1**, complex **3**). Secondly, the ligand in complex **3** is less bulky than those in **1** and **2**, which may broaden the substrate scope relative to pincer type ligands. Importantly, the precursor of complex **3** is commercially available and relatively inexpensive. Lastly, it has previously demonstrated robust catalytic activity in ethyl acetate formation from ethanol[20] as well as methanol water reformation,[36] and is used in large scale industrial applications.[34]

2.2: Results and Discussion

First, we investigated the feasibility of direct amidation by complex **3**, by using 2-methoxyethanol and benzyl amine as model substrates (see SI, Table 2.3). A number of experimental parameters, including the base, solvent, and H$_2$ removal were varied. To form the catalytically active complex **3**, the pre-catalyst **4** must be activated with a base (Scheme 2.2). Initial attempts using NaOEt or NaO^{t}Bu as the base resulted in no amide formation. Upon changing to sodium hydroxide as the base, however, amide bond formation was observed. Because the base appeared to have an effect on direct amidation, the base and counter-
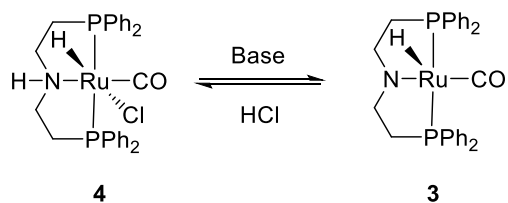
Table 2.1. Amide bond formation by acceptorless dehydrogenations of amines and alcohols with Ru-Macho catalyst

$$R\text{-}OH \ + \ R''\text{-}N(H)\text{-}R' \xrightarrow[\substack{15 \text{ mol\% KOH, 1.0 M} \\ \text{reflux, 12h, toluene} \\ \text{nitrogen flow}}]{1 \text{ mol\% } \mathbf{4}} R\text{-}C(O)\text{-}N(R')\text{-}R'' \ + \ 2H_2$$

Entry	Amine	Alcohol	Amide	Yield [%][a]
1	Ph-CH2-NH2	HO-(CH2)7-CH3	Ph-CH2-NH-C(O)-(CH2)6-CH3	91%
2	Ph-CH2-NH2	HO-(CH2)3-CH3	Ph-CH2-NH-C(O)-CH2-CH2-CH3	95%
3	Ph-CH2-NH2	HO-CH2-CH(CH3)-CH2-CH3	Ph-CH2-NH-C(O)-CH(CH3)-CH2-CH3	90%
4	Ph-CH2-NH2	HO-CH2-Ph	Ph-CH2-NH-C(O)-Ph	92%
5	Ph-CH2-NH2	HO-CH2-CH2-OMe	Ph-CH2-NH-C(O)-CH2-OMe	95%
6	MeO-C6H4-NH2	HO-CH2-CH2-OMe	MeO-C6H4-NH-C(O)-CH2-OMe	79%
7	Ph-CH2-NH2	HO-CH2-CH2-NEt2	Ph-CH2-NH-C(O)-CH2-NEt2	88%
8	Ph-CH(NH2)-CH3	HO-CH2-CH2-OMe	Ph-CH(CH3)-NH-C(O)-CH2-OMe	88%
9	H2N-CH2-C6H4-CH2-NH2	HO-CH2-CH2-OMe	MeO-CH2-C(O)-NH-CH2-C6H4-CH2-NH-C(O)-CH2-OMe	95%
10	Ph-CH2-NH2	HO-CH2CH2-(O-CH2CH2)3-OH	Ph-CH2-NH-C(O)-CH2-(O-CH2CH2)2-O-CH2-C(O)-NH-CH2-Ph	89%
11	piperidine (NH)	HO-CH2-CH2-OMe	piperidine-N-C(O)-CH2-OMe	89%
12	morpholine (NH)	HO-CH2-Ph	morpholine-N-C(O)-Ph	86%
13	Ph-CH2-N(H)-Me	HO-CH2-CH2-OMe	Ph-CH2-N(Me)-C(O)-CH2-OMe	85%
14	Ph-CH2-N(H)-Et	HO-CH2-CH2-OMe	Ph-CH2-N(Et)-C(O)-CH2-OMe	55%[b]
15	Ph-CH2-N(H)-CH2-Ph	HO-CH2-CH2-OMe	Ph-CH2-N(CH2Ph)-C(O)-CH2-OMe	35%[c]

Reaction Conditions: 1 mmol amine, 1 mmol alcohol, 0.01 mmol 3, 0.15 mmol KOH, 1.0 mL toluene, 110 °C, 12h. a Isolated yields b 24 h c 24 h in 1 mL Xylene

ion was further investigated. Among all bases evaluated (LiOH, NaOH, KOH, Na_2CO_3, K_2CO_3, NaOEt, and NaO^{t}Bu), potassium hydroxide promoted the highest yield of the desired amide (see 2.4, Table 2.3). Using KOH as the base, we investigated the solvent effect for this transformation. Among the list of both polar and nonpolar solvents examined, toluene and dioxane gave the highest yield (~66%). Because catalyst **3** can catalyze hydrogenolysis of esters and amides with the H_2 generated during dehydrogenation, removal of H_2 was necessary prevent the reverse transformation.[34]
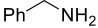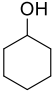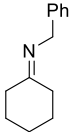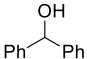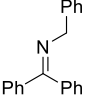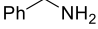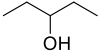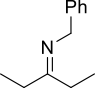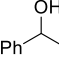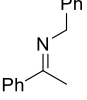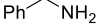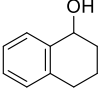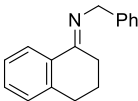
Indeed, introducing continuous nitrogen flow through the reaction flask afforded almost quantitative amide formation.

With this protocol in hand (1 mol% complex **4**, 15 mol% KOH, reflux, toluene, nitrogen flow), several amines and alcohols were examined as coupling partners for amide bond formation. A variety of amides (Table 2.1, entries 1–15) were obtained in good to excellent yields, demonstrating the efficiency and versatility of complex **3** in amide bond formation. Simple linear aliphatic alcohols coupled efficiently (entries 1–2). Similarly, aliphatic alcohols with α-branching also produced amides in high yields (entry 3). Ether and tertiary amine groups were well-tolerated in the amidation process (entries 5 & 7). An aniline substrate, which is less nucleophilic than aliphatic amines, afforded amide in 79% yield (entry 6). To test whether optically active amines were racemized or not during the amidation, an optically pure amine was subjected to the catalytic protocol. The optically pure amide was obtained in high yield (entry 8), suggesting no significant racemization occurs during the dehydrogenative coupling (see experimental). After successful amidation with a variety of mono-amines and mono-alcohols, diamines (entry 9) and diols (entry 10) were coupled to form diamides in high yields, suggesting the applicability of making polyamides using complex **3**.[18]

The ability of the secondary amines to undergo coupling stands out (Table 2.1, entries 11–15) because previously reported acceptorless dehydrogenation catalysts have limited conversion for forming tertiary amides directly from secondary amines and alcohols[5, 6, 8, 15] or require high catalyst loadings[9]. Morpholine and piperidine were both coupled in 89% and 86% yield, respectively (entries 11, 12). A linear secondary amine with moderate steric bulk was coupled in very good yield (entry 13). Systematically increasing steric bulk of the secondary amine resulted in decreasing yield (entries 13–15). Nevertheless, a more sterically encumbered secondary amine,

Table 2.2 Imine bond formation via acceptorless dehydrogenations of amines and alcohols by Ru-Macho catalyst

Entry	Amine	Alcohol	Imine	Yield [%][a]
1	Ph–NH₂	cyclohexanol (OH)	(Ph imine, cyclohexylidene)	85%
2	Ph–NH₂	Ph₂CH–OH	(Ph imine, diphenyl)	51%
3	Ph–NH₂	pentan-3-ol (OH)	(Ph imine, pentyl)	40%
4	Ph–NH₂	Ph–CH(OH)–CH₃	(Ph imine)	80%
5	Ph–NH₂	1-tetralol (OH)	(N–Ph tetralinylidene)	40%

Reaction Conditions: 1 mmol amine, 1 mmol alcohol, 0.01 mmol 3, 0.15 mmol KOH, 1.0 mL toluene, 110 °C, 8 – 12h. a) Isolated yields of reduced amines obtained by reduction of imine to amine with sodium borohydride.

dibenzylamine, underwent coupling with moderate yield (entry 15). This result suggests that further ligand tuning may open the door to the direct synthesis of more sterically hindered tertiary amides, which are very difficult to access.[3]

Acceptorless dehydrogenative catalysts have also been shown to afford secondary aldimines from primary alcohols and amines.[16, 22-26] However, synthesis of secondary ketimines via the acceptorless hydrogenation pathway remains problematic.[22, 24] Considering that complex **3** could couple secondary amines efficiently, we reasoned that ketimine formation would be feasible. Using complex **3**, cyclohexanol and benzylamine were shown to undergo coupling to generate secondary ketimines (Table 2.2, entry 1) in nearly quantitative yields on the basis of GC-MS and ¹HNMR analysis.[37] Borohydride reduction of the resulting imines leads to isolated yields for the reduced products between 40-91%. Our results represent the highest yielding examples of
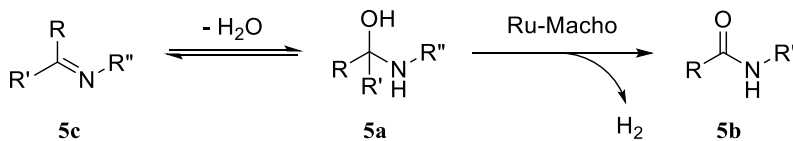
Figure 2.3 Hemiaminal 5a can either form an amide (5b) or imine (5c) depending on the identity of R'.

secondary alcohols and amines undergoing dehydrogenative coupling to generate secondary ketimines. More sterically hindered and acyclic alcohols transformed to the corresponding ketimines in moderate yields (entries 2–5).

The ability of complex **3** to form both amides and imines results from the common hemiaminal intermediate generated after the dehydrogenative coupling of the alcohol and the amine (Scheme 2.3). Typically, the hemiaminal (**5a**) undergoes another dehydrogenation via complex 3 to create the amide product (**5b**). However, if the R' substituent on the hemiaminal is a moiety other than a hydrogen atom, complex **3** is unable to undergo elimination of an equivalence of dihydrogen. Thus, imine formation is favored through dehydration in the case of secondary alcohols due to no other competing pathway.

2.3: Conclusions

The catalyst **3** (Ru-Macho) investigated here has shown utility for both amide and imine bond formation through the acceptorless dehydrogenation pathway. As an advance, we demonstrate good reactivity with secondary amines for the synthesis of tertiary amides and an improved synthesis of ketimines from secondary alcohols. The combination of commercial availability, relatively low cost, and general substrate scope makes Ru-Macho an attractive catalyst for amide and imine bond formation. Future studies will focus on stereoselective variants and using these insights towards the construction of polyamides.

2.4: Supporting Information

General Reagent Information: All reactions were set up under a nitrogen atmosphere in a Vacuum Atmospheres Company Glove box. Reactions that were carried out outside of the glove box were performed under a nitrogen atmosphere using standard Schlenk techniques. Toluene was purchased from Fischer Chemical and purged with argon for 2 hours, then dried by passing it

through two columns of neutral alumina under argon pressure. Dioxane, DMF, DMSO, chlorobenzene, xylene, and DMF were purchased from Aldrich Chemical Co or Fischer Chemical, and purged with nitrogen for 30 mins before use. Amines and alcohols were purchased at reagent grade or higher purity from Aldrich Chemical Co, or Fischer Chemical and purged with nitrogen for 30 minutes before use. [RuHCl(CO)(HN(CH$_2$CH$_2$PPh$_2$)$_2$)] (**4**) was purchased from Strem Chemicals Inc. and used as received. KOH was purchased from Fisher Chemical, ground with a mortar and pestle in the glovebox to a fine powder, and stored in the glove box. Column chromatography was performed using silica gel (Dynamic Adsorbents Inc. Silica, C-18 32-63μ, 60A) and eluted using applied air pressure with the indicated solvent system.

    General Analytical Information: All compounds were characterized by ^{1}HNMR, ^{13}CNMR, ESI-MS, and IR. NMR spectra were obtained using Bruker 500 MHz instruments. All 1HNMR and ^{13}CNMR are reported in ppm relative to TMS (0.00 ppm) unless otherwise noted. IR spectra were obtained using a Thermo Scientific Nicolet iS5 iD5 ATR IR spectrometer. GC-MS (CI) was performed using a GCT Premier Micromass MS Technologies mass spectrometer, coupled with a Waters 7890A gas chromatograph. ESI MS was performed using a LCT Premier Micromass MS Technologies mass spectrometer.

Table 2.3 Reaction Optimization
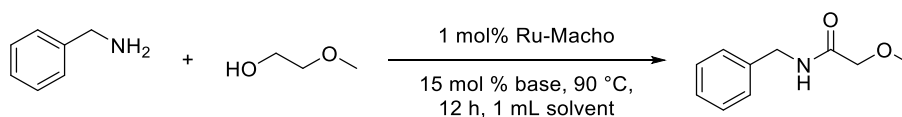
Entry	Solvent	Base	GC Yield (%)
1	Toluene	LiOH	2
2	Toluene	NaOH	32
3	Toluene	KOH	44

4	Toluene	Na_2CO_3	0
5	Toluene	K_2CO_3	5
6	Toluene	KO^{t}Bu	21
7	Toluene	NaOEt	0
8	Toluene	N/A	0
9	Diglyme	KOH	4
10	Anisole	KOH	6
11	Toluene	KOH	**66**
12	Xylene	KOH	**59**
13	DMSO	KOH	3
14	DMF	KOH	2
15	Dioxane	KOH	**66**
16	Chlorobenzene	KOH	11
17	NMP	KOH	9
18	Neat	KOH	24
19	Toluene	KOH	**98**

General Procedure for Examples in Table 2.3: A 1 dram vial was equipped with a stir bar and brought into the glove box through the antechamber, after evacuating and backfilling the antechamber with nitrogen 3 times. Once inside the glove box, the vial was charged with [RuHCl(CO)(HN(CH$_2$CH$_2$PPh$_2$)$_2$)] (**4**) (6.0 mg, 0.01 mmol, 1 mol %), a base (0.15 mmol, 15 mol %), a solvent (1 M), benzylamine (107 mg, 1 mmol, 1.0 equiv.) and 1-octanol (130 mg, 1 mmol, 1.0 equiv.) in that order. The vessel was then fitted with an air-tight septum, removed from the glove box, and heated to 90 °C in an aluminum heating block under N$_2$ pressure via a needle through the septum. During this time, nitrogen is passed through the Schlenk line allowing the hydrogen evolved from the reaction to escape the vessel. After 12 h, the vial was removed from the aluminum block and the yield of the reaction was determined by GC analysis, using a known amount of dodecane as an internal standard. In entry 19, nitrogen was flowed through the reaction.

General Procedure for Examples in Table 2.1 in Main Text: An oven dried 10 mL round bottom flask equipped with a stir bar was brought into the glove box with a reflux condenser. The

flask was charged with [RuHCl(CO)(HN(CH$_2$CH$_2$PPh$_2$)$_2$)] (4) (6.0 mg, 0.01 mmol, 1 mol %), KOH (8.2 mg, 0.15 mmol, 15 mol %), and toluene (1.0 mL), an amine (1 mmol, 1.0 equiv.) and an alcohol (1 mmol, 1.0 equiv.) in that order. After all reagents have been added to the flask, the reflux condenser was attached and secured with a keck clamp. The top of the condenser was sealed with a septum and the whole apparatus was then removed from the glove box. Once outside the glove box, the apparatus was equipped to nitrogen flow by inserting an inlet needle supplying a positive pressure of nitrogen into the septum, and an outlet needle connected to an oil bubbler. The reaction mixture was heated at reflux in a silicone oil bath overnight (12 h), then allowed to cool to RT, and the conversion determined by GC-MS (CI). The resulting residue was subjected to flash chromatography with the indicated solvent system to obtain the purified amide in the reported isolated yield.

General Procedure for Examples in Table 2.2 in Main Text: An oven dried 10 mL round bottom flask equipped with a stir bar was brought into the glove box with a reflux condenser. The flask was charged with [RuHCl(CO)(HN(CH$_2$CH$_2$PPh$_2$)$_2$)] (4) (6.0 mg, 0.01 mmol, 1 mol %), KOH (8.2 mg, 0.15 mmol, 15 mol %), and toluene (1.0 mL), an amine (1 mmol, 1.0 equiv.) and an alcohol (1 mmol, 1.0 equiv.) in that order. After all reagents had been added to the flask, the reflux condenser was attached and secured with a keck clamp. The top of the condenser was sealed with a septum and the whole apparatus was removed from the glove box. Once outside the glove box, the apparatus was equipped to nitrogen flow by inserting an inlet needle supplying a positive pressure of nitrogen into the septum, and an outlet needle connected to an oil bubbler. When the transformation was deemed complete on the basis of analysis by GC-MS (CI), the reaction mixture was allowed to cool to rt. 5 mL MeOH was added, and the resulting mixture was stirred until the solution was homogeneous. NaBH$_4$ (95 mg, 2.5 mmol, 2.5 equiv.) was added through the top of

the flask, exposing the reaction to the atmosphere. The solution was stirred for 1 h at room temperature. After 1 h, 3.5 mL 1M HCl was added drop-wise. The solution was then diluted with 50 mL of EtOAc, washed with 1M KOH (3 x 50 mL), and finally brine (3 x 50 mL). The organic layer was then dried with $MgSO_4$ and the excess solvent was removed *in vacuo*. The resulting residue was subjected to flash chromatography.

Preparation and Analysis of Compounds:

N-benzyloctanamide. (Table 2.1, Entry 1) The general procedure for Table 2.1 was followed using [RuHCl(CO)(HN($CH_2CH_2PPh_2$)$_2$)] (**4**) (5.5 mg, 0.0915 mmol, 0.01 eq.), KOH (7.7 mg, 0.137 mmol, 15 mol %), benzylamine (100 μL, 0.915 mmol, 1.0 eq.), 1-octanol (144 μL, 0.915 mmol, 1.0 eq.) and toluene (1.5 mL). The product was purified via flash chromatography with EtOAc in Hexanes (1:4) to give a clear oil (194 mg, 91% isolated yield). ^{1}HNMR (500 MHz, CDCl$_3$) δ 7.40 (m, 2H) 7.34 (m, 3H) 5.72 (br, s, 1H) 4.51 (d, *J* = 5.5 Hz, 2H) 2.27 (t, *J* = 7.5 Hz, 2H) 1.72 (m, 2H) 1.36 (m, 8H) 0.94 (t, *J* = 7.5 hz, 3H) ppm. ^{13}CNMR (125 MHz, CDCl$_3$) δ 173.0, 138.5, 128.7, 127.8, 127.5, 43.55, 36.8, 31.7, 29.3, 29.1, 25.8, 22.6, 14.1 ppm. The physical data were identical in all respects to those previously reported. [38]

***N*-benzylbutyramide. (Table 2.1, Entry 2)** The general procedure for Table 2.1 was followed using [RuHCl(CO)(HN($CH_2CH_2PPh_2$)$_2$)] (**4**) (6.0 mg, 0.01 mmol, 1 mol %), KOH (8.2 mg, 0.15 mmol, 15 mol %), benzylamine (107 mg, 1.0 mmol, 2.0 eq.), 1-butanol (74 mg, 1.0 mmol, 1.0 eq.), and toluene (1 mL). The product was purified via flash chromatography with EtOAc and hexanes (1:4) to give a white solid (168 mg, 95% isolated yield). ^{1}HNMR (500 MHz, CDCl$_3$) δ 7.35 – 7.26 (m, 5H), 6.60 (br, s, 1H), 4.45 (d, *J* = 7.5 Hz, 2H), 2.19 (t, *J* = 7 Hz, 2H), 1.69 (m, 2H), 0.96 (t, *J* = 7 Hz, 3H) ppm. ^{13}CNMR (125 MHz, CDCl$_3$) δ 173.1, 138.6, 128.7, 127.8, 127.4, 43.5, 38.6, 19.3, 13.9 ppm. The physical data were identical in all respects to those previously reported. [39]

N-benzyl-2-methylbutanamide. (Table 2.1, Entry 3) The general procedure for Table 2.1 was followed using [RuHCl(CO)(HN(CH$_2$CH$_2$PPh$_2$)$_2$)] (**4**) (6.0 mg, 0.01 mmol, 1 mol %), KOH (8.2 mg, 0.15 mmol, 15 mol %), benzylamine (107 mg, 1.0 mmol, 1.0 equiv.), 2-methyl-1-butanol (87 mg, 1.0 mmol, 1.0 equiv.), and toluene (1 mL). The product was purified via flash chromatography with EtOAc and hexanes (1:4) to give a white solid (171 mg, 90%). ^{1}HNMR (500 MHz, CDCl$_3$) δ 7.34 - 7.26 (m, 5H), 5.83 (br, s, 1H), 4.44 (m, 2H), 2.14 (m, 1H), 1.70 (m, 1H), 1.43 (m, 1H), 1.16 (d, J = 5 Hz, 3H), 0.91 (t, J = 5 Hz 3H) ppm. ^{13}CNMR (125 MHz, CDCl$_3$) δ 176.4, 138.6, 128.7, 127.8, 127.4, 43.5, 43.3, 27.4, 17.6, 12.0 ppm. The physical data were identical in all respects to those previously reported. [4]

N-benzylbenzamide. (Table 2.1, Entry 4) The general procedure for Table 2.1 was followed using [RuHCl(CO)(HN(CH$_2$CH$_2$PPh$_2$)$_2$)] (**4**) (6.0 mg, 0.01 mmol, 1 mol %), KOH (8.2 mg, 0.15 mmol, 15 mol %), benzylalcohol (108 mg, 1.0 mmol, 1.0 equiv.), benzylamine (107 mg, 1.0 mmol, 1.0 equiv.), and toluene (1 mL). The product was purified via flash chromatography with EtOAc and hexanes to give a white solid (194 mg, 92% isolated yield). (500 MHz, CDCl$_3$) δ 7.80 (d, J = 7, 2H), 7.48 (m, 1H) 7.42 (t, J = 7 Hz, 2H), 7.36–7.28 (m, 5H), 6.48 (br, s, 1H), 4.65 (d, J = 5.5 Hz, 2H) ppm. ^{13}CNMR (125 MHz, CDCl$_3$) δ 167.4, 138.2, 134.4, 131.6, 128.9, 128.7, 128.0, 127.7, 127.0, 44.2 ppm. The physical data were identical in all respects to those previously reported.[40]

N-benzyl-2-methoxyacetamide. **(Table 2.1, Entry 5)** The general procedure for Table 2.1 was followed using [RuHCl(CO)(HN(CH$_2$CH$_2$PPh$_2$)$_2$)] (**4**) (6.2 mg, 0.01 mmol, 1 mol %), KOH (8.3 mg, 0.15 mmol, 15 mol %), benzylamine (107 mg, 1.0 mmol, 1.0 equiv.), 2-methoxyethanol (76 mg, 1.0 mmol, 1.0 equiv.), and toluene (1.0 mL). The product was purified via flash chromatography with EtOAc and Hexanes (1:4) to give a clear oil (170 mg, 95% isolated yield).

^{1}HNMR (500 MHz, CDCl$_3$) δ 7.36–7.26 (m, 5H), 6.82 (br, s, 1H), 4.49 (d, J = 10 Hz, 2H), 3.95 (s, 2H), 3.40 (s, 3H) ppm. ^{13}CNMR (125 MHz, CDCl$_3$) δ 169.5, 138.1, 128.8, 127.9, 127.6, 72.0, 59.2, 42.9 ppm. The physical data were identical in all respects to those previously reported. [43]

2-methoxy-*N*-(4-methoxyphenyl)acetamide. (Table 2.1, Entry 6) The general procedure for Table 2.1 was followed using [RuHCl(CO)(HN(CH$_2$CH$_2$PPh$_2$)$_2$)] (**4**) (6.0 mg, 0.01 mmol, 1 mol %), KOH (8.2 mg, 0.15 mmol, 15 mol %), *p*-anisidine (107 mg, 1.0 mmol, 2.0 equiv.), 2-methoxyethanol (76 mg, 1.0 mmol, 1.0 equiv.), and toluene (1 mL). The product was purified via flash chromatography with EtOAc and hexanes (1:3) to give a clear oil (154 mg, 79%). HRMS (ESI/CH$_2$Cl$_2$) *m/z* calcd for C$_{10}$H$_{13}$NO$_3$Na (M + Na)$^+$: 218.0793, Found: 218.0797. ^{1}HNMR (500 MHz, CDCl$_3$) δ 8.14 (br, s, 1H), 7.47 (d, J = 9.0 Hz, 2H) 6.87 (d, J = 9.0 Hz, 2H) 4.01 (s, 2H) 3.80 (s, 3H), 3.50 (s, 3H) ppm. ^{13}CNMR (125 MHz, CDCl$_3$) δ 167.3, 156.6, 130.3, 121.6, 114.2, 72.2, 59.3, 55.5 ppm. IR (film) 3003.1, 2917.6, 2849.0, 1679.8, 1511.8, 1246.1, 1110.9, 1033.5 cm^{-1}.

***N*-benzyl-2-(diethylamino)acetamide. (Table 2.1, Entry 7)** The general procedure for Table 2.1 was followed using [RuHCl(CO)(HN(CH$_2$CH$_2$PPh$_2$)$_2$)] (**4**) (6.0 mg, 0.01 mmol, 1 mol %), KOH (8.2 mg, 0.15 mmol, 15 mol %), benzylamine (107 mg, 1.0 mmol, 1.0 equiv.), *N,N'*-diethylethanolamine (117 mg, 1.0 mmol, 1.0 equiv.), and toluene (1 mL). The product was purified via flash chromatography with EtOAc and hexanes (1:1) to give a clear oil (193 mg, 88% isolated yield). ^{1}HNMR (500 MHz, CDCl$_3$) δ 7.71 (br, s, 1H), 7.35-7.62 (m, 5H) 4.75 (d, J = 6 Hz, 2H) 3.08 (s, 2H) 2.54 (q, J = 7.0 Hz, 4H) 0.99 (t, 6H, 7.0 Hz) ppm. ^{13}CNMR (125 MHz, CDCl$_3$) δ 172.1, 138.6, 128.7, 127.6, 127.4, 57.5, 48.8, 43.0, 12.4 ppm. The physical data were identical in all respects to those previously reported. [41]

(*R*)-2-methoxy-*N*-(1-phenylethyl)acetamide. (Table 2.1, Entry 8) The general procedure for Table 2.1 was followed using [RuHCl(CO)(HN(CH$_2$CH$_2$PPh$_2$)$_2$)] (**4**) (6.0 mg, 0.01 mmol, 1 mol

%), KOH (8.2 mg, 0.15 mmol, 15 mol %), (*R*)-(+)-methylbenzylamine (121 mg, 1.0 mmol, 1.0 equiv.), 2-methoxyethanol (76 mg, 1.0 mmol, 1.0 equiv.), and toluene (1 mL). The product was purified via flash chromatography with EtOAc and hexanes (1:4) to give a colorless solid (169 mg, 88%). $[a]_D^{25}$ +109.9 (c = 2.0, MeOH) ^{1}HNMR (500 MHz, CDCl$_3$) δ 7.52-7.24 (m, 5H), 6.85 (br, s, 1H), 5.18 (m, 1H), 3.91-3.83 (m, 2H), 3.41 (s, 3H), 1.52 (d, *J* = 7.5, 3H) ppm. ^{13}CNMR (125 MHz, CDCl$_3$) δ 168.4, 143.0, 128.8, 127.4, 126.1, 72.1, 59.1, 48.0, 21.9 ppm. The physical data were identical in all respects to those previously reported. [42]

N,N'-(1,4-phenylenebis(methylene))bis(2-methoxyacetamide). (Table 2.1, Entry 9) The general procedure for Table 2.1 was followed using [RuHCl(CO)(HN(CH$_2$CH$_2$PPh$_2$)$_2$)] (**4**) (6.0 mg, 0.01 mmol, 1 mol %), KOH (8.2 mg, 0.15 mmol, 15 mol %), *p*-xylenediamine (136 mg, 1.0 mmol, 1.0 equiv.), *2*-methoxyethanol (155 mg, 2.0 mmol, 2.0 equiv.), and toluene (1 mL). The product was purified via flash chromatography with EtOAc and hexanes (9:1) to give a white solid (265 mg, 95% isolated yield). HRMS (ESI/CH$_2$Cl$_2$) *m / z* calcd for C$_{14}$H$_{20}$N$_2$O$_4$Na (M + Na)$^+$: 303.1321, Found: 303.1331. ^{1}HNMR (500 MHz, DMSO-d$_6$) δ 8.32 (t, *J* = 6.0 Hz, 1H) 7.19 (s, 4H) 4.25 (d, *J* = 6.0 Hz, 4H) 3.84 (s, 4H) 3.31 (s, *J* = 7.0 Hz, 6H) ppm. ^{13}CNMR (125 MHz, DMSO-d$_6$) δ 169.4, 138.5, 127.7, 72.0, 59.1, 41.9. IR (solid) 3029.1, 2939.7, 2831.2, 1650.8, 1532.0, 1197.4, 1109.3, 733.1 cm^{-1}

2,2'-((oxybis(ethane-2,1-diyl))bis(oxy))bis(*N*-benzylacetamide). (Table 2.1, Entry 10) The general procedure for Table 2.1 was followed using [RuHCl(CO)(HN(CH$_2$CH$_2$PPh$_2$)$_2$)] (**4**) (12.0 mg, 0.02 mmol, 1 mol %), KOH (16.4 mg, 0.3 mmol, 15 mol %), benzylamine (219 mg, 2.05 mmol, 2.05 equiv.), tetraethylene glycol (194 mg, 1.0 mmol, 1.0 equiv.), and toluene (1 mL). The product was purified via flash chromatography with EtOAc and hexanes (1:4) to give a clear oil (360 mg, 90% isolated yield). HRMS (ESI/CH$_2$Cl$_2$) *m / z* calcd for C$_{22}$H$_{28}$N$_2$O$_5$Na (M + Na)$^+$:

423.1896, found 423.1888. ^{1}HNMR (500 MHz, CDCl$_3$) δ 7.31–7.23 (m, 10H), 7.26 (br, s, 2H) 4.43 (d, J = 5.0 Hz, 4H) 3.92 (s, 4H) 3.50 (s, 8H). ^{13}CNMR (125 MHz, CDCl$_3$) δ 169.8, 138.2, 128.7, 127.8, 127.5, 70.8, 70.4, 70.0, 42.8. IR (film) 3030.1, 2913.0, 1656.8, 1529.8, 1496.6, 1454.0, 1102.6, 1028.5 cm^{-1}.

2-methoxy-1-(piperidin-1-yl)ethan-1-one. (Table 2.1, Entry 11) The general procedure for Table 2.1 was followed using . [RuHCl(CO)(HN(CH$_2$CH$_2$PPh$_2$)$_2$)] (**4**) (6.0 mg, 0.01 mmol, 1 mol %), KOH (8.2 mg, 0.15 mmol, 15 mol %), 2-methoxyethanol (76 mg, 1.0 mmol, 1.0 equiv.), piperidine (85 mg, 1.0 mmol, 1.0 equiv.) toluene (1 mL). The product was purified via flash chromatography with EtOAc and hexanes (1:4) to give clear oil (135 mg, 86% isolated yield). HRMS (ESI/CH$_2$Cl$_2$) m / z calcd for C$_8$H$_{15}$NO$_2$Na (M + Na)$^+$:180.1001, Found: 180.0997. HNMR (500 MHz, CDCl$_3$) δ 4.10 (m, 2H), 3.55 (m, 2H) 3.42 (s, 3H), 3.39 (m, 2H), 1.65 (m, 2H), 1.57 (m, 4H). ^{13}CNMR (125 MHz, CDCl$_3$) δ 167.3, 59.0, 46.00, 42.9, 26.5, 25.6, 24.5. IR (film) 2926.3, 2854.6, 1644.6, 1466.0, 1117.7 cm^{-1}.

Morpholino(phenyl)methanone. (Table 2.1, Entry 12) The general procedure for Table 2.1 was followed using [RuHCl(CO)(HN(CH$_2$CH$_2$PPh$_2$)$_2$)] (**4**) (6.0 mg, 0.01 mmol, 1 mol %), KOH (8.2 mg, 0.15 mmol, 15 mol %), morpholine (87 mg, 1.0 mmol, 1.0 equiv.), benzylalcohol (108 mg, 1.0 mmol, 1.0 equiv.), and toluene (1 mL). The product was purified via flash chromatography with EtOAc and hexanes (1:4) to give a clear oil (164 mg, 86% isolated yield). ^{1}HNMR (500 MHz, CDCl$_3$) δ 7.42 - 7.39 (m, 5H), 3.75–3.45 (m, 8H) ppm. ^{13}CNMR (125 MHz, CDCl$_3$) δ 170.5, 135.3, 129.9, 128.6, 127.1, 66.9 (2 carbons) ppm. The physical data were identical in all respects to those previously reported. [43]

***N*-benzyl-2-methoxy-*N*-methylacetamide. (Table 2.1, Entry 13)** The general procedure for Table 2.1 was followed using [RuHCl(CO)(HN(CH$_2$CH$_2$PPh$_2$)$_2$)] (**4**) (6.0 mg, 0.01 mmol, 1 mol

%), KOH (8.2 mg, 0.15 mmol, 15 mol %), *N*-methylbenzylamine (121 mg, 1.0 mmol, 1.0 equiv.), 2-methoxyethanol (76 mg, 1.0 mmol, 1.0 equiv.), and toluene (1 mL). The product was purified via flash chromatography with EtOAc and hexanes (1:4) to give a clear oil (164 mg, 88% isolated yield). Due to constrained rotational nature of the tertiary amide, product is a mixture of two rotamers (A: major, B: minor) in a 60:40 A:B ratio. NMR experiments at 350K showed coalescence of the two rotamer peaks. ^{1}HNMR (500 MHz, CDCl$_3$) δ 7.42-7.24 (m, 5H)[A][B], 4.65 (s, 2H)[A], 4.58 (s, 2H)[B], 4.21 (s, 2H)[A], 4.20 (s, 2H)[B], 3.52 (s, 3H)[A], 3.48 (s, 3H)[B], 2.99 (s, 3H)[B], 2.94 (s, 3H)[A] ppm. ^{13}CNMR (125 MHz, CDCl$_3$) δ 169.4 [B], 169.1 [A], 137.0 [A], 136.3 [B], 129.0 [A], 128.7 [A], 128.2 [A], 127.8 [B], 127.5 [B], 126.6 [B], 71.6 [B], 71.5 [A], 59.3 [B], 59.2 [A], 52.5 [B], 51.0 [A], 33.7 [B], 33.6 [A] ppm. The physical data were identical in all respects to those previously reported. [44]

***N*-benzyl-*N*-ethyl-2-methoxyacetamide. (Table 2.1, Entry 14)** The general procedure for Table 2.1 was followed using [RuHCl(CO)(HN(CH$_2$CH$_2$PPh$_2$)$_2$)] (**4**) (6.0 mg, 0.01 mmol, 1 mol %), KOH (8.2 mg, 0.15 mmol, 15 mol %), *N*-ethylbenzylamine (136 mg, 1.0 mmol, 1.0 equiv.), *2*-methoxyethanol (76 mg, 1.0 mmol, 1.0 equiv.), and toluene (1 mL). The product was purified via flash chromatography with EtOAc and hexanes (1:4) to give a white solid (113 mg, 55% isolated yield). Due to constrained rotational nature of the tertiary amide, product is a mixture of two rotamers (A: major, B: minor) in a 60:40 A:B ratio. NMR experiments at 350K in DMSO-d$_6$ showed coalescence of the two rotamer peaks. HRMS (ESI/CH$_2$Cl$_2$) *m/z* calcd for C$_{12}$H$_{17}$NO$_2$Na (M + Na)$^+$:230.1157. Found [M + Na]$^+$: 230.1148. ^{1}HNMR (500 MHz, CDCl$_3$) δ 7.36-7.22 (m, 5H)[A][B], 4.61 (s, 2H)[A], 4.52 (s, 2H)[B], 4.18 (s, 2H)[A], 4.11 (s, 2H)[B], 3.48 (s, 3H)[A], 3.42 (s, 2H)[B], 3.41 (q, *J* = 6.5 Hz, 2H)[B], 3.25 (q, *J* = 6.5 Hz, 2H)[A], 1.14 (t, *J* = 6.5 Hz, 2H)[A], 1.11 (t, *J* = 6.5 Hz, 2H)[B]. ^{13}CNMR (125 MHz, CDCl$_3$) δ 169.0 [B], 169.0 [A], 137.5

[A], 136.8 [B], 129.0 [A], 128.6 [A], 128.2 [A], 127.7 [B], 127.4 [B], 126.6 [B], 71.7 [B], 71.4 [A], 59.3 [A], 59.3 [B], 49.7 [B], 47.7 [A], 40.9 [B], 40.6 [A], 13.7 [A], 12.6 [B] ppm. IR (film) 3033.1, 2924.2, 1644.0, 1452.0, 1431.9, 1134.8, 1109.4, 1080.5 cm^{-1}.

N,N-dibenzyl-2-methoxyacetamide. (Table 2.1, Entry 15) The general procedure for Table 2.1 was followed using [RuHCl(CO)(HN(CH$_2$CH$_2$PPh$_2$)$_2$)] (**4**) (6.0 mg, 0.01 mmol, 1 mol %), KOH (8.2 mg, 0.15 mmol, 15 mol %), dibenzylamine (294 mg, 1.5 mmol, 1.5 equiv.), 2-methoxyethanol (76 mg, 1.0 mmol, 1.0 equiv.), xylene (1 mL). Reaction was heated at reflux for 24 h. Excess amine extracted by dissolving compound in EtOAc and washing with 3 x 50 mL 1 M HCl. The product was purified via flash chromatography with EtOAc and hexanes (1:4) to give a clear oil (94 mg, 35% isolated yield). HRMS (ESI/CH$_2$Cl$_2$) m / z calcd for C$_{17}$H$_{19}$NO$_2$Na (M + Na)$^+$: 292.1313, Found: 292.1323. ^{1}HNMR (500 MHz, CDCl$_3$) δ 7.37–7.15 (m, 10H), 4.59 (s, 2H) 4.43 (s, 2H) 4.20 (s, 2H) 3.46 (s, 3H) ppm. ^{13}CNMR (125 MHz, CDCl$_3$) δ 169.5, 136.9, 136.1, 129.0, 128.6, 128.4, 127.7, 127.5, 126.6, 71.5, 59.3, 48.9, 47.9. IR (film) 3028.8, 2919.4, 1649.9, 1450.9, 1429.3, 1195.8, 1128.3, 1106.4, 1080.2 cm^{-1}.

N-benzylcyclohexanamine. (Table 2, Entry 1) The general procedure for Table 2.2 was followed using [RuHCl(CO)(HN(CH$_2$CH$_2$PPh$_2$)$_2$)] (**4**) (6.0 mg, 0.01 mmol, 1 mol %), KOH (8.2 mg, 0.15 mmol, 15 mol %), cyclohexanol (100 mg, 1.0 mmol, 1.0 equiv.), benzylamine (107 mg, 1.0 mmol, 1.0 equiv.), and toluene (1 mL). The remaining mixture is purified via flash chromatography using EtOAc and hexanes (1:1) to give a tan oil (158 mg, 85% isolated yield). ^{1}HNMR (500 MHz, CDCl$_3$) δ 7.32-7.19 (m, 5H) 3.81 (s, 2H), 1.93-1.89 (m, 2H), 1.75-1.70 (m, 2H), 1.65-1.59 (m, 1H), 1.44 (s, 1H), 1.33-1.00 (m, 6H) ppm. ^{13}CNMR (125 MHz, CDCl$_3$) δ 140.9, 128.3, 127.9, 126.7, 56.1, 51.0, 33.5, 26.1, 24.9. The physical data were identical in all respects to those previously reported. [45]

***N*-benzyl-1,1-diphenylmethanamine. (Table 2, Entry 2)** The general procedure for Table 2.1 was followed using . [RuHCl(CO)(HN(CH$_2$CH$_2$PPh$_2$)$_2$)] (**4**) (6.0 mg, 0.01 mmol, 1 mol %), KOH (8.2 mg, 0.15 mmol, 15 mol %), diphenylmethanol (184 mg, 1.0 mmol, 1.0 equiv.), benzylamine (107 mg, 1.0 mmol, 1.0 equiv.), and toluene (1 mL). The remaining mixture is purified via flash chromatography using EtOAc and hexanes (1:1) to give white solid (139 mg, 85% isolated yield). ^{1}HNMR (500 MHz, CDCl$_3$) δ 7.49-7.22 (m, 15H) 4.88 (s, 1H), 3.78 (s, 2H), 1.89 (s, 1H) ppm. ^{13}CNMR (125 MHz, CDCl$_3$) δ 144.0, 140.5, 128.5, 128.5, 128.2, 127.4, 127.1, 127.0, 66.5, 51.9 ppm. The physical data were identical in all respects to those previously reported. [45]

***N*-benzylpentan-3-amine. (Table 2, Entry 3)** The general procedure for Table 2.2 was followed using [RuHCl(CO)(HN(CH$_2$CH$_2$PPh$_2$)$_2$)] (**4**) (6.0 mg, 0.01 mmol, 1 mol %), KOH (8.2 mg, 0.15 mmol, 15 mol %), 3-pentanol (87 mg, 1.0 mmol, 1.0 equiv.), benzylamine (107 mg, 1.0 mmol, 1.0 equiv.), and toluene (1 mL). The remaining mixture is purified via flash chromatography using EtOAc and hexanes (1:1) to give a tan oil (71 mg, 40% isolated yield). ^{1}HNMR (500 MHz, CDCl$_3$) δ 7.37− 7.20 (m, 5H), 3.74 (s, 2H), 2.41 (q, *J* = 6.0 Hz, 1H) 1.59 (s, 1H), 1.52−1.40 (m, 4H), 0.87 (t, *J* = 6.0 Hz, 6H) ppm. ^{13}CNMR (125 MHz, CDCl$_3$) δ 141.3, 128.7, 128.5, 127.1, 59.7, 51.5, 26.0, 10.2 ppm. The physical data were identical in all respects to those previously reported. [46]

N-benzyl-1-phenylethan-1-amine. (Table 2, entry 4) The general procedure for Table 2.2 was followed using [RuHCl(CO)(HN(CH$_2$CH$_2$PPh$_2$)$_2$)] (**4**) (6.0 mg, 0.01 mmol, 1 mol %), KOH (8.2 mg, 0.15 mmol, 15 mol %), 1-phenylethan-1-ol (122 mg, 1.0 mmol, 1.0 equiv.), benzylamine (107 mg, 1.0 mmol, 1.0 equiv.), and toluene (1 mL). The remaining mixture is purified via flash chromatography using EtOAc and hexanes (1:1) to give a tan oil (168 mg, 80% isolated yield). ^{1}HNMR (500 MHz, CDCl$_3$) δ 7.48 – 7.22 (m, 10H), 3.85 (q, *J* = 6.5 Hz, 1H), 3.70 (d, *J* = 13.0 Hz, 1H) 3.61 (d, *J* = 13.0 Hz, 1H), 1.70 (s, 1H), 1.39 (d, *J* = 6.5 Hz, 3H) ppm. (125 MHz, CDCl$_3$) δ

145.6, 140.7, 128.6, 128.4, 128.2, 127.0, 126.9, 126.7, 57.5, 51.7, 24.5 ppm. The physical data were identical in all respects to those previously reported.[45]

_N_-benzyl-1,2,3,4-tetrahydronaphthalen-1-amine. (Table 2, Entry 5) The general procedure for Table 2.2 was followed using [RuHCl(CO)(HN(CH$_2$CH$_2$PPh$_2$)$_2$)] (**4**) (6.0 mg, 0.01 mmol, 1 mol %), KOH (8.2 mg, 0.15 mmol, 15 mol %), 1,2,3,4-tetrahydronaphthalen-1-ol (148 mg, 1.0 mmol, 1.0 equiv.), benzylamine (107 mg, 1.0 mmol, 1.0 equiv.), and toluene (1 mL, 1M). The remaining mixture is purified via flash chromatography using EtOAc and hexanes (1:20) to give tan oil (94 mg, 40% isolated yield). ^{1}HNMR (500 MHz, CDCl$_3$) δ 7.60-7.24 (m, 9H), 4.10 (d, _J_ = 13.0 Hz, 1H), 4.00 (d, _J_ = 13.0 Hz, 1H), 3.95 (t, _J_ = 5.0 Hz, 1H), 3.04-2.84 (m, 2H), 2.24-2.04 (m, 3H) 1.94-1.85 (m, 1H). 1.54 (s, 1H) ppm. ^{13}CNMR (125 MHz, CDCl$_3$) 142.2, 139.5, 137.7, 129.3, 129.0, 128.5, 128.3, 127.0, 126.8, 125.9, 54.9, 51.4, 29.6, 28.4, 19.3 ppm. The physical data were identical in all respects to those previously reported. [45]

1HNMR and 13CNMR Spectra

2-methoxy-*N*-(4-methoxyphenyl)acetamide
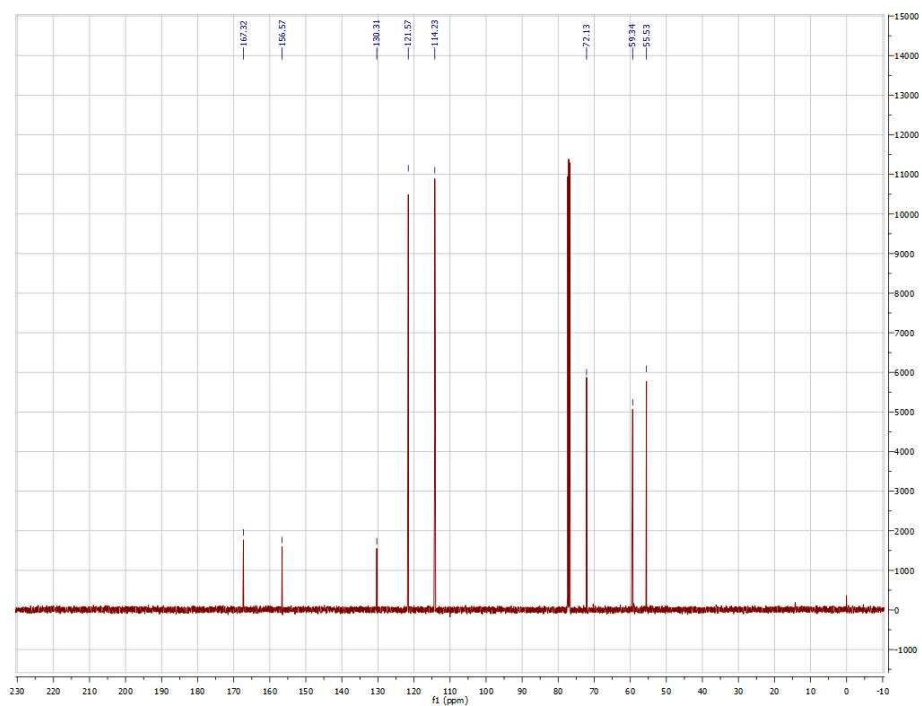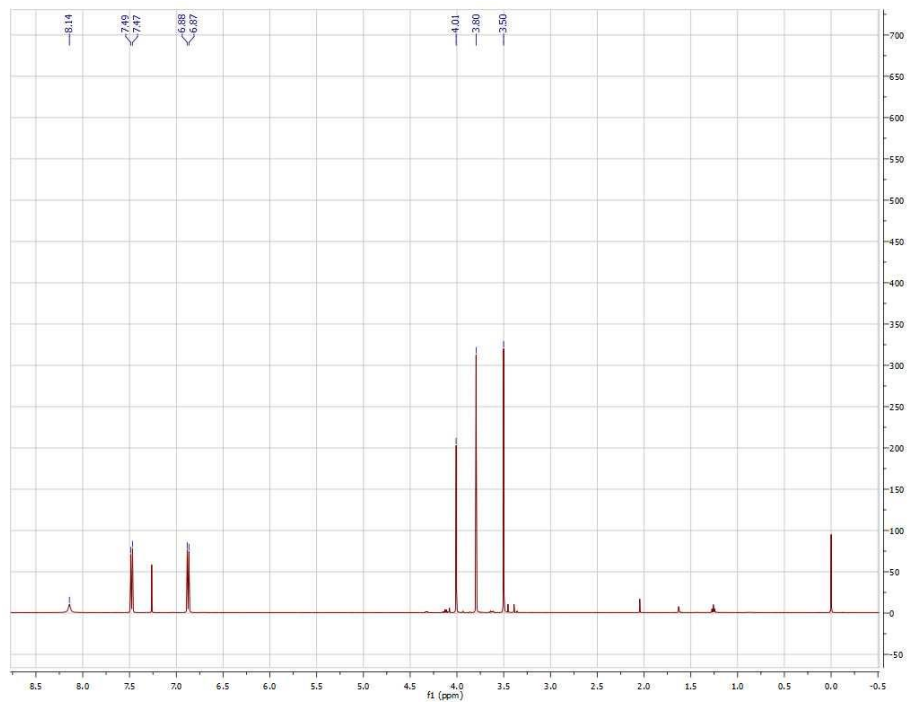
N,N'-(1,4-phenylenebis(methylene))bis(2-methoxyacetamide)
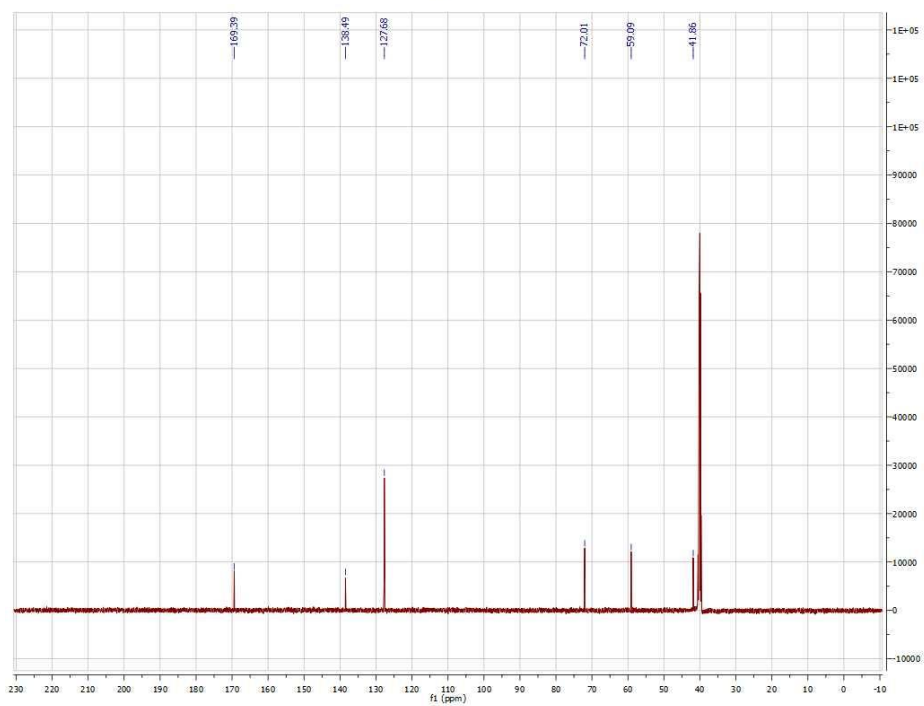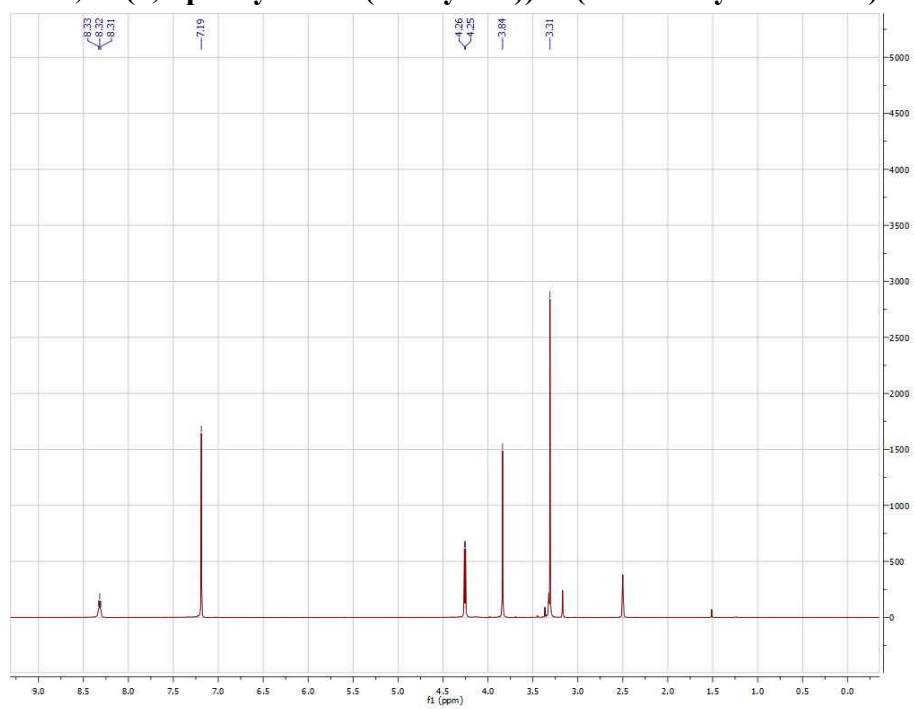
2,2'-((oxybis(ethane-2,1-diyl))bis(oxy))bis(*N*-benzylacetamide)
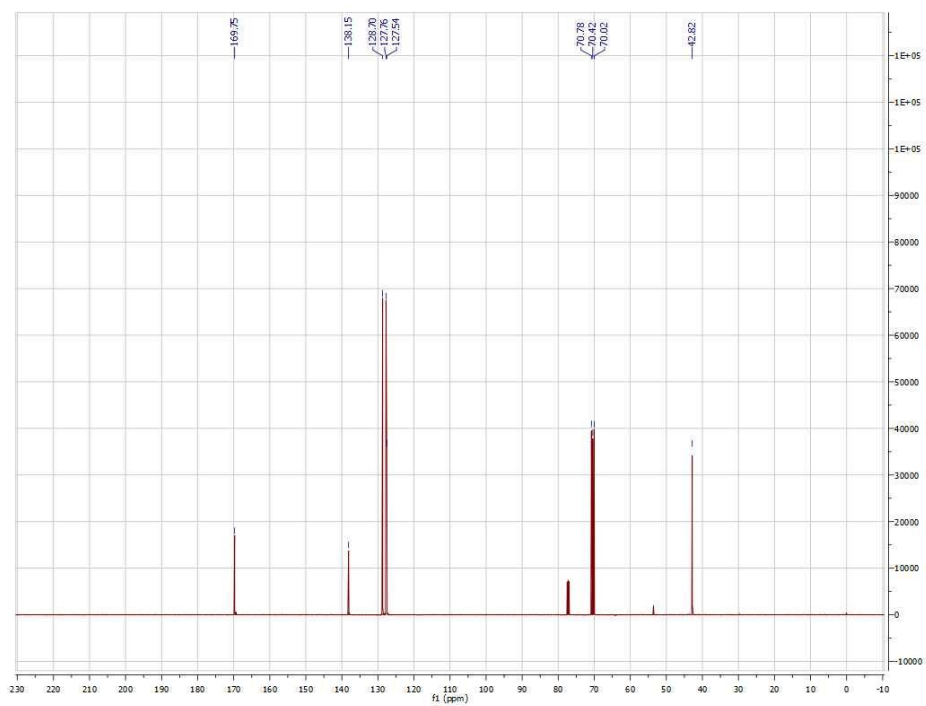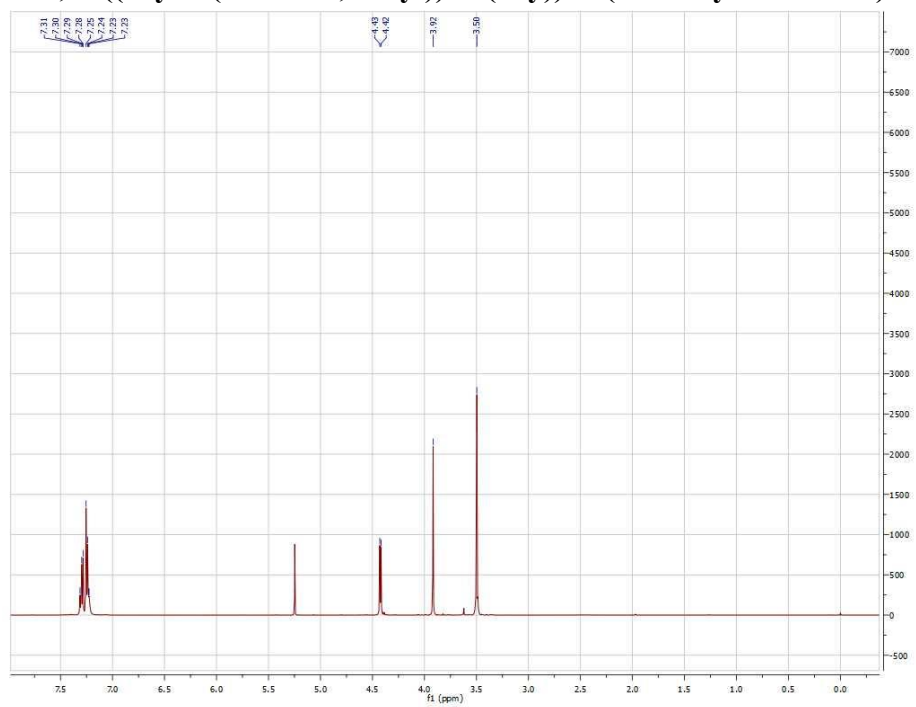
2-methoxy-1-(piperidin-1-yl)ethan-1-one
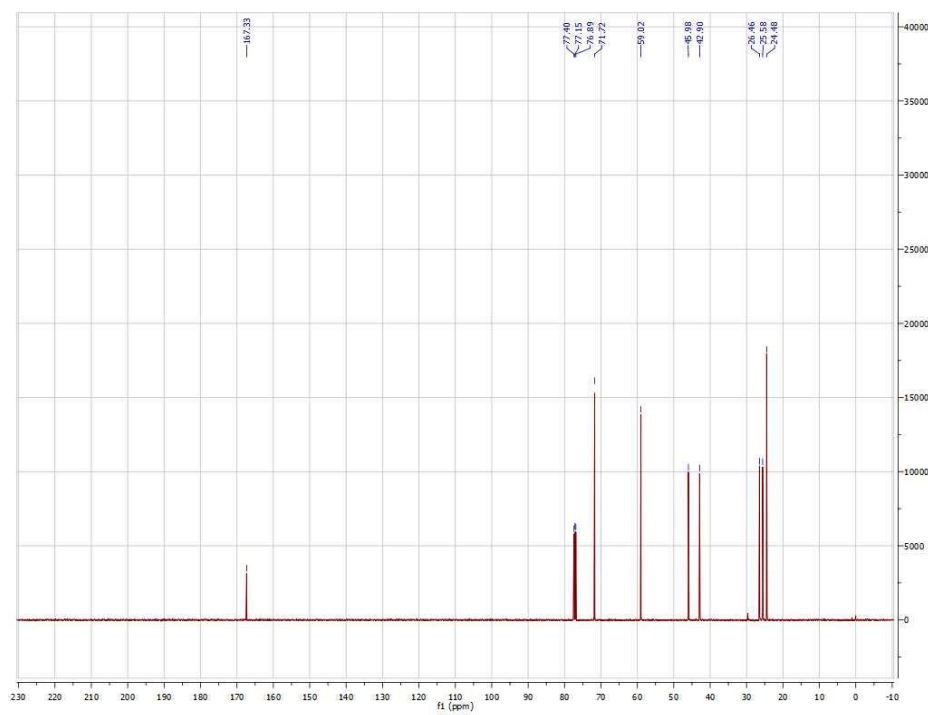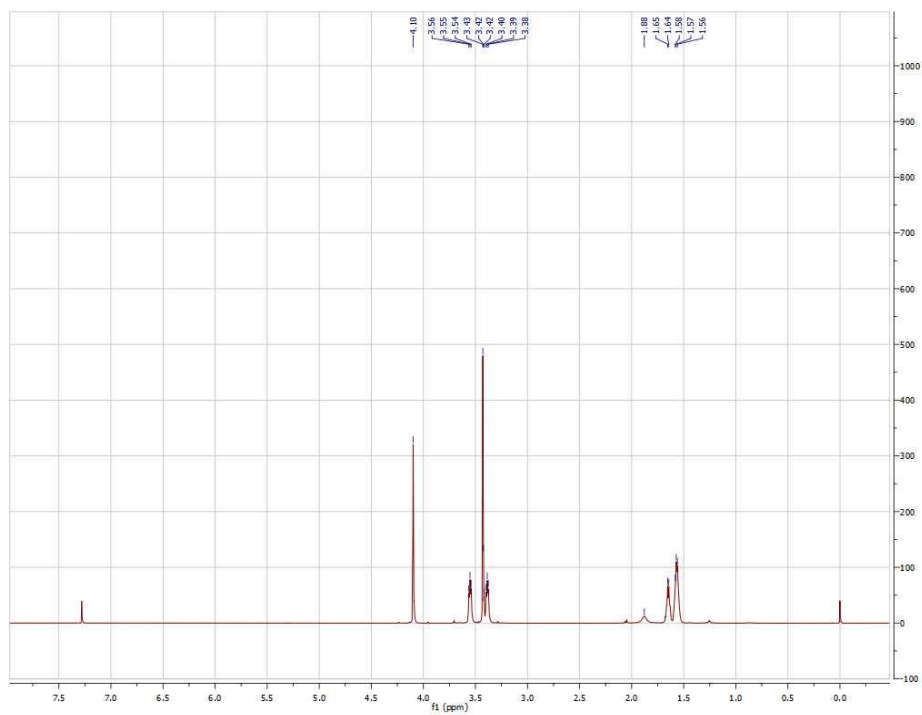
N-benzyl-*N*-ethyl-2-methoxyacetamide
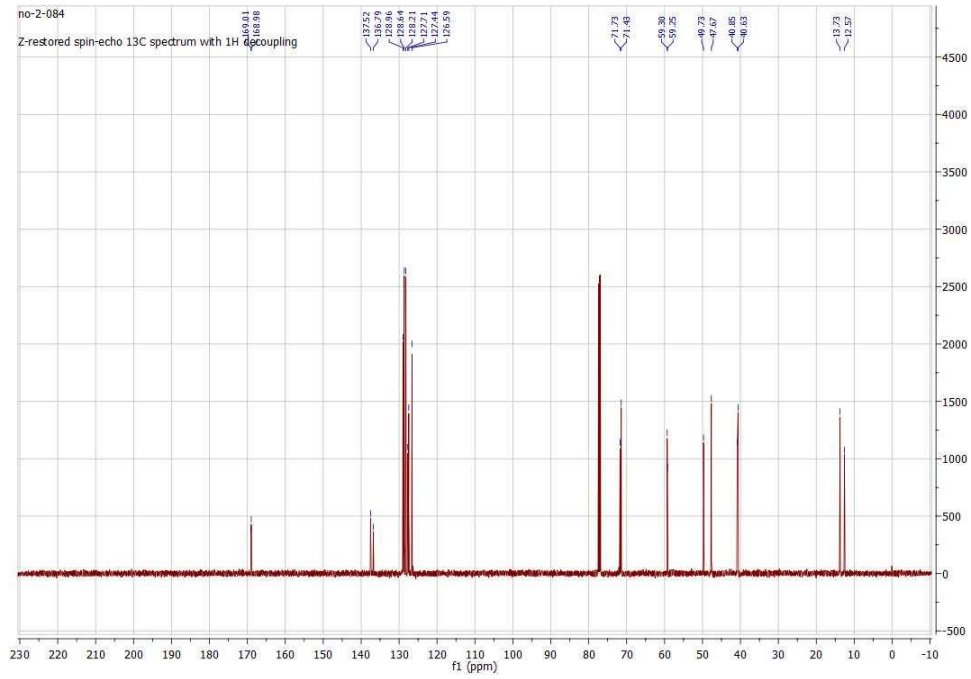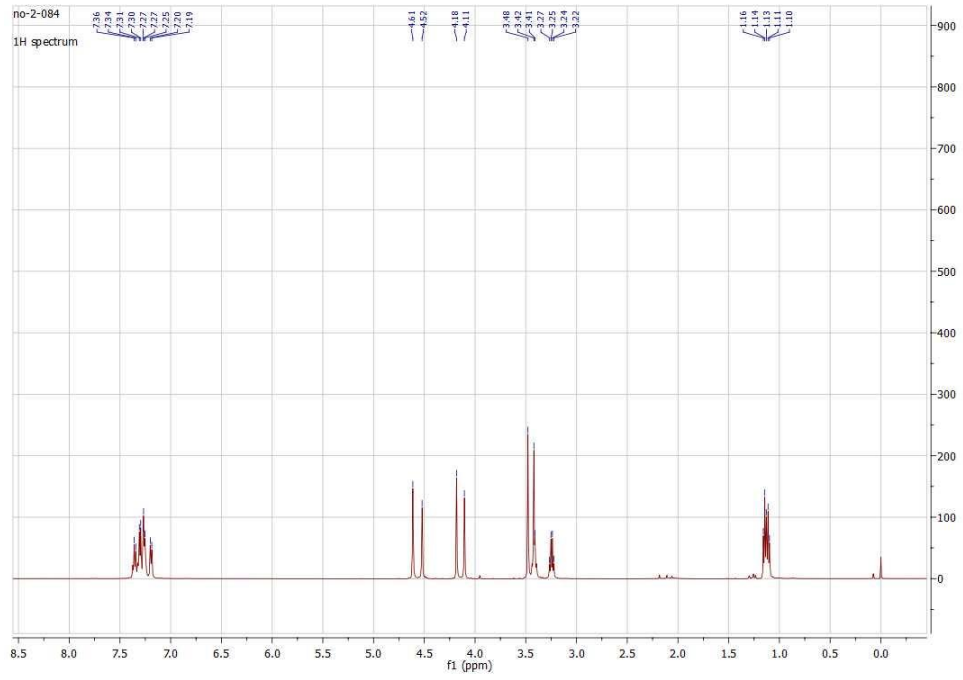
N,*N*-dibenzyl-2-methoxyacetamide
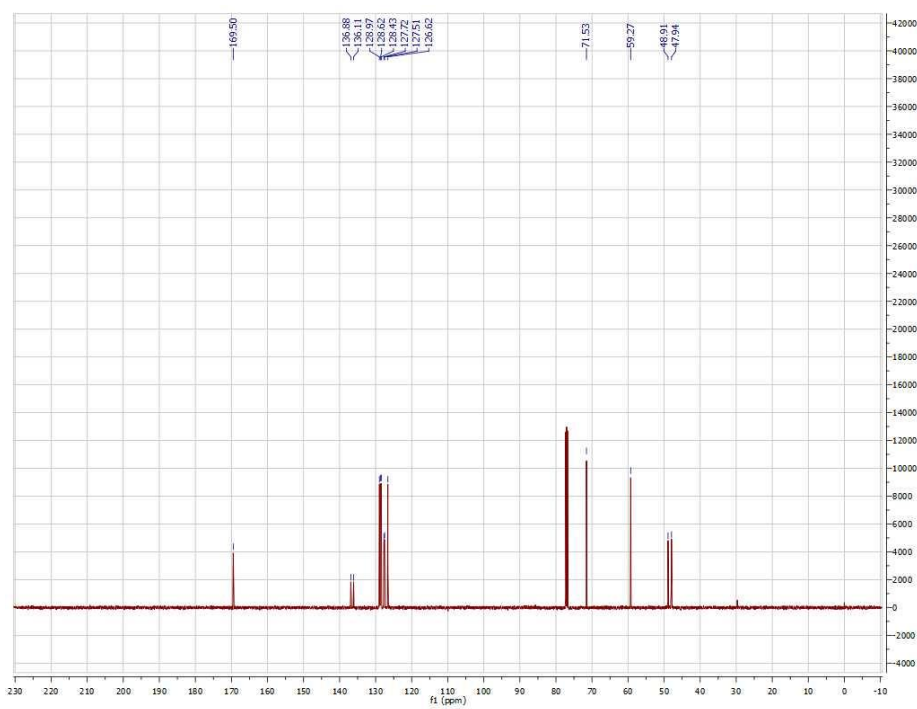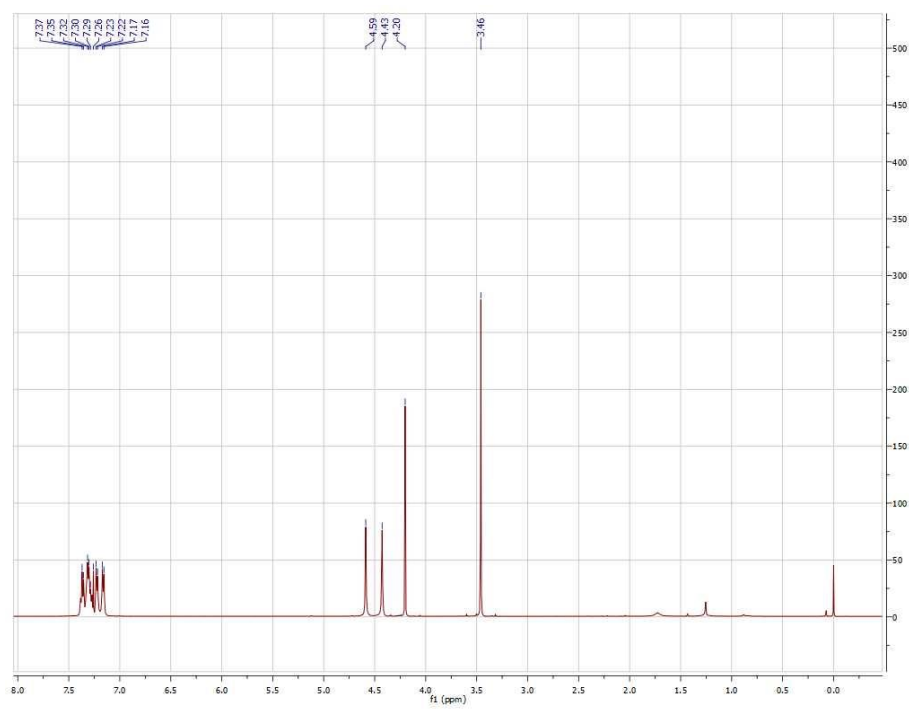
2.5 : References

1.   Montalbetti, C. A. G. N.; Falque, V., Amide bond formation and peptide coupling. *Tetrahedron* **2005,** *61* (46), 10827-10852.

2.   Valeur, E.; Bradley, M., Amide bond formation: beyond the myth of coupling reagents. *Chem. Soc. Rev.* **2009,** *38* (2), 606-631.

3.   Pattabiraman, V. R.; Bode, J. W., Rethinking amide bond synthesis. *Nature* **2011,** *480* (7378), 471-479.

4.   Constable, D. J. C.; Dunn, P. J.; Hayler, J. D.; Humphrey, G. R.; Leazer, J. L.; Linderman, R. J.; Lorenz, K.; Manley, J.; Pearlman, B. A.; Wells, A.; Zaks, A.; Zhang, T. Y., Key green chemistry research areas - a perspective from pharmaceutical manufacturers. *Green Chem.* **2007,** *9* (5), 411-420.

5.   Gunanathan, C.; Ben-David, Y.; Milstein, D., Direct synthesis of amides from alcohols and amines with liberation of H-2. *Science* **2007,** *317* (5839), 790-792.

6.   Schley, N. D.; Dobereiner, G. E.; Crabtree, R. H., Oxidative Synthesis of Amides and Pyrroles via Dehydrogenative Alcohol Oxidation by Ruthenium Diphosphine Diamine Complexes. *Organometallics* **2011,** *30* (15), 4174-4179.

7.   Gnanaprakasam, B.; Milstein, D., Synthesis of Amides from Esters and Amines with Liberation of H-2 under Neutral Conditions. *J. Am. Chem. Soc.* **2011,** *133* (6), 1682-1685.

8.   Nordstrom, L. U.; Vogt, H.; Madsen, R., Amide Synthesis from Alcohols and Amines by the Extrusion of Dihydrogen. *J. Am. Chem. Soc.* **2008,** *130* (52), 17672-+.

9.   Chen, C.; Zhang, Y.; Hong, S. H., N-Heterocyclic Carbene Based Ruthenium-Catalyzed Direct Amide Synthesis from Alcohols and Secondary Amines: Involvement of Esters. *J. Org. Chem.* **2011,** *76* (24), 10005-10010.

10.   Muthaiah, S.; Ghosh, S. C.; Jee, J. E.; Chen, C.; Zhang, J.; Hong, S. H., Direct Amide Synthesis from Either Alcohols or Aldehydes with Amines: Activity of Ru(II) Hydride and Ru(0) Complexes. *J. Org. Chem.* **2010,** *75* (9), 3002-3006.

11.   Gunanathan, C.; Milstein, D., Applications of Acceptorless Dehydrogenation and Related Transformations in Chemical Synthesis. *Science* **2013,** *341* (6143), 249-+.

12.   Dam, J. H.; Osztrovszky, G.; Nordstrom, L. U.; Madsen, R., Amide Synthesis from Alcohols and Amines Catalyzed by Ruthenium N-Heterocyclic Carbene Complexes. *Chem. Eur. J.* **2010,** *16* (23), 6820-6827.

13.   Shimizu, K.; Ohshima, K.; Satsuma, A., Direct Dehydrogenative Amide Synthesis from Alcohols and Amines Catalyzed by gamma-Alumina Supported Silver Cluster. *Chem. Eur. J.* **2009,** *15* (39), 9977-9980.

14.   Zweifel, T.; Naubron, J. V.; Grutzmacher, H., Catalyzed Dehydrogenative Coupling of Primary Alcohols with Water, Methanol, or Amines. *Angew. Chem. Int. Ed.* **2009,** *48* (3), 559-563.

15.   Srimani, D.; Balaraman, E.; Hu, P.; Ben-David, Y.; Milstein, D., Formation of Tertiary Amides and Dihydrogen by Dehydrogenative Coupling of Primary Alcohols with Secondary Amines Catalyzed by Ruthenium Bipyridine-Based Pincer Complexes. *Adv. Synth. Catal.* **2013,** *355* (13), 2525-2530.

16.   Rigoli, J. W.; Moyer, S. A.; Pearce, S. D.; Schomaker, J. M., alpha,beta-Unsaturated imines via Ru-catalyzed coupling of allylic alcohols and amines. *Org. Biomol. Chem.* **2012,** *10* (9), 1746-1749.

17.   Naota, T.; Murahashi, S. I., Ruthenium-Catalyzed Transformations of Amino-Alcohols to Lactams. *Synlett* **1991,** (10), 693-694.

18.   Zeng, H. X.; Guan, Z. B., Direct Synthesis of Polyamides via Catalytic Dehydrogenation of Diols and Diamines. *J. Am. Chem. Soc.* **2011,** *133* (5), 1159-1161.

19.   Zhang, J.; Leitus, G.; Ben-David, Y.; Milstein, D., Facile conversion of alcohols into esters and dihydrogen catalyzed by new ruthenium complexes. *J. Am. Chem. Soc.* **2005,** *127* (31), 10840-10841.

20.   Nielsen, M.; Junge, H.; Kammer, A.; Beller, M., Towards a Green Process for Bulk-Scale Synthesis of Ethyl Acetate: Efficient Acceptorless Dehydrogenation of Ethanol. *Angew. Chem. Int. Ed.* **2012,** *51* (23), 5711-5713.

21.   Spasyuk, D.; Smith, S.; Gusev, D. G., From Esters to Alcohols and Back with Ruthenium and Osmium Catalysts. *Angew. Chem. Int. Ed.* **2012,** *51* (11), 2772-2775.

22.   Zhang, G. Q.; Hanson, S. K., Cobalt-Catalyzed Acceptorless Alcohol Dehydrogenation: Synthesis of Imines from Alcohols and Amines. *Org. Lett.* **2013,** *15* (3), 650-653.

23.   Ho, H. A.; Manna, K.; Sadow, A. D., Acceptorless Photocatalytic Dehydrogenation for Alcohol Decarbonylation and Imine Synthesis. *Angew. Chem. Int. Ed.* **2012,** *51* (34), 8607-8610.

24.   Gnanaprakasam, B.; Zhang, J.; Milstein, D., Direct Synthesis of Imines from Alcohols and Amines with Liberation of H-2. *Angew. Chem. Int. Ed.* **2010,** *49* (8), 1468-1471.

25.   Maggi, A.; Madsen, R., Dehydrogenative Synthesis of Imines from Alcohols and Amines Catalyzed by a Ruthenium N-Heterocyclic Carbene Complex. *Organometallics* **2012,** *31* (1), 451-455.

26.   Esteruelas, M. A.; Honczek, N.; Olivan, M.; Onate, E.; Valencia, M., Direct Access to POP-Type Osmium(II) and Osmium(IV) Complexes: Osmium a Promising Alternative to Ruthenium for the Synthesis of Imines from Alcohols and Amines. *Organometallics* **2011,** *30* (9), 2468-2471.

27.   Zhang, M.; Neumann, H.; Beller, M., Selective Ruthenium-Catalyzed Three-Component Synthesis of Pyrroles. *Angew. Chem. Int. Ed.* **2013,** *52* (2), 597-601.

28.   Michlik, S.; Kempe, R., A sustainable catalytic pyrrole synthesis. *Nature Chem.* **2013,** *5* (2), 140-144.

29.   Montag, M.; Zhang, J.; Milstein, D., Aldehyde Binding through Reversible C-C Coupling with the Pincer Ligand upon Alcohol Dehydrogenation by a PNP-Ruthenium Catalyst. *J. Am. Chem. Soc.* **2012,** *134* (25), 10325-10328.

30.   Yang, X. Z., A Self-Promotion Mechanism for Efficient Dehydrogenation of Ethanol Catalyzed by Pincer Ruthenium and Iron Complexes: Aliphatic versus Aromatic Ligands. *Acs Catal* **2013,** *3* (12), 2684-2688.

31.   Shvo, Y.; Blum, Y.; Reshef, D.; Menzin, M., Catalytic Oxidative Coupling of Diols by Ru3(Co)12. *J. Organomet. Chem.* **1982,** *226* (1), C21-C24.

32.   Murahashi, S. I.; Naota, T.; Ito, K.; Maeda, Y.; Taki, H., Ruthenium-Catalyzed Oxidative Transformation of Alcohols and Aldehydes to Esters and Lactones. *J. Org. Chem.* **1987,** *52* (19), 4319-4327.

33.   Dobson, A.; Robinson, S. D., Complexes of the platinum metals. 7. Homogeneous ruthenium and osmium catalysts for the dehydrogenation of primary and secondary alcohols. *Inorg. Chem.* **1977,** *16* (1), 137-142.

34.   Kuriyama, W.; Matsumoto, T.; Ogata, O.; Ino, Y.; Aoki, K.; Tanaka, S.; Ishida, K.; Kobayashi, T.; Sayo, N.; Saito, T., Catalytic Hydrogenation of Esters. Development of an Efficient Catalyst and Processes for Synthesising (R)-1,2-Propanediol and 2-(l-Menthoxy)ethanol. *Org. Process Res. Dev.* **2011,** *16* (1), 166-171.

35.   Otsuka, T.; Ishii, A.; Dub, P. A.; Ikariya, T., Practical Selective Hydrogenation of alpha-Fluorinated Esters with Bifunctional Pincer-Type Ruthenium(II) Catalysts Leading to Fluorinated Alcohols or Fluoral Hemiacetals. *J. Am. Chem. Soc.* **2013,** *135* (26), 9600-9603.

36.   Nielsen, M.; Alberico, E.; Baumann, W.; Drexler, H. J.; Junge, H.; Gladiali, S.; Beller, M., Low-temperature aqueous-phase methanol dehydrogenation to hydrogen and carbon dioxide. *Nature* **2013,** *495* (7439), 85-89.

37.   Imine formation was monitored by GC-MS (CI) and 1H NMR analysis of the reaction mixture. For ease of purification the imine was reduced with sodium borohydride to the corresponding amine to prevent hydrolysis of the imine on silica gel.

38.   Smith, S. M.; Thacker, N. C.; Takacs, J. M., Efficient amide-directed catalytic asymmetric hydroboration. *J. Am. Chem. Soc.* **2008,** *130* (12), 3734-+.

39.   Chaysripongkul, S.; Pluempanupat, W.; Jang, D. O.; Chavasiri, W., Application of Cl3CCONH2/PPh3 towards the Synthesis of Bioactive Amides. *Bull. Korean Chem. Soc.* **2009,** *30* (9), 2066-2070.

40.   Moore, J. D.; Byrne, R. J.; Vedantham, P.; Flynn, D. L.; Hanson, P. R., High-load, ROMP-generated oligomeric bis-acid chlorides: Design of soluble and insoluble nucleophile scavengers. *Org. Lett.* **2003,** *5* (23), 4241-4244.

41.   Shannon, S. K.; Peacock, M. J.; Kates, S. A.; Barany, G., Solid-phase synthesis of lidocaine and procainamide analogues using backbone amide linker (BAL) anchoring. *J. Comb. Chem.* **2003,** *5* (6), 860-868.

42.   Ditrich, K., Optically active amines by enzyme-catalyzed kinetic resolution. *Synthesis-Stuttgart* **2008,** (14), 2283-2287.

43.   Ueda, T.; Konishi, H.; Manabe, K., Palladium-Catalyzed Fluorocarbonylation Using N-Formylsaccharin as CO Source: General Access to Carboxylic Acid Derivatives. *Org. Lett.* **2013,** *15* (20), 5370-5373.

44.   Stephenson, N. A.; Zhu, J.; Gellman, S. H.; Stahl, S. S., Catalytic Transamidation Reactions Compatible with Tertiary Amide Metathesis under Ambient Conditions. *J. Am. Chem. Soc.* **2009,** *131* (29), 10003-10008.

45.   Eisenberger, P.; Bailey, A. M.; Crudden, C. M., Taking the F out of FLP: Simple Lewis Acid-Base Pairs for Mild Reductions with Neutral Boranes via Borenium Ion Catalysis. *J. Am. Chem. Soc.* **2012,** *134* (42), 17384-17387.

46.   Lee, O. Y.; Law, K. L.; Yang, D., Secondary Amine Formation from Reductive Amination of Carbonyl Compounds Promoted by Lewis Acid Using the InCl3/Et3SiH System. *Org. Lett.* **2009,** *11* (15), 3302-3305.

Chapter 3 : From Racemic Alcohols to Enantiopure Amines: Ru-Catalyzed Diastereoselective Amination

Abstract: A commercially available ruthenium(II) PNP-type pincer catalyst (Ru-Macho) promotes formation of α-chiral *tert*-butanesulfinylamines from racemic secondary alcohols and Ellman's chiral *tert*-butanesulfinamide *via* a hydrogen borrowing strategy. The formation of α-chiral *tert*-butanesulfinylamines occurs in yields ranging from 31% to 89% with most examples giving >95:5 dr.

3.1 Introduction:
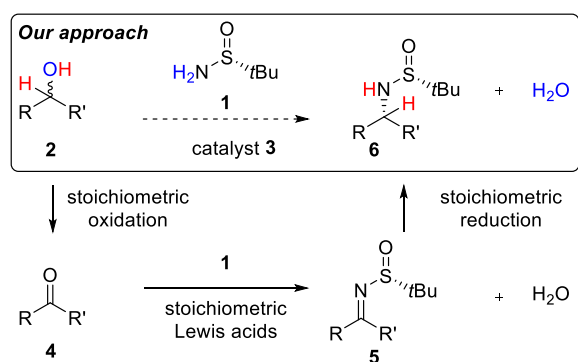
Figure 3.1 Diastereoselective Amination: Proposed catalytic strategy (one-step) versus conventional approach (three-steps)

Due to the high value of α-chiral amines in both medicinal and synthetic chemistry, there is a need to develop more efficient methods for the stereoselective construction of C–N bonds.[1, 2] Since its discovery in 1997, Ellman's sulfinamide has become a widely used reagent for the synthesis of α-chiral primary amines, with many industrially relevant applications.[3, 4] Considering the high practicality of this sulfinamide as an ammonia equivalent, we sought a catalytic method for the diastereoselective *N*-alkylation of Ellman's sulfinamide **1** using readily available secondary alcohols **2** (Figure 3.1).[5-7] This formal nucleophilic substitution would transform racemic alcohols into enantiopure amines and generate water as the only byproduct. Herein, we describe a Ru-catalyzed approach that overcomes the need for stoichiometric reagents and achieves in a single operation what traditionally requires three chemical steps (*i.e,* oxidation, condensation using Ti(OEt)$_4$, and then reduction) as shown in Figure 3.1.

The direct amination of alcohols has been demonstrated with various catalysts,[8-13] but only one single stereoselective amination has been achieved to date by Zhao and coworkers.[14] This Ir-catalyzed method is limited, however, to the synthesis of chiral anilines.[14] Guided by previous studies using Ru-pincer complexes,[5, 15-21] we proposed that racemic alcohol **2** (Figure 3.2) would undergo
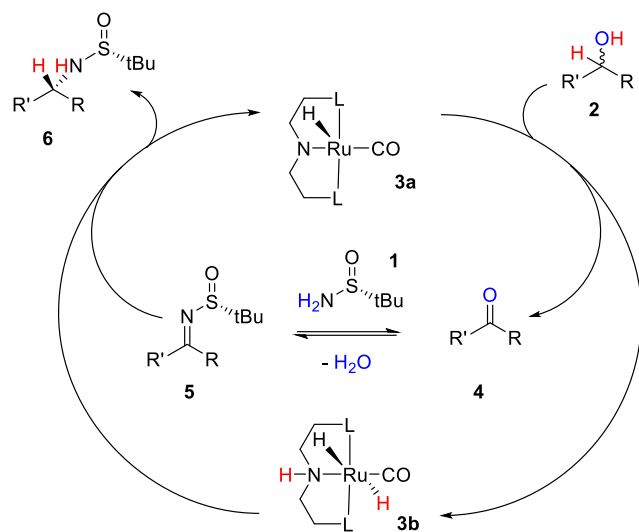
Figure 3.2 Mechanistic proposal featuring hydrogen borrowing via a ruthenium(II) pincer complex

oxidation by Ru-pincer complex **3a** to form ketone **4** and Ru-hydride **3b**. The ketone **4** would undergo condensation with sulfinamide **1** to form the sulfinylimine **5**.[22-24] Hydrogenation of imine **5** via Ru-hydride **3b** would proceed with high and predictable diastereoselectivity to generate the α-chiral sulfinylamine **6**.[22-24] To achieve this novel alkylation, we recognized the challenge of identifying a catalyst that would favor hydrogen-transfer over competing pathways (*e.g.* acceptorless dehydrogenation).[25-36] Moreover, the Ru-catalyst would need to tolerate H_2O as the main byproduct.

3.2 Results and Discussion:

To test our hypothesis, we investigated the coupling of **1** and racemic alcohol 1-phenylethanol (**2b**) with a number of Ru-pincer complexes (Table 3.1). A few structurally related pincer-complexes, including Milstein's catalyst (Table 3.1, entry 1), as well as two catalysts developed by the Gusev group (entries 2, 3) showed no desired reactivity, even though these catalysts are known to activate both C–N and C–O bonds.[25, 37-39] In a previous study,[40] we discovered that Ru-Macho[41] acted as an efficient catalyst for the dehydrogenative synthesis of

Table 3.1 Optimization of reaction conditions for the formation of *N-tert*-butanesulfinylamines

entry	catalyst	base	temp °C	% conv.[a]
1	3c	KOH	110	0%
2	3d	KOH	110	0%
3	3e	KOH	110	0%
4	3f	KOH	110	71%
5	3f	NaOH	110	36%
6	3f	Cs$_2$CO$_3$	110	4%
7	3f	K$_2$CO$_3$	110	0%
8	3f	KO*t*-Bu	110	0%
9	3f	NaOMe	110	9%
10	3f	KOH	120	89%

Reaction Conditions: 0.5 mmol 2b, 0.5 mmol 1, 1 mol % 3, 15 mol % base, 0.5 mL toluene 110 °C, 8h. a Conversion measured by GC with a known amount of dodecane standard.

amides and imines from alcohols and amines. We envisioned that this complex could potentially act as a hydrogen-transfer catalyst to afford the desired product. Indeed, Ru-Macho afforded α-chiral sulfinylamine **6** in 71% isolated yield (entry 4). By further tuning the reaction parameters, we identified the optimal conditions to be the use of toluene as solvent and KOH as base, at 120 °C (89%, entry 10). The transformation occurs efficiently using only 1 mol % catalyst loadings.

With this protocol in hand, we transformed a range of racemic alcohols into optically active amines. (Table 3.2).[42] The reaction conditions do not epimerize the chiral sulfinamide and the expected enantiomer was afforded after coupling with an achiral alcohol (entry 1). Both electron donating and electron withdrawing groups on the β-phenyl group relative to the amine could be incorporated (entries 3–7, 73–89% yield, >95:5 dr). Fluorine-containing amines were obtained in good yields (73–89%) with high diastereocontrol (>95:5 dr) (entries 5 and 6). Next, we found that chiral pyridinyl derivatives (**6h–j**) could be generated in 55–80% isolated yields, with high diastereoselectivity (>95:5 dr) (entries 8–10). A racemic alcohol bearing a larger aromatic substituent, such as the 2-napthyl group (entry 11) undergoes coupling in 84% yield and

Table 3.2 Variation of secondary alcohols used in diastereoselective amination

Reaction scheme: alcohol **2** (H–C(OH)(R')(R)) + sulfinamide **1** (H_2N–S(=O)–tBu) → with 1 mol % Ru-Macho, 15 mol % KOH, toluene, 120 °C, 6–12 h → product **6** (HN–S(=O)–tBu on C(R')(R))

entry	alcohol	time (h)	product	yield [a]	dr (R,R):(R,S) [b]
1	cyclohexyl–OH	12	**6a**	89%	> 95% ee [c]
2	Ph–CH(OH)–Me	7	**6b**	85%	>95:5
3	3-Cl-C$_6$H$_4$–CH(OH)–Me	12	**6c**	79%	>95:5 [c]
	4-X-C$_6$H$_4$–CH(OH)–Me				
4	X = Br	6	**6d**	74%	>95:5
5	X = F	6	**6e**	89%	>95:5 [c]
6	X = CF$_3$	12	**6f**	73%	>95:5
7	X = OMe	10	**6g**	78%	>95:5
8	pyridin-3-yl–CH(OH)–Me	7	**6h**	80%	>95:5
9	pyridin-2-yl–CH(OH)–Me	6	**6i**	55%	>95:5
10	pyridin-4-yl–CH(OH)–Me	6	**6j**	73%	>95:5
11	naphthalen-2-yl–CH(OH)–Me	6	**6k**	84%	>95:5 [c]
	X–CH(OH)–Me				
12	X = (CH$_2$)$_2$Ph	12	**6l**	71%	75:25
13	X = n-Bu	10	**6m**	81%	70:30
14	X = i-Pr	6	**6n**	59%	>95:5
15	1,2,3,4-tetrahydronaphthalen-1-ol	6	**6o**	36%	>95:5
16	Ph–CH(OH)–Et	12	**6p**	32%	>95:5
17	tBu–C(OH)(Me)–Me	12	**6q**	0%	N/A
18	2-Me-C$_6$H$_4$–CH(OH)–Me	12	**6r**	0%	N/A

Reaction Conditions: 0.5 mmol 1, 0.5 mmol 2, 1 mol % Ru-Macho, 15 mol % KOH, 0.5 mL toluene, 120 °C. a Isolated yields. b Determined by ^{1}H NMR. c Determined by polarimetry.

>95:5 dr (entry 12). When the aryl group was substituted for saturated hydrocarbon chains (Table 3.2, entries 12 and 13), a drop in diastereoselectivity (75:25 and 70:30 dr respectively) was observed, but the reaction yield remained between 71–81% (**6l, m**). Our observation is in agreement with previous studies by Ellman and others who found that reduction of sulfinylimines proceeds with lowered diastereocontrol when the β-substituents are similar in size.[3, 43-45] In entries 12 and 13, we propose that the lower diastereocontrol is due to the similar steric bulk of a methyl group and an *n*-butyl or (-(CH$_2$)$_2$Ph) group.[18] In contrast, an alcohol with a β-*i*-Pr group (entry 14) was shown to form the corresponding sulfinylamine with higher diastereoselectivity (>95:5) due to a greater difference in the steric bulk (**6n**).[19]
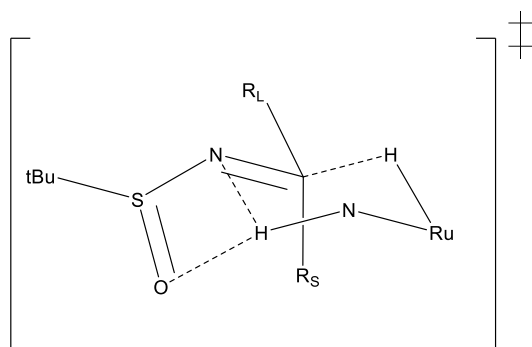
Figure 3.3 Proposed transition state for the catalytic transformation

The synthesis of α-chiral amines bearing a β-methyl group is challenging to achieve due to low diastereocontrol in the conventional use of MeLi to add to *N-tert*-butylsulfinylaldimine.[3, 4] In contrast, our method is most effective for the construction of amines bearing a β-methyl group (entries 2–15). Ru-Macho appears sensitive to the steric bulk at the β-position on the sulfinylimine intermediate during hydrogen-transfer (Figure 3.2, **5**). For example, lower isolated yields were encountered when bulkier groups were placed in the β-position on both sides of the alcohol (entries 15–16) (31–36%), but diastereoselectivities remained high (>95:5 dr) (**6o–p**). We found that more bulky substrates, (e.g., a *tert*-butyl substituted alcohol or ortho-arylated alcohol) shows no reactivity under these conditions (entries 17 and 18).

3.3 Conclusion:

In summary, this study provides an effective method for chiral amine synthesis by combining the power of the widely used Ellman's sulfinamide auxiliary with the practicality of the inexpensive and industrially relevant Ru-Macho catalyst.[41] By using a *hydrogen borrowing* strategy, α-chiral amines can be accessed directly from racemic alcohols in one step.[8-12] In addition to fewer required steps, this catalytic approach overcomes the need for use of stoichiometric Lewis acids.[3, 4] Moreover, the resulting diastereomeric products can be easily separated.[3, 4] Importantly, this methodology enables access to methyl-substituted chiral amines that are challenging to obtain with methyl organometallic reagents.[3, 4] Ongoing studies to expand substrate scope *via* catalyst design are underway.

3.4 Supporting Information

General Information: For experiments involving the glovebox, we used nitrogen atmosphere in a Vacuum Atmospheres Company Glove box and vials that were sealed under a nitrogen atmosphere. Toluene was purchased from Fisher Chemical and purged with argon for 2 hours and then dried by passing it through two columns of neutral alumina under argon pressure. Dioxane, DMF, DMSO, chlorobenzene, xylene, and DMF were purchased from Aldrich Chemical Co or Ficher Chemical and purged with nitrogen for 30 minutes before use. Alcohols were used as received from Aldrich Chemical Co or Ficher Chemical after being purged with nitrogen for 30 minutes. Some alcohols were prepared via reduction of the corresponding ketone with sodium borohydride in methanol.[3] *(R)*-(+)-2-methyl-2-propanesulfinamide was used as received from Combi-Blocks. [RuHCl(CO)(HN(CH$_2$CH$_2$PPh$_2$)$_2$)] (Ru-Macho catalyst) was purchased from Strem Chemicals Inc. and used as received. Milstein's Catalyst was used as purchased from Strem Chemicals Inc. The SNS and PNN Gusev catalysts were used as received from Aldrich Chemical Co. KOH was purchased from Fisher Chemical and then grounded with a mortar and pestle (in the glovebox) to a fine powder and stored in the glovebox. Column chromatography was performed using a Teledyne Isco CombiFlash Rf 200c with Gold high performance HP Silica Chromatography columns from Teledyne and the solvent scheme indicated.

General Analytical Information: All new compounds (*6c, 6e, 6k*) were characterized by ^{1}H NMR, ^{13}C NMR, ESI-MS, IR, and optical rotation. NMR spectra were obtained using Bruker 500 MHz instruments. All ^{1}H NMR and ^{13}C NMR are reported in ppm relative to TMS (0.00 ppm) unless otherwise noted. IR spectra were obtained using a Thermo Scientific Nicolet iS5 iD5 ATR IR spectrometer. GC-MS (CI) was performed using a GCT Premier Micromass MS Technologies

mass spectrometer, coupled with a Waters 7890A gas chromatograph. ESI-MS was performed using a LCT Premier Micromass MS Technologies mass spectrometer. Optical rotation was obtained using a Rudolph Research Analytical Autopol III Automatic Polarimeter. For known compounds, we have cited the published characterization data that we used to compare to our synthesized compounds and we have included a ^{1}H NMR spectrum to establish purity of the isolated material.

General Procedure for Examples in Table 3.1: An oven dried 1 dram vial equipped with a stir bar was brought into a nitrogen filled glove box. The vial was charged with indicated catalyst (0.01 mmol, 1 mol %), indicated base (0.15 mmol, 15 mol %), *(R)*-(+)-2-methyl-2-propanesulfinamide (61 mg, 0.5 mmol, 1.0 equiv.), 1-phenylethanol (61 mg, 0.5 mmol, 1.0 equiv.), and the indicated solvent (1 mL) in that order. After all reagents were added to the vial, the vial was sealed with a PTFE cap, electrical tape, and then removed from the glove box. The reaction vessel was heated at 110 °C in a silicone oil bath for 8 h and the resulting mixture allowed to cool to rt. Diastereomeric ratio was determined by ^{1}H NMR analysis of the unpurified reaction mixture. The peak used to determine diastereomeric ratios are noted with an asterisk and the range where the two diastereomeric peaks appear is shown with their respective integrations.

General Procedure for Examples in Table 3.2: An oven dried 5 mL conical vial equipped with a stir bar was brought a nitrogen filled glove box. The vial was charged with [RuHCl(CO)(HN(CH$_2$CH$_2$PPh$_2$)$_2$)] (6.0 mg, 0.01 mmol, 1 mol %), KOH (8.2 mg, 0.15 mmol, 15 mol %), *(R)*-(+)-2-methyl-2-propanesulfinamide (61 mg, 0.5 mmol, 1.0 equiv.), alcohol (0.5 mmol, 1.0 equiv.), and toluene (1 mL) in that order. After all reagents have been added to the vial, the vial was sealed with a PTFE cap, electrical tape, and then removed from the glove box. The reaction vessel was heated at the indicated temperature in a silicone oil bath for 6-12 h and then

allowed to cool to rt. Diasteromeric ratio was determined by ^{1}H NMR analysis of the unpurified reaction mixture. For products **6c, 6e**, and **6k**, the optical purity wasestablished by removal of the tert-butylsulfinyl group to yield the chiral amine. After purification, the optical rotation of the resulting amine was compared to literature standards via polarimetry. Removal of the tert-butylsulfinyl group was performed according to previous literature procedures.[4] The amines were purified using flash chromatography with the indicated solvent system.

Synthesis and Characterizations of Compounds:

(R)-N-cyclohexyl-2-methylpropane-2-sulfinamide (6a). The general procedure for Table 3.1 was followed using [RuHCl(CO)(HN(CH$_2$CH$_2$PPh$_2$)$_2$)] (3.0 mg, 0.05 mmol, 1 mol%), KOH (4.1 mg, 0.075 mmol, 15 mol %), *(R)*-(+)-2-methyl-2-propanesulfinamide (61 mg, 0.5 mmol, 1.0 equiv.) cyclohexanol (50 mg, 0.5 mmol, 1.0 equiv.) and toluene (1 mL). The reaction vessel was heated for 12 h in a silicone oil bath at 120 °C. The crude product was purified via flash chromatography with EtOAc in Hexanes (gradient from 0% to 100% EtOAc) to give a white solid (95.6 mg, 85% isolated yield, >95% ee. ^{1}H NMR (500 MHz, CDCl$_3$) δ 3.21 (m, 1H), 2.98 (br, s, 1H), 2.01–1.92 (m, 2H), 1.75–1.62 (m, 2H), 1.65–1.53 (m, 1H), 1.39–1.09 (m, 5H), 1.19 (s, 9H) ppm. ^{13}C NMR (125 MHz, CDCl$_3$) δ 55.5, 54.5, 35.5, 34.4, 25.8, 25.1, 24.7, 22.8 ppm. [α]$_D^{24.1}$ = -92.5° (c = 1.0, CH$_3$Cl). All spectroscopic data match previously reported values.[46]

(R)-2-methyl-N-((R)-1-phenylethyl)propane-2-sulfinamide (6b). The general procedure for Table 3.1 was followed using [RuHCl(CO)(HN(CH$_2$CH$_2$PPh$_2$)$_2$)] (3.0 mg, 0.05 mmol, 1 mol%), KOH (4.1 mg, 0.075 mmol, 15 mol %), *(R)*-(+)-2-methyl-2-propanesulfinamide (61 mg, 0.5 mmol, 1.0 equiv.), sec-phenylethylalcohol (61 mg, 0.5 mmol, 1.0 equiv.) and toluene (1 mL). The reaction vessel was heated for 7 h in a silicone oil bath at 120 °C. The crude product was purified via flash chromatography with EtOAc in Hexanes (gradient from 0% to 100% EtOAc) to give a colorless

oil (95.6 mg, 85% isolated yield, >95:5 dr (R,R : R,S)). ^{1}H NMR (500 MHz, CDCl$_3$) δ 7.36-7.27 (m, 5H), 4.59-4.51 (m, 1H), 3.43* (br, s, 1H), 1.51 (d, J = 5.0 Hz, 3H), 1.24 (s, 9H) ppm. ^{13}C NMR (125 MHz, CDCl$_3$) δ 144.1, 128.8, 127.9, 126.7, 55.5, 53.9, 22.8, 22.7 ppm. All spectroscopic data match previously reported values.[43]

(R)-N-((R)-1-(3-chlorophenyl)ethyl)-2-methylpropane-2-sulfinamide **(6c).** The general procedure for Table 3.1 was followed using [RuHCl(CO)(HN(CH$_2$CH$_2$PPh$_2$)$_2$)] (3.0 mg, 0.05 mmol, 1 mol%), KOH (4.1 mg, 0.075 mmol, 15 mol %), *(R)*-(+)-2-methyl-2-propanesulfinamide (61 mg, 0.5 mmol, 1.0 equiv.), 1-(3-chlorophenyl)ethan-1-ol (78 mg, 0.5 mmol, 1.0 equiv.) and toluene (1 mL). The reaction vessel was heated for 6 h in a silicone oil bath at 120 °C. The crude product was purified via flash chromatography with EtOAc in Hexanes (gradient from 0% to 100% EtOAc) to give a colorless oil (103 mg, 79% isolated yield, >95:5 dr (R,R : R,S)). HRMS (ESI/MeOH) *m/z* calcd for C$_{12}$H$_{18}$ClNOS (M + Na)$^+$: 282.0695, Found: 282.0687. ^{1}H NMR (500 MHz, CDCl$_3$) δ 7.45 – 7.10 (m, 4H), 4.56-4.48 (m, 1H), 3.41* (br, s, 1H), 1.50 (d, J = 6.5 Hz, 3H), 1.24 (s, 9H) ppm. ^{13}C NMR (125 MHz, CDCl$_3$) δ 146.2, 134.7, 130.2, 128.2, 126.9, 125.1, 55.7, 53.7, 22.9, 22.7 ppm. IR (film) 3210.4, 3155.5, 3057.9, 2975.9, 2954.9, 2921.1, 2864.9, 1594.8, 1573.3, 1433.5, 1389.1, 1362.2, 1329.2, 1306.1, 1258.1, 1205.3, 1052.7 cm^{-1}. The optical purity was deduced by the optical rotation of the corresponding chiral amine using a polarimeter. The chiral amine was obtained through treatment of the reaction mixture with HCl after heating the reaction for the specified time to remove the *N*-tertbutanesulfinyl group. Optical rotation of *(R)*-(+)-1-(3-chlorophenyl)ethan-1-amine [α]$_D^{24.3}$ = +27.1° (c = 1.2, MeOH). All spectroscopic data match previously reported values of the amine product.[24]

(R)-N-((R)-1-(4-bromophenyl)ethyl)-2-methylpropane-2-sulfinamide **(6d).** The general procedure for Table 3.1 was followed using [RuHCl(CO)(HN(CH$_2$CH$_2$PPh$_2$)$_2$)] (3.0 mg, 0.05

mmol, 1 mol%), KOH (4.1 mg, 0.075 mmol, 15 mol %), *(R)*-(+)-2-methyl-2-propanesulfinamide (61 mg, 0.5 mmol, 1.0 equiv.), 1-(4-bromophenyl)ethan-1-ol (100 mg, 0.5 mmol, 1.0 equiv.) and toluene (1 mL). The reaction vessel was heated for 12 h in a silicone oil bath at 120 °C. The crude product was purified via flash chromatography with EtOAc in Hexanes (gradient from 0% to 100% EtOAc) to give a tan oil (114.1 mg, 75% isolated yield, >95:5 dr (R,R : R,S)). ^{1}H NMR (500 MHz, CDCl3) δ 7.48 (d, *J* = 8.5 Hz, 2H), 7.23 (d, *J* = 8.5 Hz, 2H), 4.55-4.47 (m, 1H), 3.38* (br, s, 1H), 1.50 (d, *J* = 5.0 Hz, 3H), 1.23 (s, 9H) ppm. ^{13}C NMR (125 MHz, CDCl3) δ 143.1, 131.9, 128.4, 121.7, 55.6, 53.6, 22.8, 22.6 ppm. All spectroscopic data match previously reported values.[43]

(R)-N-((R)-1-(4-fluorophenyl)ethyl)-2-methylpropane-2-sulfinamide (6e). The general procedure for Table 3.1 was followed using [RuHCl(CO)(HN(CH2CH2PPh2)2)] (3.0 mg, 0.05 mmol, 1 mol%), KOH (4.1 mg, 0.075 mmol, 15 mol %), *(R)*-(+)-2-methyl-2-propanesulfinamide (61 mg, 0.5 mmol, 1.0 equiv.), 1-(4-fluorophenyl)ethan-1-ol (70 mg, 0.5 mmol, 1.0 equiv.) and toluene (1 mL). The reaction vessel was heated for 6 h in a silicone oil bath at 120 °C. The crude product was purified via flash chromatography with EtOAc in Hexanes (gradient from 0% to 100% EtOAc) to give a colorless oil (107 mg, 89% isolated yield, >95:5 dr (R,R : R,S)). HRMS (ESI/MeOH) *m/z* calcd for $C_{12}H_{18}FNOS$ (M + Na)[+]: 266.0991, Found: 266.0989. ^{1}H NMR (500 MHz, CDCl3) δ 7.42 – 7.34 (m, 2H), 7.08 (t, *J* = 8.6 Hz, 2H), 4.63-4.55 (m, 1H), 3.45 (br, s, 1H), 1.55 (d, *J* = 6.6 Hz, 3H), 1.29 (s, 9H). ^{13}C NMR (125 MHz, CDCl3) δ 163.3, 161.3, 139.9, 128.4, 128.3, 115.7, 115.6, 76.9, 55.6, 53.5, 22.9, 22.7 ppm. IR (film) 3207.5, 2975.2, 2928.5, 2868.7, 1602.9, 1509.4, 1478.5, 1455.7, 1363.6, 1220.9, 1051.1 cm^{-1}. The optical purity was measured by optical rotation of the corresponding chiral amine using a polarimeter. The chiral amine was obtained through treatment of the reaction mixture with HCl after heating the reaction for the specified time to remove the *N*-tert-butane sulfinyl group. Optical rotation of α-*(R)*-(+)-*p*-

fluorophenylethylamine $[\alpha]_D^{24.3}$ = +24.6° (c = 1.0, MeOH). All spectroscopic data match previously reported values of the amine product.[47]

(*R*)-2-methyl-*N*-((*R*)-1-(4-(trifluoromethyl)phenyl)ethyl)propane-2-sulfinamide (6f). The general procedure for Table 3.1 was followed using [RuHCl(CO)(HN(CH$_2$CH$_2$PPh$_2$)$_2$)] (3.0 mg, 0.05 mmol, 1 mol%), KOH (4.1 mg, 0.075 mmol, 15 mol %), (*R*)-(+)-2-methyl-2-propanesulfinamide (61 mg, 0.5 mmol, 1.0 equiv.), 1-(4-(trifluoromethyl)phenyl)ethan-1-ol (95 mg, 0.5 mmol, 1.0 equiv.) and toluene (1 mL). The reaction vessel was heated for 12 h in a silicone oil bath at 120 °C. The crude product was purified via flash chromatography with EtOAc in Hexanes (gradient from 0% to 100% EtOAc) to give a colorless oil (107 mg, 73% isolated yield, >95:5 dr (R,R : R,S)). ^{1}H NMR (500 MHz, CDCl$_3$) δ 7.61 (d, *J* = 8.0 Hz, 2H), 7.48 (d, *J* = 7.9 Hz, 2H), 4.65-4.57 (m, 1H), 3.46* (s, 1H), 1.53 (d, *J* = 6.6 Hz, 3H), 1.25 (s, 9H) ppm. ^{13}C NMR (126 MHz, CDCl$_3$) δ 148.0, 129.9 (q, *J* = 30.5 Hz) 127.0, 125.8 (q, *J* = 4.0 Hz), 122.2, 55.7, 53.8, 22.9, 22.6 ppm. All spectroscopic data match previously reported values.[43]

(*R*)-*N*-((*R*)-1-(4-methoxyphenyl)ethyl)-2-methylpropane-2-sulfinamide (6g). The general procedure for Table 3.1 was followed using [RuHCl(CO)(HN(CH$_2$CH$_2$PPh$_2$)$_2$)] (3.0 mg, 0.05 mmol, 1 mol%), KOH (4.1 mg, 0.075 mmol, 15 mol %), (*R*)-(+)-2-methyl-2-propanesulfinamide (61 mg, 0.5 mmol, 1.0 equiv.), 1-(4-methoxyphenyl)ethan-1-ol (76 mg, 0.5 mmol, 1.0 equiv.) and toluene (1 mL). The reaction vessel was heated for 10 h in a silicone oil bath at 120 °C. The crude product was purified via flash chromatography with EtOAc in Hexanes (gradient from 0% to 100% EtOAc) to give a colorless oil (63.7 mg, 50% isolated yield, >95:5 dr (R,R : R,S)). ^{1}H NMR (500 MHz, CDCl$_3$) δ 7.27 (d, *J* = 9.0 Hz, 2H) 6.88 (d, *J* = 9.0 Hz, 2H), 4.55-4.47 (m, 1 H), 3.80 (s, 3H), 3.34* (br, s, 1H), 1.49 (d, *J* = 5.0 Hz, 3H), 1.23 (s, 9H) ppm. ^{13}C NMR (125 MHz, CDCl$_3$) δ 159.2,

136.3, 127.8, 114.1, 55.4, 55.3, 53.4, 22.8, 22.7 ppm. All spectroscopic data match previously reported values.[43]

(R)-2-methyl-N-((R)-1-(pyridin-3-yl)ethyl)propane-2-sulfinamide (6h). The general procedure for Table 3.1 was followed using [RuHCl(CO)(HN(CH$_2$CH$_2$PPh$_2$)$_2$)] (3.0 mg, 0.05 mmol, 1 mol%), KOH (4.1 mg, 0.075 mmol, 15 mol %), *(R)*-(+)-2-methyl-2-propanesulfinamide (61 mg, 0.5 mmol, 1.0 equiv.), 1-(pyridin-3-yl)ethan-1-ol (61.5 mg, 0.5 mmol, 1.0 equiv.) and toluene (1 mL). The reaction vessel was heated for 7 h in a silicone oil bath at 120 °C. The crude product was purified via flash chromatography with EtOAc in Hexanes (gradient from 0% to 100% EtOAc) to give a colorless oil (90.4 mg, 80% isolated yield, >95:5 dr (R,R : R,S)). ^{1}H NMR (500 MHz, CDCl$_3$) δ 8.61 (s, 1H), 8.55 (d, *J* = 3.5 Hz, 1H), 7.70 (d, *J* = 7.8 Hz, 1H), 7.34 – 7.24 (m, 1H), 4.63-4.55 (m, 1H), 3.51* (br, s, 1H), 1.56 (d, *J* = 6.6 Hz, 3H), 1.24 (s, 9H) ppm. ^{13}C NMR (125 MHz, CDCl$_3$) δ 149.3, 148.4, 139.4, 134.4, 123.7, 55.7, 52.1, 22.8, 22.6 ppm. All spectroscopic data match previously reported values.[44]

(R)-2-methyl-N-((R)-1-(pyridin-2-yl)ethyl)propane-2-sulfinamide (6i). The general procedure for Table 3.1 was followed using [RuHCl(CO)(HN(CH$_2$CH$_2$PPh$_2$)$_2$)] (3.0 mg, 0.05 mmol, 1 mol%), KOH (4.1 mg, 0.075 mmol, 15 mol %), *(R)*-(+)-2-methyl-2-propanesulfinamide (61 mg, 0.5 mmol, 1.0 equiv.), 1-(pyridin-2-yl)ethan-1-ol (61 mg, 0.5 mmol, 1.0 equiv.) and toluene (1 mL). The reaction vessel was heated for 6 h in a silicone oil bath at 120 °C. The crude product was purified via flash chromatography with EtOAc in Hexanes (gradient from 0% to 100% EtOAc) to give a colorless oil (62 mg, 55% isolated yield, >95:5 dr (R,R : R,S)). ^{1}H NMR (500 MHz, CDCl$_3$) δ 8.56 (d, 1H, J = 4.8 Hz), 7.68 (dt, 1H, J = 7.8, 1.5 Hz), 7.30 (d, 1H, J = 7.5 Hz), 7.21 (dd, 1H, J = 5.0, 2.0 Hz), 4.85 (br, s, 1H), 4.66–4.55 (m, 1H), 1.51* (d, 3H, J = 6.5 Hz), 1.26 (s, 9H). ^{13}C

NMR (126 MHz, CDCl$_3$) δ 161.8, 149.0, 136.8, 122.3, 121.0, 55.6, 55.2, 23.3, 22.7 ppm. All spectroscopic data match previously reported values.[44]

(R)-2-methyl-N-((R)-1-(pyridin-4-yl)ethyl)propane-2-sulfinamide (6j). The general procedure for Table 3.1 was followed using [RuHCl(CO)(HN(CH$_2$CH$_2$PPh$_2$)$_2$)] (3.0 mg, 0.05 mmol, 1 mol%), KOH (4.1 mg, 0.075 mmol, 15 mol %), *(R)*-(+)-2-methyl-2-propanesulfinamide (61 mg, 0.5 mmol, 1.0 equiv.), 1-(pyridin-4-yl)ethan-1-ol (61 mg, 0.5 mmol, 1.0 equiv.) and toluene (1 mL). The reaction vessel was heated for 6 h in a silicone oil bath at 120 °C. The crude product was purified via flash chromatography with EtOAc in Hexanes (gradient from 0% to 100% EtOAc) to give a colorless oil (83 mg, 74% isolated yield, >95:5 dr (R,R : R,S)). ^{1}H NMR (500 MHz, CDCl$_3$) δ 8.58 (d, *J* = 5.5 Hz, 2H), 7.29 (d, *J* = 5.5 Hz, 2H), 4.59–4.49 (m, 1H), 3.65* (br, s, 1H), 1.52 (d, *J* = 6.1 Hz, 3H), 1.25 (s, 9H) ppm. ^{13}C NMR (126 MHz, CDCl$_3$) δ 152.7, 149.9, 121.5, 55.7, 53.3, 22.5, 22.4 ppm. All spectroscopic data match previously reported values.[44]

(R)-2-methyl-N-((R)-1-(naphthalen-2-yl)ethyl)propane-2-sulfinamide (6k). The general procedure for Table 3.1 was followed using [RuHCl(CO)(HN(CH$_2$CH$_2$PPh$_2$)$_2$)] (3.0 mg, 0.05 mmol, 1 mol%), KOH (4.1 mg, 0.075 mmol, 15 mol %), *(R)*-(+)-2-methyl-2-propanesulfinamide (61 mg, 0.5 mmol, 1.0 equiv.), 1-(naphthalen-2-yl)ethan-1-ol (76 mg, 0.5 mmol, 1.0 equiv.) and toluene (1 mL). The reaction vessel was heated for 6 h in a silicone oil bath at 120 °C. The crude product was purified via flash chromatography with EtOAc in Hexanes (gradient from 0% to 100% EtOAc) to give a colorless solid (115 mg, 84% isolated yield, >95:5 dr (R,R : R,S)). HRMS (ESI/MeOH) *m/z* calcd for C$_{16}$H$_{21}$NOS (M + Na)$^+$: 298.1241 Found: 298.1231 . ^{1}H NMR (500 MHz, CDCl$_3$) δ 7.84 – 7.75 (m, 4H), 7.53 – 7.38 (m, 3H), 4.84 – 4.61 (m, 1H), 3.50* (br, s, 1H), 1.61 (d, *J* = 6.1 Hz, 3H), 1.26 (s, 9H) ppm. ^{13}C NMR (126 MHz, CDCl$_3$) δ 141.45, 133.45, 133.15, 128.80, 128.10, 127.82, 126.45, 126.22, 125.49, 124.85, 55.66, 54.16, 22.78, 22.75 ppm. IR (film)

3294.3, 3253.9, 3055.2, 3016.4, 2978.7, 2955.3, 2926.4, 2898.7, 2865.3, 1601.1, 1507.85, 1471.2 1385.1, 1358.5, 1058.0 cm^{-1}. The optical purity was measured by the optical rotation of the corresponding chiral amine using a polarimeter. The chiral amine was obtained through treatment of the reaction mixture with HCl after heating the reaction for the specified time to remove the *N*-tert-butanesulfinyl group. Optical rotation of *(R)*-(+)-1-(naphthalen-2-yl)ethan-1-amine $[\alpha]_D^{24.3} =$ +19.6° (c = 1.0, MeOH). All spectroscopic data match previously reported values of the amine product.[48]

(R)-2-methyl-*N*-((R)-4-phenylbutan-2-yl)propane-2-sulfinamide (6l). The general procedure for Table 3.1 was followed using [RuHCl(CO)(HN(CH$_2$CH$_2$PPh$_2$)$_2$)] (3.0 mg, 0.05 mmol, 1 mol%), KOH (4.1 mg, 0.075 mmol, 15 mol %), *(R)*-(+)-2-methyl-2-propanesulfinamide (61 mg, 0.5 mmol, 1.0 equiv.), 1 4-phenylbutan-2-ol (75 mg, 0.5 mmol, 1.0 equiv.) and toluene (1 mL). The reaction vessel was heated for 12 h in a silicone oil bath at 120 °C. The crude product was purified via flash chromatography with EtOAc in Hexanes (gradient from 0% to 100% EtOAc) to give a colorless oil (90.4 mg, 75% isolated yield, 75:25 dr (R,R : R,S)). ^{1}H NMR (500 MHz, CDCl$_3$) δ 7.28 – 7.14 (m, 5H), 3.43 (m, 1H), 3.09* (br, s, 1H), 2.71 (m, 2H), 1.98 – 1.74 (m, 2H), 1.23 (d, *J* = 6.4 Hz, 3H), 1.19 (s, 9H) ppm. ^{13}C NMR (125 MHz, CDCl$_3$) δ 141.6, 128.5, 128.5, 126.0, 55.4, 51.1, 40.0, 32.2, 22.6, 21.7 ppm. All spectroscopic data match previously reported values.[43]

(R)-*N*-((R)-hexan-2-yl)-2-methylpropane-2-sulfinamide (6m). The general procedure for Table 3.1 was followed using [RuHCl(CO)(HN(CH$_2$CH$_2$PPh$_2$)$_2$)] (3.0 mg, 0.05 mmol, 1 mol%), KOH (4.1 mg, 0.075 mmol, 15 mol %), *(R)*-(+)-2-methyl-2-propanesulfinamide (61 mg, 0.5 mmol, 1.0 equiv.), 2-hexanol (51 mg, 0.5 mmol, 1.0 equiv.) and toluene (1 mL). The reaction vessel was heated for 10 h in a silicone oil bath at 120 °C. The crude product was purified via flash

chromatography with EtOAc in Hexanes (gradient from 0% to 100% EtOAc) to give a tan oil (83.5 mg, 81% isolated yield, 99:1 dr (R,R : R,S)). ^{1}H NMR (500 MHz, CDCl$_3$) δ 3.41-3.32 (m, 1H), 3.03* (br, s, 1H), 1.61-1.41 (m, 2H), 1.35-1.30 (m, 4H), 1.19 (s, 9H), 1.15 (d, *J* = 8.0, 3H), 0.91 (m, 3H) ppm. ^{13}C NMR (125 MHz, CDCl$_3$) δ 55.1, 51.2, 38.1, 27.9, 22.5, 22.4, 21.3, 13.9 ppm. All spectroscopic data match previously reported values.[45]

(*R*)-2-methyl-*N*-((*R*)-3-methylbutan-2-yl)propane-2-sulfinamide (6n). The general procedure for Table 3.1 was followed using [RuHCl(CO)(HN(CH$_2$CH$_2$PPh$_2$)$_2$)] (3.0 mg, 0.05 mmol, 1 mol%), KOH (4.1 mg, 0.075 mmol, 15 mol %), *(R)*-(+)-2-methyl-2-propanesulfinamide (61 mg, 0.5 mmol, 1.0 equiv.), 3-methyl-butan-2-ol (44 mg, 0.5 mmol, 1.0 equiv.) and toluene (1 mL). The reaction vessel was heated for 6 h in a silicone oil bath at 120 °C. The crude product was purified via flash chromatography with EtOAc in Hexanes (gradient from 0% to 100% EtOAc) to give a colorless oil (56 mg, 59% isolated yield, >95:5 dr (R,R : R,S)). ^{1}H NMR (500 MHz, CDCl$_3$) δ 3.38 – 3.29 (m, 1H), 3.24* (br, s, 1H), 1.82 (qt, *J* = 13.8, 6.8 Hz, 1H), 1.27 (d, *J* = 11.1 Hz, 9H), 1.15 (d, *J* = 6.5 Hz, 3H), 0.97 (dd, *J* = 15.7, 8.0 Hz, 6H) ppm. ^{13}C NMR (126 MHz, CDCl$_3$) δ 55.8, 34.0, 22.6, 18.8, 17.2, 16.8 ppm. All spectroscopic data match previously reported values.[45]

(*R*)-2-methyl-*N*-((*R*)-1,2,3,4-tetrahydronaphthalen-1-yl)propane-2-sulfinamide (6o). The general procedure for Table 3.1 was followed using [RuHCl(CO)(HN(CH$_2$CH$_2$PPh$_2$)$_2$)] (3.0 mg, 0.05 mmol, 1 mol%), KOH (4.1 mg, 0.075 mmol, 15 mol %), *(R)*-(+)-2-methyl-2-propanesulfinamide (61 mg, 0.5 mmol, 1.0 equiv.), 1,2,3,4-tetrahydronaphthalen-1-ol (76 mg, 0.5 mmol, 1.0 equiv.) and toluene (1 mL). The reaction vessel was heated for 6 h in a silicone oil bath at 120 °C. The crude product was purified via flash chromatography with EtOAc in Hexanes (gradient from 0% to 100% EtOAc) to give a brown oil (43.9 mg, 36% isolated yield, >95:5 dr (R,R : R,S)). ^{1}H NMR (500 MHz, CDCl$_3$) δ 7.47 (dd, *J* = 5.0 , 3.5 Hz, 1H), 7.24-7.16 (m, 2H),

7.09 (dd, J = 5.0, 3.5 Hz, 1H), 4.58-4.55 (m, 1H), 3.21* (d, J = 2.5 Hz, 1H), 2.89-2.65 (m, 2H), 2.05-1.83 (m, 3H), 1.80-1.73 (m, 1H), 1.20 (s, 9H) ppm. ^{13}C NMR (125 MHz, CDCl$_3$) δ 137.8, 136.7, 129.7, 129.3, 127.6, 126.6, 55.5, 52.8, 30.6, 29.1, 22.7, 18.2 ppm. All spectroscopic data match previously reported values.[45]

(*R*)-2-methyl-N-((*R*)-1-phenylpropyl)propane-2-sulfinamide (6p). The general procedure for Table 3.1 was followed using [RuHCl(CO)(HN(CH$_2$CH$_2$PPh$_2$)$_2$)] (3.0 mg, 0.05 mmol, 1 mol%), KOH (4.1 mg, 0.075 mmol, 15 mol %), *(R)*-(+)-2-methyl-2-propanesulfinamide (61 mg, 0.5 mmol, 1.0 equiv.), 1-phenyl-1-propanol (68 mg, 0.5 mmol, 1.0 equiv.) and toluene (1 mL). The reaction vessel was heated for 12 h in a silicone oil bath at 120 °C. The crude product was purified via flash chromatography with EtOAc in Hexanes (gradient from 0% to 100% EtOAc) to give a colorless oil (38.4 mg, 32% isolated yield, >95:5 dr (R,R : R,S)). ^{1}H NMR (500 MHz, CDCl$_3$) δ 7.39 – 7.21 (m, 5H), 4.33 – 4.20 (m, 1H), 3.53* (br, s, 1H), 2.09 – 1.99 (m, 1H), 1.86 – 1.66 (m, 1H), 1.23 (s, 9H), 0.80 (t, J = 7.4 Hz, 3H). ^{13}C NMR (126 MHz, CDCl$_3$) δ 142.3, 128.7, 127.9, 127.3, 60.6, 55.8, 29.4, 22.7, 10.1. All spectroscopic data match previously reported values.[43]

¹H NMR spectrum of *6b* (CDCl₃, 25° C)
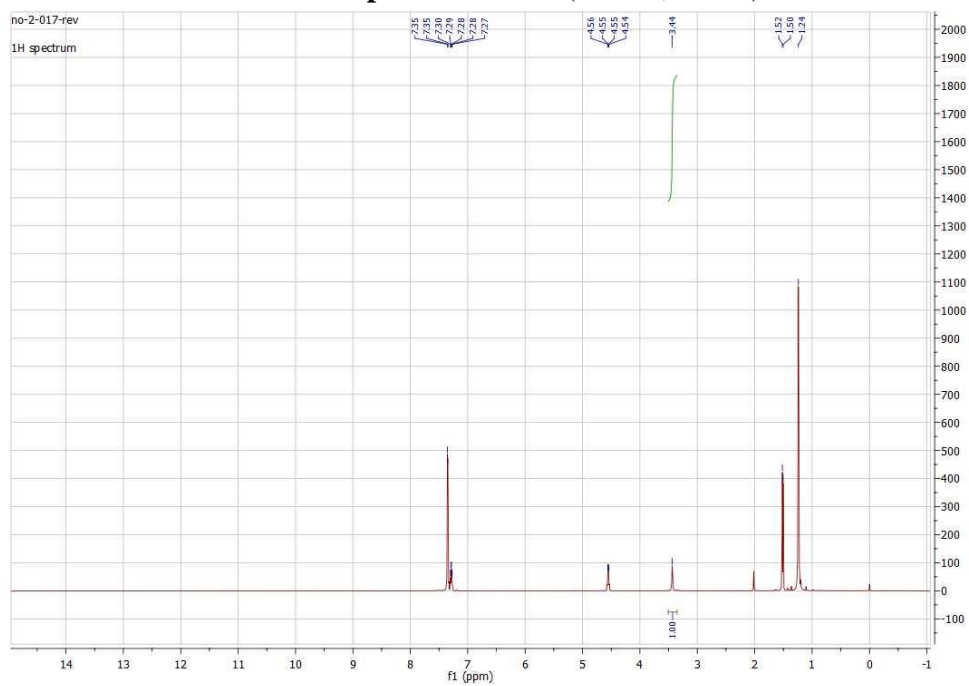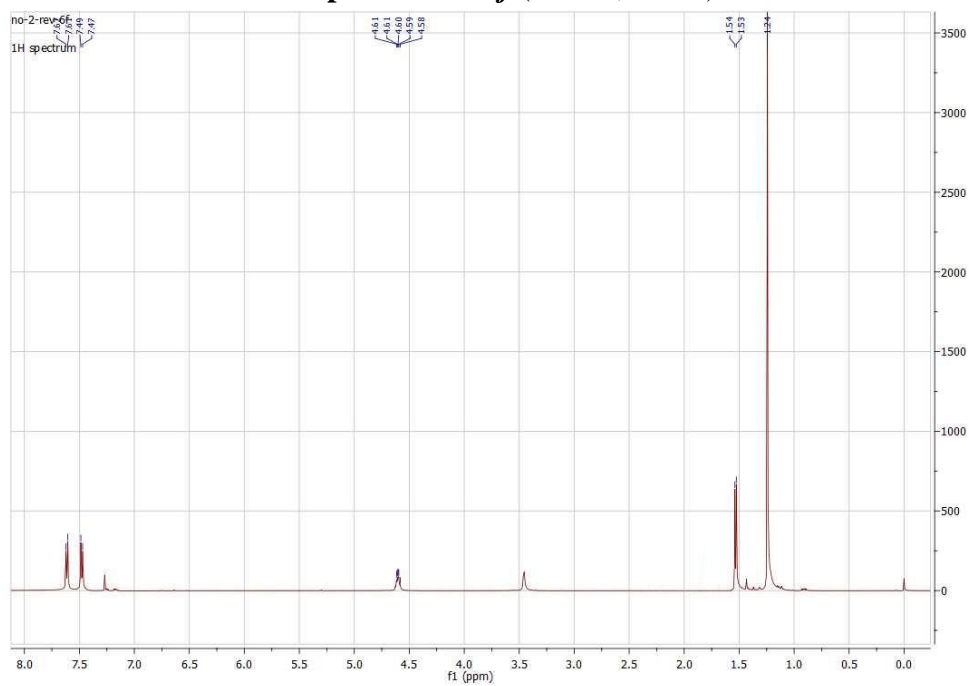

¹H and ¹³C NMR spectra of *6c* (CDCl₃, 25° C)
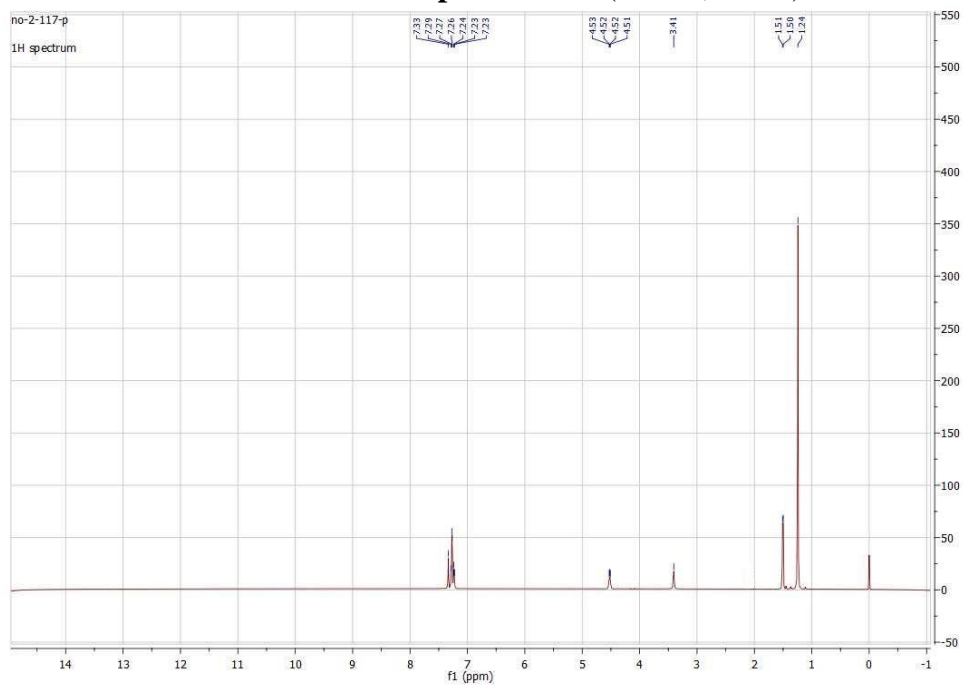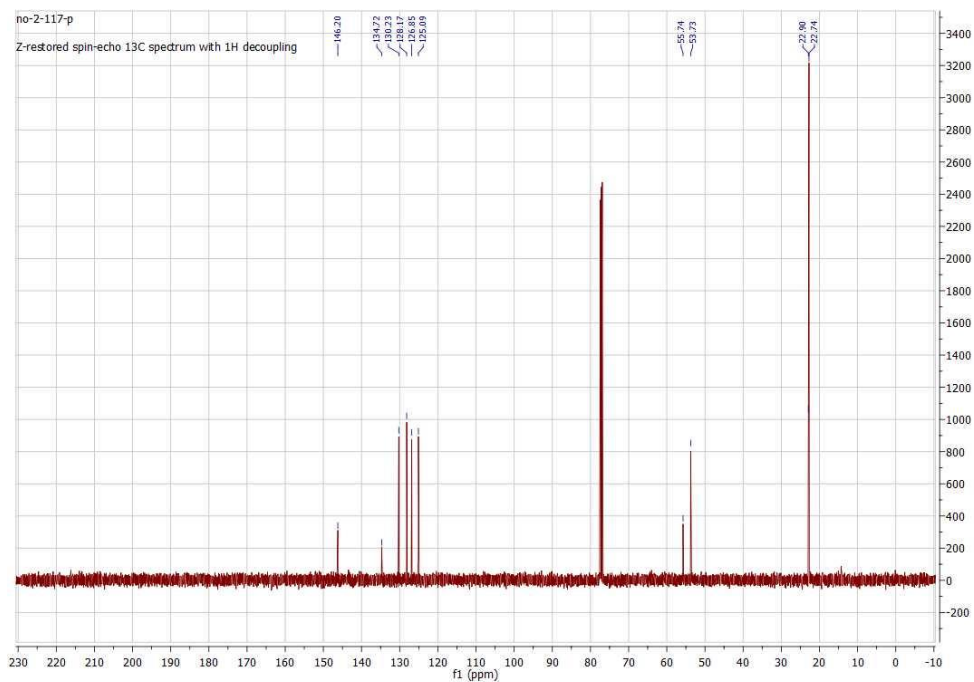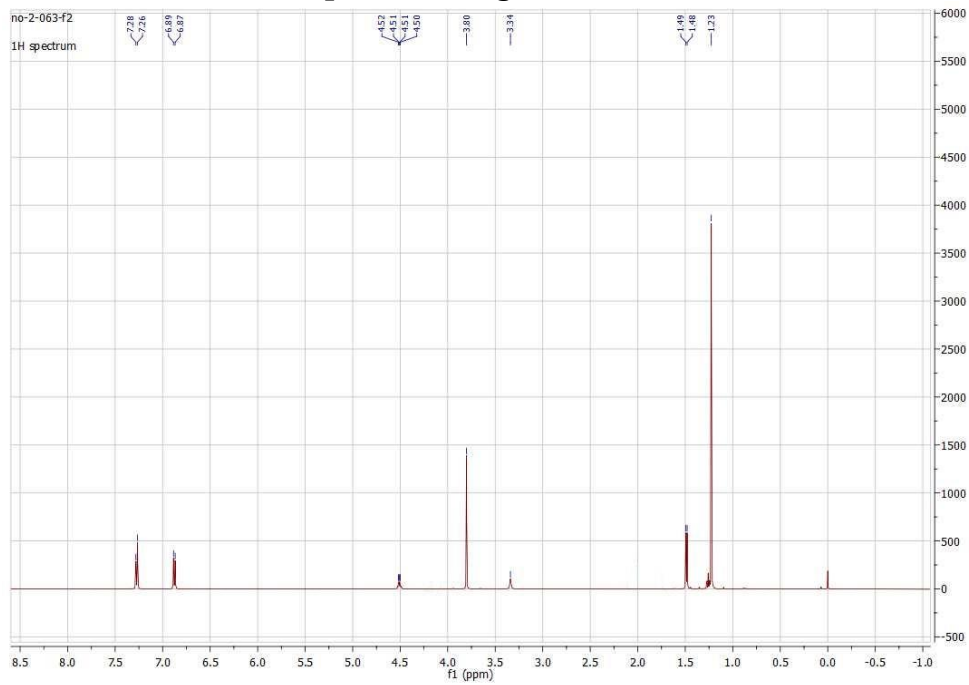
¹H and spectra of *6d* (CDCl₃, 25° C)
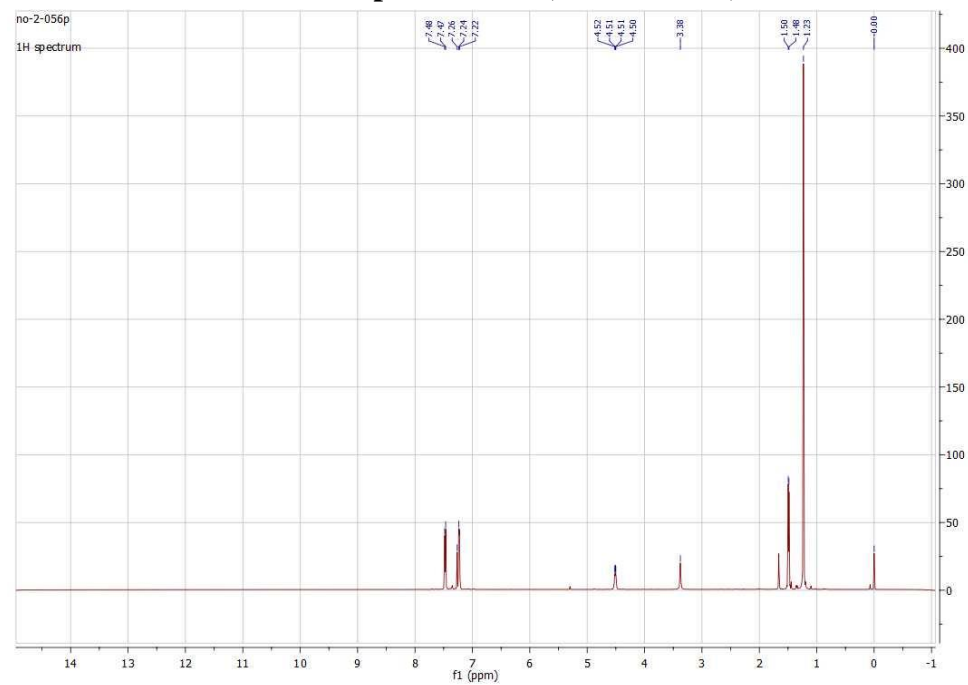
^{1}H and ^{13}C NMR spectra of *6e* (CDCl$_3$, 25° C)
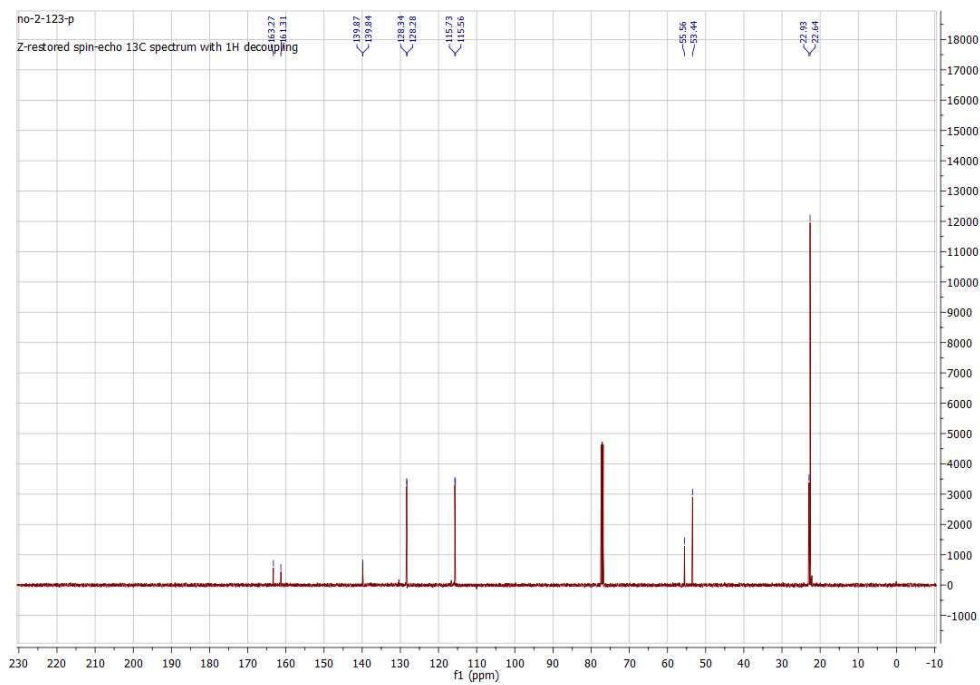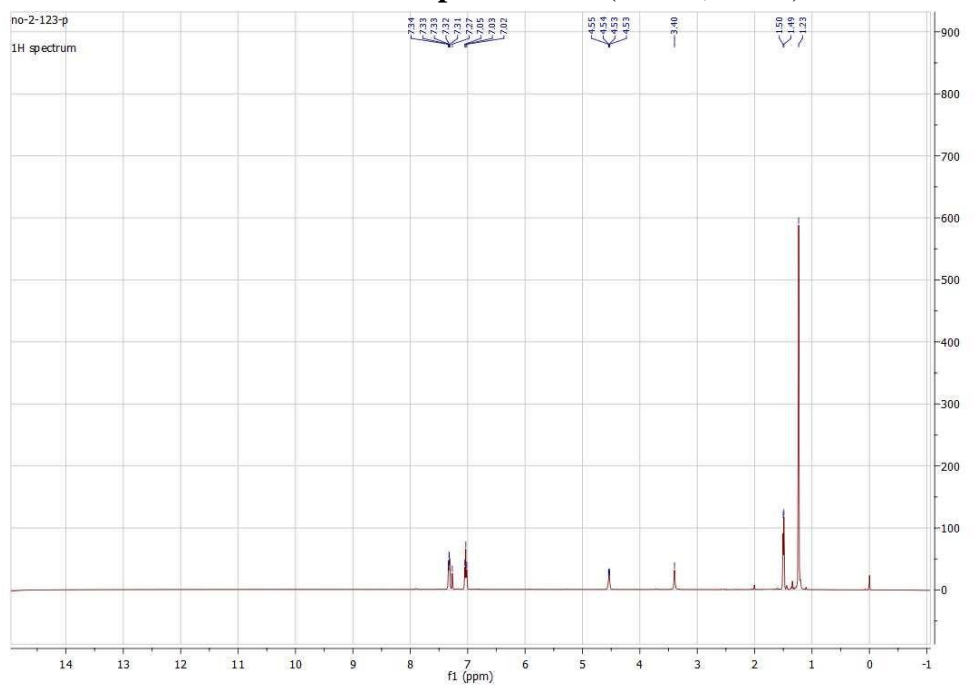
¹H spectrum of *6f* (CDCl₃, 25° C)

¹H spectrum of *6g* (CDCl₃, 25° C)

^{1}**H spectrum of** *6h* (CDCl$_3$, 25° C)
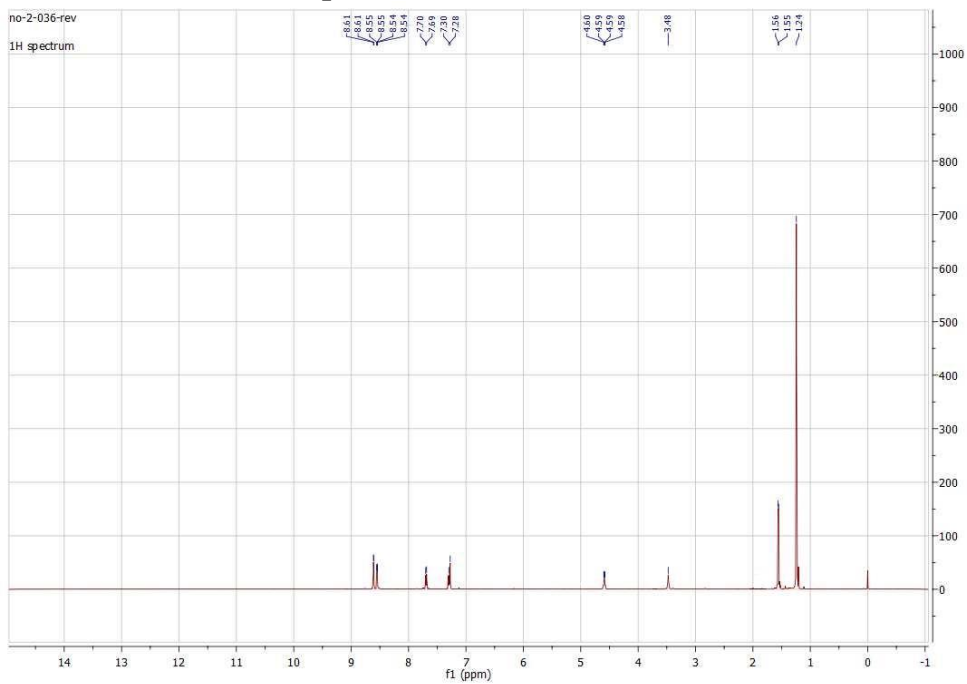
^{1}**H spectrum of** *6i* (CDCl$_3$, 25° C)
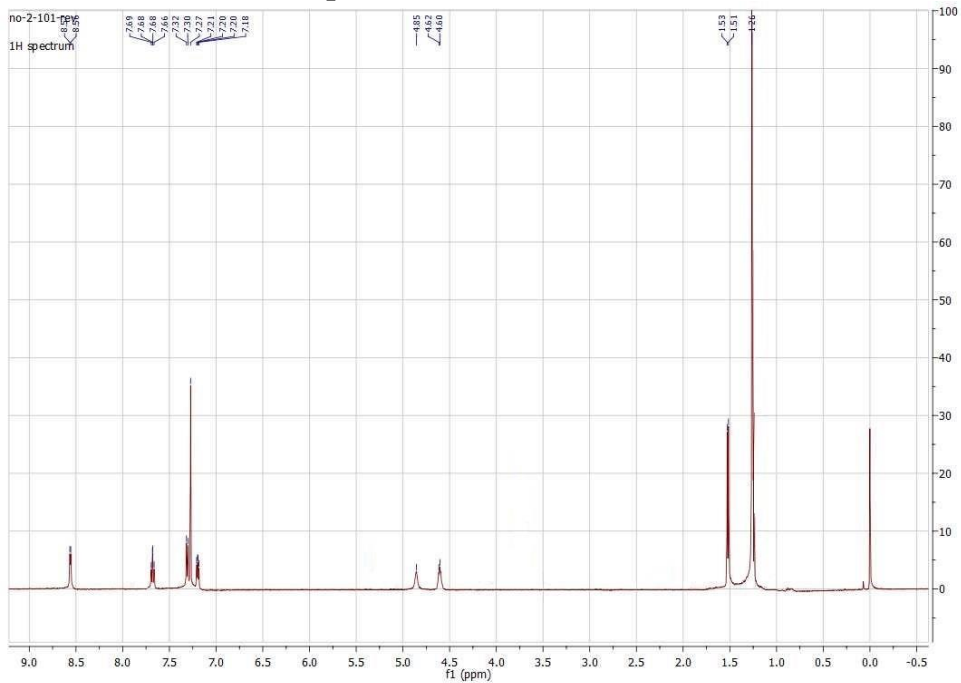
^{1}H spectrum of *6j* (CDCl$_3$, 25° C)
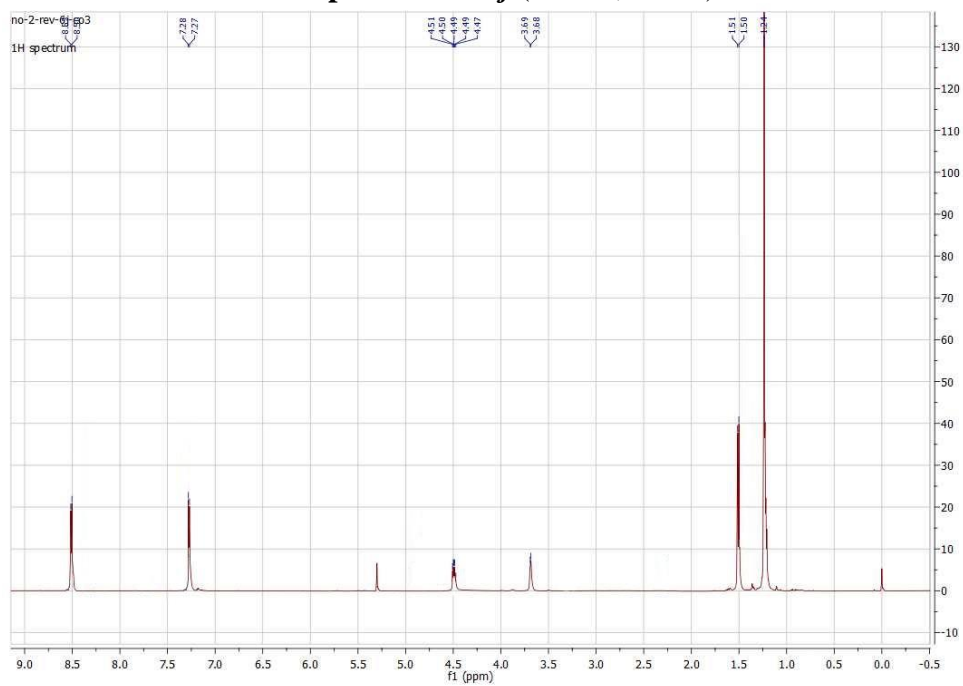
^{1}H spectrum of *6k* (CDCl$_3$, 25° C)
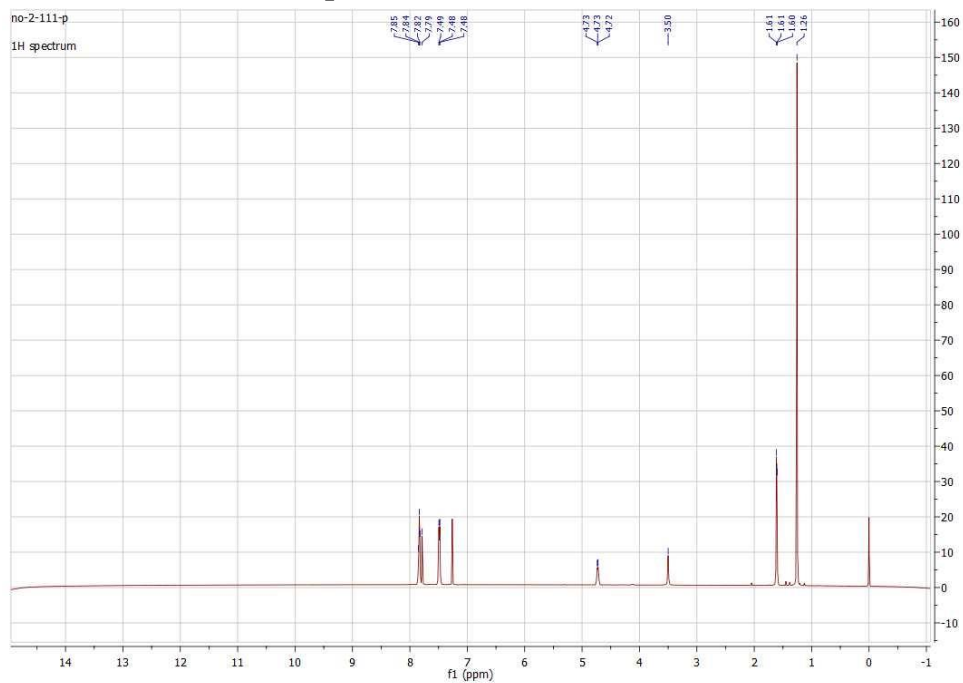
^{1}H and ^{13}C NMR spectra of *6l* (CDCl$_3$, 25° C)

no-2-052p

1H spectrum

no-2-111-p

Z-restored spin-echo 13C spectrum with 1H decoupling
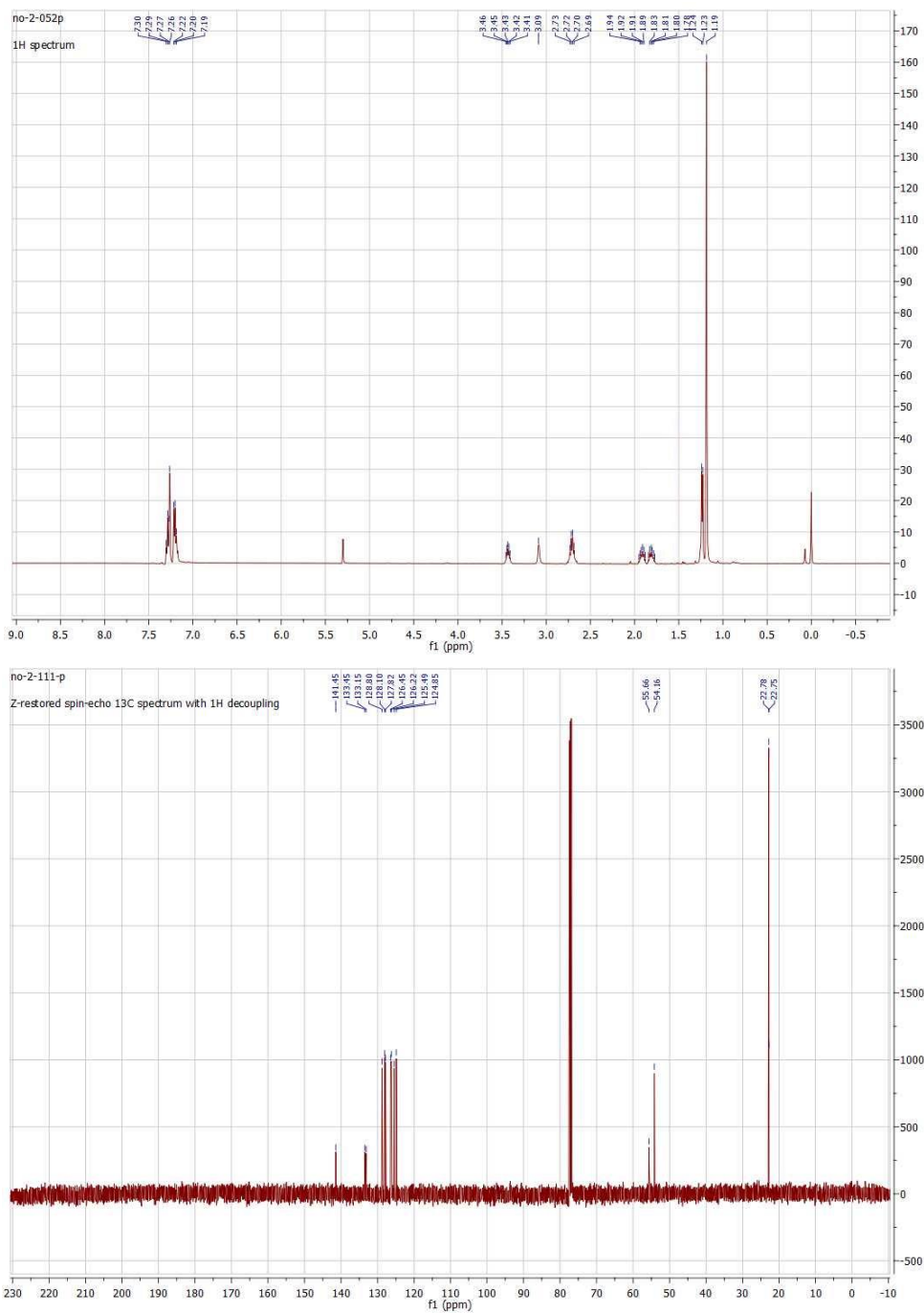
^{1}**H spectrum of *6m*** (CDCl$_3$, 25° C)
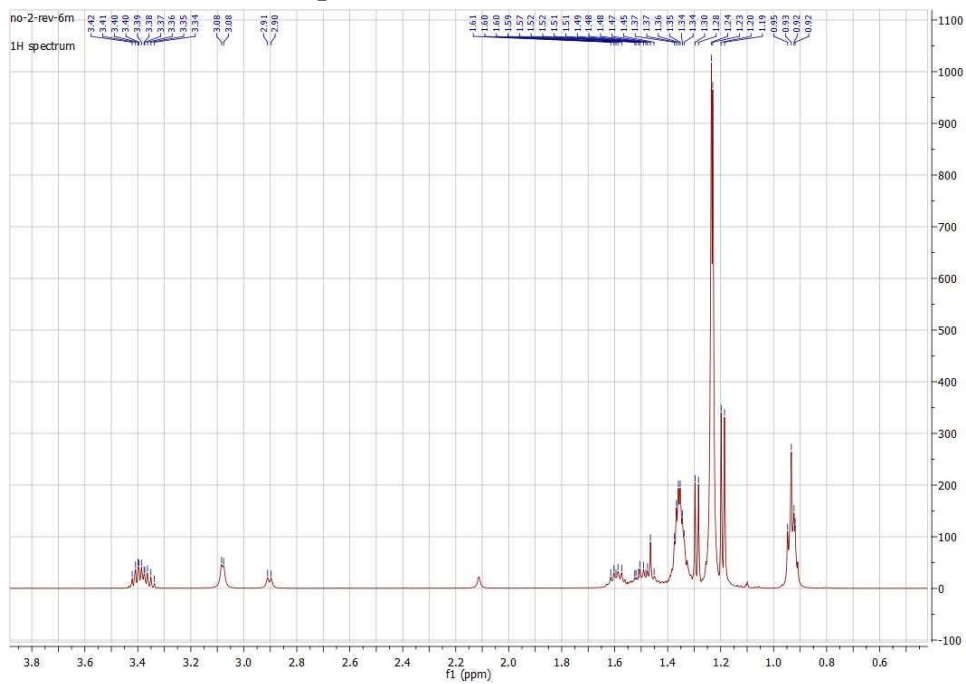
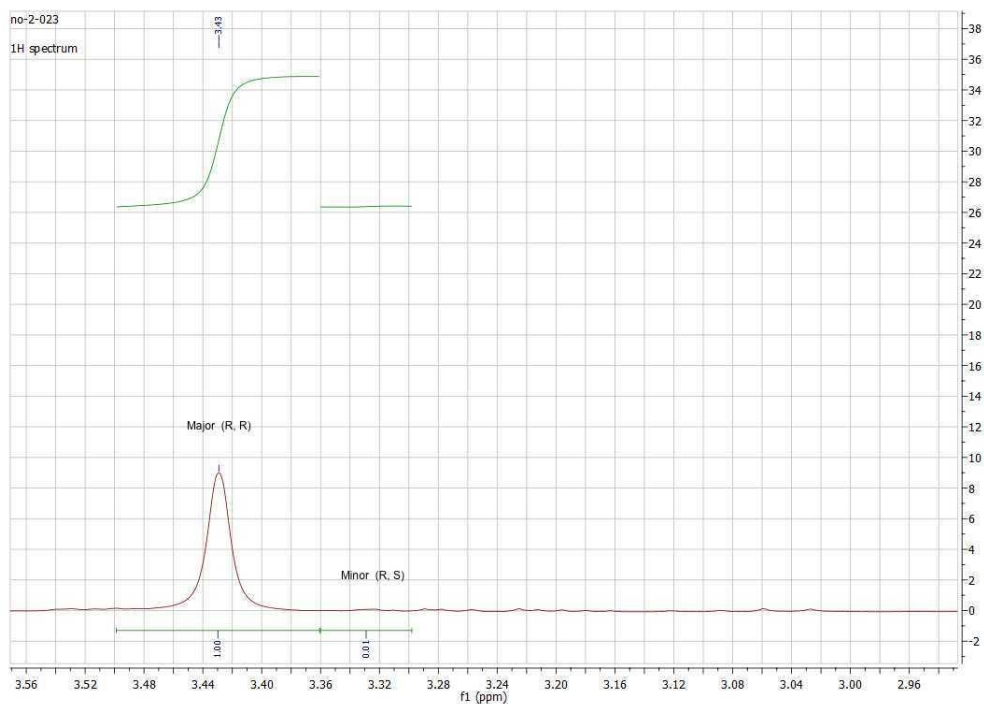# ^{1}**H spectrum of *6n*** (CDCl$_3$, 25° C)
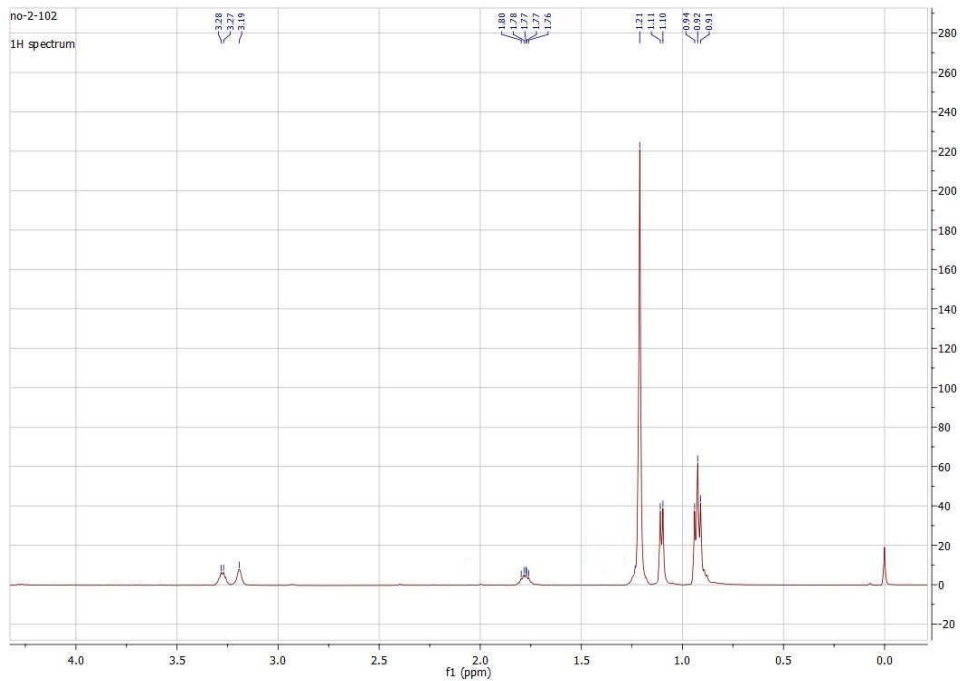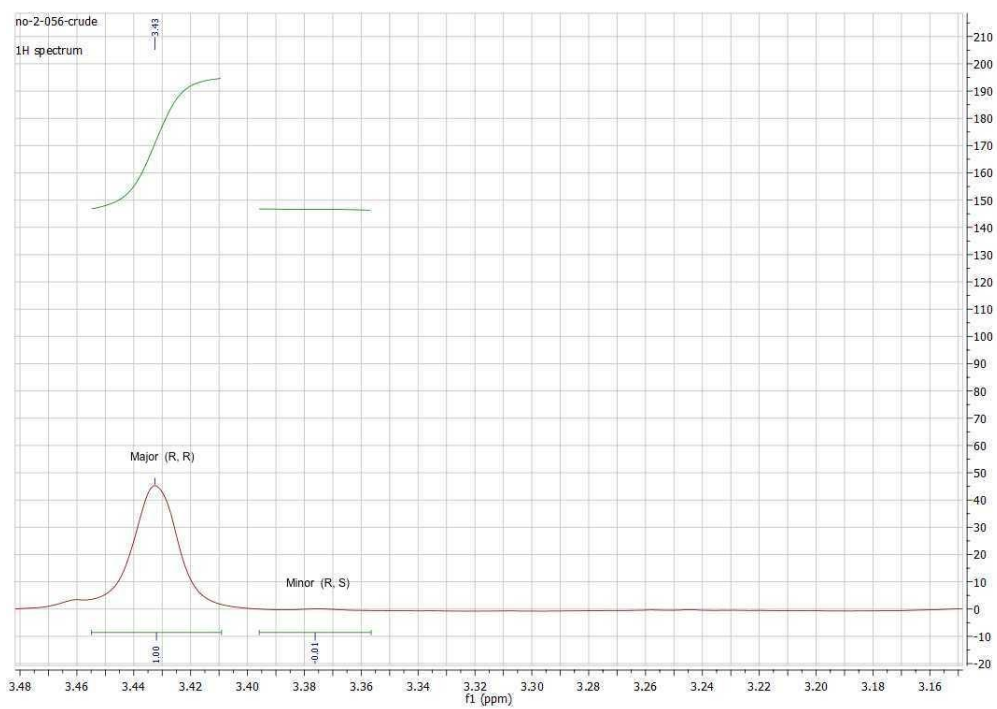
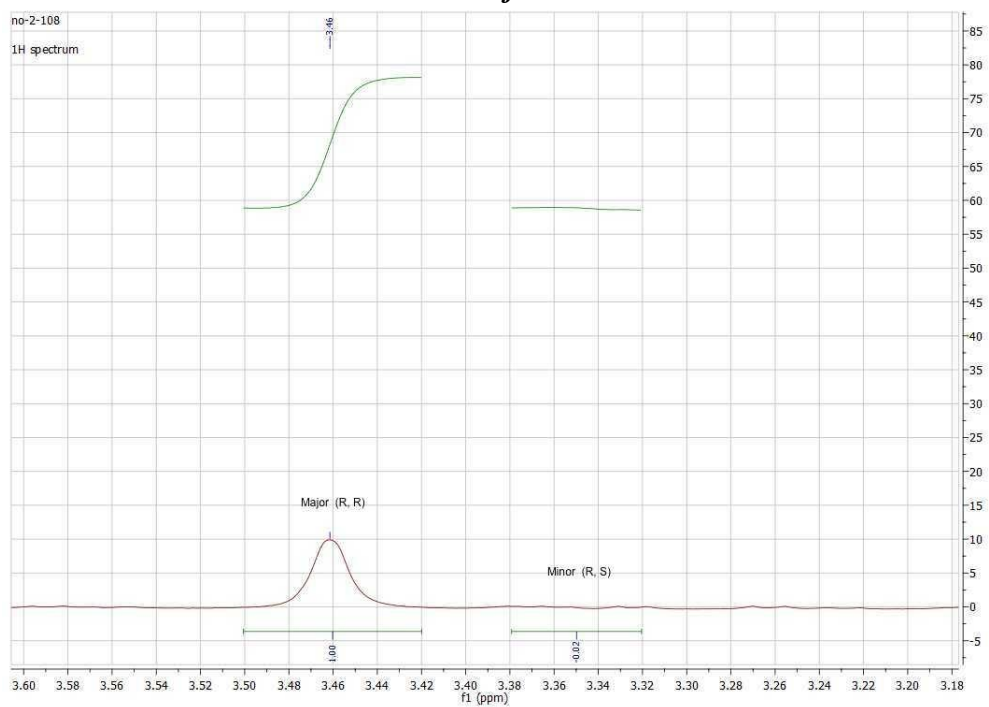# ^{1}**H spectrum of** *6o* (CDCl$_3$, 25° C)
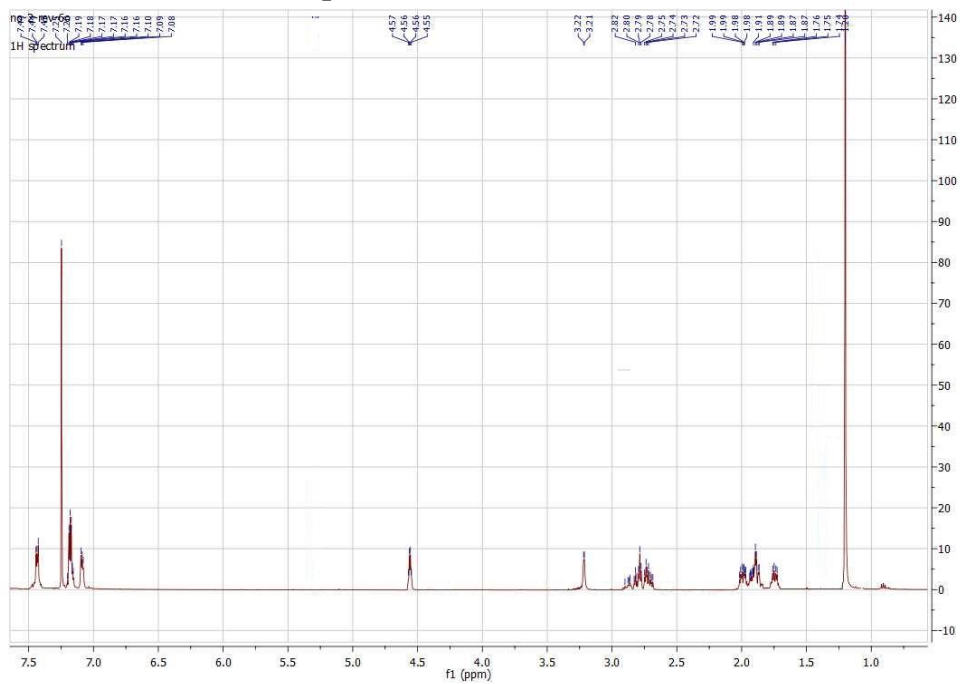
^{1}**H spectrum of** *6p* (CDCl$_3$, 25° C)
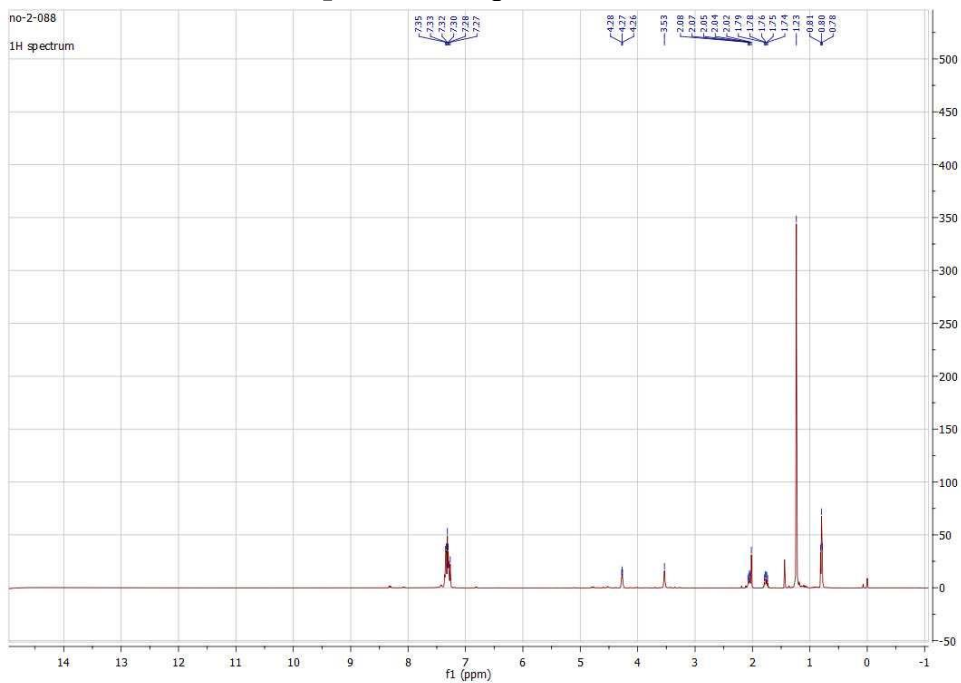
¹H NMR of reaction mixture used for dr calculations
6b

6d

6f

6g

6h

no-2-048-crude

1H spectrum

3.53

Major (R, R)

Minor (R, S)

1.00

0.01

f1 (ppm)

6i

no-2-101

1H spectrum

Major (R, R)

Minor (R, S)

-0.02

1.00

f1 (ppm)

6j

no-2-04

1H spectrum

—3.65

Major (R, R)

Minor (R, S)

1.00   0.01

3.72 3.71 3.70 3.69 3.68 3.67 3.66 3.65 3.64 3.63 3.62 3.61 3.60 3.59 3.58 3.57 3.56 3.55 3.54 3.53 3.52 3.51
f1 (ppm)

6l

no-2-052

1H spectrum

—3.10   —2.94
         —2.93

Major (R, R)

Minor (R, S)

1.00   0.50

3.22 3.20 3.18 3.16 3.14 3.12 3.10 3.08 3.06 3.04 3.02 3.00 2.98 2.96 2.94 2.92 2.90 2.88 2.86 2.84 2.82 2.80 2.78
f1 (ppm)

80

6m

6n

81

6o

6p

3.5 Reference

1.   Nugent, T. C., *Chiral Amine Synthesis: Methods, Developments and Applications*. WILEY-VCH Verlag GmbH & Co. KGaA,Weinheim: 2010.

2.   Nugent, T. C.; El-Shazly, M., Chiral Amine Synthesis - Recent Developments and Trends for Enamide Reduction, Reductive Amination, and Imine Reduction (vol 352, pg 753, 2010). *Adv. Synth. Catal.* **2011,** *353* (6), Cp6-Cp6.

3.   Robak, M. T.; Herbage, M. A.; Ellman, J. A., Synthesis and Applications of tert-Butanesulfinamide. *Chem. Rev.* **2010,** *110* (6), 3600-3740.

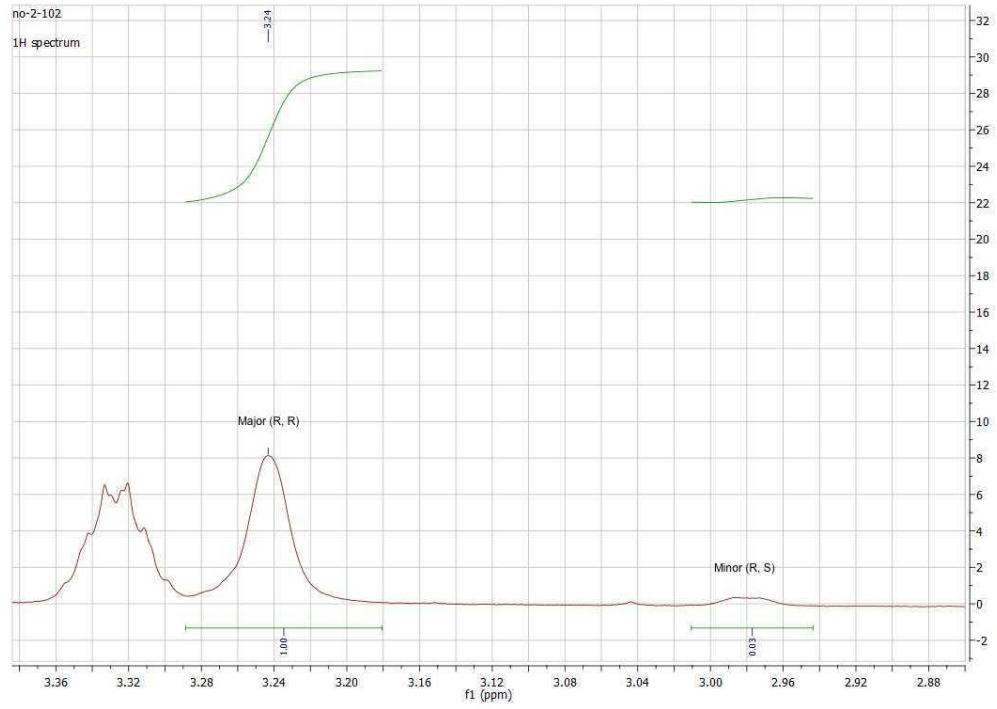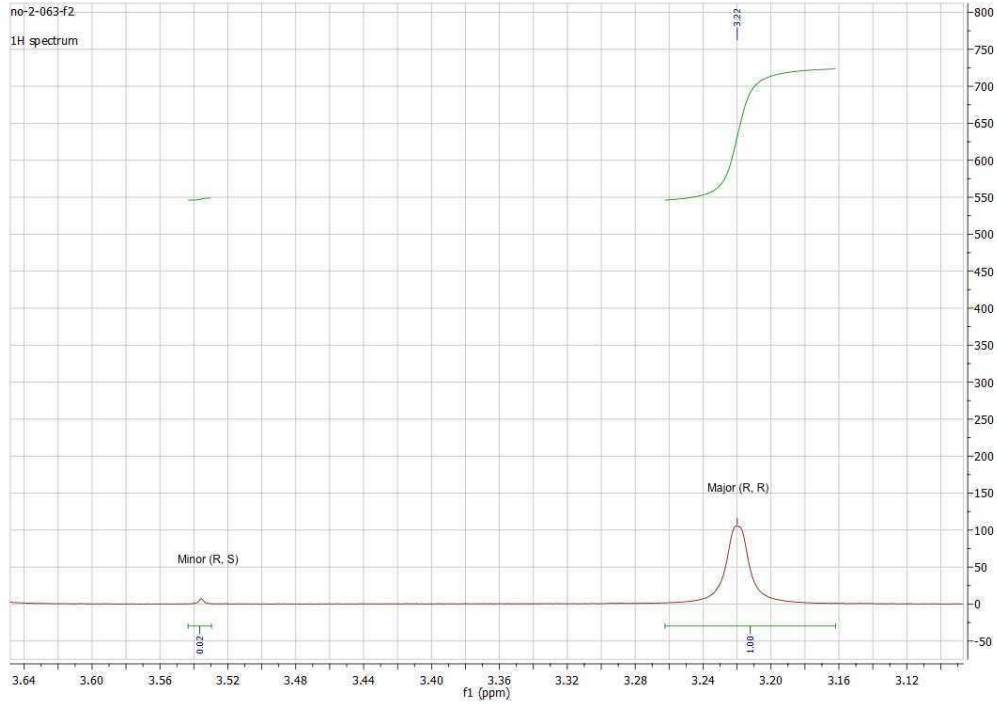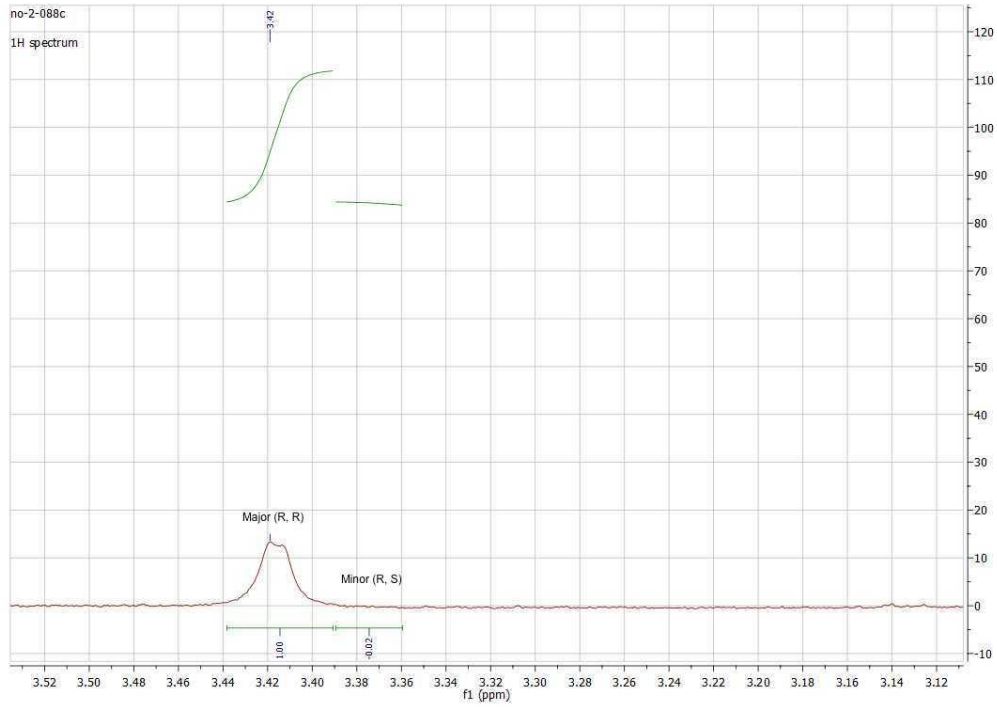4.   Liu, G. C.; Cogan, D. A.; Ellman, J. A., Catalytic asymmetric synthesis of tert-butanesulfinamide. Application to the asymmetric synthesis of amines. *J. Am. Chem. Soc.* **1997,** *119* (41), 9913-9914.

5.   Gunanathan, C.; Milstein, D., Selective Synthesis of Primary Amines Directly from Alcohols and Ammonia. *Angew. Chem. Int. Ed.* **2008,** *47* (45), 8661-8664.

6.   Klinkenberg, J. L.; Hartwig, J. F., Catalytic Organometallic Reactions of Ammonia. *Angew. Chem. Int. Ed.* **2011,** *50* (1), 86-95.

7.   Pingen, D.; Muller, C.; Vogt, D., Direct Amination of Secondary Alcohols Using Ammonia. *Angew. Chem. Int. Ed.* **2010,** *49* (44), 8130-8133.

8.   Bahn, S.; Imm, S.; Neubert, L.; Zhang, M.; Neumann, H.; Beller, M., The Catalytic Amination of Alcohols. *Chemcatchem* **2011,** *3* (12), 1853-1864.

9.   Watson, A. J. A.; Williams, J. M. J., The Give and Take of Alcohol Activation. *Science* **2010,** *329* (5992), 635-636.

10.   Hamid, M. H. S. A.; Slatford, P. A.; Williams, J. M. J., Borrowing hydrogen in the activation of alcohols. *Adv. Synth. Catal.* **2007,** *349* (10), 1555-1575.

11.   Guillena, G.; J. Ramón, D.; Yus, M., Hydrogen Autotransfer in the N-Alkylation of Amines and Related Compounds using Alcohols and Amines as Electrophiles. *Chem. Rev.* **2009,** *110* (3), 1611-1641.

12.   Dobereiner, G. E.; Crabtree, R. H., Dehydrogenation as a Substrate-Activating Strategy in Homogeneous Transition-Metal Catalysis. *Chem. Rev.* **2010,** *110* (2), 681-703.

13.   Imm, S.; Bahn, S.; Neubert, L.; Neumann, H.; Beller, M., An Efficient and General Synthesis of Primary Amines by Ruthenium-Catalyzed Amination of Secondary Alcohols with Ammonia. *Angew. Chem. Int. Ed.* **2010,** *49* (44), 8126-8129.

14.   Zhang, Y.; Lim, C. S.; Sim, D. S. B.; Pan, H. J.; Zhao, Y., Catalytic Enantioselective Amination of Alcohols by the Use of Borrowing Hydrogen Methodology: Cooperative Catalysis by Iridium and a Chiral Phosphoric Acid. *Angew. Chem. Int. Ed.* **2014,** *53* (5), 1399-1403.

15.   Monrad, R. N.; Madsen, R., Ruthenium-catalysed synthesis of 2-and 3-substituted quinolines from anilines and 1,3-diols. *Org. Biomol. Chem.* **2011,** *9* (2), 610-615.

16.   Yamaguchi, K.; He, J. L.; Oishi, T.; Mizuno, N., The "Borrowing Hydrogen Strategy" by Supported Ruthenium Hydroxide Catalysts: Synthetic Scope of Symmetrically and Unsymmetrically Substituted Amines. *Chem. Eur. J.* **2010,** *16* (24), 7199-7207.

17.   Watson, A. J. A.; Maxwell, A. C.; Williams, J. M. J., Ruthenium-Catalyzed Oxidation of Alcohols into Amides. *Org. Lett.* **2009,** *11* (12), 2667-2670.

18.   Hamid, M. H. S. A.; Allen, C. L.; Lamb, G. W.; Maxwell, A. C.; Maytum, H. C.; Watson, A. J. A.; Williams, J. M. J., Ruthenium-Catalyzed N-Alkylation of Amines and Sulfonamides Using Borrowing Hydrogen Methodology. *J. Am. Chem. Soc.* **2009,** *131* (5), 1766-1774.

19.   Zhang, J.; Balaraman, E.; Leitus, G.; Milstein, D., Electron-Rich PNP- and PNN-Type Ruthenium(II) Hydrido Borohydride Pincer Complexes. Synthesis, Structure, and Catalytic Dehydrogenation of Alcohols and Hydrogenation of Esters. *Organometallics* **2011,** *30* (21), 5716-5724.

20.   Tillack, A.; Hollmann, D.; Mevius, K.; Michalik, D.; Bahn, S.; Beller, M., Salt-free synthesis of tertiary amines by ruthenium-catalyzed amination of alcohols. *Eur. J. Org. Chem.* **2008,** (28), 4745-4750.

21.   Hollmann, D.; Tillack, A.; Michalik, D.; Jackstell, R.; Beller, M., An improved ruthenium catalyst for the environmentally benign amination of primary and secondary alcohols. *Chem-Asian J* **2007,** *2* (3), 403-410.

22.   Xiao, X.; Wang, H. W.; Huang, Z. Y.; Yang, J.; Bian, X. X.; Qin, Y., Selective diethylzinc reduction of imines in the presence of ketones catalyzed by Ni(acac)(2). *Org. Lett.* **2006,** *8* (1), 139-142.

23.   Pablo, O.; Guijarro, D.; Kovacs, G.; Lledos, A.; Ujaque, G.; Yus, M., A Versatile Ru Catalyst for the Asymmetric Transfer Hydrogenation of Both Aromatic and Aliphatic Sulfinylimines. *Chem. Eur. J.* **2012,** *18* (7), 1969-1983.

24.   Guijarro, D.; Pablo, O.; Yus, M., Asymmetric Synthesis of Chiral Primary Amines by Transfer Hydrogenation of N-(tert-Butanesulfinyl)ketimines. *J. Org. Chem.* **2010,** *75* (15), 5265-5270.

25.   Gunanathan, C.; Ben-David, Y.; Milstein, D., Direct synthesis of amides from alcohols and amines with liberation of H-2. *Science* **2007,** *317* (5839), 790-792.

26.   Schley, N. D.; Dobereiner, G. E.; Crabtree, R. H., Oxidative Synthesis of Amides and Pyrroles via Dehydrogenative Alcohol Oxidation by Ruthenium Diphosphine Diamine Complexes. *Organometallics* **2011,** *30* (15), 4174-4179.

27.   Gnanaprakasam, B.; Milstein, D., Synthesis of Amides from Esters and Amines with Liberation of H-2 under Neutral Conditions. *J. Am. Chem. Soc.* **2011,** *133* (6), 1682-1685.

28.   Nordstrom, L. U.; Vogt, H.; Madsen, R., Amide Synthesis from Alcohols and Amines by the Extrusion of Dihydrogen. *J. Am. Chem. Soc.* **2008,** *130* (52), 17672-+.

29.   Chen, C.; Zhang, Y.; Hong, S. H., N-Heterocyclic Carbene Based Ruthenium-Catalyzed Direct Amide Synthesis from Alcohols and Secondary Amines: Involvement of Esters. *J. Org. Chem.* **2011,** *76* (24), 10005-10010.

30.   Muthaiah, S.; Ghosh, S. C.; Jee, J. E.; Chen, C.; Zhang, J.; Hong, S. H., Direct Amide Synthesis from Either Alcohols or Aldehydes with Amines: Activity of Ru(II) Hydride and Ru(0) Complexes. *J. Org. Chem.* **2010,** *75* (9), 3002-3006.

31.   Dam, J. H.; Osztrovszky, G.; Nordstrom, L. U.; Madsen, R., Amide Synthesis from Alcohols and Amines Catalyzed by Ruthenium N-Heterocyclic Carbene Complexes. *Chem. Eur. J.* **2010,** *16* (23), 6820-6827.

32.   Shimizu, K.; Ohshima, K.; Satsuma, A., Direct Dehydrogenative Amide Synthesis from Alcohols and Amines Catalyzed by gamma-Alumina Supported Silver Cluster. *Chem. Eur. J.* **2009,** *15* (39), 9977-9980.

33.   Zweifel, T.; Naubron, J. V.; Grutzmacher, H., Catalyzed Dehydrogenative Coupling of Primary Alcohols with Water, Methanol, or Amines. *Angew. Chem. Int. Ed.* **2009,** *48* (3), 559-563.

34.   Srimani, D.; Balaraman, E.; Hu, P.; Ben-David, Y.; Milstein, D., Formation of Tertiary

Amides and Dihydrogen by Dehydrogenative Coupling of Primary Alcohols with Secondary

Amines Catalyzed by Ruthenium Bipyridine-Based Pincer Complexes. *Adv. Synth. Catal.* **2013,**

355 (13), 2525-2530.

35.   Rigoli, J. W.; Moyer, S. A.; Pearce, S. D.; Schomaker, J. M., alpha,beta-Unsaturated

imines via Ru-catalyzed coupling of allylic alcohols and amines. *Org. Biomol. Chem.* **2012,** *10*

(9), 1746-1749.

36.   Naota, T.; Murahashi, S. I., Ruthenium-Catalyzed Transformations of Amino-Alcohols to

Lactams. *Synlett* **1991,** (10), 693-694.

37.   Bertoli, M.; Choualeb, A.; Lough, A. J.; Moore, B.; Spasyuk, D.; Gusev, D. G., Osmium

and Ruthenium Catalysts for Dehydrogenation of Alcohols. *Organometallics* **2011,** *30* (13),

3479-3482.

38.   Spasyuk, D.; Smith, S.; Gusev, D. G., From Esters to Alcohols and Back with Ruthenium

and Osmium Catalysts. *Angew. Chem. Int. Ed.* **2012,** *51* (11), 2772-2775.

39.   Spasyuk, D.; Smith, S.; Gusev, D. G., Replacing Phosphorus with Sulfur for the Efficient

Hydrogenation of Esters. *Angew. Chem. Int. Ed.* **2013,** *52* (9), 2538-2542.

40.   Oldenhuis, N. J.; Dong, V. M.; Guan, Z., Catalytic acceptorless dehydrogenations: Ru-

Macho catalyzed construction of amides and imines. *Tetrahedron* **2014,** *70* (27ΓÇô28), 4213-

4218.

41.   Kuriyama, W.; Matsumoto, T.; Ogata, O.; Ino, Y.; Aoki, K.; Tanaka, S.; Ishida, K.;

Kobayashi, T.; Sayo, N.; Saito, T., Catalytic Hydrogenation of Esters. Development of an

Efficient Catalyst and Processes for Synthesising (R)-1,2-Propanediol and 2-(l-

Menthoxy)ethanol. *Org. Process Res. Dev.* **2011,** *16* (1), 166-171.

42.   Paul, C. E.; Rodríguez-Mata, M.; Busto, E.; Lavandera, I.; Gotor-Fernández, V.; Gotor, V.; García-Cerrada, S.; Mendiola, J.; de Frutos, Ó.; Collado, I., Transaminases Applied to the Synthesis of High Added-Value Enantiopure Amines. *Org. Process Res. Dev.* **2013**.

43.   Colyer, J. T.; Andersen, N. G.; Tedrow, J. S.; Soukup, T. S.; Faul, M. M., Reversal of diastereofacial selectivity in hydride reductions of N-tert-butanesulfinyl imines. *J. Org. Chem.* **2006,** *71* (18), 6859-6862.

44.   Chelucci, G.; Baldino, S.; Chessa, S.; Pinna, G. A.; Soccolini, F., An easy route to optically active 1-substituted-1-pyridyl-methylamines by diastereoselective reduction of enantiopure N-tert-butanesulfinyl ketimines. *Tetrahedron-Asymmetr* **2006,** *17* (22), 3163-3169.

45.   Tanuwidjaja, J.; Peltier, H. M.; Ellman, J. A., One-pot asymmetric synthesis of either diastereomer of tert-butanesulfinyl-protected amines from ketones. *J. Org. Chem.* **2007,** *72* (2), 626-629.

46.   Beck, E. M.; Hyde, A. M.; Jacobsen, E. N., Chiral Sulfinamide/Achiral Sulfonic Acid Cocatalyzed Enantioselective Protonation of Enol Silanes. *Org. Lett.* **2011,** *13* (16), 4260-4263.

47.   Gao, Y.; Zou, Z. M.; Yu, L. M.; Xu, H.; Liu, B.; Zhu, Y. Q.; Hu, F. Z.; Yang, H. Z., Synthesis and herbicidal activity of 2-cyano-3-methylthio-3-substituted methylaminoacrylates. *Chin. J. Chem.* **2006,** *24* (4), 521-526.

48.   Pallavicini, M.; Bolchi, C.; Fumagalli, L.; Valoti, E.; Villa, L., Highly efficient resolutions with isopropylidene glycerol 3-carboxy-2-naphthoate. *Tetrahedron-Asymmetr* **2002,** *13* (20), 2277-2282.

Chapter 4 : Biodegradable Dendronized Polymers for Efficient mRNA Delivery

Abstract: As chemically modified messenger RNAs become less immunogenic and more stable against RNases, the need for synthetic vectors that can efficiently deliver mRNA into cells has increased significantly. Based on a dendronized polypeptide (denpol) architecture, we describe here the development of a synthetic vector system for efficient delivery of mRNAs. The optimized denpols show high efficiency of mRNA delivery to a variety of cells including primary murine dendritic cells (BMDCs), giving it potential use for anti-tumor immunotherapy.

4.1 Introduction:

Originally thought to be too unstable and immunogenic for the treatment of diseases, messenger RNA (mRNA) has reemerged as a promising therapeutic for cancers, vaccines, and stem-cell therapy.[1-5] In accordance, the demand and applicability for synthetic vectors tailored to mRNA delivery has also increased greatly.[6-8] Much like other nucleic acids, mRNA is a large anionic polymer and does not readily pass through the cell membrane unassisted.[8] However, since mRNA only requires delivery to the cellular cytoplasm, it avoids the drawbacks of protein expression via plasmid DNA (pDNA) or viral vector delivery (e.g. insertive mutagenesis, delivery to nucleus.) Recently, synthetic vectors such as liposomes[3, 6, 9-13] and cationic polymers,[4, 14-22] many of which were originally developed for pDNA or siRNA delivery, as well as physical delivery methods,[8, 23-26] have been used to deliver mRNA to the cytoplasm for various applications. Nevertheless, mRNA delivery is significantly understudied compared to siRNA and pDNA delivery methods.[8]

As a notable application, mRNA–based prophylactic and therapeutic antitumor immunity has vitalized the field of immuno-oncology. Peptide or protein antigens isolated from tumors are

A Functional denondronized polymer (denpol)

Delivery To Cells → Controlled Protein Expression

mRNA Polymer Complex

mRNA

B

Denpol Backbone (M$_n$ ~ 16 kDa, PDI ~ 1.6)

$R_1 =$

PEG

or

TEG

· 4 TFA

Peptide Dendron
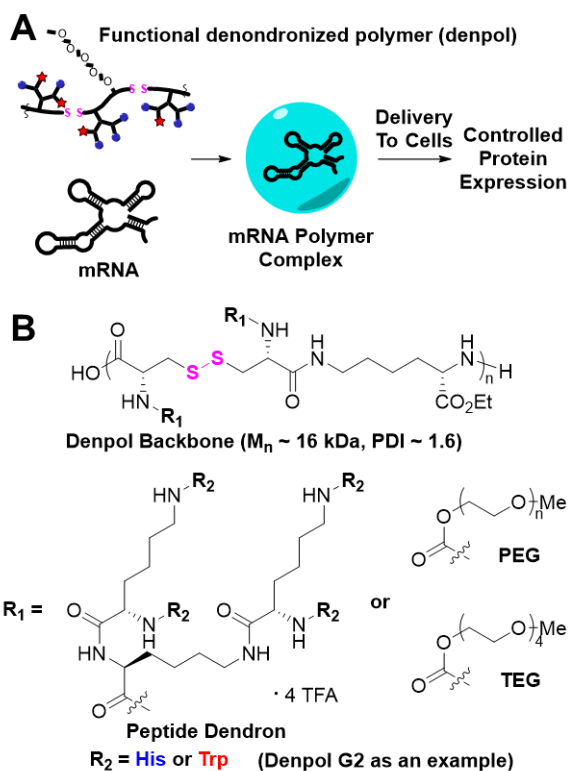$R_2 =$ His or Trp   (Denpol G2 as an example)

Figure 4.1 Concept and general structure of Denpol for mRNA delivery.

coded into mRNA and delivered *ex vivo* or *in vivo* to dendritic cells. Upon translation of the mRNA, major histocompatibility complexes (MHC) present the coded antigen and activate T-cells against the tumor.[27] Liposomes and cationic polymers are currently used for this application, [1, 6-8, 10] but inefficient delivery to immune cells is hindering further clinical applications.[1, 27, 28] On closer inspection, some of the synthetic mRNA delivery vectors were found to be reformulated or modified based on siRNA or pDNA delivery vectors. While the repurposed materials showed some efficacy, there was little discussion about what specific variables or changes were important for effective mRNA delivery. Based on a dendronized polymer system our lab previously created for siRNA delivery,[29] herein we report biodegradable polymeric vectors for efficient delivery of mRNA to various cells (Figure 4.1A). We investigated key factors that contribute to increased mRNA delivery with a specific goal to improve transfections in immune cells.

4.2 Results and Discussion:

The dendronized polypeptide (denpol) system initially developed by our lab for siRNA delivery[29] contains an L-lysine- dicysteine polymer backbone having multiple lysine dendrons grown on the surface to achieve a vector combining the conformational flexibility of a linear polymer and the beneficial multivalent interactions of a dendrimer (Figure 4.1). Additionally, the

disulfide linkages in the polymer backbone can be reduced inside the cellular cytoplasm and acts as a selective release mechanism. The initial report of denpol demonstrated that surface functionalization of the lysine dendrons with histidine (His) and tryptophan (Trp) was vital for effective siRNA delivery. Histidine provides the buffering capacity needed to escape the endosome during lysosomal maturation, and the indole ring of Trp binds the nucleic acids via π-stacking and improves cellular uptake.[29] The optimal vector obtained for siRNA delivery contained a G2 lysine dendron functionalized with a 3:1 ratio of His:Trp. For the purpose of mRNA delivery, several structural parameters were varied to optimize the performance. First, given the less ordered secondary structure of single stranded mRNA compared to double stranded siRNA, we hypothesized a higher generation lysine dendron or additional Trp may be required to effectively complex and deliver mRNA. Therefore, denpols containing G2 or G3 lysine dendrons functionalized with higher amounts of tryptophan were studied. Second, we envisioned that the long anionic mRNA might increase aggregation during nanoparticle assembly with denpol. To prevent this from occurring, denpols functionalized with either short tetraethylene glycol (TEG) or long polyethylene glycol (PEG2K, M_n=2000 Da) units on the backbone were investigated.

The synthesis of the denpols was completed in the same manner as previously reported using conventional peptide coupling chemistry and a "graft-from" approach (for a detailed synthesis scheme and characterization details see the supporting information 4.4, Figure 4.13.)[29] Figure 4.1B shows a generalized G2 denpol structure, where the R_1 group can either be a lysine dendron or a TEG/PEG group, and the R_2 group can either be a His or Trp. A series of denpols were synthesized by varying the amount of TEG/PEG and the His:Trp molar ratio. For example, G2 25 TEG 3:1 represents a denpol that has 75 mol% G2 lysine dendrons and 25 mol% TEG on the backbone, and 75 mol% His 25 mol% Trp (3:1 ratio of His:Trp) functionalized on the surface

of the lysine dendrons (as determined by ^{1}HNMR). Figure 4.5 represents the complete family of denpols made and used in the study. His:Trp ratios of 3:1, 2:1, 1:1, 1:2 and 1:3 were targeted for functionalization to the G2 and G3 lysine dendrons. Results from the initial transfections (*vida infra*) were used to select denpol vectors for further study.

The non-PEGylated G2 and G3 denpols were tested first to determine if a higher generation or more Trp had a positive effect on transfection ability. To assay mRNA delivery, NIH 3T3 cells were treated with a firefly luciferase (FLuc, 5-methylcytidine, pseudouridine modified) mRNA/denpol nanoplex. Fifteen hours after transfection, D-Luciferin was added, and luminescence was measured with an IVIS camera. Lipofectamine MessengerMax (LF MM) was used as a positive control. Naked mRNA with no delivery vector and untreated cells were used as negative controls. The initial transfection conditions used were based on those optimized for siRNA transfections. The vector was used starting at an N:P ratio of 45 (molar ratio of protonated amines of the vector to phosphates of the mRNA). To form nanoparticles, 200 ng of mRNA solution was added directly to a 10 mg/mL solution of the vector and mixed via pipette. The mixture was then diluted to a final volume with OptiMEM and mixed again with a pipette before incubation with the cells. The G2 denpols produced luminescence comparable to the positive control, whereas the G3 denpols were largely ineffective (Figure 4.2A). Interestingly, higher luminescence was observed when decreasing the His:Trp ratio from 3:1 to 2:1, but quickly drops off in efficiency when approaching 1:1, suggesting an optimal ratio of ~ 2:1. When the ratio is decreased to 1:2 or 1:3, the vectors become cytotoxic and ineffective (Figure 4.5), therefore only ratios of 3:1, 2:1, or 1:1 were used for further studies. We hypothesize delivery efficiency decreases and toxicity increases as tryptophan increases past 1:1 because the denpol becomes too hydrophobic to bind mRNA and may disrupt the cell membrane.
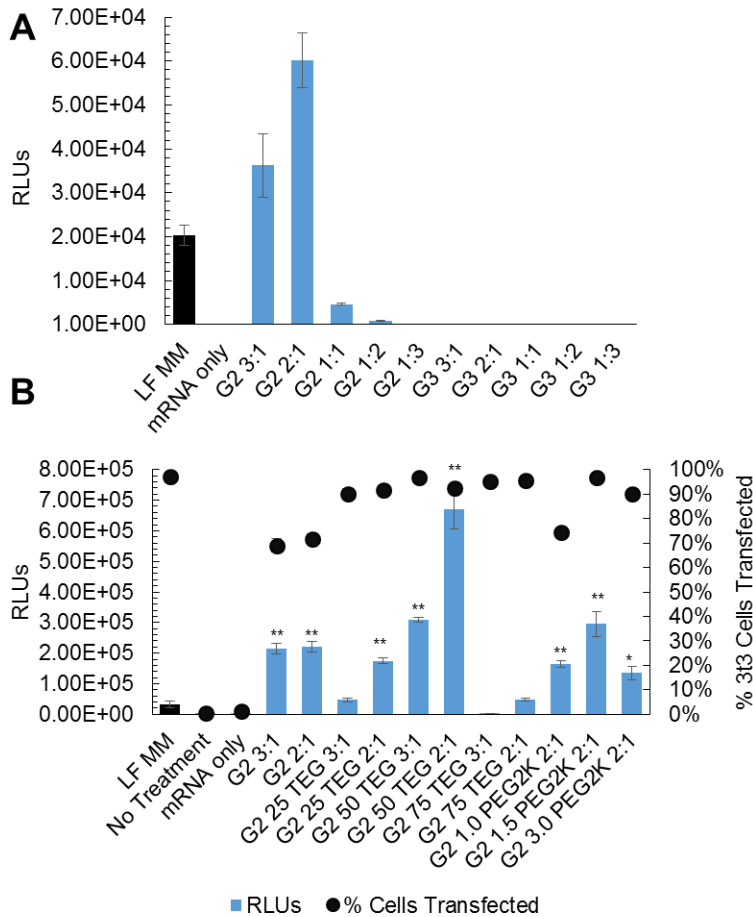
Figure 4.2 Transfection of 3T3 cells with denpols (70% confluence, 24 h exposure to transfection media, 200 ng Fluc mRNA per well). A) Screen of the His:Trp ratio for non-PEGylated denpols (N:P = 45). B) Screen of the denpol library created for study. (N:P = 10) * = P < 0.01, ** = P < 0.001

Notably, the PEGylated denpols show excellent serum tolerance for mRNA delivery. When denpol and mRNA were complexed and then added to complete media (10% fetal bovine serum (FBS) in OptiMEM) instead of buffer alone, a universal increase in transfection efficiency was observed (Figure 4.6). Based on this observation, the rest of the study was completed using at least 10% FBS. Increasing the amount of FBS to 80% in the transfection media had little or no effect on the transfection ability of the PEGylated denpols, but drastically diminished the efficacy of the non-PEGylated denpols (Figure 4.7). Presumably, PEGylation reduces nonspecific interactions with serum components and enhances the colloidal stability for the mRNA complexes.

To find out the optimal formulation for mRNA delivery, differing N:P ratios for the PEGylated and non-PEGylated denpols were tested via transfection to find the optimal N:P ratio for mRNA delivery. Luminescence was greatest for the PEGylated denpols surveyed between 5-15 N:P, drastically reducing the amount of vector needed for mRNA transfections compared to

siRNA transfections (Figure 4.8). This was further confirmed using gel shift assays, which showed that all denpols bound mRNA by an N:P of 5 (Figure 4.9). Luminescence of non-PEGylated denpols plateaued after an N:P of 10 and did not increase at higher N:P ratios. Luminescence of PEGylated denpols peaked between an N:P of 10-15 and then decreased when more than the optimal amount of denpol was used (Figure 4.8).

After optimized conditions had been identified (10% FBS, N:P 10) the denpols were all tested against each other to find the best vectors (Figure 4.2B, Figure 4.10 shows all vectors screened). In general, the vectors containing a His:Trp ratio of 2:1 and G2 lysine dendron gave the highest expression. G2 50 TEG 2:1 had the highest luminescence of the vectors measured. Excitingly, the best denpol vector is much more effective for delivering mRNA into cells, exhibiting 10 folds increase in luminescence compared to the positive control (LF MM). No cytotoxicity was observed via lactate dehydrogenase (LDH) assay, except for the vectors with a His:Trp ratio below 1:2 as mentioned above (Figure 4.5). Further transfection studies were performed using cyanine 5 (cy-5) mRNA in conjunction with flow cytometry to examine cellular uptake and the percentage of cells with mRNA associated. Ideally, a synthetic mRNA vector would induce high amounts of mRNA association in 100% of the cells intended for delivery. Indeed, the most effective vectors were able to associate mRNA to a majority of the cells (>70% contained cy-5 labeled mRNA, Figure 4.2B) with the best vectors associating over 90% of cells.

Dynamic light scattering (DLS) was used to examine the size and zeta potential of the denpol nanoparticles. DLS in PBS showed that the effective non-PEGylated nanoparticles (G2 2:1 and G2 3:1) initially formed nanoparticles in the $100 - 200$ nm range (Figure 4.3A) but aggregated over time (Figure 4.11). The PEGylated denpols formed stable nanoparticles between $100 - 200$ nm and did not aggregate with time. G3 denpols tended to aggregate quickly and form cloudy

precipitates, which could not be measured via DLS. Atomic force microscopy (AFM) was used to confirm nanoparticle size (Figure 4.12). Zeta potential measurements in PBS revealed negatively charged particles. The DLS data and transfection data agrees with the knowledge that nanoparticles in the 50 – 200 nm size range are generally optimal for cellular uptake.[30] The DLS measurements in combination the transfection results agree with our initial hypothesis that mRNA is more prone to aggregation during

A

Denpol	d (nm)	PDI	ZP (mV)
G2 3:1	140	0.31	-8.3
G2 2:1	163	0.30	-6.3
G2 3.0 PEG2k 2:1	106	0.22	-2.1
G2 1.5 PEG2k 2:1	136	0.21	-7.8
G2 1.0 PEG2k 2:1	155	0.29	-8.0
G2 25 TEG 3:1	126	0.35	-10.1
G2 25 TEG 2:1	160	0.28	-7.5
G2 50 TEG 3:1	153	0.23	-8.6
G2 50 TEG 2:1	131	0.19	-9.2
G2 75 TEG 3:1	180	0.24	-10.1
G2 75 TEG 2:1	191	0.32	-13.4

B
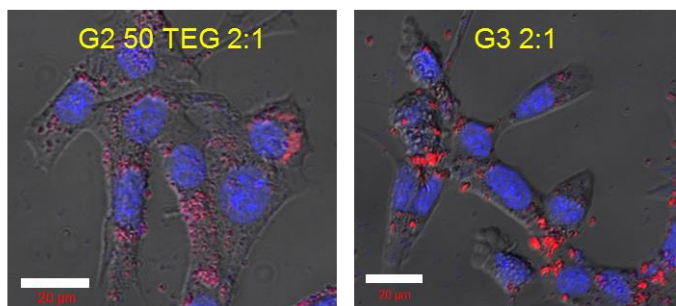
Figure 4.3 Denpol nanoparticle characterization. N:P = 10 A) Diameter is based on Z-Avg in PBS. Zeta potential measurements are in PBS B) Confocal microscopy image highlighting a colloidally stable (G2 50 TEG 2:1) denpol versus a denpol that aggregates (G3 3:1). White bar represents 20 μm.

formulation compared to siRNA (e.g., G2 3:1 does not aggregate when formulated with siRNA)[29]. Accordingly, when TEG/PEG was functionalized to the backbone, colloidal stability was regained, and transfection efficiency increased.

Confocal microscopy using cy-5 labeled FLuc mRNA was used to visualize internalization of the denpol/mRNA nanoparticles (Figure 4.3B). Images of the G3 denpols shows large clusters of nanoparticles on the surface of the cells and aggregates on the floor of the well, but shows little internalization (Figure 4.3B). TEG/PEGylated G2 denpol/mRNA complexes showed more dispersed nanoparticles. There were no obvious differences between the 3:1 and 2:1 denpols when
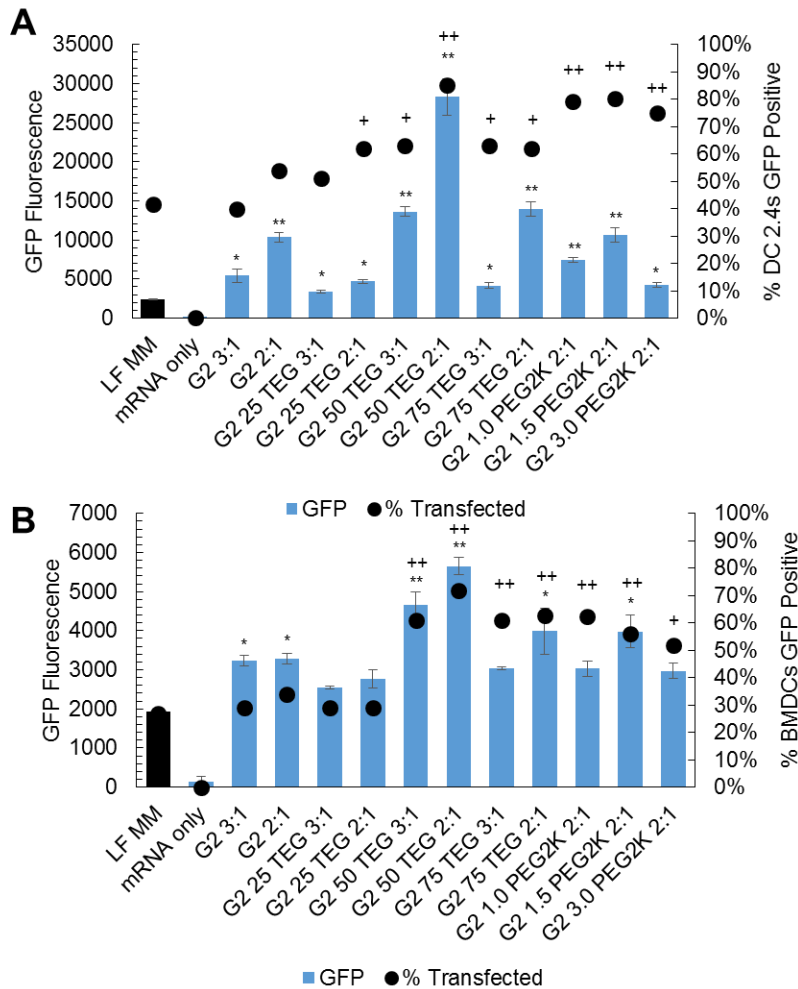
Figure 4.4. Transfections in dendritic cells. N:P = 15, 200 ng Cy-5 labeled eGFP mRNA per well. For GFP fluorescence * = P < 0.01, ** = P < 0.001 relative to LF MM. For GFP positive cells + = P < 0.01, ++ = P < 0.001 relative to LF MM A) DC 2.4 cells, 70% confluent, 24 h exposure B) primary BMDCs, 60k per well, 12 h exposure.

examined. The confocal images corroborate the DLS results, as one can visually see the large aggregates from the G3 denpols are not able to enter the cellular endosome or cytoplasm, and thus inefficiently deliver mRNA.

As discussed in the introduction, the delivery of antigen coding mRNA to dendritic cells can excite T cell activity against tumors; however, nucleic acid delivery to dendritic cells is notorious for being inefficient.[1, 6-8, 10] Given the high efficiency of denpol for mRNA delivery to 3T3 cells, the denpol system was tested in immortalized murine dendritic cells (DC 2.4) cells to confirm if transfection would be operative in an immune cell line. Using the transfection conditions optimized in 3T3 cells, it was observed that the same denpols that were active in 3T3 cells were also active in DC 2.4 (Figure 4.4A). Again, the most effective denpol showed ~ 10 fold higher GFP expression than the positive control (LF MM). Flow cytometry using GFP mRNA showed that for the most effective denpol vectors a

majority of cells (~70%) were GFP positive. After confirming that denpol was effective to deliver mRNA into DC 2.4 cells, further transfections using primary murine bone marrow derived, dendritic cells (BMDCs) *ex vivo* were attempted. The best denpols tested transfected ~60% of the BMDCs expressed GFP and provided significant production of GFP after only one treatment (Figure 4.4B). Additionally, the successful delivery of both GFP (996 nucleotides) and FLuc (1929 nucleotides) mRNA shows that denpol can efficiently accommodate mRNA of different length. The high efficiency of delivery to both DC 2.4 and BMDC cells demonstrates the promise of denpol vectors for further studies of mRNA-based vaccination.

4.3 Conclusion:

In conclusion, we have developed a denpol vector system that is highly efficient for mRNA delivery to various cells. Through the study, we identified several important factors for designing effective mRNA delivery vectors. The study first demonstrated that increasing the amount of tryptophan on the dendron surface increases transfection efficiency, presumably due to the increased binding to the less ordered structure of mRNA. Then, we showed TEG/PEGylation increased transfection ability, serum tolerance, and colloidal stability of the denpol/mRNA nanoparticles by reducing the propensity of mRNA for aggregation. Finally, denpol was demonstrated to transfect both DC2.4 and BMDCs at high efficiency, showing great promise for future investigations with mRNA adjuvanting. Further studies on both new designs of denpol vectors and biological applications of mRNA delivery are currently underway in our laboratory.

4.4 Supplementary Information:

General Information: Unless otherwise noticed, all reagents were used as received from commercial suppliers without further purification. Protected amino acids were purchased from Advanced ChemTech (Loiusville, KY) and Aroz Technologies, LLC. (Cincinnati, OH). Coupling

reagents were purchased from GL Biochem Ltd. (Shanghai, China). FLuc mRNA (5meC, Ψ), Cyanine 5 FLuc mRNA (5meC, Ψ), and Cyanine 5 EGFP mRNA (5meC, Ψ) were obtained from TriLink Biotechnologies (Sorrento Mesa, CA). Lipofectamine MessangerMAX was purchased from Invitrogen (Carlsbad, CA). Pierce™ LDH Cytotoxicity Assay Kit was purchased from ThermoFisher (San Jose, CA). All reactions were performed using HPLC grade solvent unless otherwise noted. All water used in biological experiments was nanopure water obtained from Barnstead Nanopure Diamond (Waltham, MA). Unmodified NIH 3T3 cells were a generous gift from Professor Young Jik Kwon (Department of Chemical Engineering, UC Irvine, CA). Unmodified DC 2.4 cells and BMDCs were a generous gift from Professor Aaron Esser-Kahn's lab (Department of Chemistry, UC Irvine, CA). The BMDCs were harvested according to the procedure outlined in "Stimulation of Innate Immune Cells by Light-activated TLR7/8 Agonists" (IACUC protocol # 2012-3048).[31] Dulbecco's modified Eagle's medium (DMEM), fetal bovine serum (FBS), and OptiMEM were purchased from Invitrogen (Carlsbad, CA).

General Analytical Information: The molecular weight and molecular weight distribution of the Denpol backbone was measured by gel permeation chromatography (GPC). ^{1}HNMR spectra were obtained using 500 and 600 MHz Bruker instruments. [1] HNMR chemical shifts were reported as values in ppm relative to deuterated solvents indicated. GPC was performed on an Agilent 1100 SEC system using a OHpak SB-803 HQ column from Shodex. The molecular weight was determined with respect to poly(ethylene glycol) (PEG) S3 standards purchased from Aldrich. DMF with 0.1% LiBr (wt/v) was used as the eluent at a flow rate of 1.0 mL/min with column temperature at 45°C. The size and zeta potential of denpol/mRNA polyplexes were measured at 633 nm using Zetasizer (NanoZS) dynamic light scattering instrument (Malvern Instruments, Malvern, UK) at 25 °C with detection angle of 173˚. Confocal images were obtained

using a Ziess LSM 700 (Carl Zeiss AG, Oberkochen, Germany). Flow cytometry was performed on a BD ACCURI C6 flow cytometer (BD Biosciences, San Jose). AFM images were all taken on an MFP-3D StandAlone AFM (Asylum Research, Santa Barbara, CA) through tapping-mode using a monolithic silicon TESP-10 tip (NanoAndMore USA, Watsonville, CA) with resonant frequency =320 kHz and a spring constant k =42 N/m.
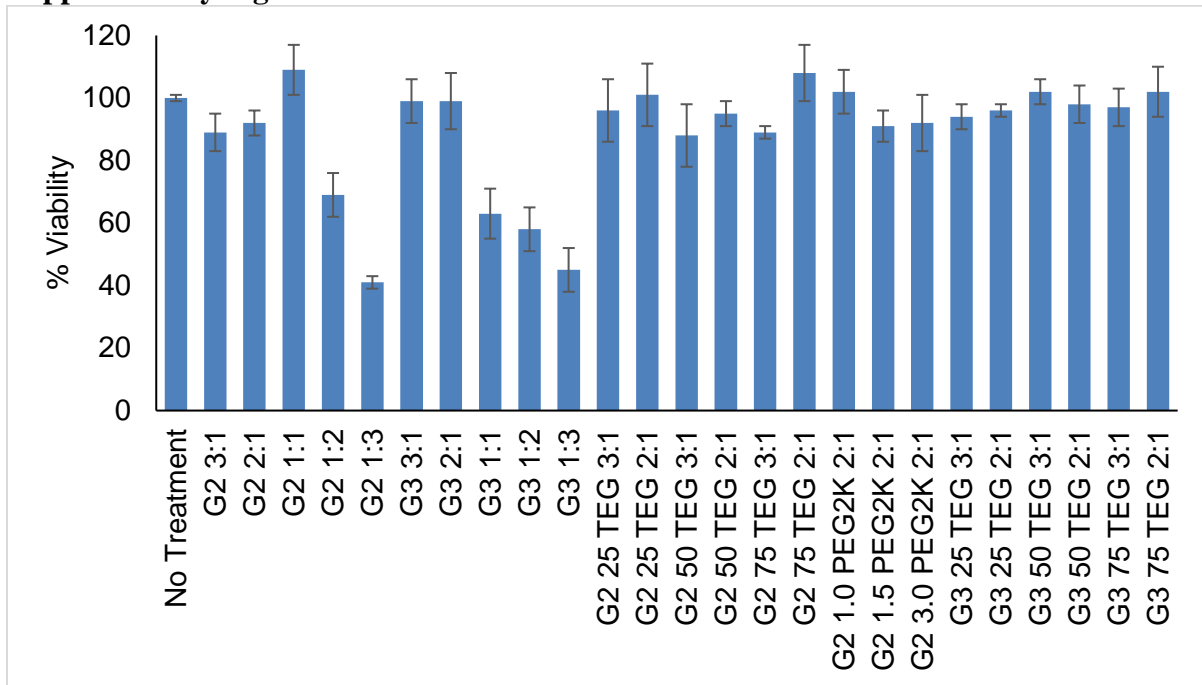
Supplementary Figures:

Figure 4.5 Cytotoxicity of the denpol vectors against 3T3 cells assayed using a LDH assay
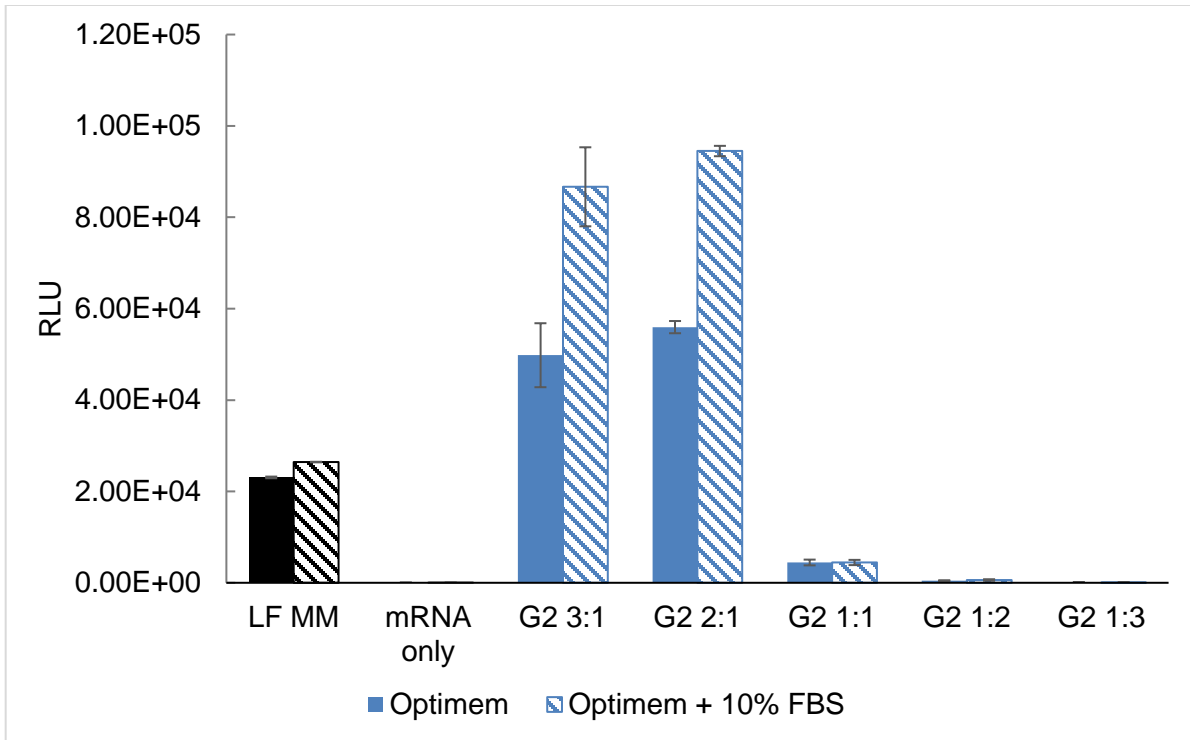
Figure 4.6 Effect of 10% FBS on denpol transfections
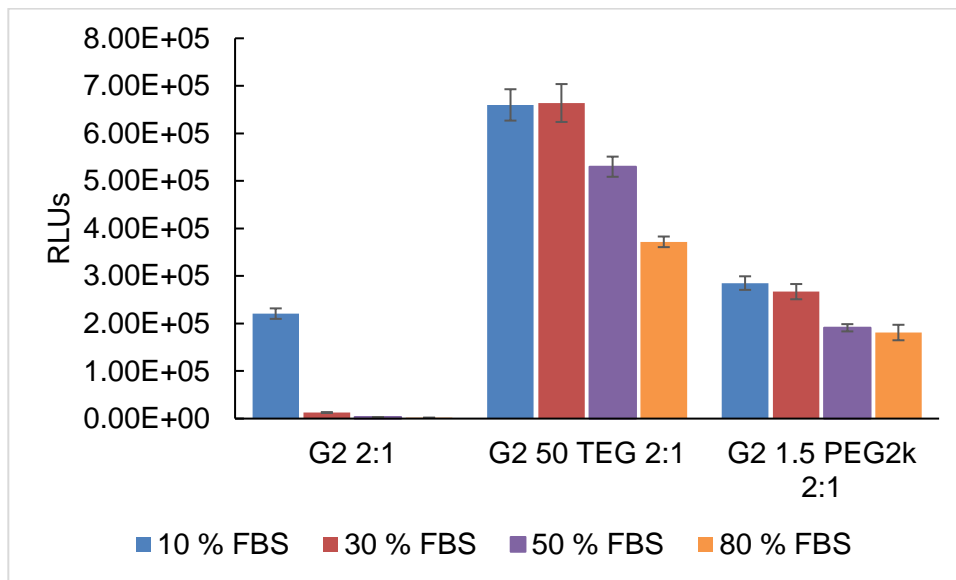
Figure 4.7 Effects of increasing FBS concentration in transfection efficiency. N:P = 10, 200 ng FLuc mRNA, 24 hours exposure to transfection media.
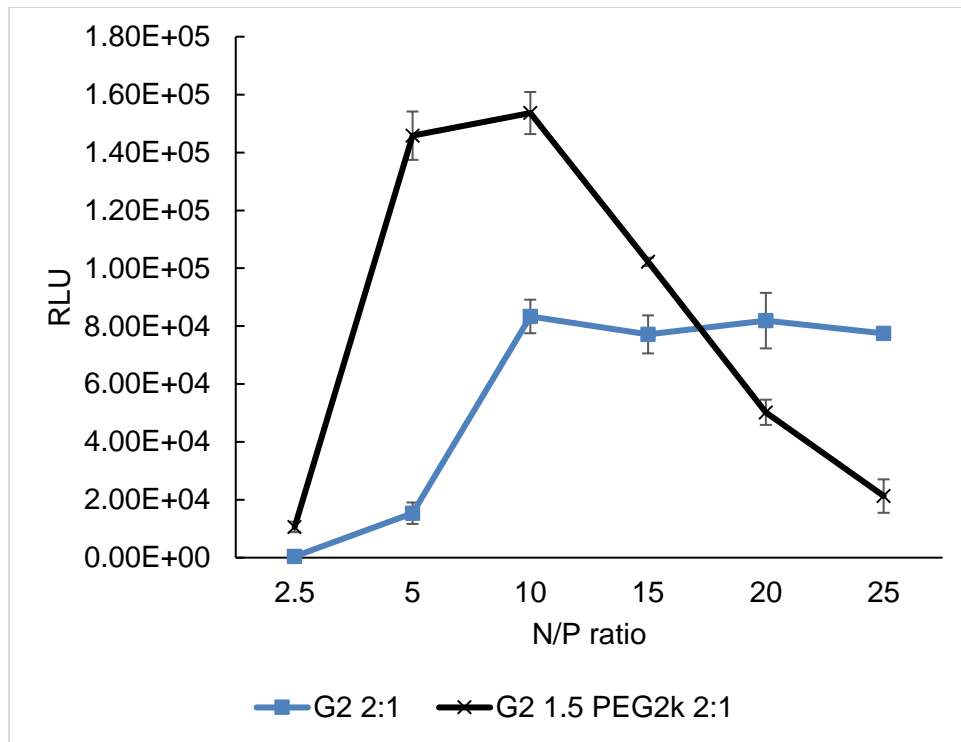
Figure 4.8 Representative N:P screen of a non-PEGylated and PEGylated vector. Non-PEGylated vectors tended to plateau after N:P 10 and had slightly diminished luminescence after N:P 30. PEGylated vectors Peaked between N:P 5 – 15 and had a maximum at N:P 10.
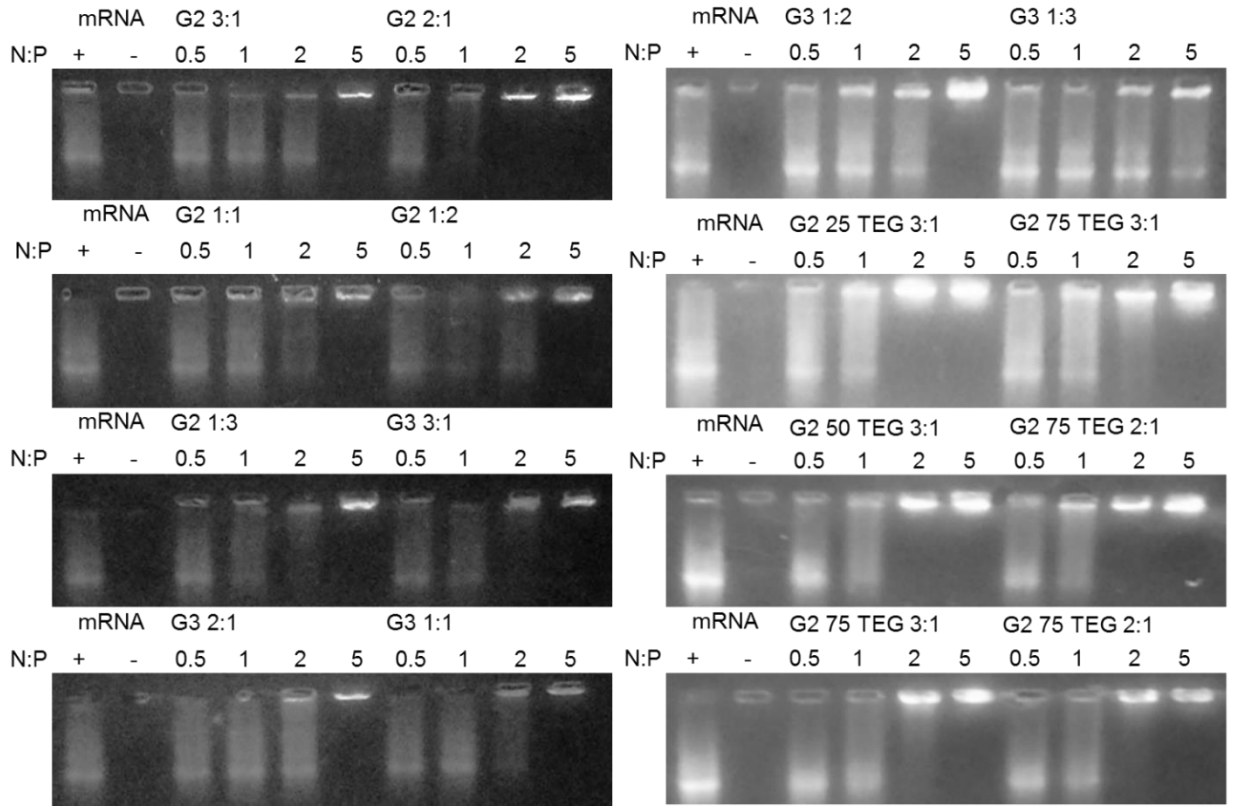
Figure 4.9 Representative gel shift binding assays in 1% agarose. All vectors surveyed bound mRNA by N:P 5.
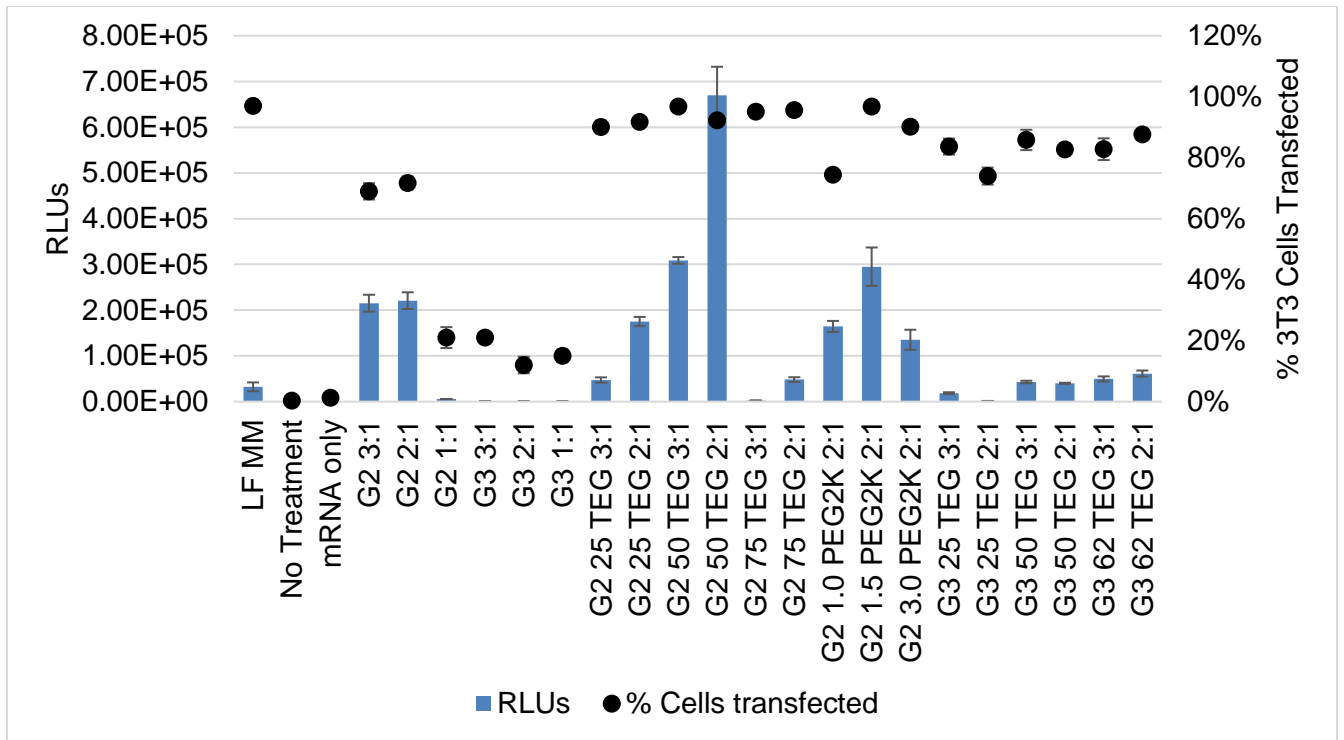
Figure 4.10 Complete screen of all denpols made
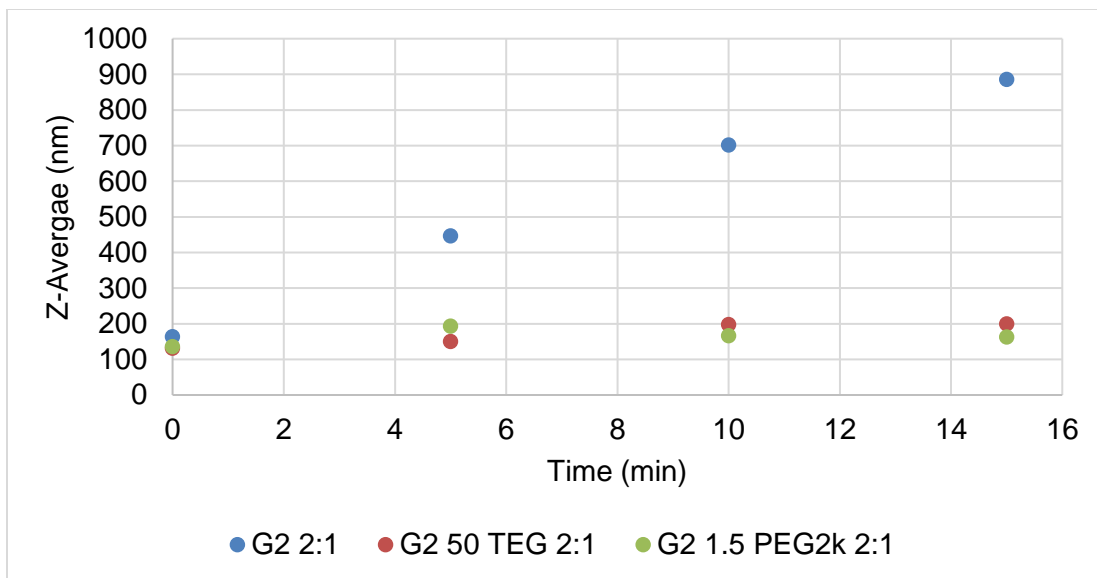
Figure 4.11 Aggregation of non-PEG/TEGylated polymers over time
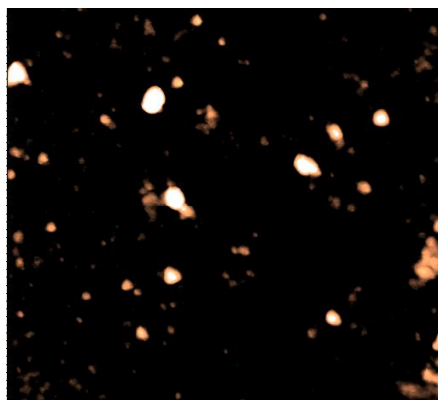
Figure 4.12 Dry AFM of G2 1.5 PEG2k 2:1 mRNA denpol nanoparticles on mica. Each side represents 5 μm.

Synthesis of Denpols (DP):
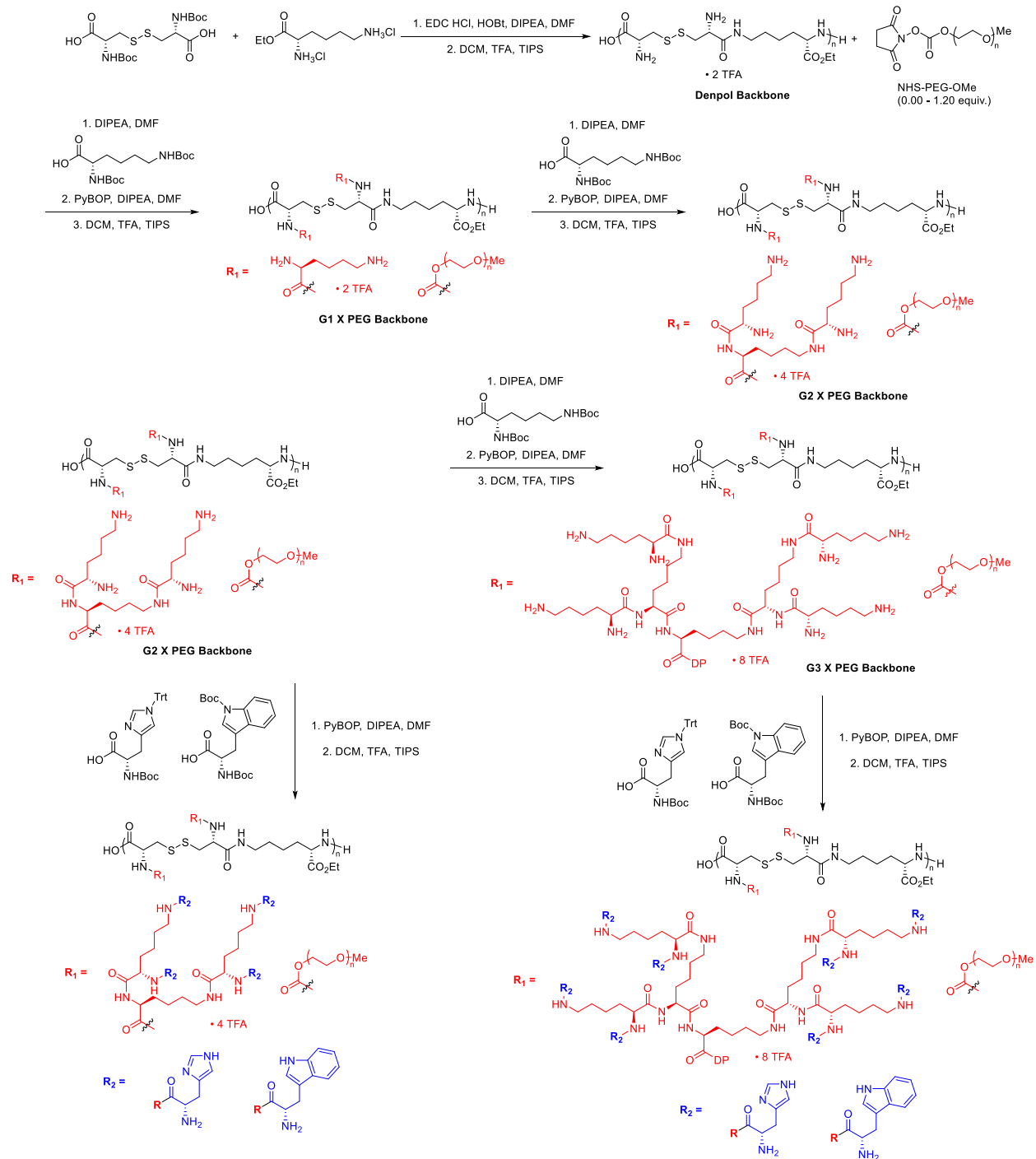
Figure 4.13 General synthetic scheme for Denpol. Amounts of NHS-PEG-OMe and dendron on the surface of the denpol backbone are specified in the procedures.

Typical procedure for Denpol functionalization:

In a 1 dram vial equipped with a stir bar, the specified DP (10.0 mg, 1.00 equiv) was dissolved in 1 mL of DMF. After the denpol backbone was completely dissolved, Boc-His(Boc)-OH, and Boc-Trp(Boc)-OH were added in the corresponding ratios. After all reagents had been solubilized, PyBOP (10.00 equiv.) and DIPEA (12.00 equiv.) were added, and the 1 dram vial was sealed with nitrogen and stirred over-night. After 12 h, 3 mL of MeOH was added to the reaction, and the mixture was purified via dialysis (MWCO = 6 – 8 kD) against MeOH for 12 h. After 12 h the mixture was concentrated *in vacuo* (no heating), yielding a solid film. The Boc groups were removed by suspending the solid in a mixture of TFA (1.5 mL), DCM (0.75 mL), anisole (0.75 mL), and TIPS (0.1 mL) and stirring for 4 h under nitrogen. The mixture was concentrated *in vacuo* (no heating), resuspended in methanol, and then precipitated in cold ether. The precipitate was pelleted via centrifugation, and the supernatant was discarded. The precipitate was purified via dialysis (MWCO = 6 – 8 kD) against MeOH for 24 h and then concentrated *in vacuo*. All denpols were characterized by ^{1}H NMR. The final functionalization ratio was calculated using the same methodology as previously reported.[29]

Histidine Tryptophan functionalized G2 Denpols:

See procedure for typical denpol functionalization

G2 3:1 (77.4 H 22.6 W): Boc-His(Boc)-OH (6.00 equiv.) and Boc-Trp(Boc)-OH (2.00 equiv.). Clear colorless solid. 71% isolated yield.

G2 2:1 (66 H 34 W): Boc-His(Boc)-OH (4.80 equiv.) and Boc-Trp(Boc)-OH (3.20 equiv.). Clear colorless solid. 62% isolated yield.

G2 1:1 (55 H 45 W): Boc-His(Boc)-OH (4.00 equiv.) and Boc-Trp(Boc)-OH (4.00 equiv.). Clear colorless solid. 89% isolated yield.

G2 1:2 (39 H 61 W): Boc-His(Boc)-OH (3.20 equiv.) and Boc-Trp(Boc)-OH (4.80 equiv.). Clear colorless solid. 78% isolated yield.

G2 1:3 (27 H 73 W): Boc-His(Boc)-OH (2.00 equiv.) and Boc-Trp(Boc)-OH (6.00 equiv.). Clear colorless solid. 74% isolated yield

Denpol G3 backbone

G3 backbone In a 25 mL RB flask equipped with a stir bar, DP G2 (76.3 mg, 1.00 equiv, 0.037 mmol) was dissolved in 4 mL of DMF. After the denpol backbone was completely dissolved, Boc-Lys(Boc)-OH DCHA was added. After all reagents had been solubilized, PyBOP (191.1 mg, 10.00 equiv., 0.37 mmol) and DIPEA (103.4 µL, 12.00 equiv., 0593 mmol) were added, and the flask was sealed with nitrogen and stirred over-night. After 12 h, 8 mL of MeOH was added to the reaction, and the mixture was purified via dialysis (MWCO = 6 – 8 kD) against MeOH for 12 h. After 12 h the mixture was concentrated *in vacuo* (no heating), yielding a solid film. The Boc groups were removed by suspending the solid in a mixture of TFA (3.0 mL), DCM (1.5 mL), anisole (1.5 mL), and TIPS (0.2 mL) and stirring for 4 h under nitrogen. The mixture was concentrated *in vacuo* (no heating), suspended in methanol, and then precipitated in cold diethyl ether. The precipitate was pelleted via centrifugation, and the supernatant was discarded. The precipitate was purified via dialysis (MWCO = 6 – 8 kD) against MeOH for 24 h and then concentrated *in vacuo*. Clear colorless solid. 93% isolated yield.

Histidine Tryptophan functionalized G3 Denpols:

See procedure for typical denpol functionalization.

G3 3:1 (71 H 29 W): Boc-His(Boc)-OH (12.00 equiv.) and Boc-Trp(Boc)-OH (4.00 equiv.). Clear colorless solid. 93% isolated yield.

G3 2:1 (66 H 34 W): Boc-His(Boc)-OH (9.60 equiv.) and Boc-Trp(Boc)-OH (6.40 equiv.). Clear colorless solid. 91% isolated yield.

G3 1:1 (53 H 47 W): Boc-His(Boc)-OH (8.00 equiv.) and Boc-Trp(Boc)-OH (8.00 equiv.). Clear colorless solid. 82% isolated yield.

G3 1:2 (33 H 67 W): Boc-His(Boc)-OH (6.40 equiv.) and Boc-Trp(Boc)-OH (9.60 equiv.). Clear colorless solid. 78% isolated yield.

G3 1:3 (28 H 72 W): Boc-His(Boc)-OH (4.00 equiv.) and Boc-Trp(Boc)-OH (12.00 equiv.). Clear colorless solid. 86% isolated yield.

G1 TEG Backbones:

NHS-TEG-OMe and NHS-PEG2k-OMe was prepared according to previous literature.[32]

Typical procedure for functionalization of denpol G0 backbone with TEG or PEG:

In a 25 mL RB flask equipped with a stir bar, DP backbone (50 mg, 1.00 equiv., 0.083 mmol) was dissolved in 4 mL of DMF and DIPEA (57.6 µL, 5.00 equiv., 0.330 mmol) was added. The reaction was cooled to 0°C and the NHS-TEG-OMe or NHS-PEG-OMe was added in the corresponding amount. The flask was sealed with nitrogen and stirred for 4 h. After stirring, Boc-Lys(Boc)-OH DCHA (86.6 mg, 2.00 equiv., 0.165 mmol) and PyBOP (128.9 mg, 3.00 equiv. 0.248 mmol) are added. After 12 h, 8 mL of MeOH was added to the reaction, and the mixture was purified via dialysis (MWCO = 6 – 8 kD) against MeOH for 12 h. After 12 h the mixture was concentrated *in vacuo* (no heating), yielding a solid film. The Boc groups were removed by suspending the solid in a mixture of TFA (3.0 mL), DCM (1.5 mL), anisole (1.5 mL), and TIPS (0.2 mL) and stirring for 4 h under nitrogen. The mixture was concentrated *in vacuo* (no heating), resuspended in methanol, and then precipitated in cold diethyl ether. The precipitate was pelleted via centrifugation, and the supernatant was discarded. The precipitate was purified via dialysis

(MWCO = 6 – 8 kD) against MeOH for 24 h and then concentrated *in vacuo*. % TEG or PEG functionalization was determined via ^{1}H NMR. % functionalization represents % of TEG or PEG per SRU. The compounds are named to represent which polymer (TEG or PEG) is functionalized off the backbone and in what percent.

G1 25 TEG: (23% by NMR) NHS-TEG-OMe (20.6 mg, 0.50 equiv., 0.0415 mmol). Clear colorless solid. 81% isolated yield.

G1 50 TEG: (42% by NMR) NHS-TEG-OMe (41.1 mg, 1.0 equiv., 0.083 mmol). Clear colorless solid. 68% isolated yield.

G1 75 TEG: (62% by NMR) NHS-TEG-OMe (61.7 mg, 1.50 equiv., 0.124 mmol). Clear colorless solid. 83% isolated yield.

G2 TEG Backbones:

Typical Procedure for synthesis of G2 lysine dendrons on the TEGylated (or PEG) DP backbones: In a 25 mL RB flask equipped with a stir bar, DPBBTEG G1 (1.00 equiv) was dissolved in DMF. After the DPBBTEG G1 was completely dissolved, Boc-Lys(Boc)-OH DCHA (4.00 equiv) was added. After all reagents had been solubilized, PyBOP (6.00 equiv.) and DIPEA (8.00 equiv.) were added, and the flask was sealed with nitrogen and stirred over-night. After 12 h, 8 mL of MeOH was added to the reaction, and the mixture was purified via dialysis (MWCO = 6 – 8 kD) against MeOH for 12 h. After 12 h the mixture was concentrated *in vacuo* (no heating), yielding a solid film. The Boc groups were removed by suspending the solid in a mixture of TFA (3.0 mL), DCM (1.5 mL), anisole (1.5 mL), and TIPS (0.2 mL) and stirring for 4 h under nitrogen. The mixture was concentrated *in vacuo* (no heating), resuspended in methanol, and then precipitated in cold diethyl ether. The precipitate was pelleted via centrifugation, and the supernatant was

discarded. The precipitate was purified via dialysis (MWCO = 6 – 8 kD) against MeOH for 24 h and then concentrated *in vacuo*.

G2 TEG 25: Clear colorless solid. 93% isolated yield.

G2 TEG 50: Clear colorless solid. 91% isolated yield.

G2 TEG 75: Clear colorless solid. 88% isolated yield.

Histidine Tryptophan functionalized TEG G2 Denpols:

See procedure for typical DP functionalization.

G2 25 TEG 3:1 (74 H 26 W): Boc-His(Boc)-OH (4.62 equiv.) and Boc-Trp(Boc)-OH (1.54 equiv.). Clear colorless solid. 59% isolated yield.

G2 25 TEG 2:1 (63 H 32 W): Boc-His(Boc)-OH (4.01 equiv.) and Boc-Trp(Boc)-OH (2.16 equiv.). Clear colorless solid. 87% isolated yield.

G2 50 TEG 3:1 (73 H 27 W): Boc-His(Boc)-OH (3.48 equiv.) and Boc-Trp(Boc)-OH (1.16 equiv.). Clear colorless solid. 85% isolated yield.

G2 50 TEG 2:1 (64 H 36 W): Boc-His(Boc)-OH (3.02 equiv.) and Boc-Trp(Boc)-OH (1.62 equiv.). Clear colorless solid. 71% isolated yield.

G2 75 TEG 3:1 (71 H 29 W): Boc-His(Boc)-OH (2.28 equiv.) and Boc-Trp(Boc)-OH (0.76 equiv.). Clear colorless solid. 85% isolated yield.

G2 75 TEG 2:1 (61 H 39 W): Boc-His(Boc)-OH (1.98 equiv.) and Boc-Trp(Boc)-OH (1.06 equiv.). Clear colorless solid. 77% isolated yield

G3 TEG Backbones:

Typical Procedure for synthesis of G3 lysine dendrons on the TEGylated DP backbones:

In a 25 mL RB flask equipped with a stir bar, DPBBTEG G2 (1.00 equiv.) was dissolved in DMF. After the DPBBTEG G2 was completely dissolved, Boc-Lys(Boc)-OH DCHA (8.00 equiv.) was

added. After all reagents had been solubilized, PyBOP (10.00 equiv.) and DIPEA (12.00 equiv.) were added, and the flask was sealed with nitrogen and stirred over-night. After 12 h, 8 mL of MeOH was added to the reaction, and the mixture was purified via dialysis (MWCO = 6 – 8 kD) against MeOH for 12 h. After 12 h the mixture was concentrated *in vacuo* (no heating), yielding a solid film. The Boc groups were removed by suspending the solid in a mixture of TFA (3.0 mL), DCM (1.5 mL), anisole (1.5 mL), and TIPS (0.2 mL) and stirring for 4 h under nitrogen. The mixture was concentrated *in vacuo* (no heating), resuspended in methanol, and then precipitated in cold diethyl ether. The precipitate was pelleted via centrifugation, and the supernatant was discarded. The precipitate was purified via dialysis (MWCO = 6 – 8 kD) against MeOH for 24 h and then concentrated *in vacuo*.

G3 25 TEG Backbone: Clear colorless solid. 91% isolated yield.

G3 50 TEG Backbone: Clear colorless solid. 90% isolated yield.

G3 75 TEG Backbone: Clear colorless solid. 93% isolated yield

Histidine Tryptophan functionalized TEG G3 Denpols:

See procedure for typical DP functionalization.

G3 25 TEG 3:1 (73 H 27 W): Boc-His(Boc)-OH (9.24 equiv.) and Boc-Trp(Boc)-OH (3.08 equiv.). Clear colorless solid. 80% isolated yield.

G3 25 TEG 2:1 (64 H 36 W): Boc-His(Boc)-OH (8.01 equiv.) and Boc-Trp(Boc)-OH (4.31 equiv.). Clear colorless solid. 81% isolated yield.

G3 50 TEG 3:1 (74 H 26 W): Boc-His(Boc)-OH (6.96 equiv.) and Boc-Trp(Boc)-OH (2.32 equiv.). Clear colorless solid. 78% isolated yield.

G3 50 TEG 2:1 (64 H 36 W): Boc-His(Boc)-OH (6.03 equiv.) and Boc-Trp(Boc)-OH (3.24 equiv.). Clear colorless solid. 84% isolated yield.

G3 75 TEG 3:1 (73 H 27 W): Boc-His(Boc)-OH (4.56 equiv.) and Boc-Trp(Boc)-OH (1.52 equiv.). Clear colorless solid. 70% isolated yield.

G3 75 TEG 2:1 (62 H 38 W): Boc-His(Boc)-OH (3.95 equiv.) and Boc-Trp(Boc)-OH (2.13 equiv.). Clear colorless solid. 73% isolated yield.

G1 PEG 2k Backbones:

See typical procedure for functionalization of denpol G0 backbone with TEG or PEG

G1 1.0 PEG2k Backbone: NHS-PEG2k-OMe (0.01 equiv.). Clear colorless solid. 68% isolated yield.

G1 1.5 PEG2k Backbone: NHS-PEG2k-OMe (0.02 equiv.). Clear colorless solid. 59% isolated yield.

G1 3.0 PEG2k Backbone: NHS-PEG2k-OMe (0.05 equiv.). Clear colorless solid. 69%% isolated yield.

G2 PEG 2k Backbones:

See typical procedure for synthesis of G2 lysine dendrons on the TEGylated (or PEG) DP backbones:

G2 1.0 PEG2k Backbone: Clear colorless solid. 89% isolated yield.

G2 1.5 PEG2k Backbone: Clear colorless solid. 71% isolated yield.

G2 3.0 PEG2k Backbone: Clear colorless solid. 72% isolated yield.

Histidine Tryptophan functionalized Peg 2k G2 Denpols:

See procedure for typical DP functionalization.

G1 1.0 PEG2k 2:1 (64 H 36 W): Boc-His(Boc)-OH (5.20 equiv.) and Boc-Trp(Boc)-OH (2.80 equiv.). Clear colorless solid. 67% isolated yield.

G1 1.5 PEG2k 2:1 (67 H 33 W): Boc-His(Boc)-OH (5.20 equiv.) and Boc-Trp(Boc)-OH (2.80 equiv.). Clear colorless solid. 74% isolated yield.

G1 3.0 PEG2k 2:1 (65 H 35 W): Boc-His(Boc)-OH (5.20 equiv.) and Boc-Trp(Boc)-OH (2.80 equiv.). Clear colorless solid. 68% isolated yield.

Denpol mRNA transfection protocol:

Before performing the mRNA transfections, the area was sterilized with bleach and RNAase ZAP (Ambion), and special care was take to use RNAase free products when handling the mRNA. Transfections were performed in triplicate in a cell culture treated clear-bottom 96-well plate (Corning). Lipofectamine messangerMAX was used as a positive control, and was prepared as instructed in the manual. After synthesis, characterization, and purification of DP, a 10 mg/mL solution was prepared using RNAase free water. DP and mRNA are mixed using the indicated N:P (Protonated primary amines on Denpol:Deprotonated phosphate groups on RNA) ratio. The mRNA was thawed and diluted to a concentration of 0.05 μg/μL with optimem buffer. DP was added to a 200 μL vial. Next, the mRNA solution was added and mixed by pipetting up and down 10 times. Finally, the mixture is diluted with optimem such that 20 μL will contain 200 ng of mRNA. The mixture was then incubated at room temperature for 5 minutes. During this time the culture media of the cells to be transfected was changed to 80 μL of 10% FBS in Optimem. 20 μL of the mixture was then added to each well, and then the plate was returned to the incubator.

Imaging of FLuc mRNA transfected cells:

After the specified time of incubation with the transfection mixture, enough D-Luciferin was added to reach a concentration of 150 μg/mL. After addition, the cells were incubated for 5 minutes and then imaged using a IVIS camera to determine luminescence. After imagining the cells were discarded or the culture media was changed back to 10% FBS in DMEM if further experimentation was required.

Preparation of samples for dynamic light scattering (DLS) measurements:

The FLuc mRNA was thawed and diluted to a concentration of 0.05 μg/μL with low salt PBS buffer. DP was added to a 200 μL vial. Next, the mRNA solution was added and mixed by pipetting up and down 10 times. The mixture was diluted to 100 μL with low salt PBS The mixture was incubated at room temperature for 5 minutes. During the incubation, 80 μL of the selected media is added to a 100 μL cuvette. After 5 minutes 20 μL of the mRNA DP mixture is added to the cuvette and mixed via pipetting up and down 10 times. The cuvette is then placed in the instrument and the measurements are made.

Procedure for confocal microscopy:

Confocal laser microscopy was used to track cyanine-5 labeled mRNA in the transfected cells. Unmodified NIH 3T3 fibroblast cells were seeded at a density of 15000 cells/well on an 8-well chamber slide (Lab-Tek , Rochester, NY) 24h before transfection. Cy-5 labeled mRNA was complexed with different denpols at an N:P of 10 and transfected to the cells under the aforementioned conditions. Confocal fluorescence spectroscopy was performed at 4 h and 24 h post transfection. The nucleus was counter-stained with 0.5 μg/mL solution of Hoechst 33342. All confocal images were acquired using a Zeiss LSM 700 inverted laser-scanning confocal

microscope. A 63× plan apochromatic numerical aperture of 1.4 oil immersion DIC III objective or 20× plan apochromatic numerical aperture of 0.8 DIC II objective was used for all experiments. A 639 nm laser and a 606-700 nm band-pass filter were used to obtain the images of Cy-5 labeled mRNA. A 405 nm laser and a 400-498 nm band-pass filter were used to obtain the images of the Hoechst 33342 counter-stained nuclei. The fluorescent images were scanned separately and overlaid together with the differential interference contrast image (DIC). The cells were scanned as a z-stack of two-dimensional images (1024×1024 pixels) and an image cutting approximately through the middle of the cellular height was selected to present the intracellular mRNA localization.

Gel shift assay to survey mRNA binding:

The binding of mRNA to denpol was studied by agarose gel electrophoresis. Both mRNA and denpol were diluted with 10 mM pH 7.4 phosphate buffer. Different amount of denpol solutions (10 mg/mL) were added to 5 µL of a .04 µg/µL mRNA solution to achieve the specified N:P ratios. The same buffer was added to adjust the final volume to 10.0 µL, followed by 5 min incubation at room temperature. 2.5 µL 6X gel loading dye was added to each sample and 10 µL of the mixture was loaded to each well in 1% agarose gel with 1X GelRed dye. The electrophoresis was run in TAE buffer (pH 7.9) at 60 V for 45 min and the gel was visualized under a UV trans illuminator.

Flow cytometry measurements:

Before flow cytometry, the cells are harvested from the 96 well plate via trypsin for the 3T3 and DC 2.4 cells and pipetting for the BMDC cells followed by centrifugation. The cells are washed with PBS and spun down 3 additional times to remove excess Cy-5 labeled mRNA (if it was used). 5000 events were recorded per sample. Each value reported is the average of 3 samples.

LDH cytotoxicity assay:

NIH 3t3 cells seeded in a 96 well plate were treated with denpol mRNA nanoparticles at an N:P ratio of 30, formulated as specified above. After 24 h incubation with the nano particles, 50 µL of the supernatant was taken and cytotoxicity was measured using a Pierce™ LDH Cytotoxicity Assay Kit (ThermoFisher) as directed in the manual.

AFM imaging:

Polyplexes were prepared at an N/P ratio of 10 as described above. mRNA polyplexes were prepared in water. After incubation for 20 min at room temperature, a drop of the solution was placed on freshly cleaved mica, and dried using an air gun to avoid drying effects before measurement. The images were all taken on an MFP-3D StandAlone AFM (Asylum Research, Santa Barbara, CA) through tapping-mode using a monolithic silicon TESP-10 tip (NanoAndMore USA, Watsonville, CA) with resonant frequency =320 kHz and a spring constant k =42 N/m.

¹H NMR characterizations of denpols:

¹HNMR of the polymer samples used a 10 second relaxation time to ensure chain relaxation and to help with resolution. Methanol and water were unable to be completely removed from the polymer samples. The actual percentage functionalization of the Denpols as determined by integration is listed after the name of the denpols. As the polymer samples become more functionalized, the spectra become complex and peak resolution becomes difficult. Unless fully resolved, ranges of peaks are listed.

G2 3:1 (77.4 H 22.6 W): ¹H NMR (600 MHz, D₂O) δ 8.61 – 7.97 (m, 5H), 7.70 – 6.95 (m, 13H), 4.67 – 4.52 (m, 1H), 4.52 – 3.87 (m, 15H), 3.53 – 2.62 (m, 34H), 2.07 – 0.71 (m, 48H).

G2 2:1 (66 H 34 W): ¹H NMR (600 MHz, D₂O) δ 8.58 – 8.01 (m, 5H), 7.70 – 6.88 (m, 18H), 4.67 – 4.49 (m, 1H), 4.49 – 3.86 (m, 15H), 3.64 – 2.69 (m, 34H), 2.09 – 0.67 (m, 47H).

G2 1:1 (55 H 45 W): ¹H NMR (600 MHz, D₂O) δ 8.66 – 8.02 (m, 4H), 7.69 – 6.82 (m, 19H), 4.66 – 4.52 (m, 1H), 4.49 – 3.87 (m, 15H), 3.47 – 2.54 (m, 33H), 2.02 – 0.63 (m, 52H).

G2 1:2 (39 H 61 W): ¹H NMR (600 MHz, D₂O) δ 8.62 – 7.95 (m, 4H), 7.67 – 6.80 (m, 25H), 4.64 – 4.49 (m, 1H), 4.50 – 3.82 (m, 15H), 3.59 – 2.60 (m, 33H), 2.09 – 0.60 (m, 50H).

G2 1:3 (27 H 73 W): ¹H NMR (600 MHz, D₂O) δ 8.61 – 7.95 (m, 2H), 7.70 – 6.75 (m, 28H), 4.67 – 4.49 (m, 1H), 4.51 – 3.79 (m, 15H), 3.71 – 2.50 (m, 33H), 2.05 – 0.54 (m, 47H).

G3 Backbone: ¹H NMR (600 MHz, CD₃OD) δ 4.74 – 4.56 (m, 5H), 4.57 – 4.28 (m, 8H), 4.27 – 4.08 (m, 2H), 4.13 – 3.96 (m, 4H), 3.96 – 3.81 (m, 4H), 3.45 – 3.09 (m, 34H), 3.09 – 2.85 (m, 19H), 2.16 – 1.07 (m, 101H).

G3 3:1 (71 H 29 W): ¹H NMR (600 MHz, D₂O) δ 8.44 – 7.77 (m, 14H), 7.66 – 6.81 (m, 43H), 4.66 – 4.52 (m, 2H), 4.43 – 3.89 (m, 35H), 3.52 – 2.61 (m, 73H), 2.08 – 0.55 (m, 105H).

G3 2:1 (66 H 34 W): ^{1}H NMR (600 MHz, D$_2$O) δ 8.21 – 7.69 (m, 12H), 7.69 – 6.71 (m, 45H), 4.52 – 3.80 (m, 35H), 3.52 – 2.61 (m, 64H), 2.10 – 0.38 (m, 93H).

G3 1:1 (53 H 47 W): ^{1}H NMR (600 MHz, D$_2$O) δ 8.17 – 7.67 (m, 11H), 7.63 – 6.68 (m, 57H), 4.48 – 3.79 (m, 35H), 3.49 – 2.51 (m, 69H), 2.00 – 0.43 (m, 100H).

G3 1:2 (33 H 67 W): ^{1}H NMR (600 MHz, D$_2$O) δ 8.22 – 7.69 (m, 11H), 7.67 – 6.70 (m, 61H), 4.44 – 3.79 (m, 35H), 3.47 – 2.47 (m, 68H), 1.96 – 0.42 (m, 102H).

G3 1:3 (28 H 72 W): ^{1}H NMR (600 MHz, D$_2$O) δ 8.04 – 7.66 (m, 6H), 7.63 – 6.70 (m, 70H), 4.49 – 3.73 (m, 35H), 3.47 – 2.39 (m, 67H), 1.95 – 0.45 (m, 93H).

G1 25 TEG: ^{1}H NMR (600 MHz, CD$_3$OD) δ 4.80 – 4.71 (m, 2H), 4.71 – 4.59 (m, 1H), 4.60 – 4.47 (m, 0.5 H), 4.47 – 4.30 (m, 1.39H), 4.29 – 4.10 (m, 3H), 4.12 – 3.90 (m, 1.5H), 3.80 – 3.50 (m, 6.47H), 3.36 (s, 0.7H), 3.28 – 3.11 (m, 7H), 3.10 – 2.87 (m, 4.8H), 2.04 – 1.81 (m, 4H), 1.79 – 1.63 (m, 4H), 1.64 – 1.32 (m, 7.2H), 1.26 (t, J = 6.9 Hz, 3H).

G1 50 TEG: ^{1}H NMR (600 MHz, CD$_3$OD) δ 4.72 – 4.61 (m, 1H), 4.60 – 4.49 (m, 0.47H), 4.48 – 4.32 (m, 1.72H), 4.30 – 4.10 (m, 4H), 4.11 – 3.96 (m, 1H), 3.79 – 3.51 (m, 12.1H), 3.37 (s, 1.2H), 3.29 – 3.08 (m, 3.67H), 3.08 – 2.86 (m, 3.9H), 2.03 – 1.81 (m, 3.16H), 1.81 – 1.65 (m, 3.02H), 1.66 – 1.34 (m, 6.28H), 1.27 (t, J = 6.7 Hz, 3H).

G1 75 TEG: ^{1}H NMR (600 MHz, CD$_3$OD) δ 4.64 – 4.50 (m, 0.65H), 4.50 – 4.32 (m, 1.54H), 4.32 – 4.10 (m, 4.12H), 4.10 – 3.96 (m, 0.54H), 3.87 – 3.49 (m, 16.84H), 3.28 – 3.10 (m, 3.46H), 3.10 – 2.83 (m, 2.25H), 2.04 – 1.82 (m, 1.78H), 1.84 – 1.66 (m, 1.77H), 1.66 – 1.34 (m, 4.66H), 1.34 – 1.10 (m, 3H).

G2 TEG 25: ^{1}H NMR (500 MHz, CD$_3$OD) δ 4.69 – 4.26 (m, 4H), 4.25 – 4.08 (m, 3H), 4.08 – 3.90 (m, 1H), 3.90 – 3.76 (m, 1H), 3.76 – 3.49 (m, 6H), 3.44 – 3.03 (m, 32H), 3.04 – 2.77 (m, 7H), 2.06 – 1.76 (m, 8H), 1.76 – 1.60 (m, 8H), 1.60 – 1.28 (m, 15H), 1.28 – 1.15 (m, 3H).

G2 TEG 50: ^{1}H NMR (500 MHz, CD$_3$OD) δ 4.63 – 4.46 (m, 1H), 4.46 – 4.27 (m, 2H), 4.27 – 4.07 (m, 3H), 4.07 – 3.90 (m, 1H), 3.90 – 3.78 (m, 1H), 3.75 – 3.47 (m, 11H), 3.45 – 3.04 (m, 24H), 3.03 – 2.75 (m, 5H), 2.07 – 1.76 (m, 5H), 1.76 – 1.61 (m, 5H), 1.61 – 1.29 (m, 11H), 1.29 – 1.15 (m, 3H).

G2 TEG 75: ^{1}H NMR (500 MHz, CDCl$_3$) δ 4.62 – 4.49 (m, 1H), 4.49 – 4.30 (m, 2H), 4.30 – 4.09 (m, 4H), 4.09 – 3.94 (m, 1H), 3.94 – 3.80 (m, 1H), 3.83 – 3.48 (m, 17H), 3.48 – 3.09 (m, 11H), 3.09 – 2.83 (m, 3H), 2.06 – 1.81 (m, 3H), 1.80 – 1.65 (m, 3H), 1.65 – 1.33 (m, 7H), 1.33 – 1.18 (m, 3H).

G2 25 TEG 3:1 (74 H 26 W): ^{1}H NMR (600 MHz, CD$_3$OD) δ 8.91 – 8.57 (m, 5H), 7.74 – 6.93 (m, 12H), 4.59 – 3.95 (m, 14H), 3.78 – 2.72 (m, 80H), 1.93 – 1.00 (m, 69H).

G2 25 TEG 2:1 (63 H 32 W): ^{1}H NMR (600 MHz, CD$_3$OD) δ 8.94 – 8.58 (m, 4H), 7.73 – 6.92 (m, 18H), 4.59 – 3.95 (m, 21H), 3.80 – 2.74 (m, 120H), 2.16 – 1.02 (m, 98H).

G2 50 TEG 3:1 (73 H 27 W): ^{1}H NMR (600 MHz, CD$_3$OD) δ 8.89 – 8.62 (m, 3H), 7.72 – 6.94 (m, 9H), 4.52 – 3.96 (m, 18H), 3.80 – 2.79 (m, 278H), 2.09 – 1.10 (m, 38H).

G2 50 TEG 2:1 (64 H 36 W): ^{1}H NMR (600 MHz, CD$_3$OD) δ 8.91 – 8.60 (m, 3H), 7.72 – 6.94 (m, 12H), 4.60 – 3.92 (m, 16H), 3.85 – 2.73 (m, 71H), 2.15 – 1.04 (m, 47H).

G2 75 TEG 3:1 (71 H 29 W): ^{1}H NMR (600 MHz, CD$_3$OD) δ 8.93 – 8.69 (m, 2H), 7.75 – 7.00 (m, 7H), 4.63 – 4.02 (m, 18H), 3.86 – 2.78 (m, 91H), 2.11 – 1.07 (m, 41H).

G2 75 TEG 2:1 (61 H 39 W): ^{1}H NMR (600 MHz, CD$_3$OD) δ 9.01 – 8.71 (m, 2H), 7.76 – 6.97 (m, 8H), 4.69 – 3.96 (m, 16H), 3.83 – 2.77 (m, 75H), 2.10 – 1.01 (m, 35H).

G3 25 TEG Backbone: ^{1}H NMR (600 MHz, CD$_3$OD) δ 4.78 – 4.69 (m, 1H), 4.69 – 4.59 (m, 1H), 4.48 – 4.27 (m, 3H), 4.27 – 4.11 (m, 2H), 4.10 – 3.96 (m, 2H), 3.96 – 3.82 (m, 2H), 3.76 – 3.52

(m, 4H), 3.44 – 3.08 (m, 12H), 3.08 – 2.80 (m, 9H), 2.06 – 1.63 (m, 23H), 1.63 – 1.32 (m, 23H), 1.32 – 1.15 (m, 3H).

G3 25 TEG Backbone: ^{1}H NMR (600 MHz, CD$_3$OD) δ 4.79 – 4.70 (m, 1H), 4.69 – 4.49 (m, 1H), 4.52 – 4.28 (m, 3H), 4.28 – 4.11 (m, 3H), 4.11 – 3.97 (m, 1H), 3.97 – 3.81 (m, 2H), 3.81 – 3.53 (m, 9H), 3.48 – 3.09 (m, 13H), 3.09 – 2.87 (m, 7H), 2.07 – 1.65 (m, 19H), 1.65 – 1.33 (m, 19H), 1.33 – 1.22 (m, 3H).

G3 75 TEG Backbone: ^{1}H NMR (600 MHz, CD$_3$OD) δ 4.72 – 4.51 (m, 1H), 4.51 – 4.30 (m, 2H), 4.30 – 4.12 (m, 3H), 4.12 – 3.97 (m, 1H), 3.97 – 3.84 (m, 1H), 3.83 – 3.52 (m, 13H), 3.47 – 3.11 (m, 12H), 3.09 – 2.85 (m, 4H), 2.05 – 1.82 (m, 5H), 1.81 – 1.67 (m, 5H), 1.68 – 1.34 (m, 11H), 1.35 – 1.21 (m, 3H).

G3 75 TEG 3:1 (73 H 27 W): ^{1}H NMR (500 MHz, CD$_3$OD) δ 8.93 – 8.63 (m, 9H), 7.72 – 7.53 (m, 3H), 7.56 – 7.31 (m, 12H), 7.31 – 7.18 (m, 4H), 7.18 – 6.95 (m, 6H), 4.82 – 4.61 (m, 1H), 4.61 – 3.99 (m, 26H), 3.82 – 2.69 (m, 85H), 2.18 – 1.09 (m, 108H).

G3 25 TEG 2:1 (64 H 36 W): ^{1}H NMR (500 MHz, CD$_3$OD) δ 8.89 – 8.51 (m, 8H), 7.67 – 7.48 (m, 4H), 7.48 – 7.24 (m, 12H), 7.24 – 7.11 (m, 5H), 7.14 – 6.87 (m, 9H), 4.65 – 4.51 (m, 1H), 4.53 – 3.89 (m, 26H), 3.75 – 2.76 (m, 87H), 2.05 – 1.02 (m, 103H).

G3 25 TEG 3:1 (74 H 26 W): ^{1}H NMR (600 MHz, CD$_3$OD) δ 8.90 – 8.65 (m, 7H), 7.66 – 7.51 (m, 3H), 7.51 – 7.29 (m, 9H), 7.29 – 7.16 (m, 3H), 7.16 – 6.95 (m, 4H), 4.66 – 4.55 (m, 1H), 4.52 – 3.96 (m, 24H), 3.75 – 2.80 (m, 81H), 1.94 – 1.07 (m, 88H).

G3 50 TEG 2:1 (64 H 36 W): ^{1}H NMR (600 MHz, CD$_3$OD) δ 8.91 – 8.57 (m, 6H), 7.67 – 7.51 (m, 3H), 7.50 – 7.26 (m, 9H), 7.26 – 7.14 (m, 3H), 7.14 – 6.93 (m, 7H), 4.50 – 3.93 (m, 25H), 3.74 – 2.77 (m, 74H), 2.00 – 1.00 (m, 72H).

G3 50 TEG 3:1 (73 H 27 W): ^{1}H NMR (600 MHz, CD$_3$OD) δ 8.91 – 8.66 (m, 4H), 7.72 – 7.54 (m, 2H), 7.54 – 7.29 (m, 6H), 7.28 – 7.17 (m, 2H), 7.17 – 6.95 (m, 3H), 4.68 – 4.54 (m, 1H), 4.54 – 3.97 (m, 22H), 3.77 – 2.76 (m, 76H), 2.01 – 1.00 (m, 63H).

G3 75 TEG 2:1 (62 H 38 W): ^{1}H NMR (600 MHz, CD$_3$OD) δ 8.90 – 8.63 (m, 4H), 7.71 – 7.52 (m, 2H), 7.54 – 7.29 (m, 6H), 7.28 – 7.17 (m, 2H), 7.17 – 6.95 (m, 5H), 4.66 – 4.52 (m, 1H), 4.50 – 3.97 (m, 21H), 3.81 – 2.81 (m, 76H), 2.01 – 1.04 (m, 56H).

G1 1.0 PEG2k Backbone: ^{1}H NMR (600 MHz, D$_2$O) δ 4.72 – 4.62 (m, 2H), 4.43 – 4.31 (m, 1H), 4.30 – 4.16 (m, 2H), 4.16 – 4.01 (m, 2H), 3.80 – 3.68 (m, 1H), 3.49 – 2.91 (m, 19H), 2.05 – 1.85 (m, 4H), 1.85 – 1.66 (m, 4H), 1.67 – 1.34 (m, 7H), 1.34 – 1.17 (m, 3H).

G1 1.5 PEG2k Backbone: ^{1}H NMR (600 MHz, D$_2$O) δ 4.71 – 4.58 (m, 1H), 4.44 – 4.32 (m, 1H), 4.30 – 4.16 (m, 1H), 4.15 – 4.01 (m, 1H), 3.81 – 3.66 (m, 1H), 3.47 – 2.93 (m, 9H), 2.08 – 1.67 (m, 5H), 1.67 – 1.35 (m, 4H), 1.35 – 1.21 (m, 1H).

G1 3.0 PEG2k Backbone: ^{1}H NMR (600 MHz, D$_2$O) δ 4.71 – 4.61 (m, 2H), 4.45 – 4.32 (m, 1H), 4.32 – 4.18 (m, 2H), 4.18 – 4.00 (m, 1H), 3.83 – 3.65 (m, 6H), 3.34 – 2.93 (m, 9H), 2.05 – 1.85 (m, 4H), 1.85 – 1.67 (m, 4H), 1.66 – 1.35 (m, 7H), 1.35 – 1.20 (m, 3H).

G2 1.0 PEG2k Backbone: ^{1}H NMR (600 MHz, CD$_3$OD) δ 4.77 – 3.95 (m, 8H), 3.97 – 3.83 (m, 2H), 3.76 – 3.62 (m, 2H), 3.44 – 3.10 (m, 14H), 3.10 – 2.85 (m, 9H), 2.12 – 1.82 (m, 11H), 1.81 – 1.67 (m, 10H), 1.67 – 1.33 (m, 20H), 1.33 – 1.19 (m, 3H).

G2 1.5 PEG2k Backbone: ^{1}H NMR (600 MHz, CD$_3$OD) δ 4.75 – 4.26 (m, 5H), 4.26 – 3.96 (m, 3H), 3.96 – 3.79 (m, 1H), 3.76 – 3.59 (m, 2H), 3.47 – 3.08 (m, 20H), 3.08 – 2.86 (m, 8H), 2.13 – 1.81 (m, 9H), 1.81 – 1.66 (m, 9H), 1.66 – 1.33 (m, 17H), 1.33 – 1.16 (m, 3H).

G2 3.0 PEG2k Backbone: ^{1}H NMR (600 MHz, CD$_3$OD) δ 4.76 – 4.29 (m, 4H), 4.27 – 4.13 (m, 2H), 4.15 – 3.95 (m, 2H), 3.95 – 3.83 (m, 2H), 3.78 – 3.61 (m, 7H), 3.50 – 3.09 (m, 24H), 3.09 –

2.89 (m, 8H), 2.14 – 1.82 (m, 10H), 1.82 – 1.67 (m, 10H), 1.67 – 1.34 (m, 18H), 1.34 – 1.21 (m,

3H).

G1 1.0 PEG2k 2:1 (64 H 36 W): ^{1}H NMR (600 MHz, CD$_3$OD) δ 8.14 – 7.81 (m, 5H), 7.68 – 7.50

(m, 3H), 7.43 – 7.29 (m, *J* = 6.4 Hz, 3H), 7.29 – 6.82 (m, 14H), 4.76 – 4.61 (m, 2H), 4.58 – 3.94

(m, 19H), 3.71 – 2.77 (m, 71H), 2.05 – 1.05 (m, 60H).

G1 1.5 PEG2k 2:1 (67 H 33 W): ^{1}H NMR (600 MHz, CD$_3$OD) δ 8.28 – 7.87 (m, 5H), 7.71 – 7.52

(m, 2H), 7.44 – 7.29 (m, 3H), 7.29 – 6.89 (m, 13H), 4.72 – 4.59 (m, 2H), 4.57 – 3.95 (m, 18H),

3.75 – 2.78 (m, 69H), 2.01 – 1.03 (m, 61H).

G1 3.0 PEG2k 2:1 (65 H 35 W[1]H NMR (600 MHz, CD$_3$OD) δ 8.19 – 7.82 (m, 5H), 7.75 – 7.55

(m, 3H), 7.44 – 7.31 (m, 3H), 7.32 – 6.93 (m, 13H), 4.77 – 4.63 (m, 1H), 4.57 – 4.00 (m, 18H),

3.75 – 2.83 (m, 58H), 2.13 – 1.05 (m, 73H).

¹H NMR spectra of denpols:

G2 3:1 (77 H 23 W):
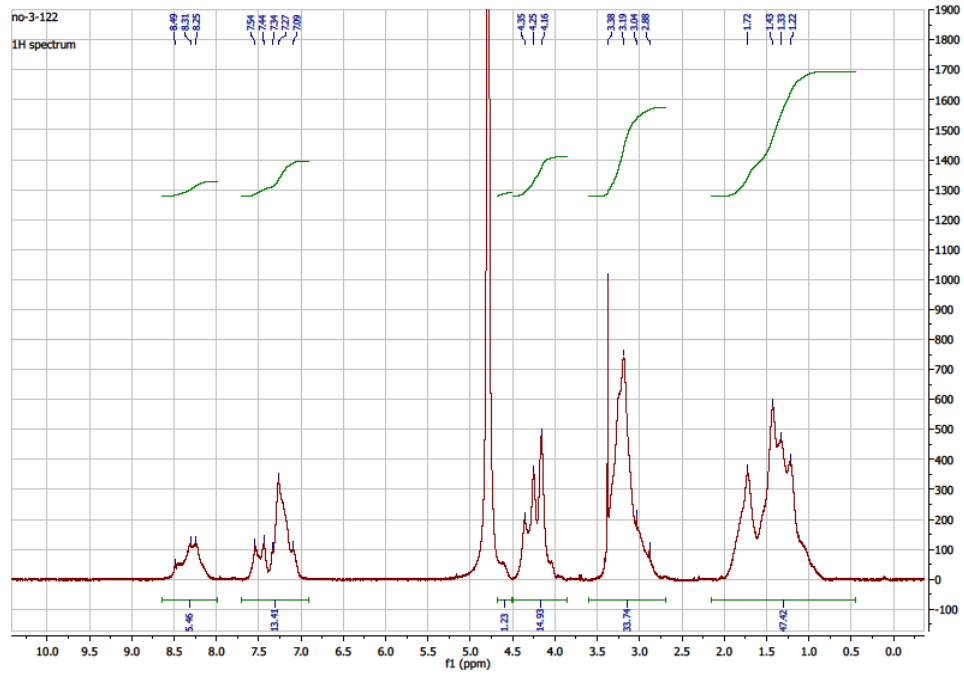
G2 2:1 (66 H 34 W):
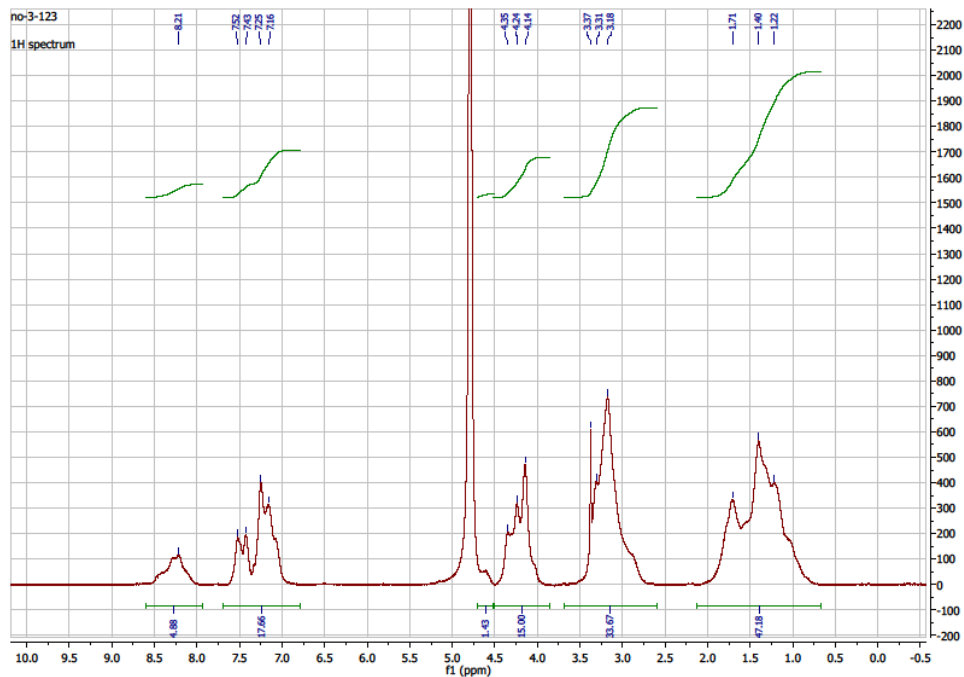
G2 1:1 (55 H 45 W):
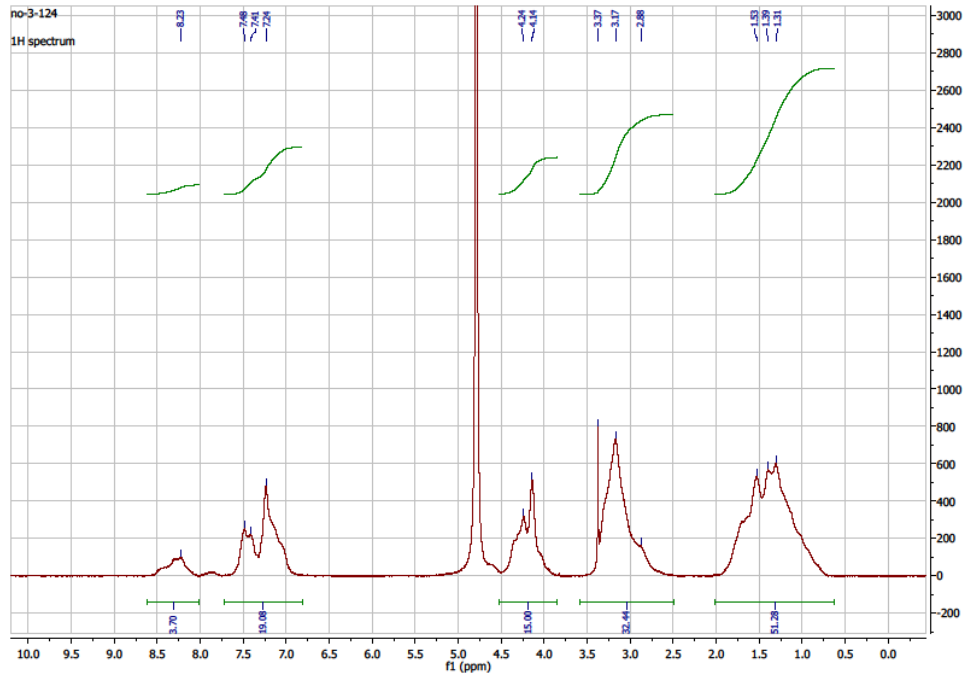
G2 1:2 (39 H 61 W):
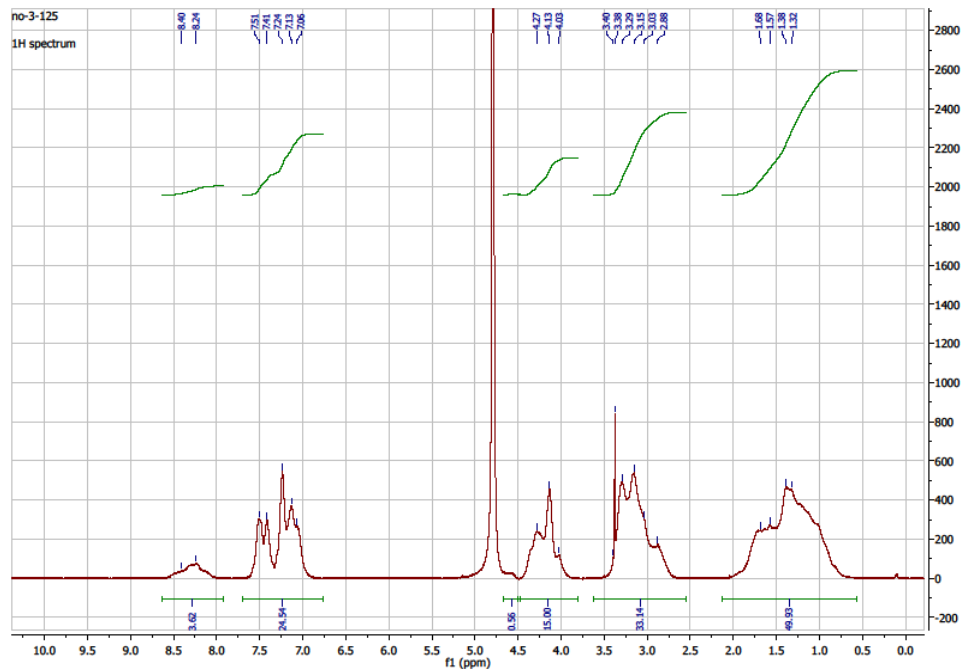
G2 1:3 (27 H 73 W):
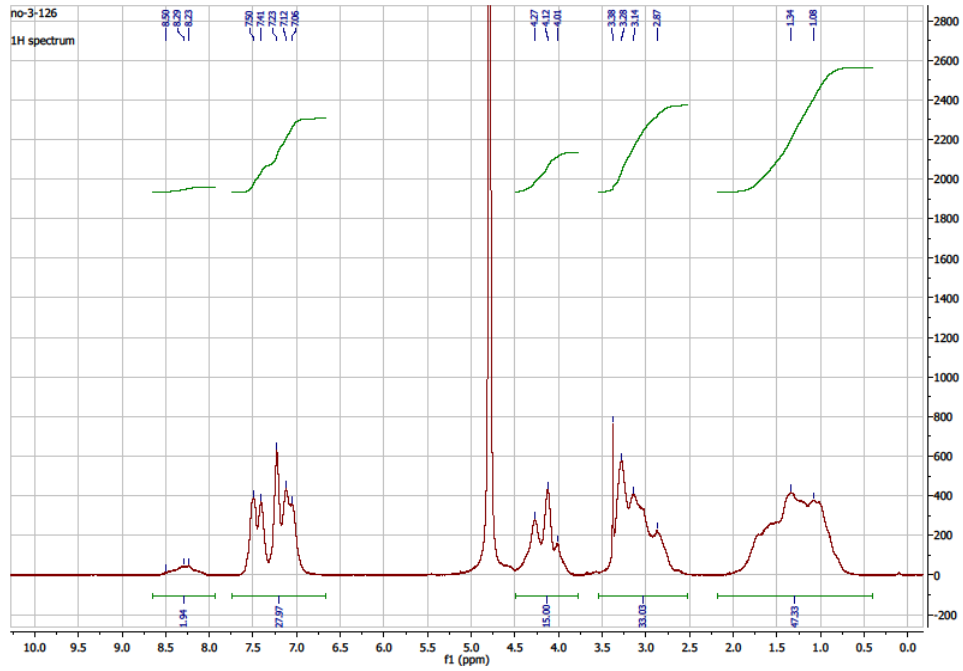
G3 Backbone:
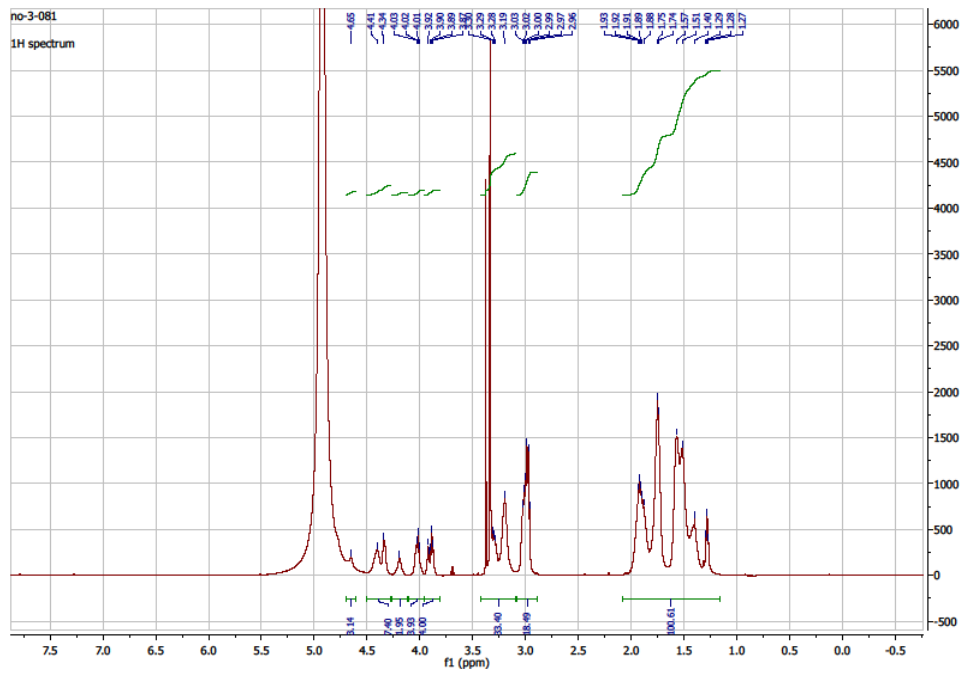
G3 3:1 (71 H 29 W):
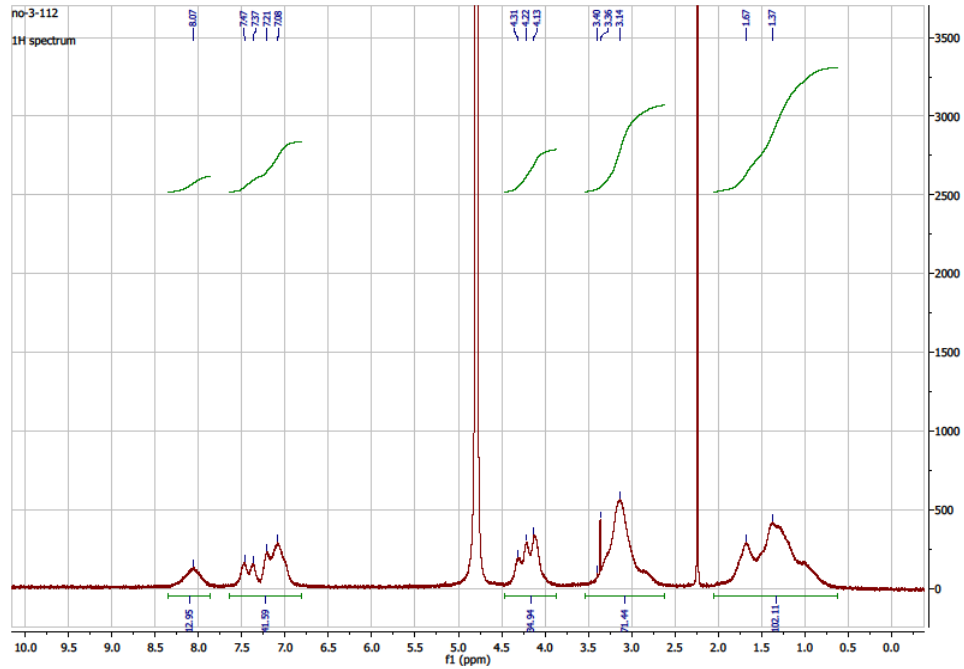
G3 2:1 (66 H 34 W):
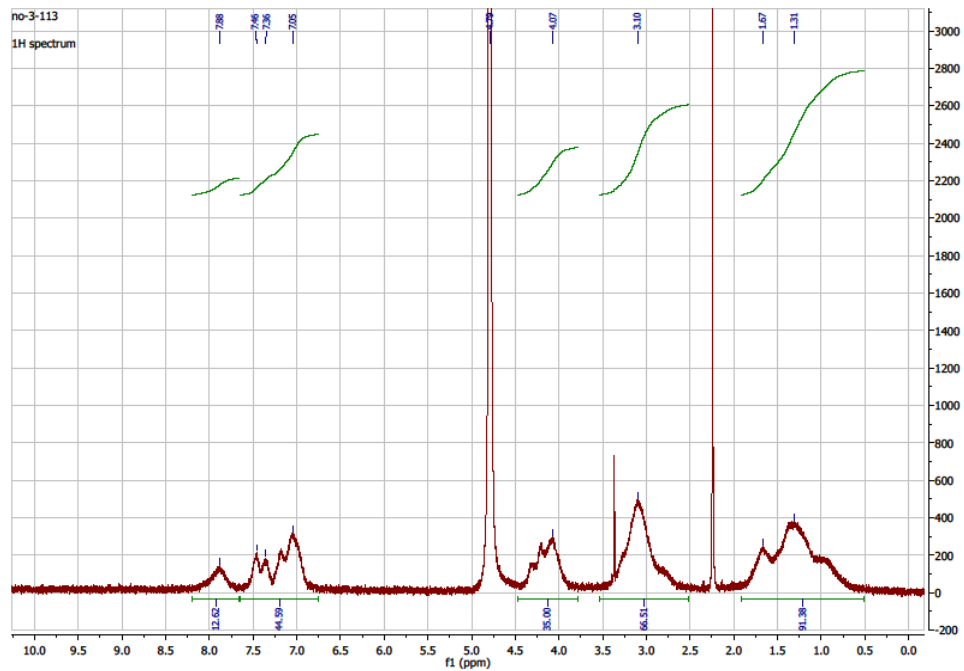
G3 1:1 (53 H 47 W):
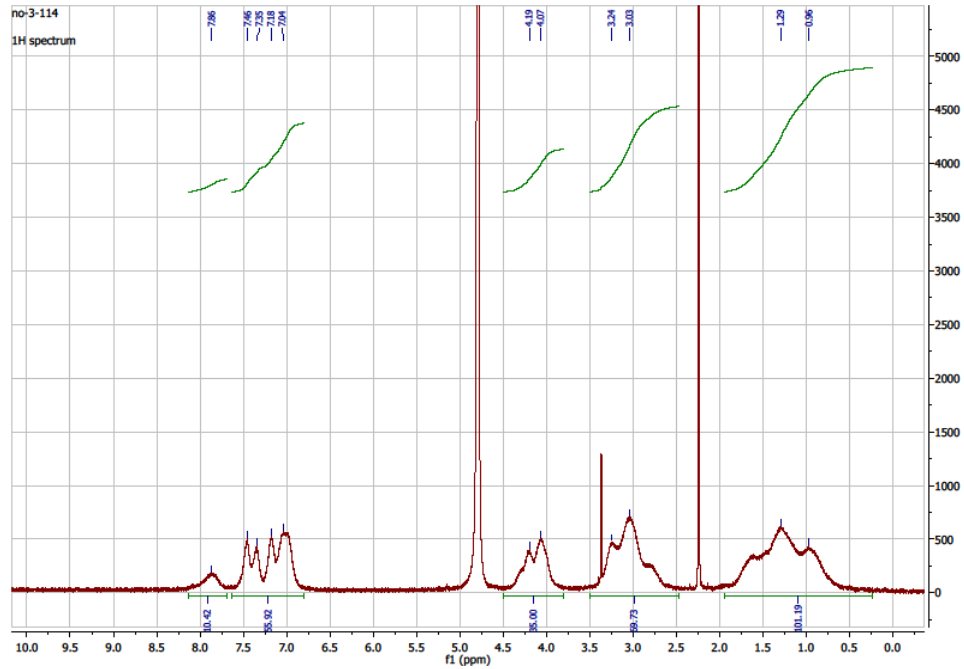
G3 1:2 (33 H 67 W):
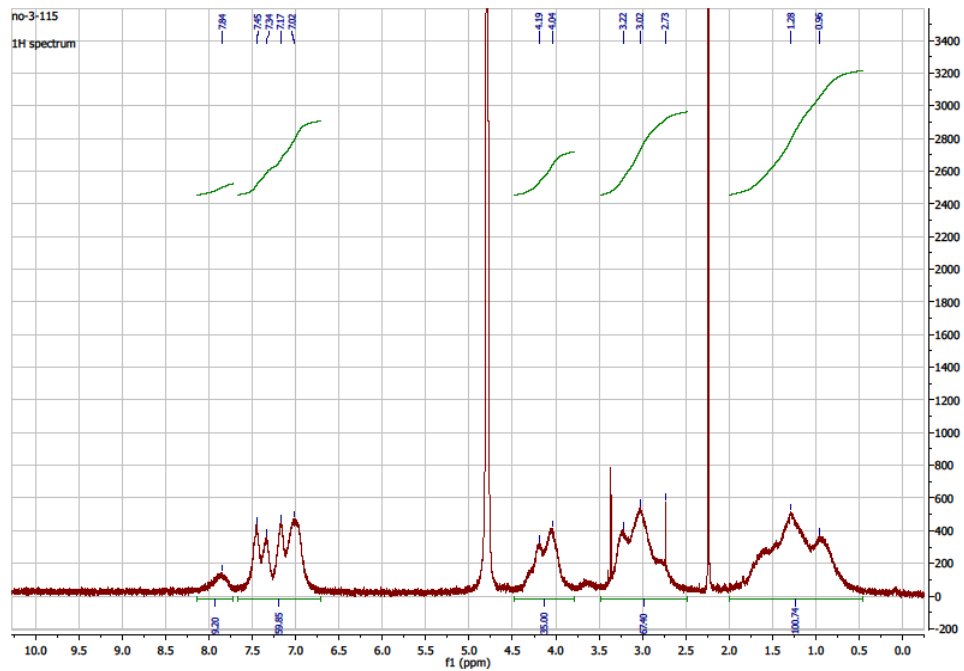
G3 1:3 (28 H 72 W):
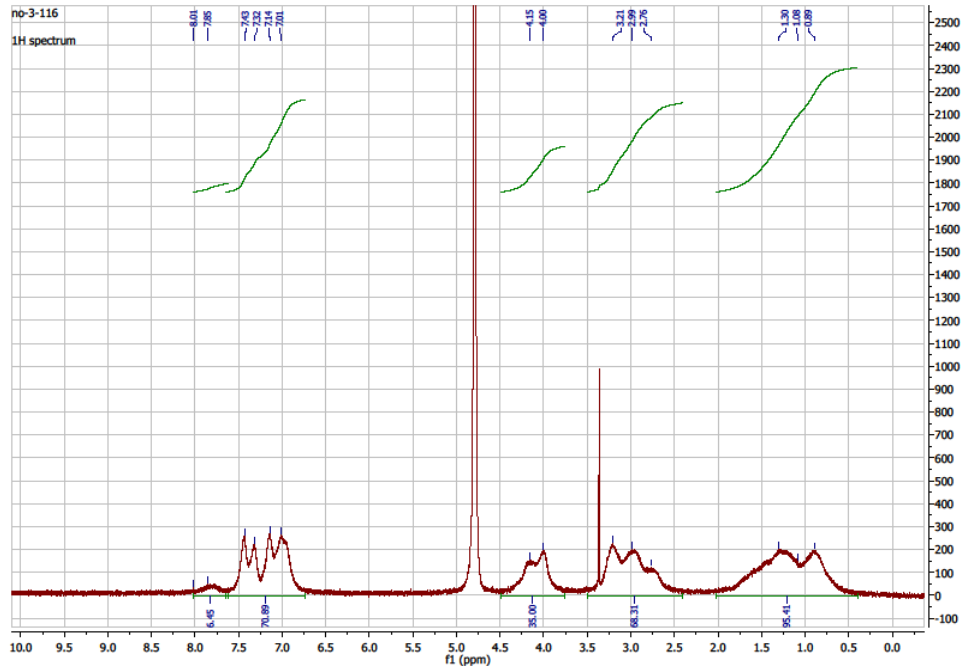
G1 25 TEG:
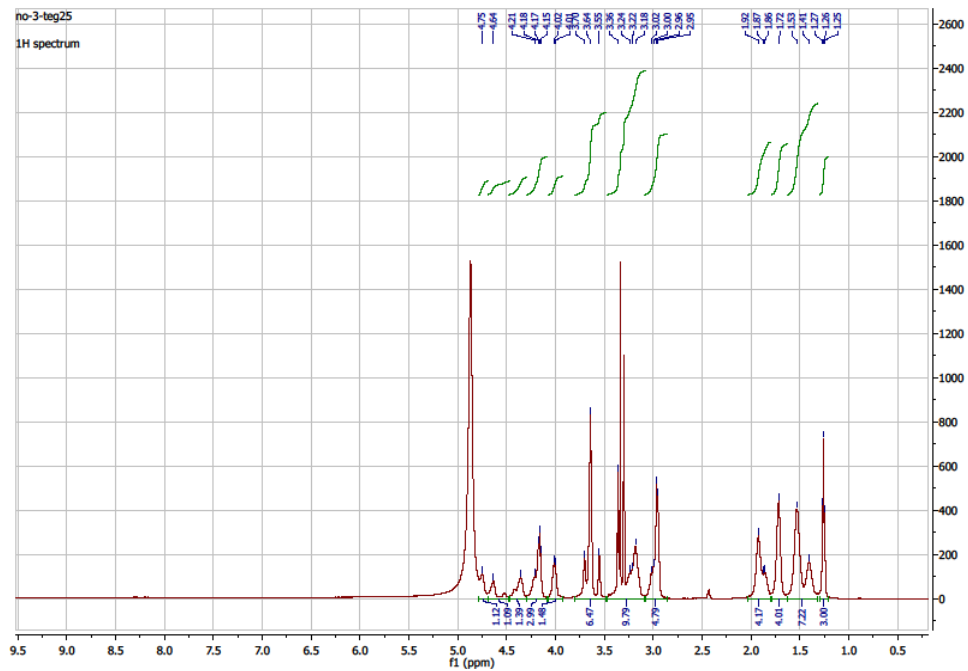
G1 50 TEG:
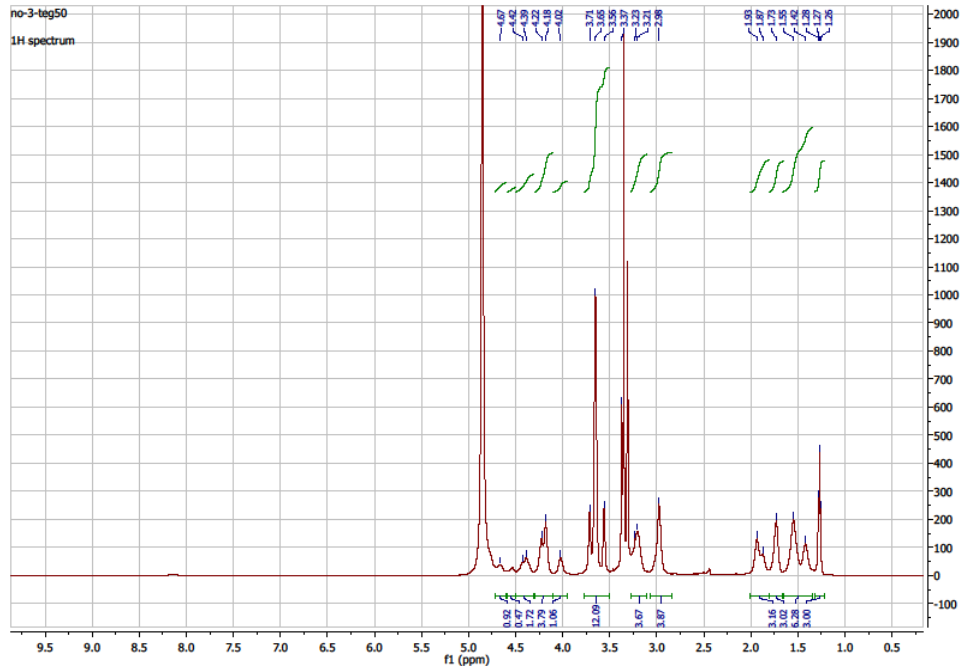
G1 75 TEG:
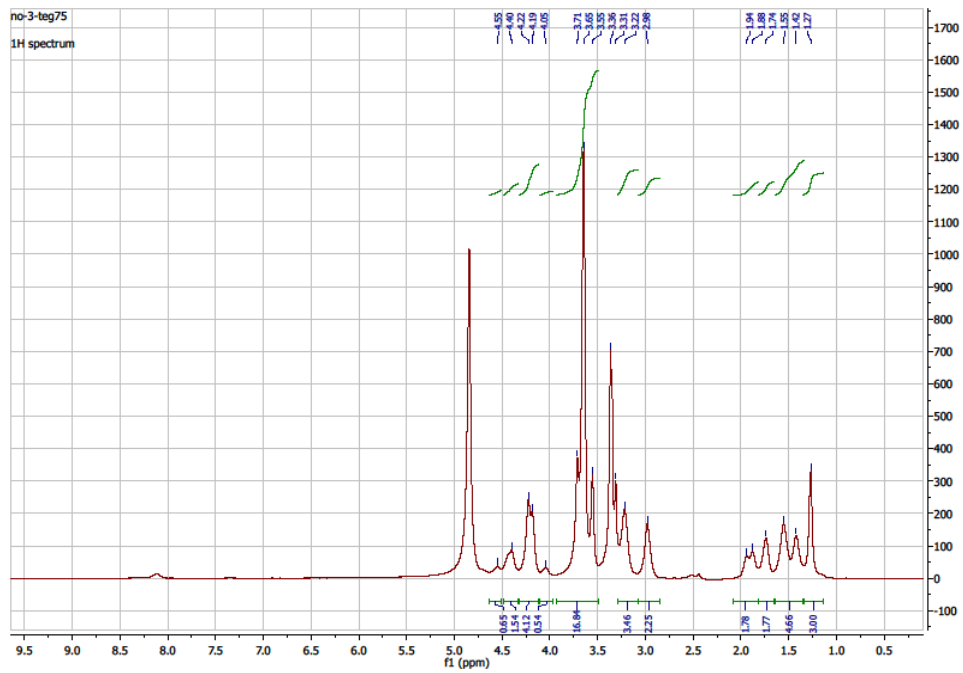
G2 TEG 25:
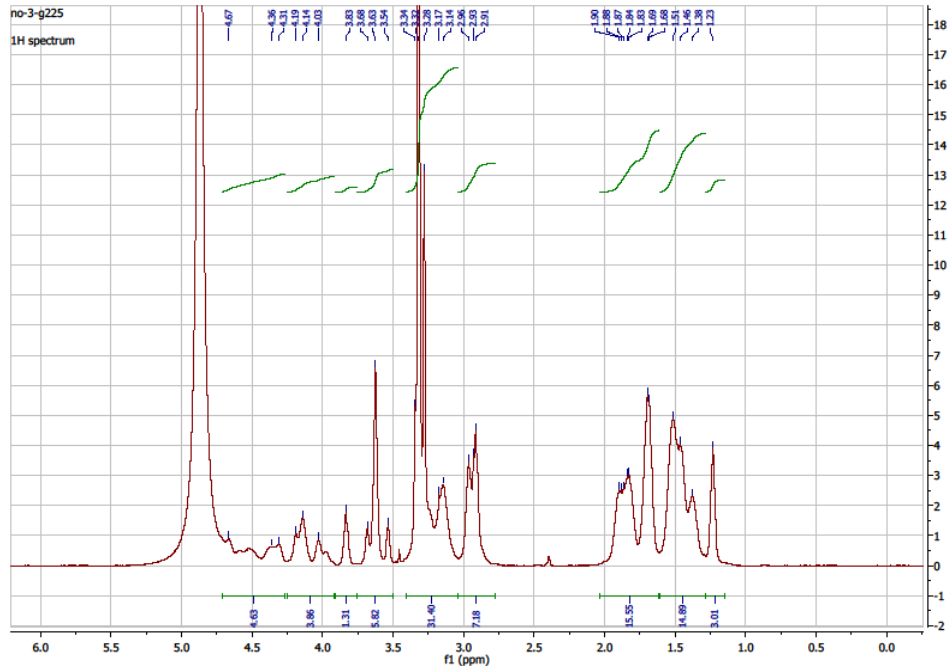
G2 TEG 50:
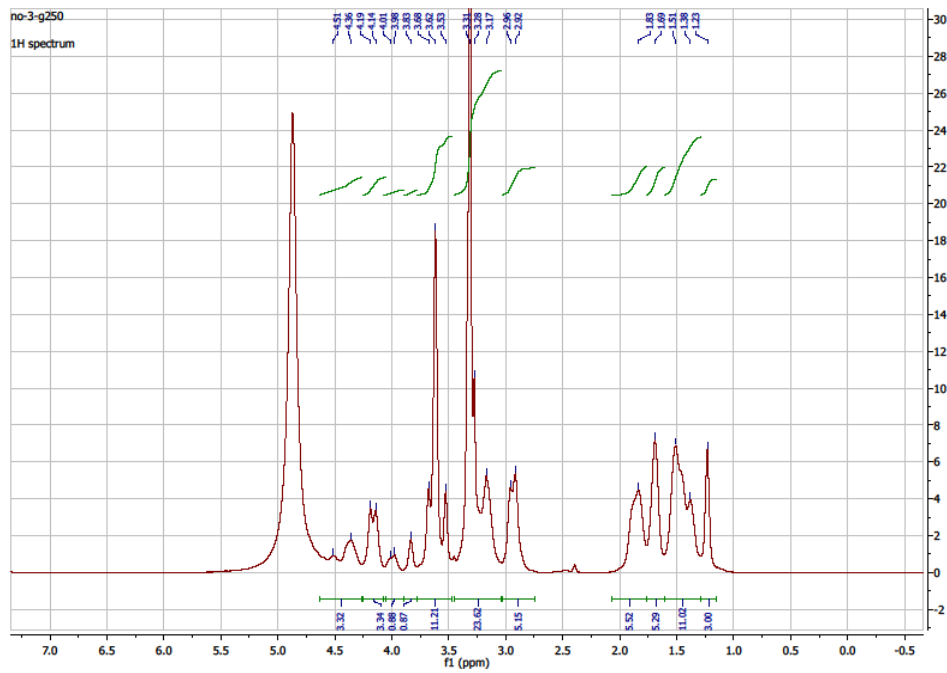
G2 TEG 75:
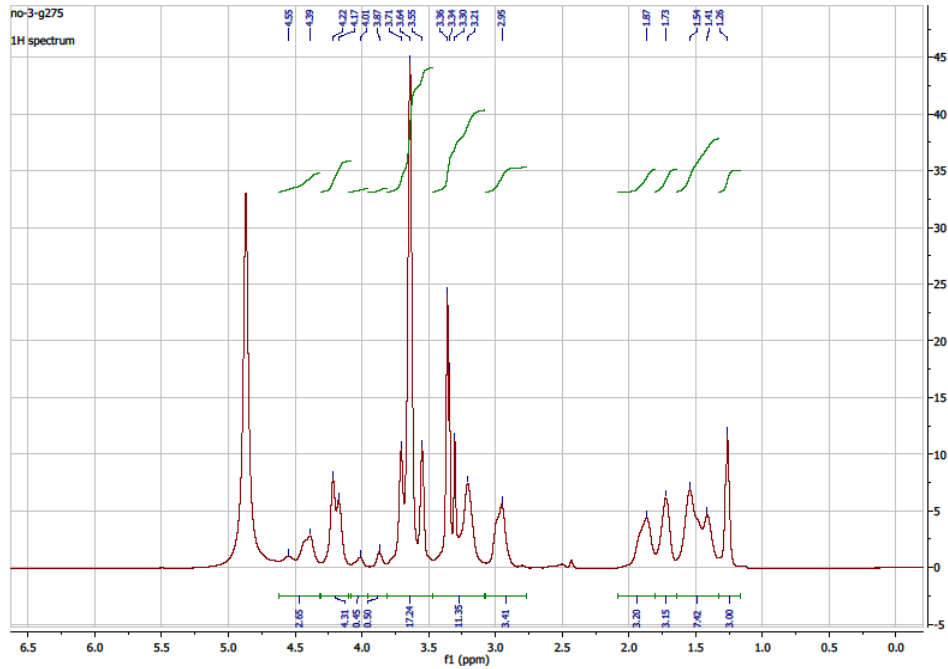
G2 25 TEG 3:1 (74 H 26 W):
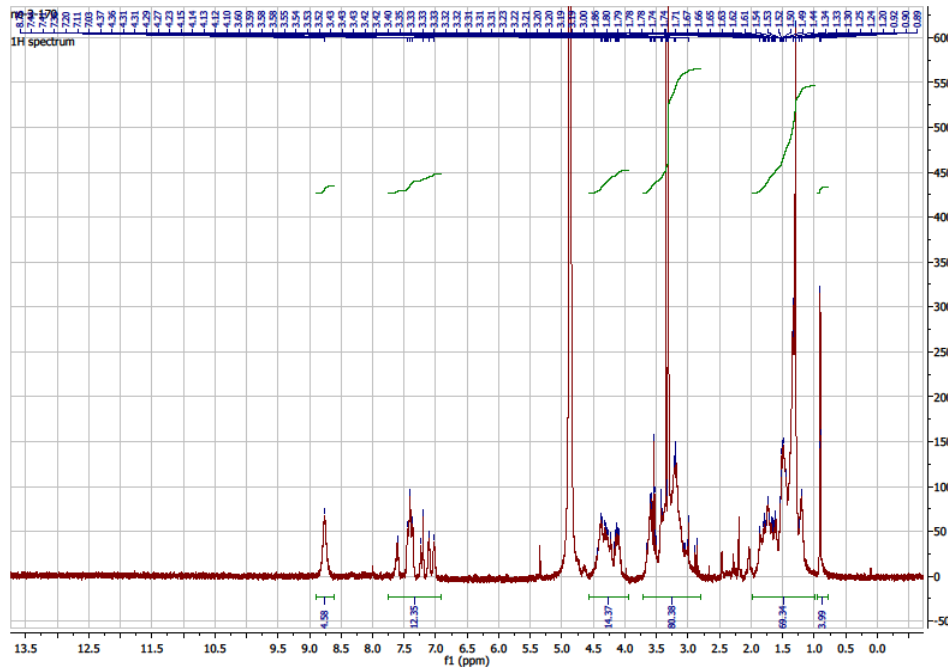
G2 25 TEG 2:1 (63 H 32 W):
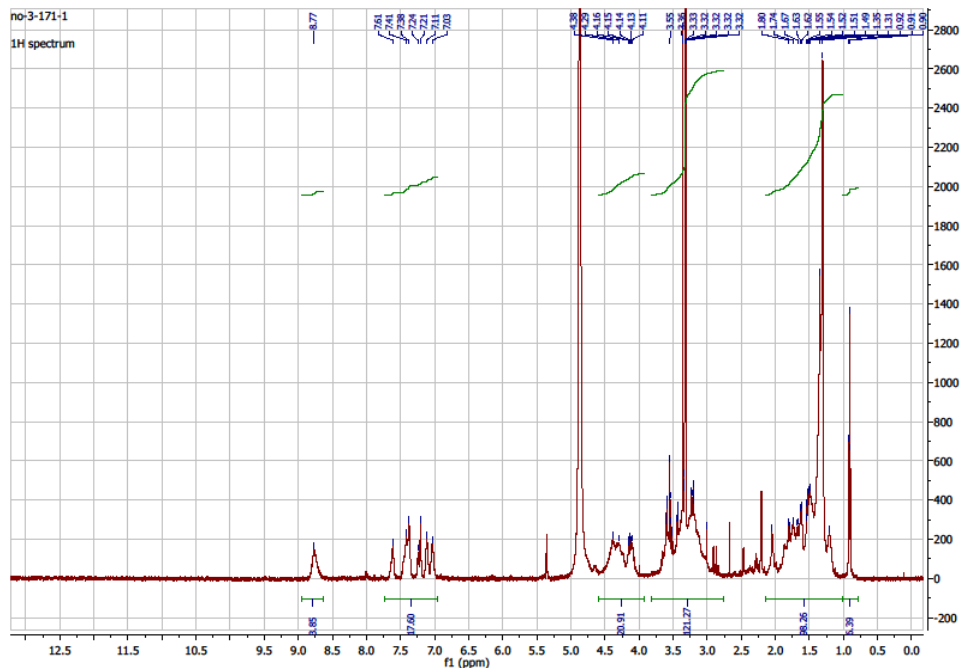
G2 50 TEG 3:1 (73 H 27 W):
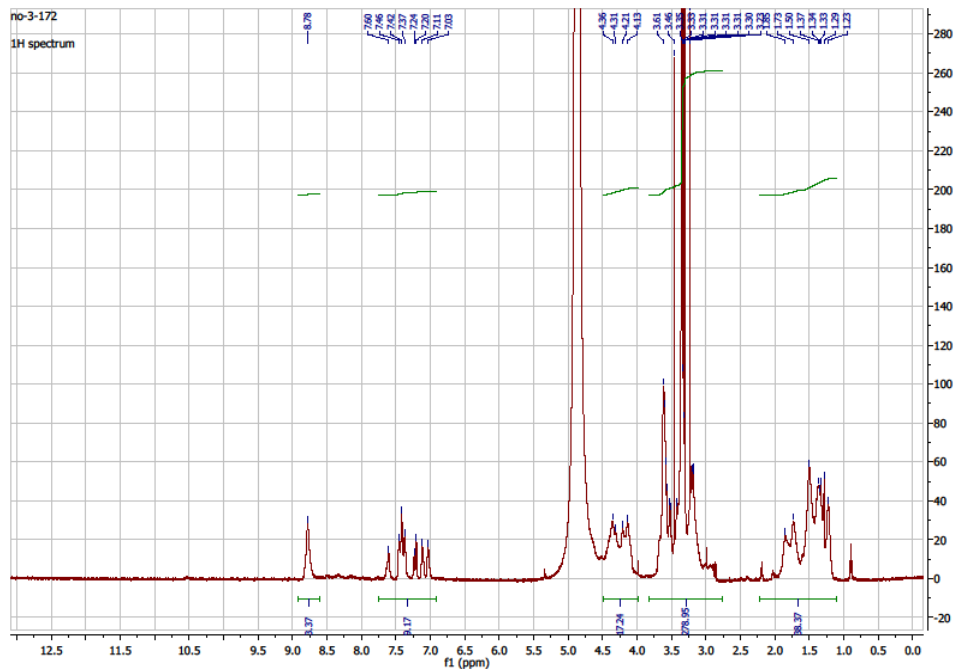
G2 50 TEG 2:1 (64 H 36 W):
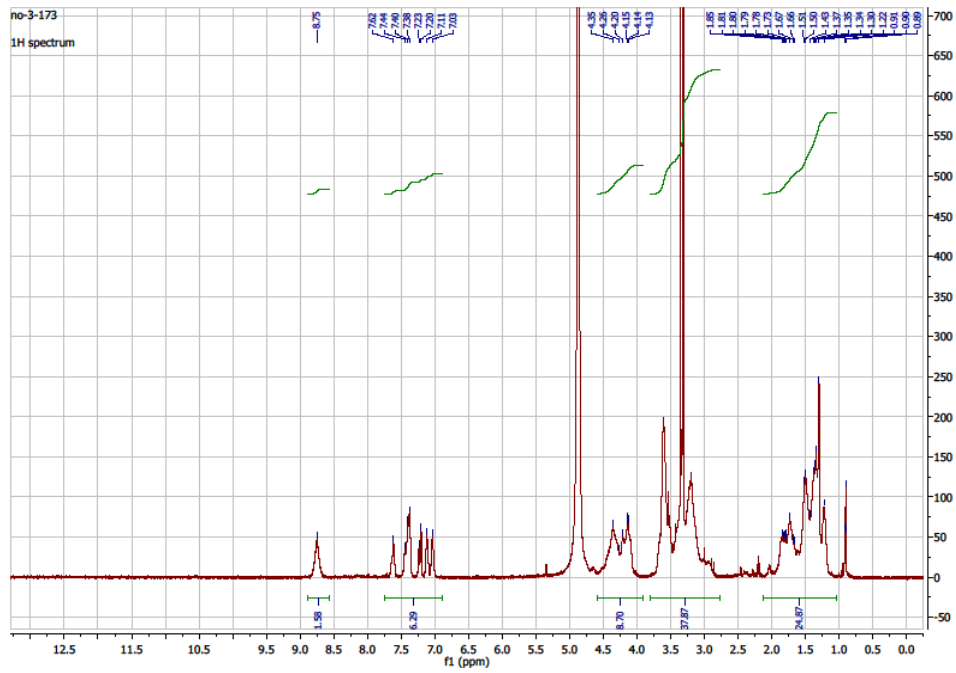
G2 75 TEG 3:1 (71 H 29 W):
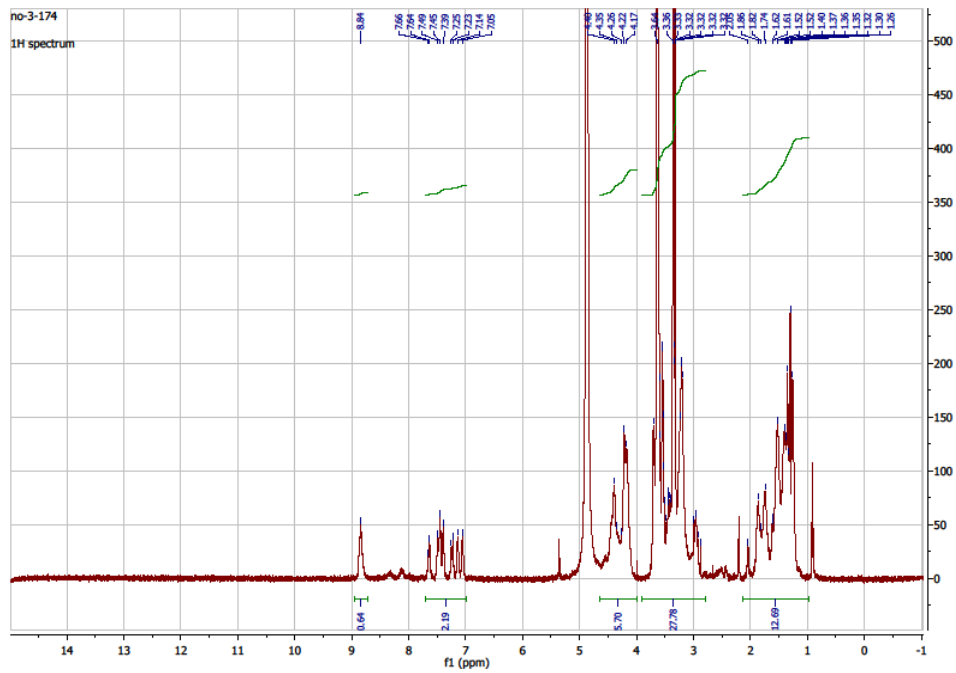
G2 75 TEG 2:1 (61 H 39 W):
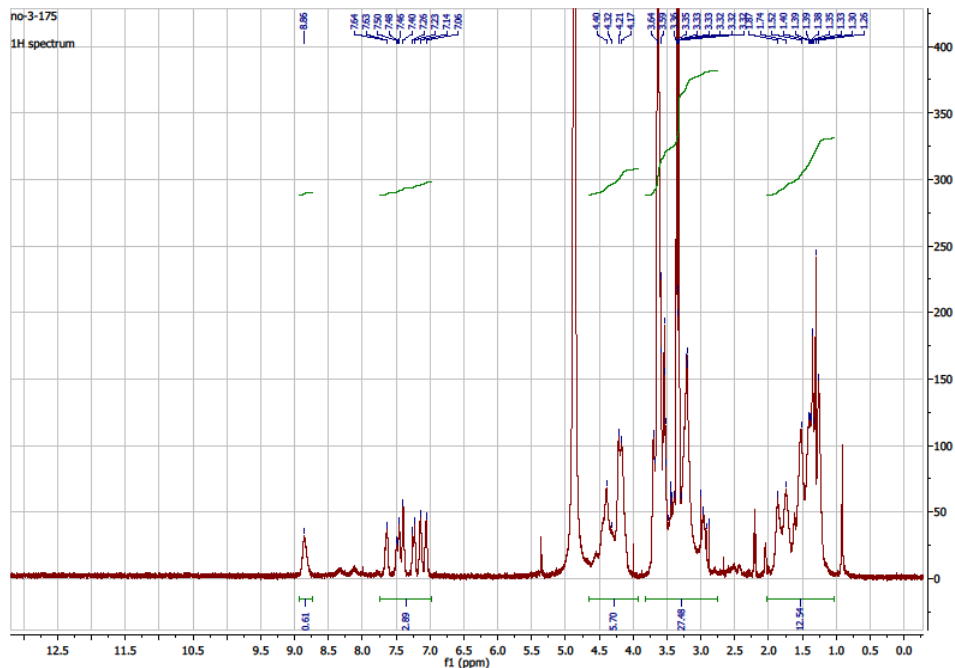
G3 25 TEG Backbone:
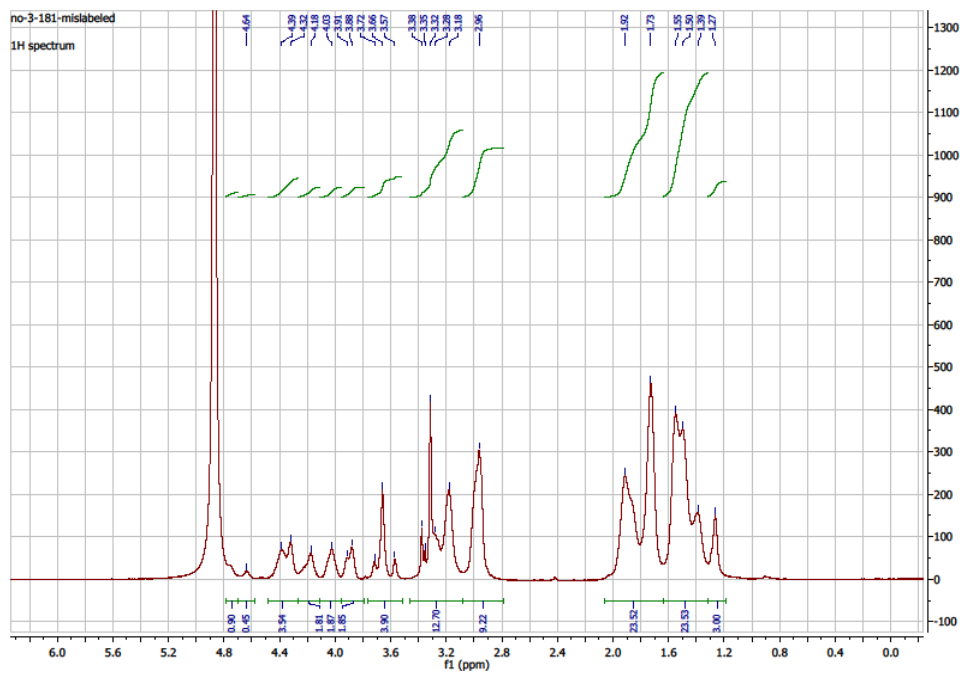
G3 50 TEG Backbone:
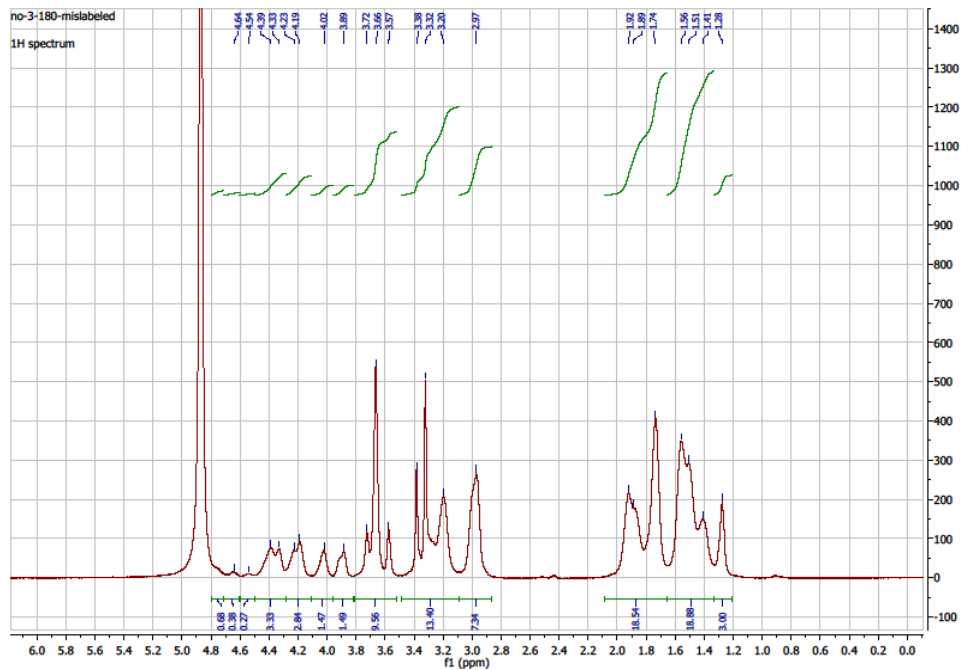
G3 75 TEG Backbone:
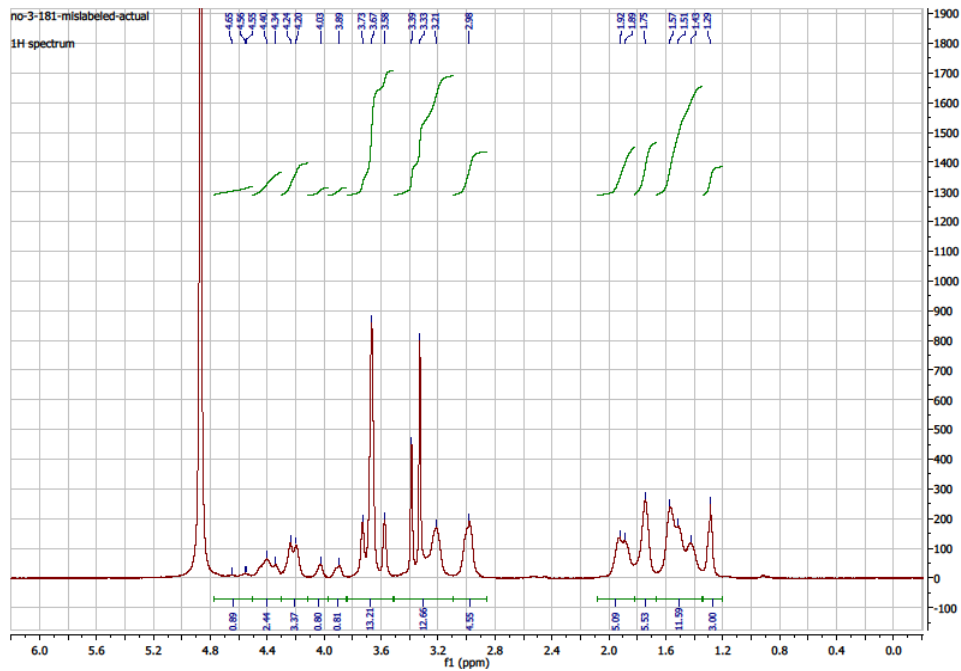
G3 25 TEG 3:1 (73 H 27 W):
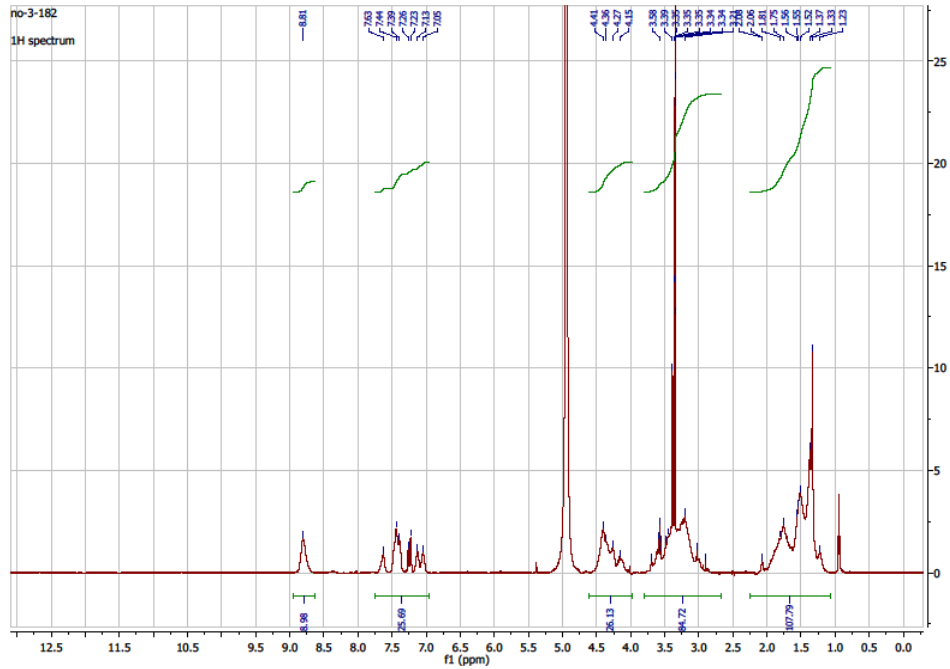
G3 25 TEG 2:1 (64 H 36 W):
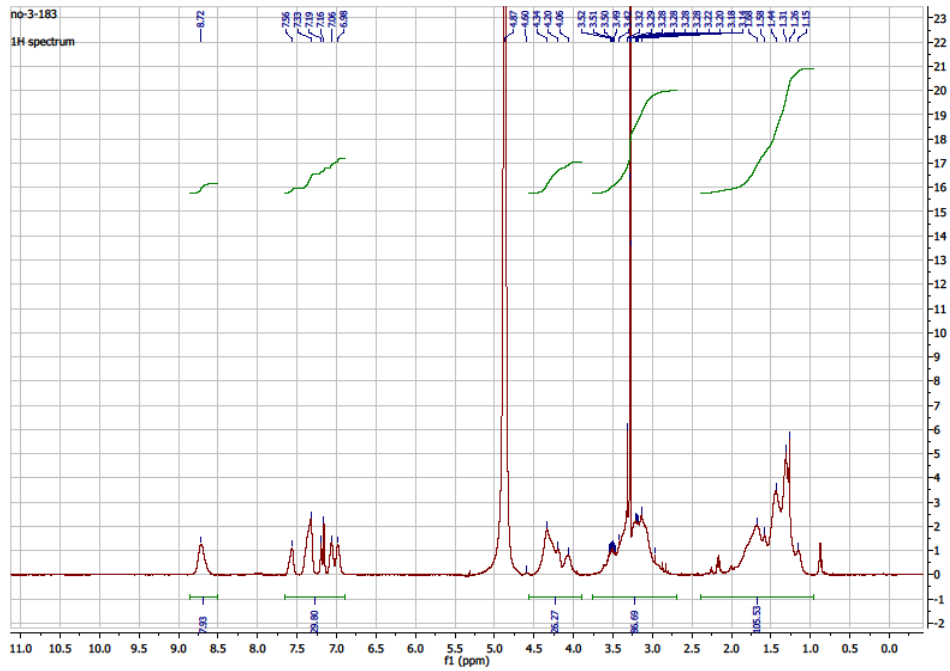
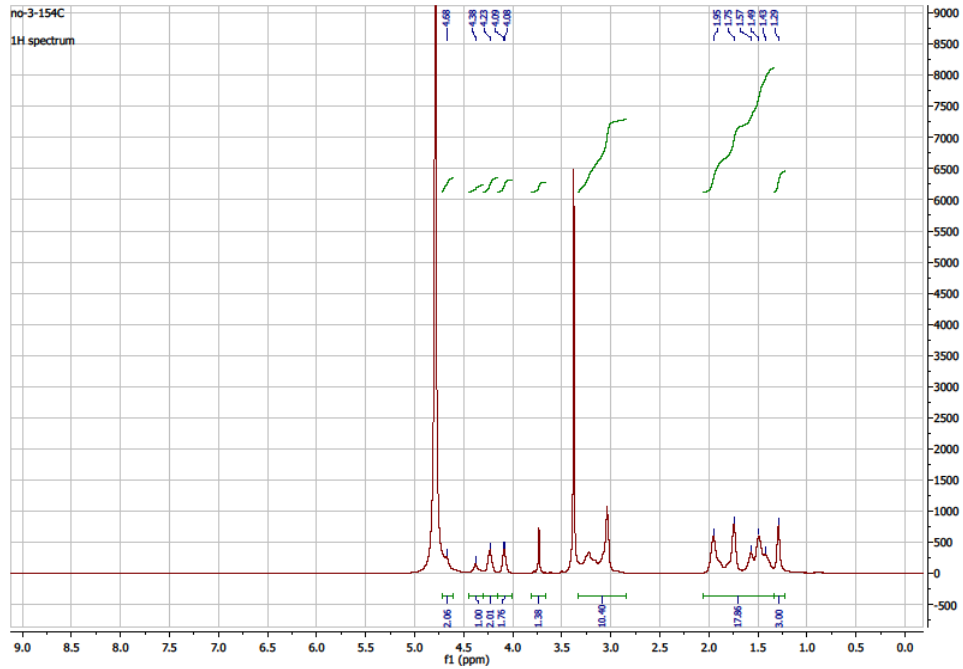# G3 50 TEG 3:1 (74 H 26 W):
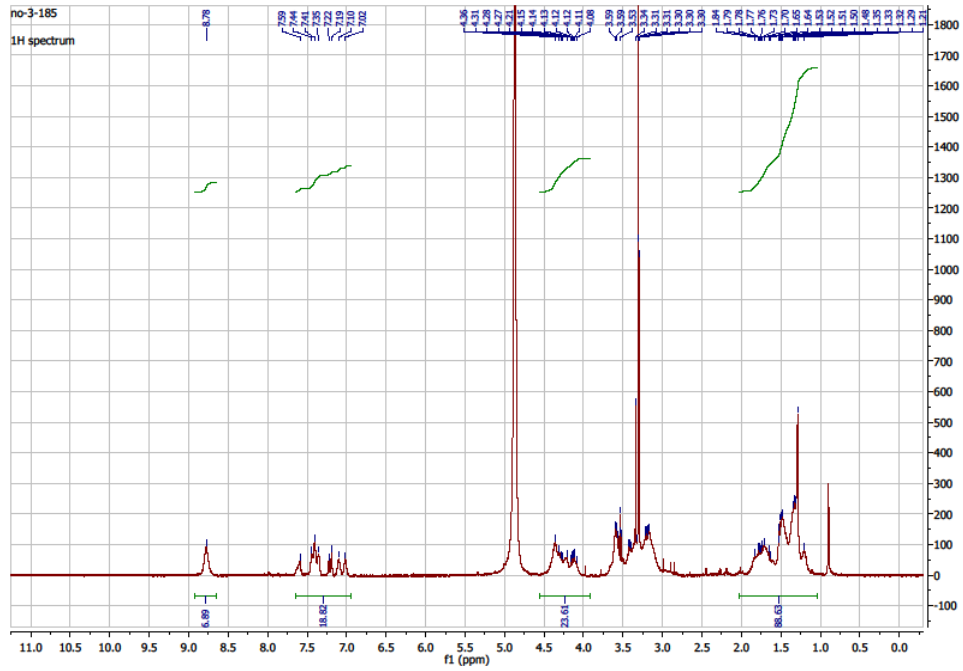
G3 50 TEG 2:1 (64 H 36 W):
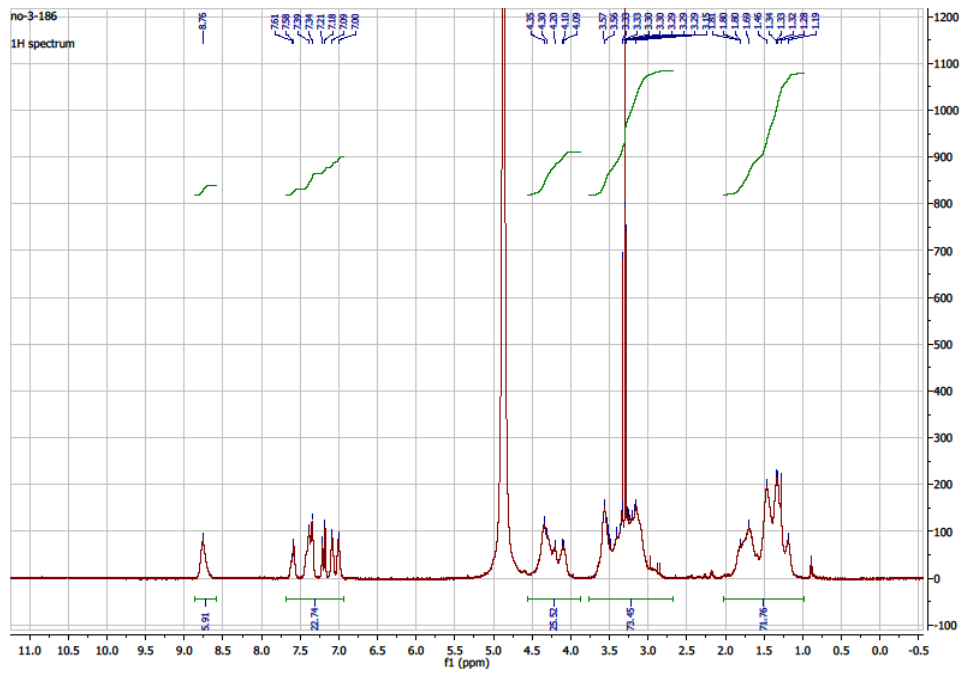
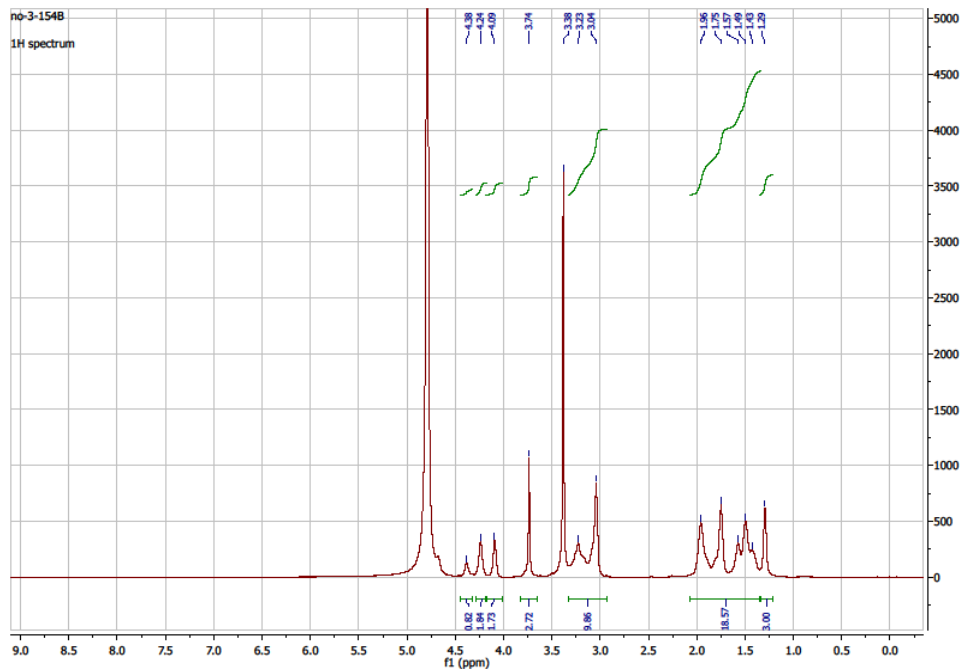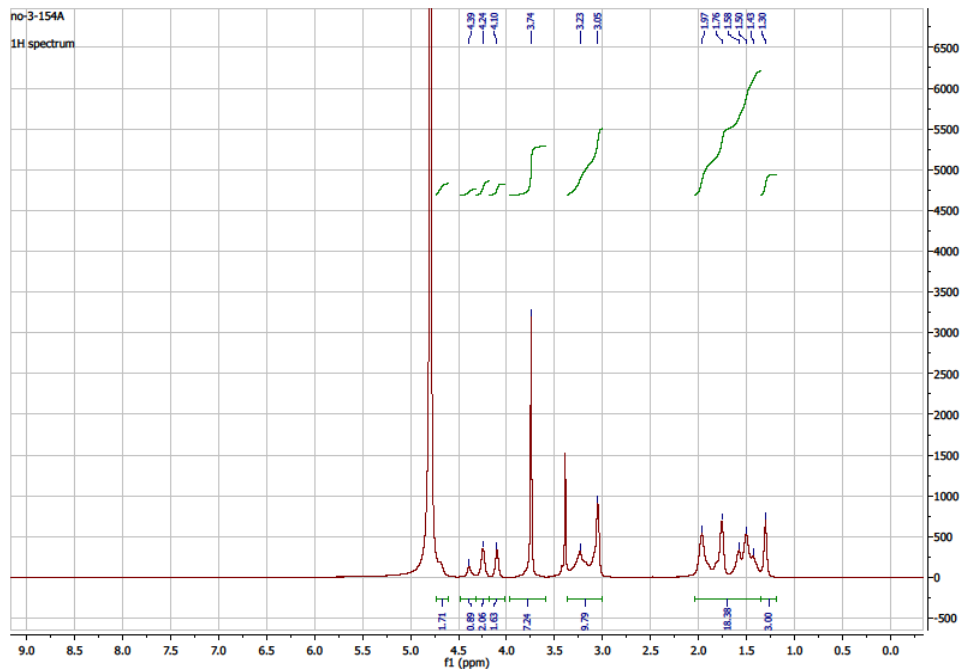**G3 75 TEG 3:1 (73 H 27 W):**
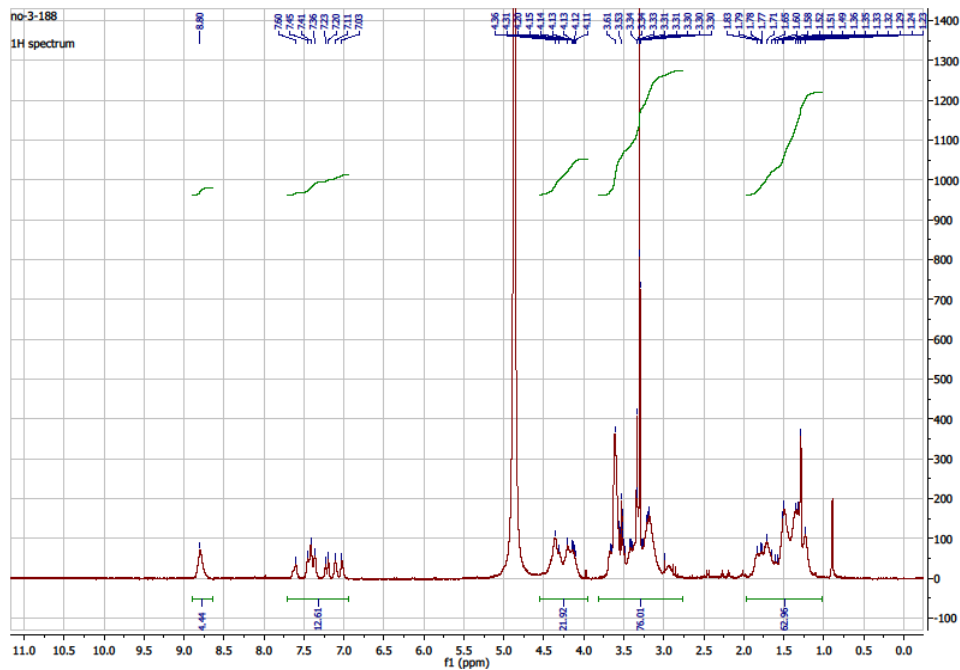
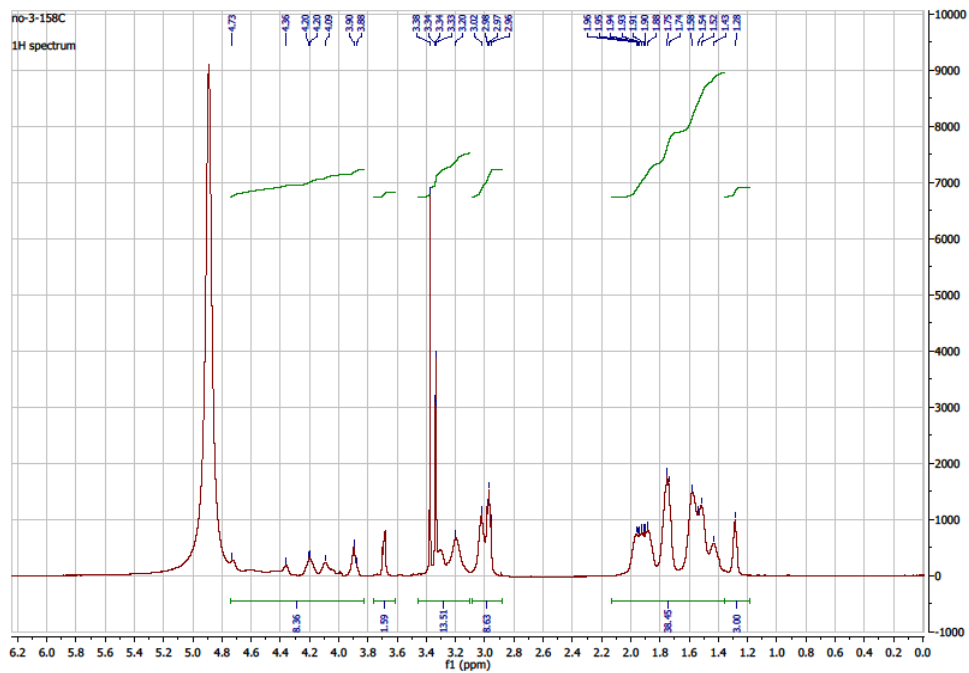**G3 75 TEG 2:1 (62 H 38 W):**
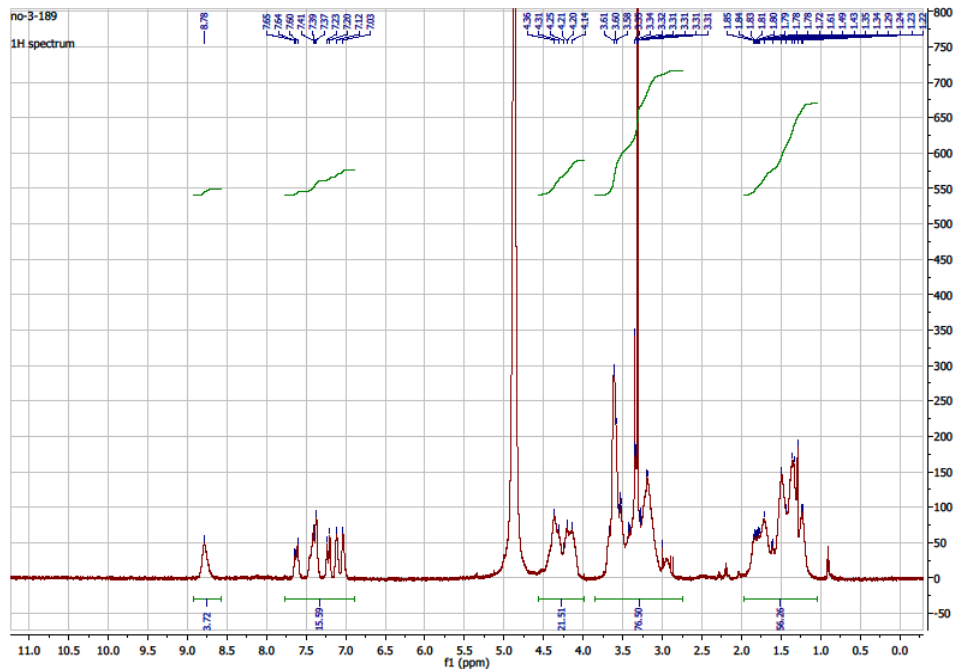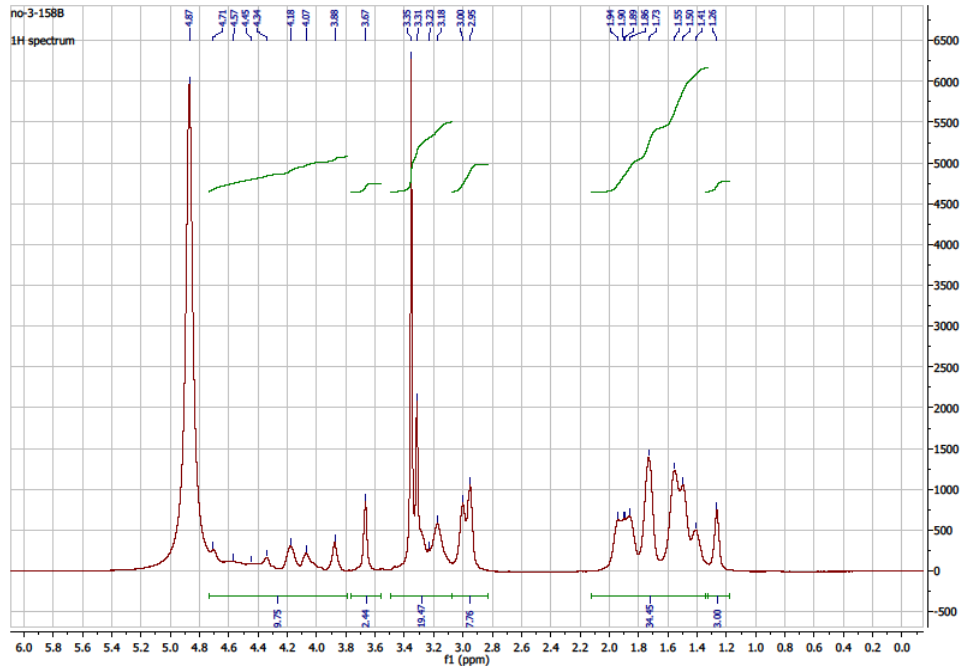
G1 1.0 PEG2k Backbone:
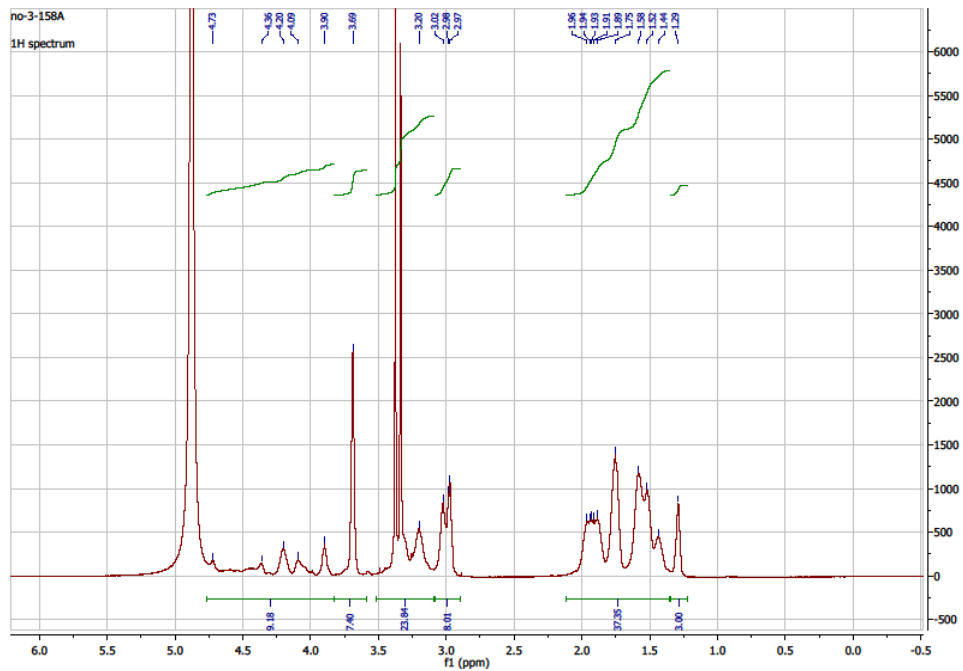

G1 1.5 PEG2k Backbone:
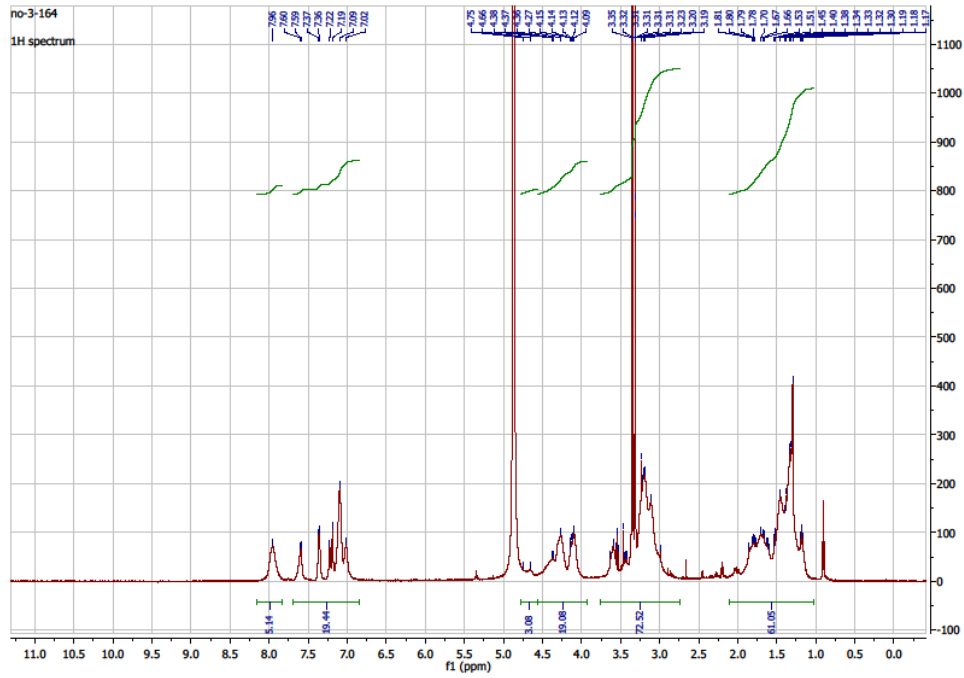
G1 3.0 PEG2k Backbone:

G2 1.0 PEG2k Backbone:

G2 1.5 PEG2k Backbone:

G2 3.0 PEG2k Backbone:

G1 1.0 PEG2k 2:1 (64 H 36 W):

G1 1.5 PEG2k 2:1 (67 H 33 W):
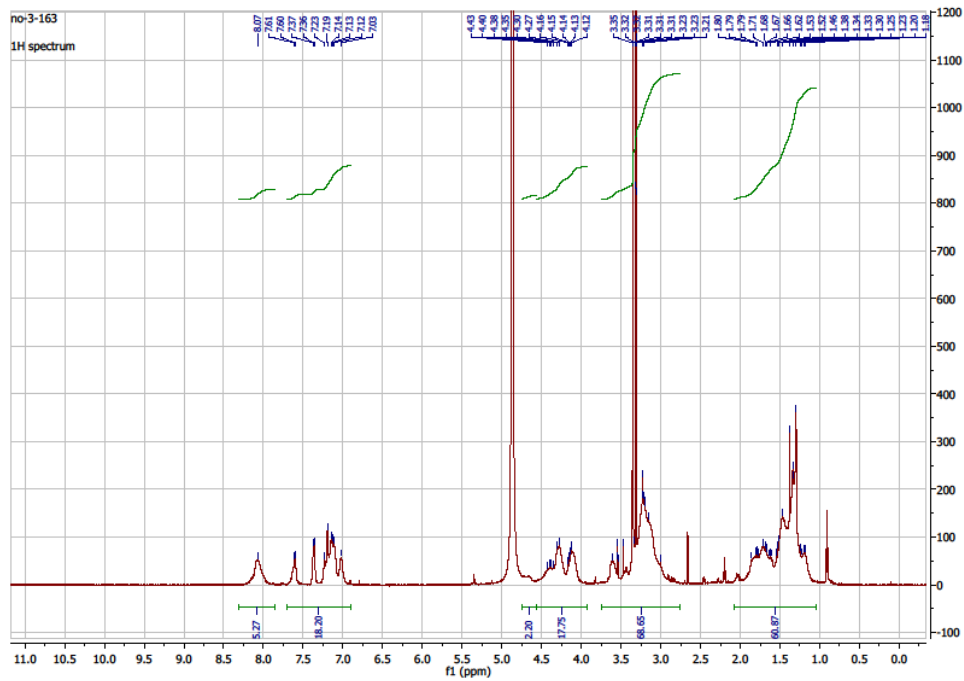
G1 3.0 PEG2k 2:1 (65 H 35 W):
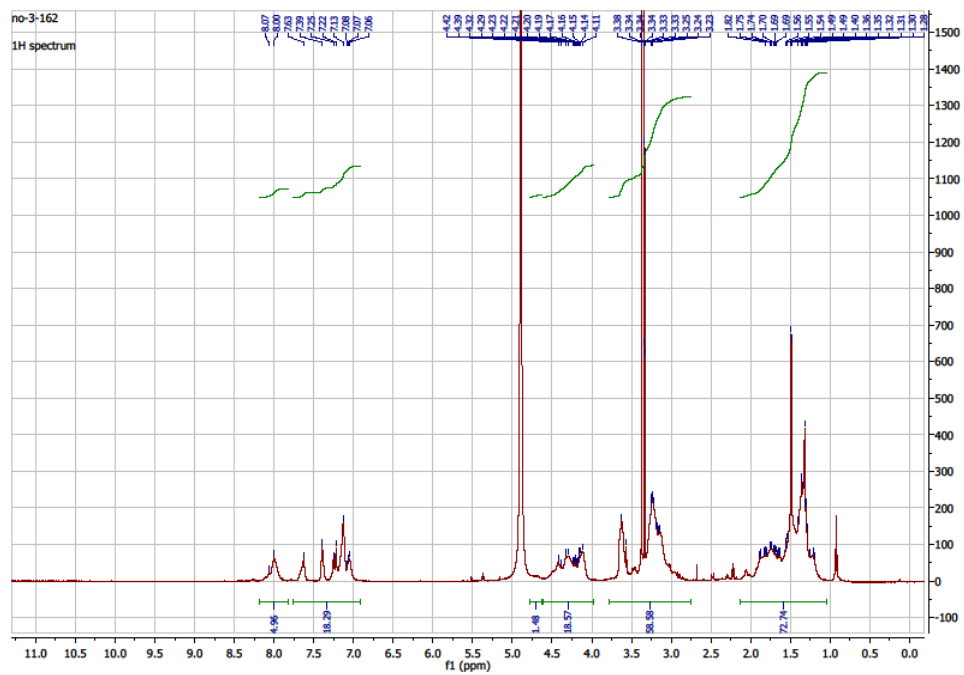
Flow Cytometry Output:

DC 2.4 cells

LF MM
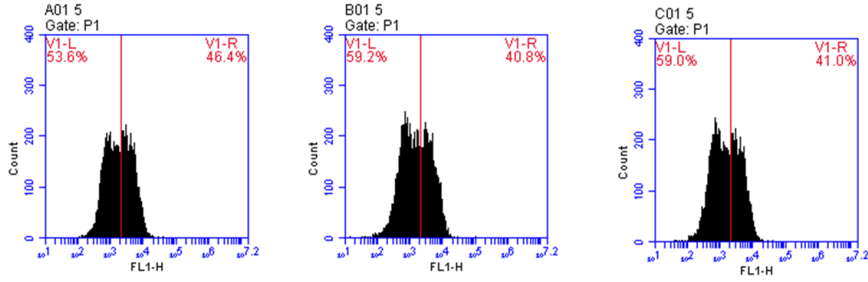
	Count	% of All	Mean FL1-H
1	5,000	79.12	2,599.14
2	5,000	85.91	2,4004.12
3	5,000	86.32	2,683.18

mRNA only
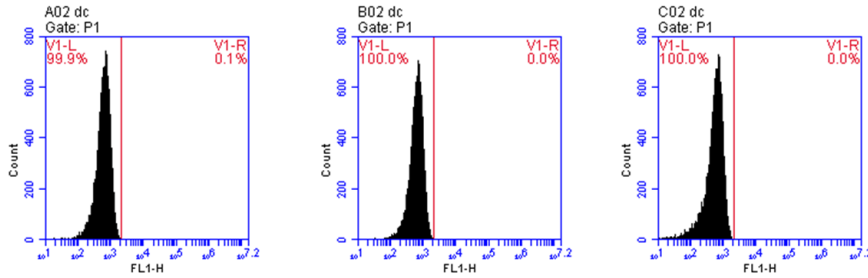
	Count	% of All	Mean FL1-H
1	10,000	89.65	399.1
2	10,000	86.91	323.3
3	10,000	87.12	344.1

G2 3:1
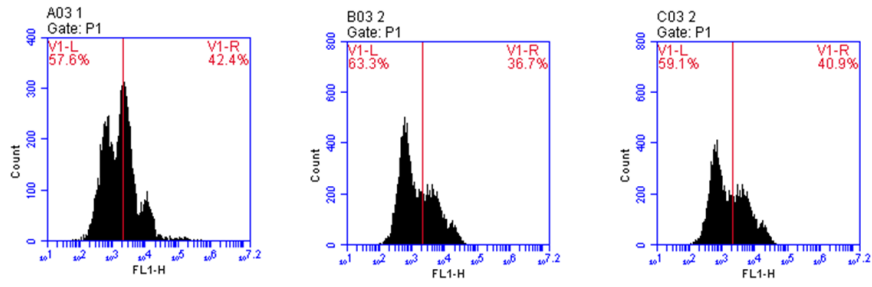
	Count	% of All	Mean FL1-H
1	5,000	81.44	5,124.04
2	5,000	82.66	3,801.32
3	5,000	83.11	3,969.96

G2 2:1
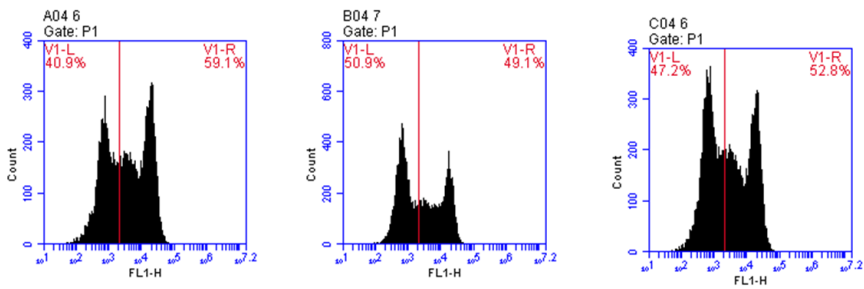
	Count	% of All	Mean FL1-H
1	10,000	80.00	10,276.09
2	10,000	72.26	9,801.32
3	10,000	89.01	10,969.96

G2 25 TEG 2:1
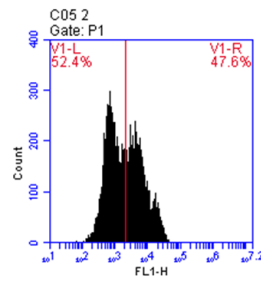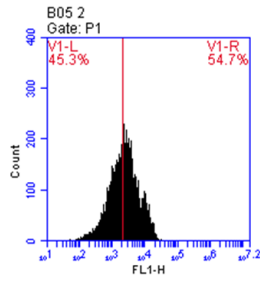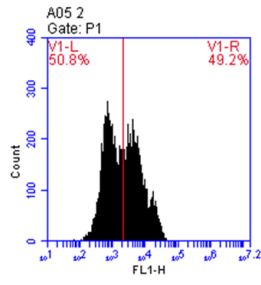
	Count	% of All	Mean FL1-H
1	5,000	82.24	3,664.09
2	5,000	85.88	3,423.12
3	5,000	82.98	3,659.96

G2 25 TEG 3:1
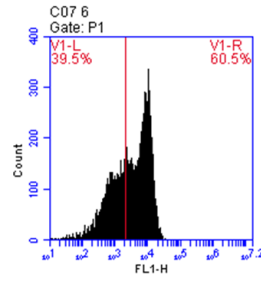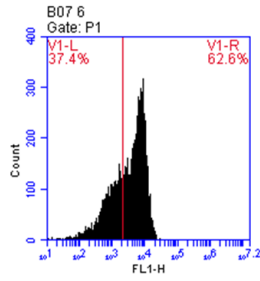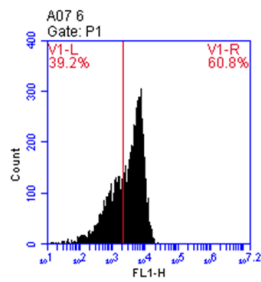
	Count	% of All	Mean FL1-H
1	5,000	87.56	5,055.45
2	5,000	89.53	4,729.82
3	5,000	80.47	5,155.71

G2 50 TEG 3:1
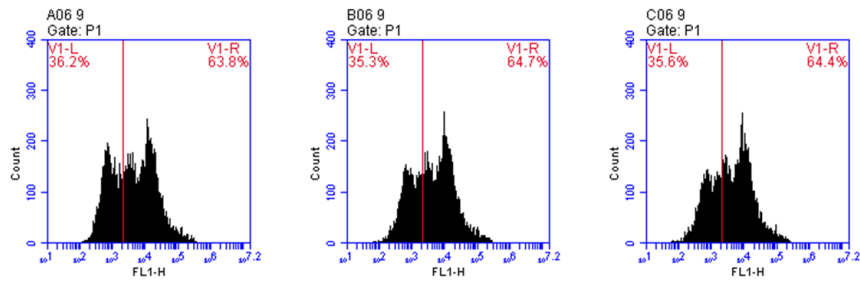
	Count	% of All	Mean FL1-H
1	5,000	90.85	13,848.27
2	5,000	82.67	12,635.90
3	5,000	86.77	12,544.60

G2 50 TEG 2:1
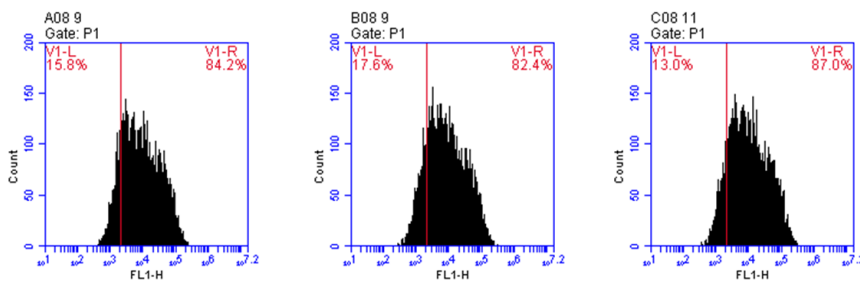
	Count	% of All	Mean FL1-H
1	5,000	87.87	23,659.82
2	5,000	81.49	29,092.82
3	5,000	87.01	29,940.34

G2 75 TEG 3:1
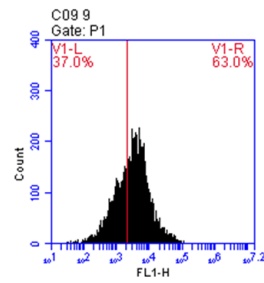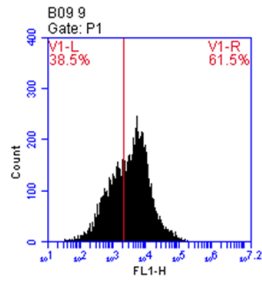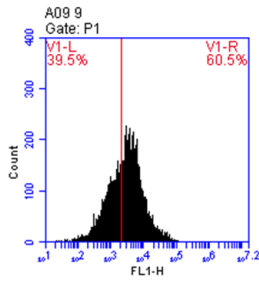
	Count	% of All	Mean FL1-H
1	5,000	88.32	4,127.82
2	5,000	88.34	4,483.27
3	5,000	86.71	4,173.36

G2 75 TEG 2:1
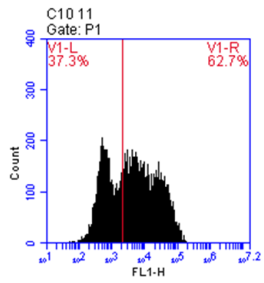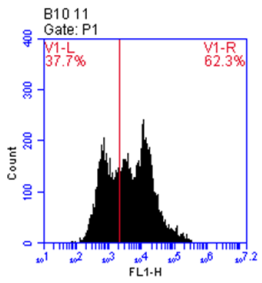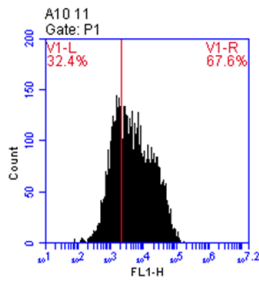
	Count	% of All	Mean FL1-H
1	5,000	87.99	13,328.76
2	5,000	77.55	13,603.87
3	5,000	86.61	14,198.87

G2 1.0 PEG 2k 2:1
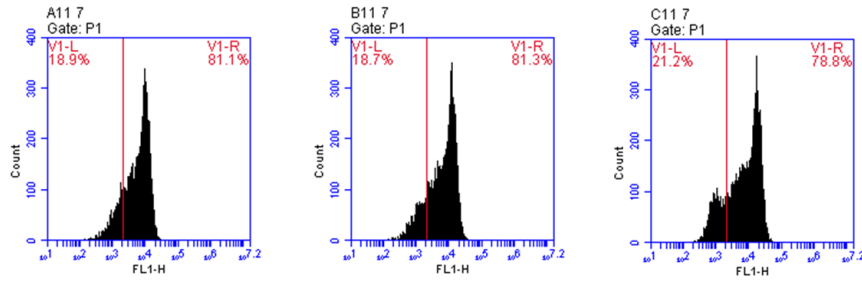
	Count	% of All	Mean FL1-H
1	5,000	79.91	7,122.91
2	5,000	81.82	8,2879.07
3	5,000	82.36	8,631.24

G2 1.5 PEG 2k 2:1
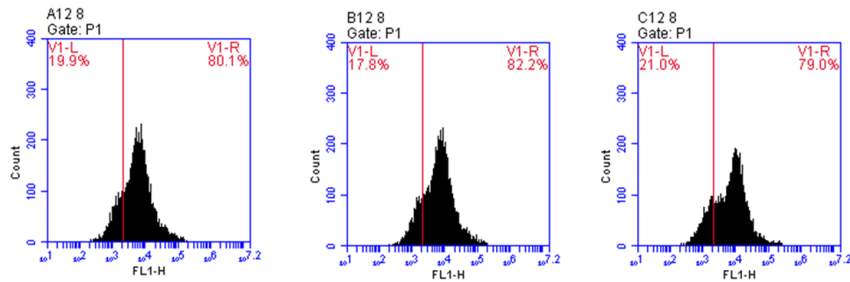
	Count	% of All	Mean FL1-H
1	5,000	77.84	10,523.56
2	5,000	81.78	12,465.91
3	5,000	88.12	11,769.73

G2 3.0 PEG 2k 2:1
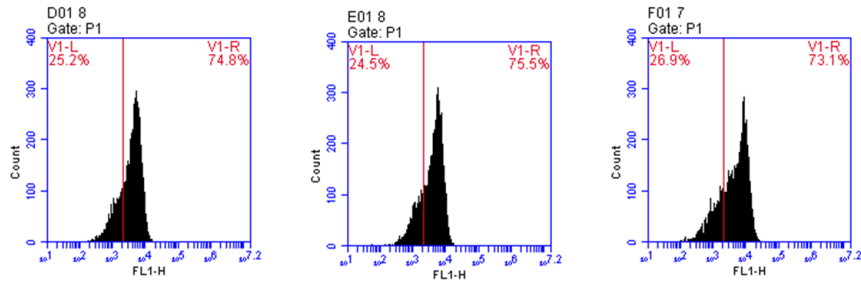
	Count	% of All	Mean FL1-H
1	5,000	82.00	4,167.13
2	5,000	85.93	4,593.51
3	5,000	76.93	4,839.97

BMDC Cells

LF MM
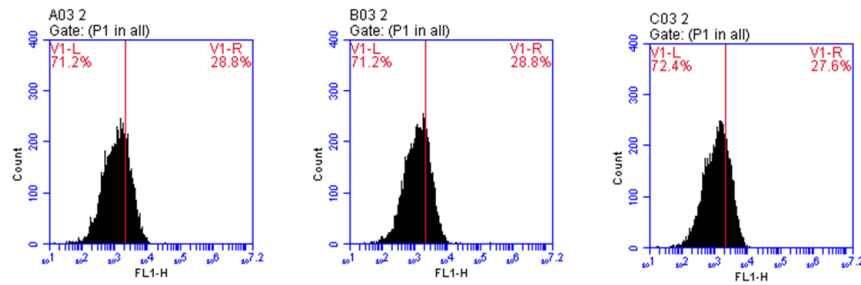
	Count	% of All	Mean FL1-H
1	5,000	66.19	1,970.12
2	5,000	62.22	1,939.12
3	5,000	66.31	1,535.91

mRNA only
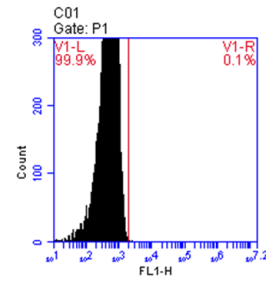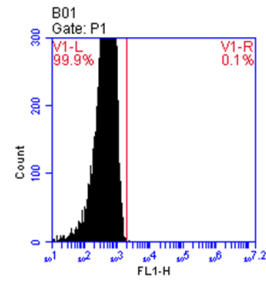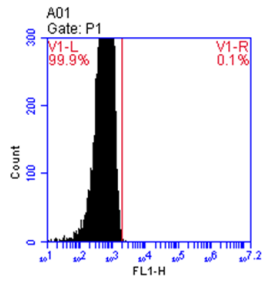
	Count	% of All	Mean FL1-H
1	5,000	60.31	329.14
2	5,000	62.22	318.56
3	5,000	66.16	341.29

G2 3:1
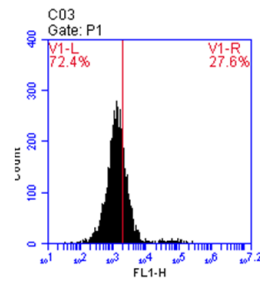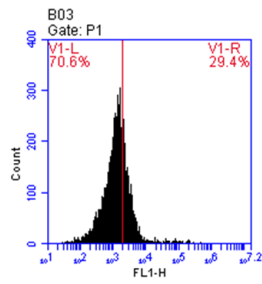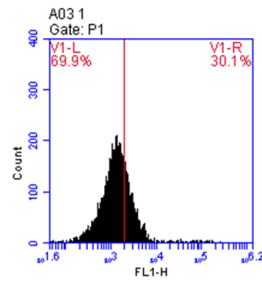
	Count	% of All	Mean FL1-H
1	5,000	66.49	3,379.18
2	5,000	77.88	3,272.67
3	5,000	63.18	3,036.29

G2 2:1
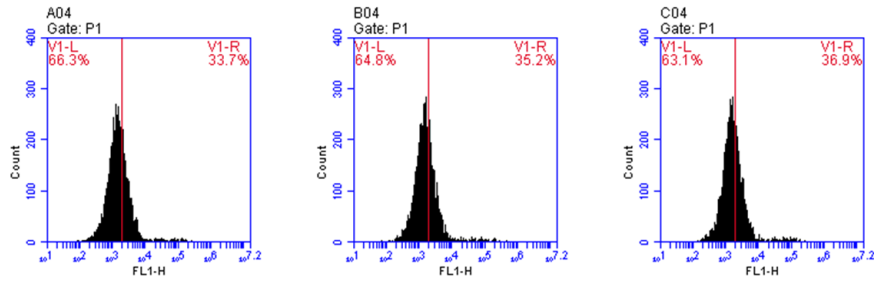
	Count	% of All	Mean FL1-H
1	5,000	57.89	3,147.03
2	5,000	64.26	3,296.16
3	5,000	65.04	3,012.59

G2 25 TEG 2:1
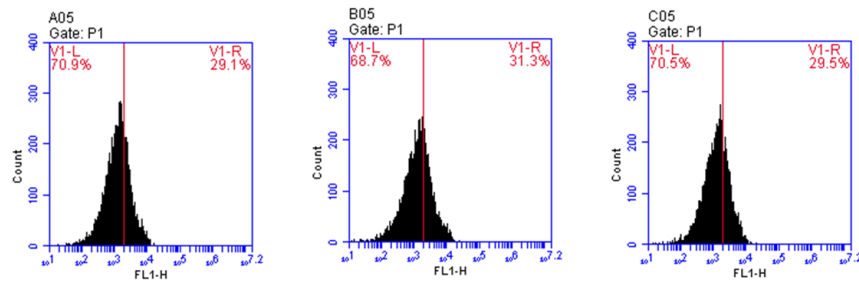
	Count	% of All	Mean FL1-H
1	5,000	60.31	2,332.51
2	5,000	60.71	2,345.31
3	5,000	66.16	2,755.94

G2 25 TEG 3:1
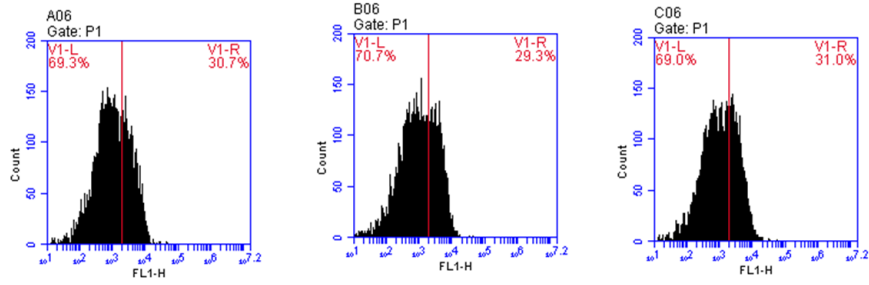
	Count	% of All	Mean FL1-H
1	5,000	61.24	3,025.06
2	5,000	64.60	2,913.07
3	5,000	59.88	2,562.80

G2 50 TEG 3:1
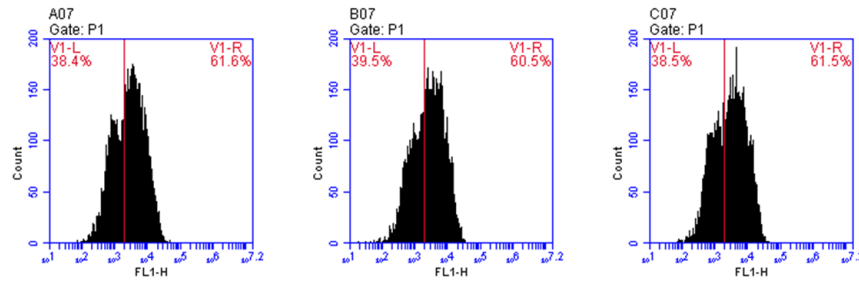
	Count	% of All	Mean FL1-H
1	5,000	64.54	4,518.09
2	5,000	66.23	4,320.75
3	5,000	62.21	4,926.54

G2 50 TEG 2:1
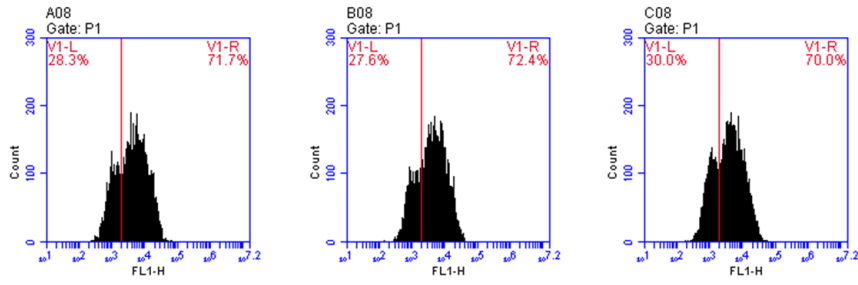
	Count	% of All	Mean FL1-H
1	5,000	60.09	5,745.55
2	5,000	64.21	5,799.99
3	5,000	65.26	5,996.12

G2 75 TEG 3:1
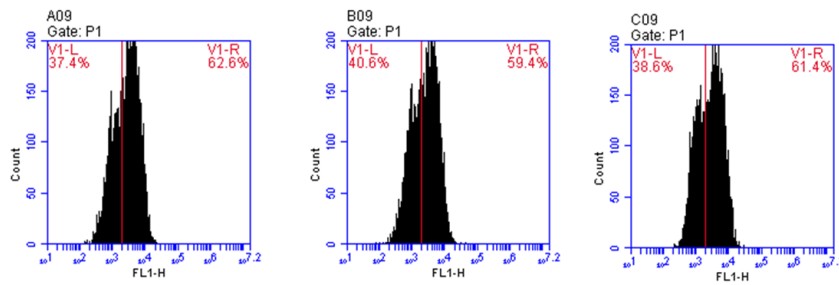
	Count	% of All	Mean FL1-H
1	5,000	60.32	3,398.50
2	5,000	54.62	3,001.84
3	5,000	58.54	3,012.98

G2 75 TEG 2:1
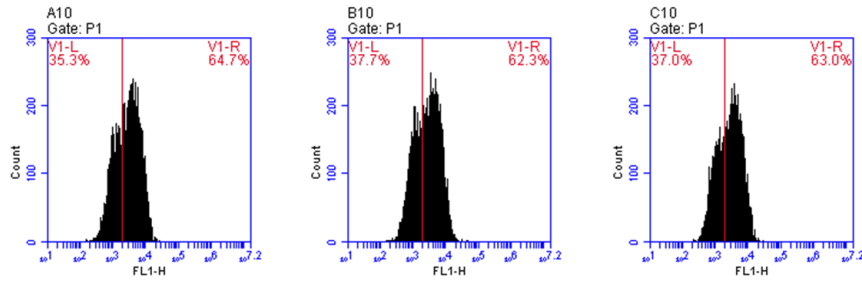
	Count	% of All	Mean FL1-H
1	5,000	69.76	3,874.57
2	5,000	64.74	3,816.52
3	5,000	62.82	3,990.91

G2 1.0 PEG 2k 2:1
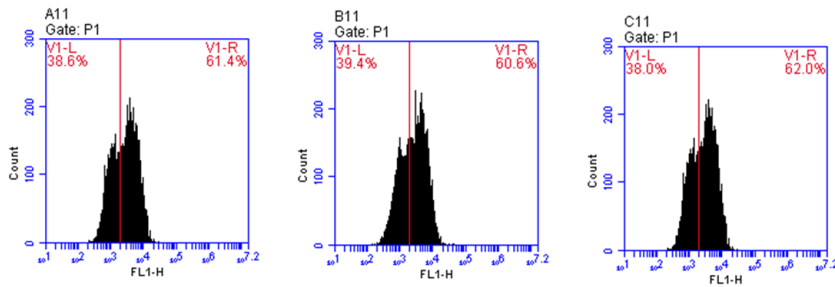
	Count	% of All	Mean FL1-H
1	5,000	58.64	3,043.23
2	5,000	54.62	3,290.07
3	5,000	31.36	3,057.12

G2 1.5 PEG 2k 2:1
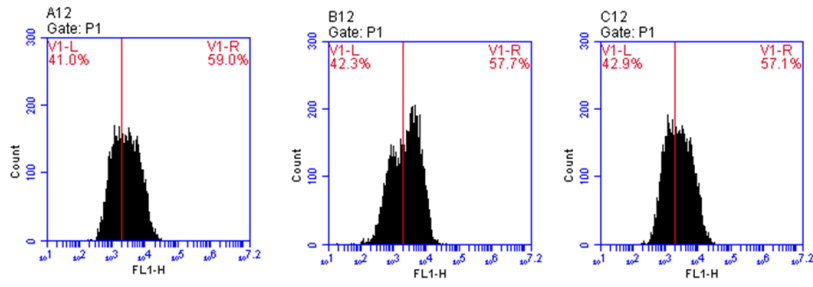
	Count	% of All	Mean FL1-H
1	5,000	53.77	3,950.17
2	5,000	62.22	3,912.98
3	5,000	58.18	3,786.73

G2 3.0 PEG 2k 2:1
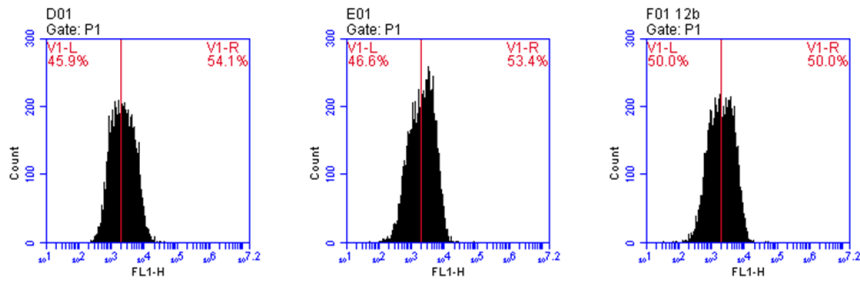
	Count	% of All	Mean FL1-H
1	5,000	68.17	3,088.93
2	5,000	68.96	2,920.68
3	5,000	71.26	2,975.93

4.5 References:

1.   Youn, H.; Chune, J. K., Modified mRNA as an alternative to plasmid DNA (pDNA) for transcript replacement and vaccination therapy. *Expert Opinion on Biological Therapy* **2015,** *15* (9), 1337-1348.

2.   Kariko, K.; Muramatsu, H.; Welsh, F. A.; Ludwig, J.; Kato, H.; Akira, S.; Weissman, D., Incorporation of Pseudouridine Into mRNA Yields Superior Nonimmunogenic Vector With Increased Translational Capacity and Biological Stability. *Mol. Ther.* **2008,** *16* (11), 1833-1840.

3.   Kariko, K.; Muramatsu, H.; Keller, J. M.; Weissman, D., Increased Erythropoiesis in Mice Injected With Submicrogram Quantities of Pseudouridine-containing mRNA Encoding Erythropoietin. *Mol. Ther.* **2012,** *20* (5), 948-953.

4.   Kormann, M. S. D.; Hasenpusch, G.; Aneja, M. K.; Nica, G.; Flemmer, A. W.; Herber-Jonat, S.; Huppmann, M.; Mays, L. E.; Illenyi, M.; Schams, A.; Griese, M.; Bittmann, I.; Handgretinger, R.; Hartl, D.; Rosenecker, J.; Rudolph, C., Expression of therapeutic proteins after delivery of chemically modified mRNA in mice. *Nat. Biotechnol.* **2011,** *29* (2), 154-U96.

5.   Heil, F.; Hemmi, H.; Hochrein, H.; Ampenberger, F.; Kirschning, C.; Akira, S.; Lipford, G.; Wagner, H.; Bauer, S., Species-specific recognition of single-stranded RNA via toll-like receptor 7 and 8. *Science* **2004,** *303* (5663), 1526-1529.

6.   Deering, R. P.; Kommareddy, S.; Ulmer, J. B.; Brito, L. A.; Geall, A. J., Nucleic acid vaccines: prospects for non-viral delivery of mRNA vaccines. *Expert Opinion on Drug Delivery* **2014,** *11* (6), 885-899.

7.   Sahin, U.; Kariko, K.; Tureci, O., mRNA-based therapeutics - developing a new class of drugs. *Nat. Rev. Drug Discovery* **2014,** *13* (10), 759-780.

8.   Yin, H.; Kanasty, R. L.; Eltoukhy, A. A.; Vegas, A. J.; Dorkin, J. R.; Anderson, D. G., Non-viral vectors for gene-based therapy. *Nat. Rev. Genet.* **2014,** *15* (8), 541-555.

9.   Phua, K. K. L.; Leong, K. W.; Nair, S. K., Transfection efficiency and transgene expression kinetics of mRNA delivered in naked and nanoparticle format. *J. Controlled Release* **2013,** *166* (3), 227-233.

10.   Schlake, T.; Thess, A.; Fotin-Mleczek, M.; Kallen, K. J., Developing mRNA-vaccine technologies. *RNA Biol.* **2012,** *9* (11), 1319-1330.

11.   Malone, R. W.; Felgner, P. L.; Verma, I. M., Cationic Liposome-Mediated Rna Transfection. *Proc. Natl. Acad. Sci. U. S. A.* **1989,** *86* (16), 6077-6081.

12.   Zangi, L.; Lui, K. O.; von Gise, A.; Ma, Q.; Ebina, W.; Ptaszek, L. M.; Spater, D.; Xu, H. S.; Tabebordbar, M.; Gorbatov, R.; Sena, B.; Nahrendorf, M.; Briscoe, D. M.; Li, R. A.; Wagers, A. J.; Rossi, D. J.; Pu, W. T.; Chien, K. R., Modified mRNA directs the fate of heart progenitor cells and induces vascular regeneration after myocardial infarction. *Nat. Biotechnol.* **2013,** *31* (10), 898-+.

13.   Kauffman, K. J.; Dorkin, J. R.; Yang, J. H.; Heartlein, M. W.; DeRosa, F.; Mir, F. F.; Fenton, O. S.; Anderson, D. G., Optimization of Lipid Nanoparticle Formulations for mRNA Delivery in Vivo with Fractional Factorial and Definitive Screening Designs. *Nano Lett.* **2015,** *15* (11), 7300-7306.

14.   Cheng, C.; Convertine, A. J.; Stayton, P. S.; Bryers, J. D., Multifunctional triblock copolymers for intracellular messenger RNA delivery. *Biomaterials* **2012,** *33* (28), 6868-6876.

15.   Uzgun, S.; Nica, G.; Pfeifer, C.; Bosinco, M.; Michaelis, K.; Lutz, J. F.; Schneider, M.; Rosenecker, J.; Rudolph, C., PEGylation Improves Nanoparticle Formation and Transfection Efficiency of Messenger RNA. *Pharm. Res.* **2011,** *28* (9), 2223-2232.

16.	Perche, F.; Benvegnu, T.; Berchel, M.; Lebegue, L.; Pichon, C.; Jaffres, P. A.; Midoux, P., Enhancement of dendritic cells transfection in vivo and of vaccination against B16F10 melanoma with mannosylated histidylated lipopolyplexes loaded with tumor antigen messenger RNA. *Nanomedicine-Nanotechnology Biology and Medicine* **2011,** *7* (4), 445-453.

17.	Crowley, S. T.; Poliskey, J. A.; Baumhover, N. J.; Rice, K. G., Efficient expression of stabilized mRNA PEG-peptide polyplexes in liver. *Gene Ther.* **2015,** *22* (12), 993-999.

18.	Avci-Adali, M.; Behring, A.; Keller, T.; Krajewski, S.; Schlensak, C.; Wendel, H. P., Optimized conditions for successful transfection of human endothelial cells with in vitro synthesized and modified mRNA for induction of protein expression. *Journal of Biological Engineering* **2014,** *8*.

19.	Debus, H.; Baumhof, P.; Probst, J.; Kissel, T., Delivery of messenger RNA using poly(ethylene imine)-poly(ethylene glycol)-copolymer blends for polyplex formation: Biophysical characterization and in vitro transfection properties. *J. Controlled Release* **2010,** *148* (3), 334-343.

20.	Wang, Y. H.; Su, H. H.; Yang, Y.; Hu, Y. X.; Zhang, L.; Blancafort, P.; Huang, L., Systemic Delivery of Modified mRNA Encoding Herpes Simplex Virus 1 Thymidine Kinase for Targeted Cancer Gene Therapy. *Mol. Ther.* **2013,** *21* (2), 358-367.

21.	Uchida, S.; Itaka, K.; Uchida, H.; Hayakawa, K.; Ogata, T.; Ishii, T.; Fukushima, S.; Osada, K.; Kataoka, K., In Vivo Messenger RNA Introduction into the Central Nervous System Using Polyplex Nanomicelle. *PLoS One* **2013,** *8* (2).

22.	Dong, Y. Z.; Dorkin, J. R.; Wang, W. H.; Chang, P. H.; Webber, M. J.; Tang, B. C.; Yang, J.; Abutbul-Ionita, I.; Danino, D.; DeRosa, F.; Heartlein, M.; Langer, R.; Anderson, D. G.,

Poly(glycoamidoamine) Brushes Formulated Nanomaterials for Systemic siRNA and mRNA Delivery in Vivo. *Nano Lett.* **2016,** *16* (2), 842-848.

23.   Ponsaerts, P.; Van der Sar, S.; Van Tendeloo, V. F.; Jorens, P. G.; Berneman, Z. N.; Singh, P. B., Highly efficient mRNA-based gene transfer in feeder-free cultured H9 human embryonic stem cells. *Cloning Stem Cells* **2004,** *6* (3), 211-216.

24.   Ponsaerts, P.; Van Tendeloo, V. F. I.; Berneman, Z. N., Cancer immunotherapy using RNA-loaded dendritic cells. *Clin. Exp. Immunol.* **2003,** *134* (3), 378-384.

25.   Van Tendeloo, V. F. I.; Ponsaerts, P.; Lardon, F.; Nijs, G.; Lenjou, M.; Van Broeckhoven, C.; Van Bockstaele, D. R.; Berneman, Z. N., Highly efficient gene delivery by mRNA electroporation in human hematopoietic cells: superiority to lipofection and passive pulsing of mRNA and to electroporation of plasmid cDNA for tumor antigen loading of dendritic cells. *Blood* **2001,** *98* (1), 49-56.

26.   Strobel, I.; Berchtold, S.; Gotze, A.; Schulze, U.; Schuler, G.; Steinkasserer, A., Human dendritic cells transfected with either RNA or DNA encoding influenza matrix protein M1 differ in their ability to stimulate cytotoxic T lymphocytes. *Gene Ther.* **2000,** *7* (23), 2028-2035.

27.   Phua, K. K. L.; Nair, S. K.; Leong, K. W., Messenger RNA (mRNA) nanoparticle tumour vaccination. *Nanoscale* **2014,** *6* (14), 7715-7729.

28.   Midoux, P.; Pichon, C., Lipid-based mRNA vaccine delivery systems. *Expert Review of Vaccines* **2015,** *14* (2), 221-234.

29.   Zeng, H. X.; Little, H. C.; Tiambeng, T. N.; Williams, G. A.; Guan, Z. B., Multifunctional Dendronized Peptide Polymer Platform for Safe and Effective siRNA Delivery. *J. Am. Chem. Soc.* **2013,** *135* (13), 4962-4965.

30.   Oh, N.; Park, J. H., Endocytosis and exocytosis of nanoparticles in mammalian cells. *International Journal of Nanomedicine* **2014,** *9*, 51-63.

31.   Ryu, K. A.; Stutts, L.; Tom, J. K.; Mancini, R. J.; Esser-Kahn, A. P., Stimulation of Innate Immune Cells by Light-Activated TLR7/8 Agonists. *J. Am. Chem. Soc.* **2014,** *136* (31), 10823-10825.

32.   Shirasaki, Y.; Takahashi, H.; Yamaguchi, M.; Inoue, J., Molecular design to enhance the penetration into the retina via ocular instillation. *Bioorg. Med. Chem. Lett.* **2008,** *18* (19), 5174-5177..

Chapter 5 : Mechanical Gradient Formation via Metal-Ligand Interactions

Abstract:

Mechanical gradients are often employed in nature to prevent damage from large forces by creating a smooth transition from strong to weak biological materials. Synthetic mimics of these natural structures are highly desired to improve distribution of stresses at interfaces, and reduce contact deformation in non-biological materials. Current synthetic gradient materials suffer from steep, irregular transitions and relatively small ranges in mechanical properties. Inspired by the polychaete worm jaw, we report a novel route to generate stiffness gradients in polymeric materials via incorporation of monodentate, dynamic metal-ligand crosslinks. Through spatial control of metal ion content, we create a continuous mechanical gradient that spans over a 100-fold difference in stiffness.

5.1: Introduction

Materials that provide form and function in living organisms generate and withstand tremendous forces. For example, the club of a peacock mantis shrimp (*Odontodactylus scyllarus*) can experience up to 700 N during a strike.[1] This massive force must be ameliorated when transferring between the hard club and soft tissues of the shrimp to prevent serious damage. Cleverly, the dissipation of these forces is accomplished through a continuous gradient in mechanical properties from hard to soft. Gradients like this allow the forces to be distributed over a large area to prevent stress buildup and catastrophic failures in the tissues of living organisms.[2] Synthetic analogs of these natural mechanical gradients have been long pursued to create stronger materials with improved thermal stress dissipation, mechanical stress dissipation, and fracture toughness at interfaces.[2]

Polychaete Worm Jaw:

Bioinspired Synthetic gradient:

Cu

In Nature

= Histidine

= Copper
   Zinc

Protein Network

Mechanical Gradients

Synthetic

= Imidazole

= Copper
   Zinc
   Cobalt

Acrylate network

Higher metal concentration
More cross links
Higher stiffness
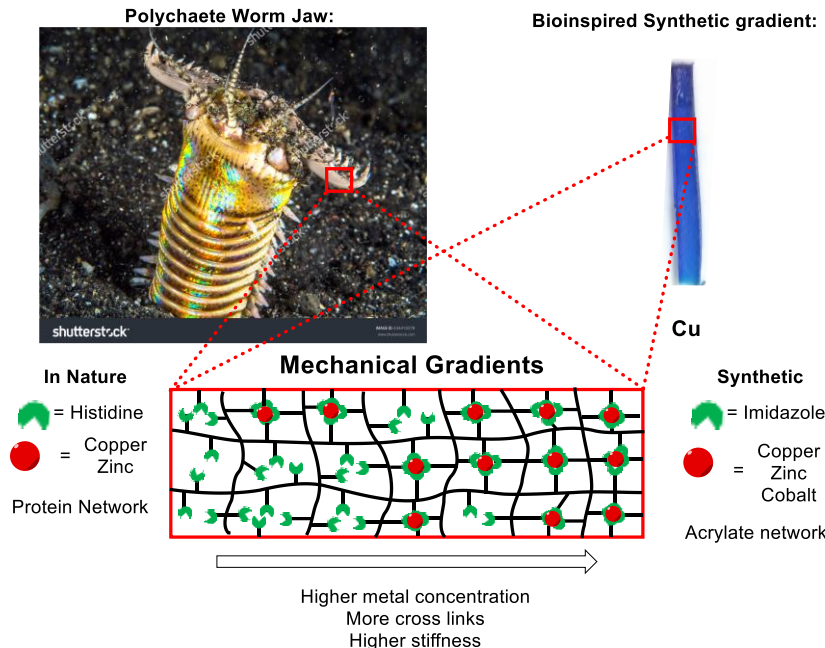
Figure 5.1 Comparison of the gradient found in the Polychaete worm jaw and the gradient made in this work

Synthetic mechanical gradients are generally obtained in a layered or lateral orientation. Layered gradients are printed layer-by-layer onto surfaces and are not true continuous gradients due to the segmented fabrication process.[3-5] Some lateral gradients are able to obtain smooth transitions,[6-10] but there are fewer examples due to the higher synthetic effort required to generate them. Notable examples of previously reported lateral gradients include photoinduced crosslinking of cellulose nano crystals,[7] ordering of carbon nanotube films,[11] and cellulose nanofibril/polymer nanopapers.[12] While these and other synthetic analogs are functional mechanical gradients,[6, 8-10, 13-18] they often suffer from relatively small ranges in stiffness (~ 1 order of magnitude), noncontiguous stepwise transitions, and require specialty equipment to fabricate. To improve upon these systems, we sought a synthetic solution that could span a greater range of mechanical properties with a true continuous gradient and facile synthesis.

Many examples of gradient materials exist in nature[19-24], but when searching for routes to gradient formation, the jaw of the polychaete worm became a unique source of inspiration (Figure 5.1). In contrast to the mineralization and covalent crosslinking used to form many natural gradients[25-27], the polychaete worm relies on metal-ligand interactions to create a rigid jaw tip to

162

inject venom.[25-27] Specifically, by creating a gradient of zinc (or copper) through a histidine rich protein network, the increasing number of metal-histidine interactions act as crosslinks and create a mechanical gradient, which can prevent damage to the jaw tip during biting and venom injection.

Our previously reported studies investigated control of mechanical properties by altering metal identity (Zn, Cu, Co) and concentration in an imidazole metallopolymer network. [28, 29] We employed monodentate imidazole ligands to create dynamic metal-ligand crosslinks, which in the presence of a weakly binding solvent (acetonitrile, ACN) facilitated ligand exchange and metal incorporation (no gelation). Upon solvent removal the rate of ligand exchange was sufficiently lowered to create appreciable crosslinks that tuned mechanical properties based on metal concentration.

5.2: Results and Discussion

Herein, we leverage our understanding of monodentate, labile imidazole ligands to generate a gradient crosslinked metallopolymer network, to achieve gradient mechanical properties mimicking the polychaete jaw (Figure 5.1). To incorporate a gradient of metal into the material, we imagined that we could suspend a polymer sample in a metal solution, and slowly raise it out of the solution while increasing metal concentration. The dynamic nature of the crosslink in the presence of ACN would allow for rapid crosslink exchange and metal incorporation into the bulk of the material. Subsequently, upon removal of the solvent, the dynamic metal-ligand interactions would have drastically lowered exchange rates, increasing the local hardness and Young's modulus (E). The synthesis of the imidazole-containing network (ICN) is described in Figure 5.2A. An imidazole-containing acrylate monomer (IMZa) was copolymerized with butyl acrylate (BA) and 1,4-butanediol diacrylate (BDDA) via UV-initiated polymerization to achieve the ICN. BA was used to lower the glass transition temperature, enhance ligand
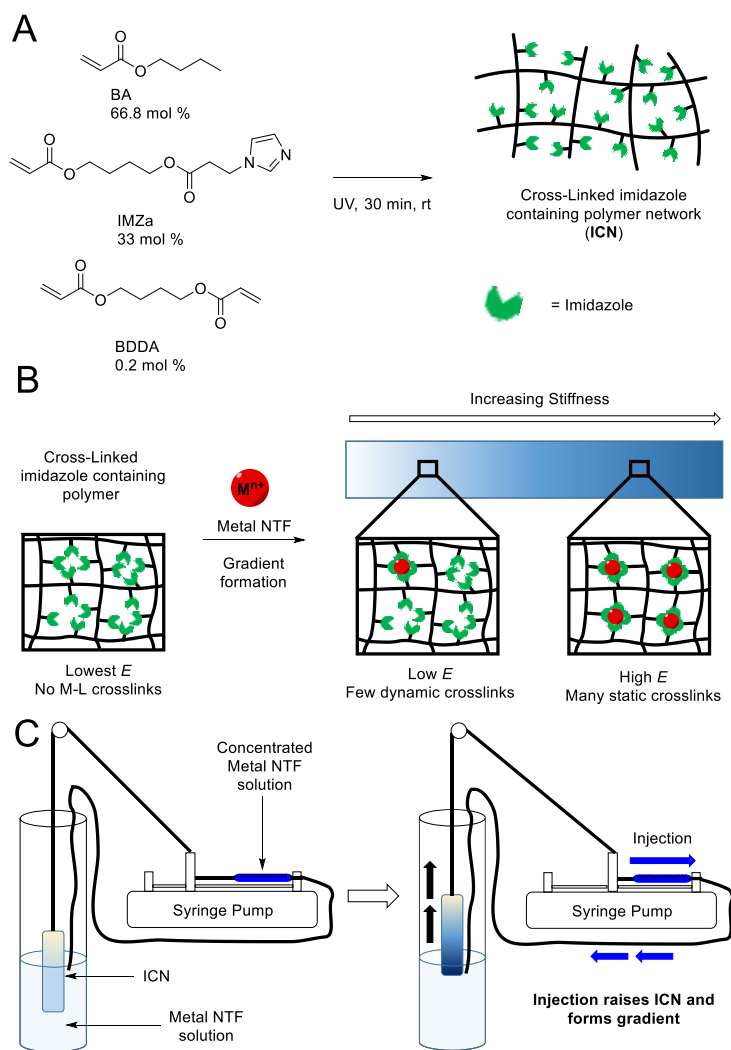
Figure 5.2 A) Synthetic route used to achieve the ICN. B) Cartoon depicting metal incorporation into the ICN to form ICN-M. C) Cartoon depicting the use of a common laboratory syringe pump to fashion the CGP

mobility, and create an initial polymer with the desired mechanical properties. The BA, IMZa and BDDA were used in a 66.5:33:0.5 mol ratio, respectively, to achieve the polymer network. These monomer incorporation ratios were selected based on our previous study, where IMZa incorporation over ~35 mol% gave diminished returns of increased mechanical properties.[29] After the synthesis of the ICN, a metal salt (Zn, Cu, or Co) was incorporated via controlled diffusion to form ICN-M. [Bis(trifluoromethylsulfonyl)-imide] (NTF) was selected as the counter ion for all metals due to its well-characterized behaviour, thermal stability, and high mobility in the solid state.

To create the metal gradient, a simple device was designed from a common laboratory syringe pump. The device, termed a **c**ontinuous **g**radient **p**atterner (CGP, Figure 5.2C) works by first attaching the polymer sample via string to the pusher block of the syringe pump and then suspending the sample in a graduated cylinder with lightly stirring solution of a metal NTF salt dissolved in ACN. A 1 mL syringe containing a highly concentrated metal NTF salt solution in
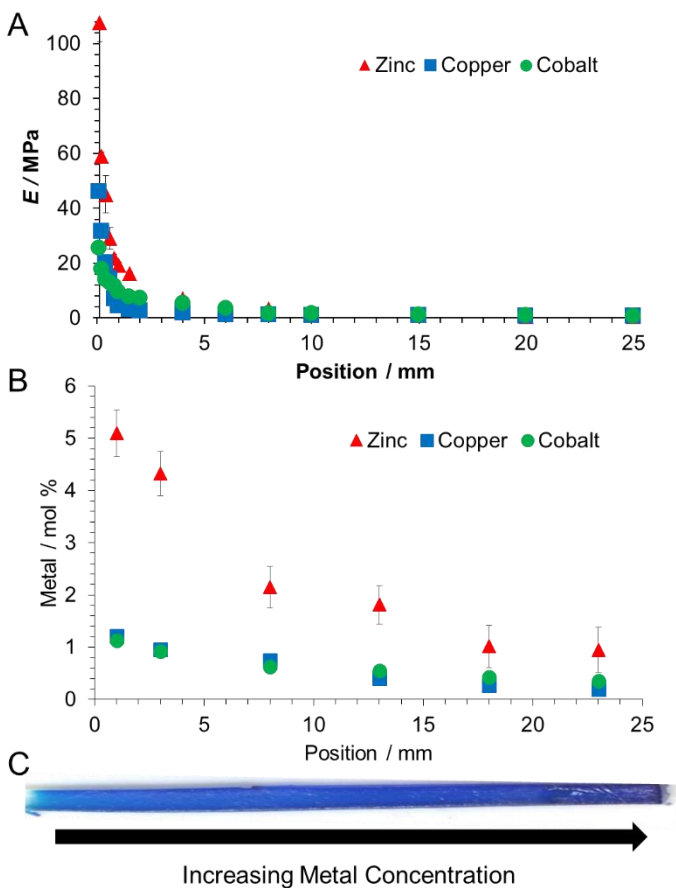
Figure 5.3. A) Spatial Young's modulus (*E*) as determined by Nano indentation. B) Relative metal concentration along the lateral axis as determined by XPS C) image of the ICN-Cu sample

ACN was adjusted to the length of the sample, such that, while the additional metal solution was being injected into the graduated cylinder, the sample would be slowly raised out of the solution, allowing a gradient to be formed. All ICN-M gradient samples were formed starting with the molar ratio of 0.167 metal atoms per imidazole. During the continuous CGP process, more metal salt was gradually added to finally raise the molar ratio to 0.25 metal atoms per imidazole in the end (See SI for detailed calculations). These selected values were determined experimentally, as both too much (Figure 5.5) and too little added metal resulted in consistently weaker materials. The syringe pump was set on the lowest flow rate, which typically allowed the polymer sample to raise out from the metal solution over 2 days, giving sufficient time for the metal to incorporate into the bulk. After completion of the process, any residual solvent was removed from the crosslinked samples in a vacuum oven.

After the metal incorporation and removal of ACN, the mechanical properties of ICN-M samples were studied via nanoindentation using a Nanovea nanoindenter. The Young's modulus (stiffness, *E*) and local hardness were calculated based on single indentation of a spherical tip. Nanoindentation was selected for characterization because it is non-destructive and allows for

small and precisely controlled testing areas. Each ICN-M sample was tested along its length axis to illustrate gradient formation. Young's modulus results (Figure 5.3A) illustrate that the highest stiffness for all ICN-M samples occur at the end of the sample in the metal solution the longest and that all samples display gradual stiffness decrease along their length axis. ICN-Zn displayed the highest stiffness for all tested samples at 108 ± 7 MPa (Table 5.1). Additionally, ICN-Zn possessed the largest and most gradually decreasing gradient span from 108 ± 7 to 0.59 ± 0.04 MPa. To the best of our knowledge, at over two orders of magnitude (227 fold increase), this stiffness gradient represents the largest, continuous synthetic mechanical gradient made to date. In fact, this range in stiffness closely matches the magnitude of gradient observed in squid beaks, a benchmark for many gradient materials.[20] After ICN-Zn, ICN-Cu displayed the next highest maximum stiffness (46.1 ± 0.8 MPa), followed by ICN-Co (25 ± 2 MPa)(Table 5.1). The local hardness of all specimens was also determined via nanoindentation (Figure 5.6, Table 5.3). In general, the observed hardness gradients spanned over one order of magnitude. Interestingly, ICN-Co displays the highest hardness of all samples, rather than ICN-Zn. This may be because Co-imidazole complexes exist as ML_6 species, while Zn-imidazole complexes exist as ML_4 complexes. This higher degree of crosslinks per metal atom could lead to a higher resistance to permanent shape change i.e. hardness.

To confirm that the stiffness and hardness gradient was arising from the incorporation of a gradient of metal ions, X-ray Photoelectron Spectroscopy (XPS) using a Kratos Axis SUPRA, was employed to determine relative metal concentrations along the lateral axis of the specimen. XPS was chosen because it can detect small metal concentrations, examine spatially distinct locations along the lateral axis, and is generally non-destructive to the sample. An argon gas cluster ion source (GCIS) was used to remove surface contaminants (Ar2000+, 5 keV) and observe the bulk

material. Region scans of the major atomic components (C, O, N) of the ICN were used to determine the relative abundance of the metal ions (Zn, Cu, and Co) and confirm that the correct atomic ratios of elements were present for the ICN. Indeed, along the lateral axis of the specimen, gradients of all 3 metals were observed (Figure 5.3B). ICN-Zn contains the largest relative percentage of metal (ranging from 0.9 – 5.1%, Table 5.2) while ICN-Co and ICN-Cu contained less relative metal (ranging from 0.35 – 1.13 % and 0.1 – 1.21 % respectively, Table 5.2). Depth profiling using a 20 keV 2000 Ar+ GCIS suggests that the metal is able to penetrate into the bulk of the material in similar relative amounts (Figure 5.7). Determination of metal concentration below 1 mm was not accurate as the survey area of the XPS must be kept away from the edge to minimize interference from the carbon tape used to adhere the sample to the slide. The excellent correlation between the metal concentration gradient observed by XPS and the mechanical gradient observed via nanoindentation implies that metal-imidazole interactions cause the strengthening of the material. We hypothesize that the dramatic change in stiffness over the last 1 mm of the material may be due to the ability of the metal to permeate better into the end of the material from the great surface area exposed to the solution, and is also in the solution the longest. This spike in stiffness may also be related to the changing metal to ligand ratio. In our previous study[29], we observed significant changes in Young's modulus between 0.22 and 0.25 metal atoms per imidazole. If the sample is in this range at the end of these samples, a similar dramatic increase in Young's modulus could be observed. Incorporation of the metal into the polymer at the molar ratio of 0.25:1 would give roughly 7.5 mol % metal. Especially in the case of the zinc, we imagine that the bulk mol % of metal is closest to approaching this ideal amount.

Table 5.1 Minimal and maximal stiffness of each ICN material.

Metal	Max E[a]	Min E[a]	Fold Increase
Zinc	107 ± 7	0.47 ± 0.02	227
Copper	46 ± 1	0.34 ± 0.01	135
Cobalt	25 ± 2	0.38 ± 0.01	66

[a] Young's modulus (E) is measured in MPa

Table 5.2 Minimal and maximal relative metal amount of each ICN material.

Metal	Max Metal mol %[a]	Min Metal mol %[a]	Fold Increase
Zinc	5.1 ± 0.5	0.9 ± 0.4	5.7
Copper	1.13 ± 0.07	0.35 ± 0.05	3.2
Cobalt	1.21 ± 0.06	0.11 ± 0.01	11.2

[a] Metal mol % was determined via XPS and is relative to the carbon, nitrogen and oxygen content of the polymer

While the same metal concentrations for M-NTf solutions were used for all samples during swelling, the gradient behaviour for ICN-M samples differed based on metal selection. ICN-Zn formed a significantly stiffer gradient than both ICN-Cu and ICN-Co. This agrees with the XPS data, which demonstrates the ICN-Zn had higher metal incorporation across the lateral axis. In an attempt to rationalize why ICN-Zn would have more metal than ICN-Co and ICN-Cu, we note here that Zn^{2+} species are known to form only ML_4 complexes with imidazole ligands, while Co^{2+} and Cu^{2+} can from six coordinate species.[28, 29] While studying complexation of metal into a swollen polymer is not straightforward, we hypothesize that higher coordination number would hinder penetration of the metal deeper into the sample. This dissimilar metal mobility could affect network formation. We are currently pursuing routes to better quantify these possible effects.

5.3: Conclusions

In summary, the ICN-Zn network demonstrated in this work represents the largest continuous gradient change in mechanical properties observed to date at over 2 orders of

magnitude. While this alone is a dramatic improvement in these types of materials, the accessibility and ease of synthesis is another marked improvement. Using only a 2-step synthesis and common laboratory syringe pump, the ICN-M gradient materials can be reliably produced. With more rigorous engineering control (pull rate, temperature, metal added) we think gradients with over 3 orders of magnitude in young's modulus could feasibly be obtained. In addition, the flexibility of this system will allow for a variety of different mechanical gradients to be studied using different metals, labile ligands, and counterions. Ongoing studies pursuing these goals, as well as gaining more mechanistic insight are currently being completed in our lab.

5.4 Supporting Information

General Information

^{1}H NMR spectra were recorded at 500 MHz. Chemical shifts were reported in standard format as values in ppm relative to the signal of deuterated solvents. All metal salts were stored and weighed in a Nitrogen glove box to minimize water absorption and ensure accurate measurements. $Cu(NTf_2)_2$ was purchased from Aldrich. $Zn(NTf_2)_2$ was purchased from Strem Chemicals, Inc. $Co(NTf_2)_2$ was purchased from Alfa Aesar. $Cu(NTf_2)_2$ was obtained in hydrate form and the water content, reported in the Certificate of Analysis (determined by Karl Fischer titration), was used to calculate the molecular weight of the copper hydrate. For butyl acrylate, inhibitors were removed by passing through basic alumina column prior to polymerization. 1-hydroxycyclohexyl phenyl ketone, technical grade, was used as received and was not passed through basic column before polymerization. UV polymerization was performed with a UVP BL-15 longwave UV lamp (P/N 95-0130-01, 0.305 amps, 120 V, 60 Hz) at a distance of approximately 1.5 inches. The syringe pump used in the CGP was a Fisher Scientific model No. 78-01001.

Synthesis and polymerization

Synthesis of IMZa
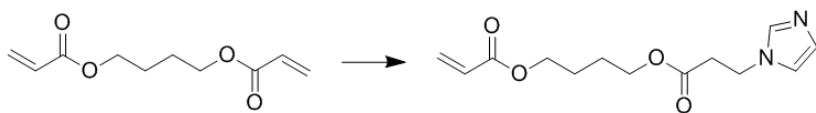
The synthesis of **IMZa** was carried out as previously described.[28] Characterization matched previous literature values.

Polymerization of ICN
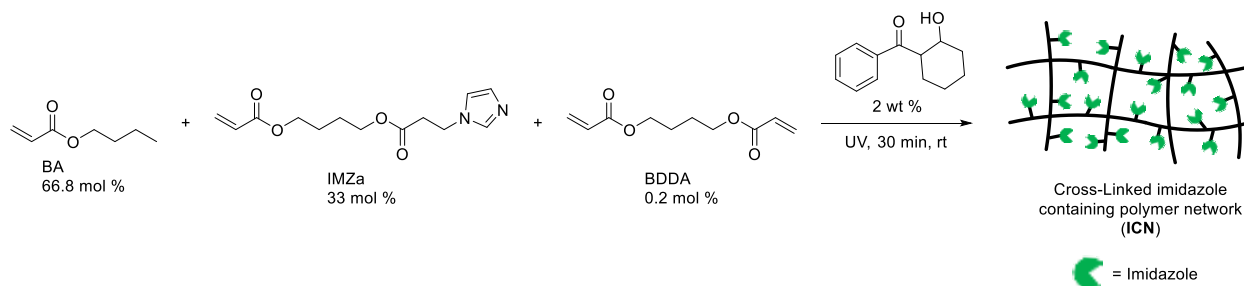
In a glass vial IMZa (7.44 mmol, 1.98 g, 33 mol%), butyl acrylate (13.7 mmol, 1.76 g, 66.8 mol%), butane diol diacrylate (0.0744 mmol, 0.0147 g, 0.2 mol%), and 1-hydroxycyclohexyl phenyl ketone (0.0751 g, 2 wt% w.r.t. total monomer) were combined. Next, reagents were purged with N_2 for 5 minutes. After purging, a small amount of monomer solution was saved for NMR analysis to determine the exact amount of IMZa in the monomer solution. The purged monomer solution was transferred to a Teflon dish (54 mm x 35 mm x 1.5 mm) and pre-polymerized with UV light for 5 minutes. The viscous gel was then covered with a plastic overhead slip and weighted glass sheet, followed by UV irradiation for 30 min. After polymerization, the ICN sheet was peeled from the Teflon mold and plastic sheet, before being stored under vacuum to prevent imidazole oxidation. The mol% of IMZa in ICN was calculated from the monomer mixture, as the ratio of imidazole peaks to acrylate peaks.
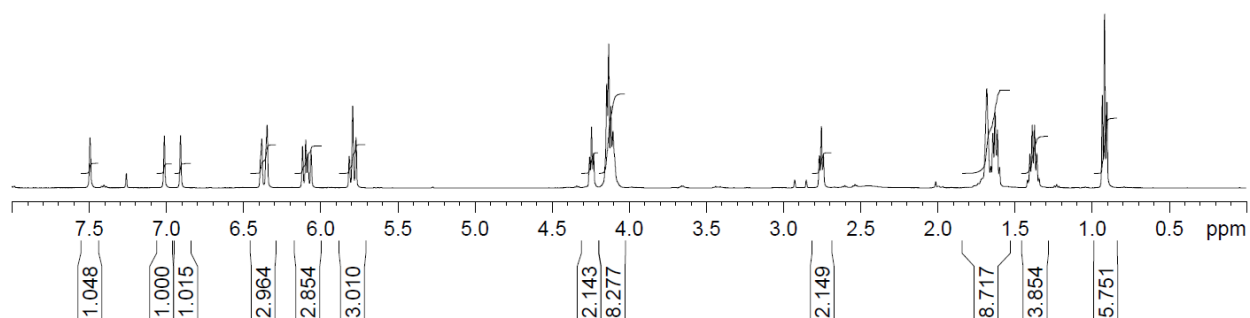
Figure 5.4 Monomer mixture from ICN polymerization. IMZa peak at 7.0 ppm was compared to BA peak at 0.9 ppm to determine IMZa percentage.

Formation of the Gradient Material

The polymer sample is suspended using tweezers in 90 mL of a stirring acetonitrile solution with the appropriate amount of metal (*vida infra*). The other end of the string is attached to the pusher arm of a syringe pump using tape. Using a 1 mL syringe and tubing, the amount of metal to be added *(vida infra)* is dissolved in an amount of acetonitrile equivalent to the swollen length of the polymer. For example, if the sample is 3 cm long while swollen, the plunger of the syringe (with the tubing attached, to account for the dead volume of the tubing) is drawn up 3 cm and that volume is used. The added solution concentration can vary slightly due to the adjustment for length for each sample. The end of the tubing is placed in the stirring solution, and the syringe pump is started. The syringe pump was set to a speed that allowed the sample to be slowly pulled up over 2 days. See Image of Apparatus below.

Calculation of swell solution concentration

Since the mol % of IMZa is known, the mmol of imidazole per length can be determined using the mass and length of the polymer. Using equation S1 the total metal needed (in mmol) at length l to form the gradient can be calculated:

Equation 5.1: $Total\ mmol\ metal = \int_{l_f}^{l_i} x \left(y_f - (y_f - y_i)\frac{l}{l_i} \right) l\ dl$

Where:

x = mmol of IMZa per length

y_f = final metal atoms per IMZa

y_i = initial metal atoms per IMZa

l_i = initial length submerged in solution

l_f = final length submerged in solution

Then using equation S2 the initial amount of metal needed can be calculated:

Equation 5.2: $Initial\ mmol\ metal\ needed = x \times y_i \times l_i$

Finally Equation S3 is used to determine the amount to add via the syringe:

Equation 5.3: $mmol\ metal\ needed\ in\ syringe = Total\ mmol\ metal - Initial\ mmol\ metal$

Bulk characterization

Instrumented indentation procedure of ICN-M samples

The hardness and modulus of elasticity were measured by nanoindenter (Nanovea, Irvine, CA, USA) using a spherical-conical diamond indenter with tip radius and cone angle of 100µm and 120° respectively. The depth and compliance of the instrument was calibrated with fused silica prior to testing, and all tests were performed at 40% humidity and 23°C. In order to stay within the spherical zone of the indenter tip (0-28.5µm), the applied load was based on the hardness of the sample at each test location. The loading rate was based on the applied load so that loading and unloading would each take 30 seconds. The resting period at maximum load was always 2 minutes to reduce the effect of creep on the elastic modulus measurement. The applied load and loading rate ranged from 0.5-20mN and 1-40mN/min respectively. The hardness and elastic modulus were calculated using ASTM E2546 (the Oliver & Pharr method).

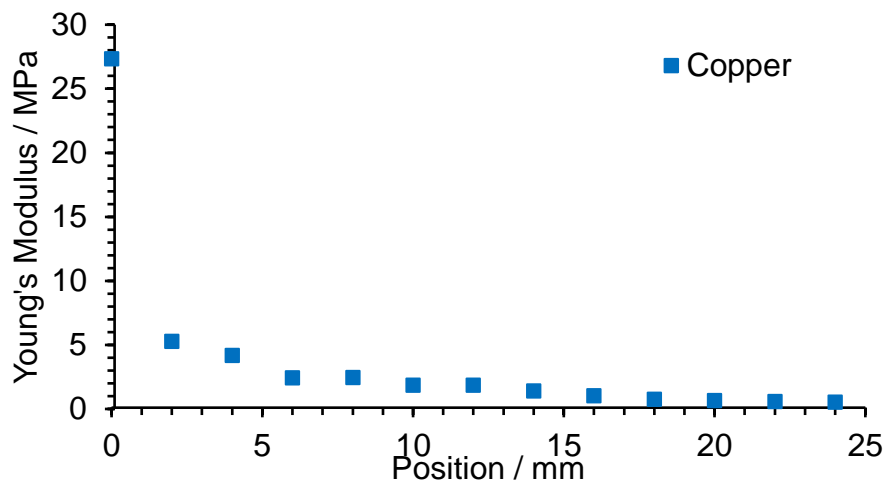**Instrumented indentation of preliminary ICN-M samples**

Figure 5.5 Preliminary data for higher metal content (0.1 copper per imidazole initial, 1 copper per imidazole final) ICN-Cu shows weaker ICN-Cu stiffness.

Tabulated Young's modulus data

Table 5.3 Stiffness of ICN-M samples associated with Figure 5.3A.

| Young's modulus by Metal (MPa)				Young's modulus by Metal (MPa)			
Position (mm)	Zinc	Copper	Cobalt	Position (mm)	Zinc	Copper	Cobalt
0.1	108 ± 7	46 ± 0.8	25 ± 2	4	7.1 ± 0.5	1.8 ± 0.3	5.4 ± 0.1
0.2	59 ± 2	32 ± 3	17.8 ± 0.6	6	4.0 ± 0.4	1.21 ± 0.05	3.52 ± 0.09
0.4	45 ± 7	20 ± 2	14 ± 1	8	3.4 ± 0.2	1.05 ± 0.02	1.5 ± 0.2
0.6	29 ± 4	14 ± 1	12.8 ± 0.8	10	1.49 ± 0.05	0.94 ± 0.01	1.6 ± 0.1
0.8	22 ± 1	7.0 ± 0.6	12 ± 1	15	1.1 ± 0.1	0.85 ± 0.01	1.15 ± 0.02
1	19 ± 1	4 ± 1	9.5 ± 0.2	20	0.63 ± 0.03	0.70 ± 0.01	0.87 ± 0.02
1.5	16.3 ± 0.6	3.0 ± 0.1	7.6 ± 0.2	25	0.59 ± 0.04	0.61 ± 0.01	0.63 ± 0.01
2	7.3 ± 0.6	2.5 ± 0.2	7.2				

Hardness data of ICN-M samples
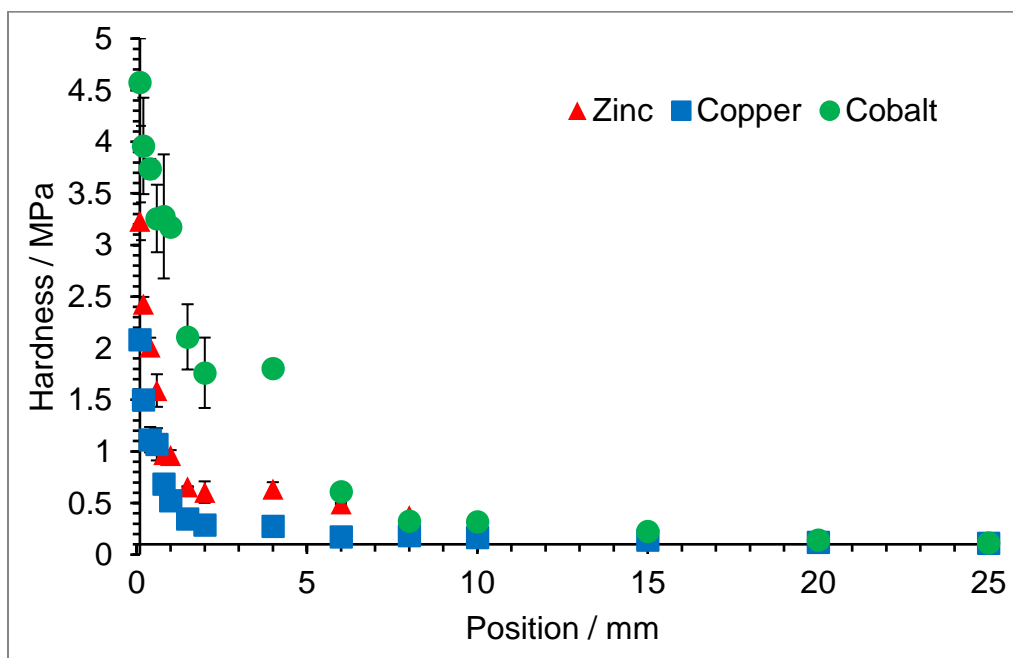
Figure 5.6 Spatial Hardness as determined by Nano indentation.

XPS procedure

X-ray photoelectron spectra were obtained using a Kratos AXIS Supra device. All measurements were made at a vacuum of < 5 e -7 torr. All samples were mounted to glass microscope slides using double-sided carbon tape. Region scans were obtained using a monochromic aluminum source at an energy of 1486.69 eV, a magnification of 1 e 37, and a resolution of 20. All surfaces were cleaned using GCIS 2000 Ag+ 5 keV etching over 12 minutes before region scans were collected. Regions scans of the Cu (3/2 2p), Zn (3/2 2p), Co (3/2 2p), O (1s), N (1s), and C (1s) were collected in the ranges of 965-925 eV, 1057-1012 eV, 810-773 eV, 543-525 eV, 410-390 eV, 300-277 eV respectively. Integrated regions from the C, O, N regions, as well as the appropriate metals were divided by their relative sensitivity factor to derive the mol % of each element. Region scans were taken at 1, 3, 8, 13, 18, and 23 mm from the hard end of the sample. Depth profiling studies were carried out using a more powerful GCIS (Ar 2000+ 20 eV) over 100 minutes. Etching was performed for 10 minutes then region scans were performed. During the depth profiling experiments, only region scans of the metal of interest and carbon were collected to minimize the time the GCIS filament was active.

Table 5.4 Tabulated XPS data of Figure 5.3B.

Distance from hard end (mm)	mol % Zn[a]	St. Dev. Zn	mol % Cu[a]	St. dev. Cu	mol % Co[a]	St. dev. Co
1	5.1	0.45	1.13	0.079	1.21	0.064
3	4.3	0.42	0.92	0.075	0.95	0.053
8	2.1	0.40	0.62	0.073	0.74	0.046
13	1.8	0.36	0.54	0.065	0.40	0.032
18	1.0	0.40	0.42	0.065	0.27	0.021
23	0.9	0.43	0.35	0.050	0.20	0.018

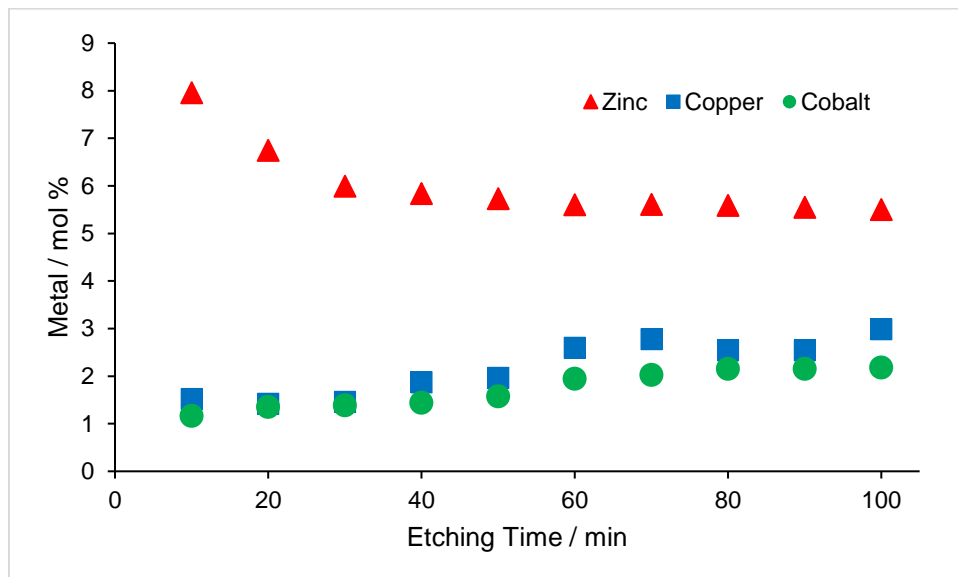[a] Relative to mol % of C, O, and N

XPS Depth Profiling

Figure 5.7 Depth profiling with a 20 keV 2000 Ar+ GCIS. Measurements were take 5.5 mm from the stiff end. mol % was calculated only relative to carbon, due to the limited time the GCIS filament could be active.

5.5: References

1. Weaver, J. C.; Milliron, G. W.; Miserez, A.; Evans-Lutterodt, K.; Herrera, S.; Gallana, I.; Mershon, W. J.; Swanson, B.; Zavattieri, P.; DiMasi, E.; Kisailus, D., The Stomatopod Dactyl Club: A Formidable Damage-Tolerant Biological Hammer. *Science* **2012,** *336* (6086), 1275-1280.

2. Suresh, S., Graded materials for resistance to contact deformation and damage. *Science* **2001,** *292* (5526), 2447-2451.

3. Libanori, R.; Erb, R. M.; Reiser, A.; Le Ferrand, H.; Suess, M. J.; Spolenak, R.; Studart, A. R., Stretchable heterogeneous composites with extreme mechanical gradients. *Nat Commun* **2012,** *3*.

4. Ionov, L., Hydrogel-based actuators: possibilities and limitations. *Mater Today* **2014,** *17* (10), 494-503.

5.   Claussen, K. U.; Scheibel, T.; Schmidt, H. W.; Giesa, R., Polymer Gradient Materials: Can Nature Teach Us New Tricks? *Macromol Mater Eng* **2012,** *297* (10), 938-957.

6.   Claussen, K. U.; Giesa, R.; Schmidt, H. W., Longitudinal polymer gradient materials based on crosslinked polymers. *Polymer* **2014,** *55* (1), 29-38.

7.   Fox, J. D.; Capadona, J. R.; Marasco, P. D.; Rowan, S. J., Bioinspired Water-Enhanced Mechanical Gradient Nanocomposite Films That Mimic the Architecture and Properties of the Squid Beak. *J Am Chem Soc* **2013,** *135* (13), 5167-5174.

8.   Kim, J.; Mok, M. M.; Sandoval, R. W.; Woo, D. J.; Torkelson, J. M., Uniquely broad glass transition temperatures of gradient copolymers relative to random and block copolymers containing repulsive comonomers. *Macromolecules* **2006,** *39* (18), 6152-6160.

9.   Wang, Y. Q.; Wang, Y.; Zhang, H. F.; Zhang, L. Q., A novel approach to prepare a gradient polymer with a wide damping temperature range by in-situ chemical modification of rubber during vulcanization. *Macromol Rapid Comm* **2006,** *27* (14), 1162-1167.

10.   Zhang, X. L.; Hassanzadeh, P.; Miyake, T.; Jin, J.; Rolandi, M., Squid beak inspired water processable chitosan composites with tunable mechanical properties. *J Mater Chem B* **2016,** *4* (13), 2273-2279.

11.   Lin, Z. Q.; Gui, X. C.; Zeng, Z. P.; Liang, B. H.; Chen, W. J.; Liu, M.; Zhu, Y.; Cao, A. Y.; Tang, Z. K., Biomimetic Carbon Nanotube Films with Gradient Structure and Locally Tunable Mechanical Property. *Adv Funct Mater* **2015,** *25* (46), 7173-7179.

12.   Wang, B. C.; Benitez, A. J.; Lossada, F.; Merindol, R.; Walther, A., Bioinspired Mechanical Gradients in Cellulose Nanofibril/Polymer Nanopapers. *Angew Chem Int Edit* **2016,** *55* (20), 5966-5970.

13. Wang, D.; Zhang, H.; Guo, J.; Cheng, B. C.; Cao, Y.; Lu, S. J.; Zhao, N.; Xu, J., Biomimetic Gradient Polymers with Enhanced Damping Capacities. *Macromol Rapid Comm* **2016,** *37* (7), 655-661.

14. Karabanova, L. V.; Mikhalovsky, S. V.; Lloyd, A. W.; Boiteux, G.; Sergeeva, L. M.; Novikova, T. I.; Lutsyk, E. D.; Meikle, S., Gradient semi-interpenetrating polymer networks based on polyurethane and poly(vinyl pyrrolidone). *J Mater Chem* **2005,** *15* (4), 499-507.

15. Qin, C. L.; Zhao, D. Y.; Bai, X. D.; Zhang, X. G.; Zhang, B.; Jin, Z.; Niu, H. J., Vibration damping properties of gradient polyurethane/vinyl ester resin interpenetrating polymer network. *Mater Chem Phys* **2006,** *97* (2-3), 517-524.

16. Ahmed, A.; Smith, J.; Zhang, H. F., Gradient porous materials by emulsion centrifugation. *Chem Commun* **2011,** *47* (42), 11754-11756.

17. Li, X. R.; MacEwan, M. R.; Xie, J. W.; Siewe, D.; Yuan, X. Y.; Xia, Y. N., Fabrication of Density Gradients of Biodegradable Polymer Microparticles and Their Use in Guiding Neurite Outgrowth. *Adv Funct Mater* **2010,** *20* (10), 1632-1637.

18. Karpiak, J. V.; Ner, Y.; Almutairi, A., Density Gradient Multilayer Polymerization for Creating Complex Tissue. *Adv Mater* **2012,** *24* (11), 1466-1470.

19. Chai, H.; Lee, J. J. W.; Constantino, P. J.; Lucas, P. W.; Lawn, B. R., Remarkable resilience of teeth. *P Natl Acad Sci USA* **2009,** *106* (18), 7289-7293.

20. Miserez, A.; Schneberk, T.; Sun, C. J.; Zok, F. W.; Waite, J. H., The transition from stiff to compliant materials in squid beaks. *Science* **2008,** *319* (5871), 1816-1819.

21. Fischer, S. F.; Thielen, M.; Loprang, R. R.; Seidel, R.; Fleck, C.; Speck, T.; Buhrig-Polaczek, A., Pummelos as Concept Generators for Biomimetically Inspired Low Weight Structures with Excellent Damping Properties. *Adv Eng Mater* **2010,** *12* (12), B658-B663.

22. Ruggeberg, M.; Burgert, I.; Speck, T., Structural and mechanical design of tissue interfaces in the giant reed Arundo donax. *J R Soc Interface* **2010,** *7* (44), 499-506.

23. Harrington, M. J.; Waite, J. H., How Nature Modulates a Fiber's Mechanical Properties: Mechanically Distinct Fibers Drawn from Natural Mesogenic Block Copolymer Variants. *Adv Mater* **2009,** *21* (4), 440-+.

24. Li, X. R.; Xie, J. W.; Lipner, J.; Yuan, X. Y.; Thomopoulos, S.; Xia, Y. N., Nanofiber Scaffolds with Gradations in Mineral Content for Mimicking the Tendon-to-Bone Insertion Site. *Nano Lett* **2009,** *9* (7), 2763-2768.

25. Lichtenegger, H. C.; Schoberl, T.; Bartl, M. H.; Waite, H.; Stucky, G. D., High abrasion resistance with sparse mineralization: Copper biomineral in worm jaws. *Science* **2002,** *298* (5592), 389-392.

26. Lichtenegger, H. C.; Schoberl, T.; Ruokolainen, J. T.; Cross, J. O.; Heald, S. M.; Birkedal, H.; Waite, J. H.; Stucky, G. D., Zinc and mechanical prowess in the jaws of Nereis, a marine worm. *P Natl Acad Sci USA* **2003,** *100* (16), 9144-9149.

27. Waite, J. H.; Lichtenegger, H. C.; Stucky, G. D.; Hansma, P., Exploring molecular and mechanical gradients in structural bioscaffolds. *Biochemistry-Us* **2004,** *43* (24), 7653-7662.

28. Mozhdehi, D.; Ayala, S.; Cromwell, O. R.; Guan, Z. B., Self-Healing Multiphase Polymers via Dynamic Metal-Ligand Interactions. *J. Am. Chem. Soc.* **2014,** *136* (46), 16128-16131.

29. Mozhdehi, D.; Neal, J. A.; Grindy, S. C.; Cordeau, Y.; Ayala, S.; Holten-Andersen, N.; Guan, Z. B., Tuning Dynamic Mechanical Response in Metallopolymer Networks through Simultaneous Control of Structural and Temporal Properties of the Networks. *Macromolecules* **2016,** *49* (17), 6310-6321.